

Adsorption Engineering

MOTOYUKI SUZUKI

Professor, Institute of Industrial Science, University of Tokyo, Tokyo 1



KODANSHA

1990



ELSEVIER

Copublished by
KODANSHA LTD., Tokyo
and
ELSEVIER SCIENCE PUBLISHERS B. V., Amsterdam

exclusive sales rights in Japan
KODANSHA LTD.
12-21, Otowa 2-chome, Bunkyo-ku, Tokyo 112, Japan

for the U.S.A. and Canada
ELSEVIER SCIENCE PUBLISHING COMPANY, INC.
655 Avenue of the Americas, New York, NY 10010, U.S.A.

for the rest of the world
ELSEVIER SCIENCE PUBLISHERS B. V.
25 Sara Burgerhartstraat, P.O. Box 211, 1000 AE Amsterdam, The Netherlands

Library of Congress Cataloging-in-Publication Data

Suzuki, Motoyuki, 1941-
Adsorption engineering / Motoyuki Suzuki.
p. cm. -- (Chemical engineering monographs : vol. 25)
Includes bibliographical references
ISBN 0-444-98802-5 (U.S.)
1. Adsorption. I. Title. II. Series. Chemical engineering
monographs : v. 25.
TP156.A35S89 1989
660'.28423--dc20

89-23532
CIP

ISBN 0-444-98802-5 (Vol. 25)
ISBN 0-444-41295-6 (Series)

ISBN 4-06-201485-8 (Japan)

Copyright © 1990 by Kodansha Ltd.

All rights reserved.

No part of this book may be reproduced in any form, by photostat, microfilm, retrieval system, or any other means, without the written permission of Kodansha Ltd. (except in the case of brief quotation for criticism or review).

Printed in Japan

CHEMICAL ENGINEERING MONOGRAPHS

Advisory Editor: Professor S.W. CHURCHILL, Department of Chemical Engineering, University of Pennsylvania, Philadelphia, PA 19104, U.S.A

- Vol. 1 Polymer Engineering (Williams)
- Vol. 2 Filtration Post-Treatment (Wakeman)
- Vol. 3 Multicomponent Diffusion (Cussler)
- Vol. 4 Transport in Porous Catalysts (Jackson)
- Vol. 5 Calculation of Properties Using Corresponding-State Methods (Šterbáček et al.)
- Vol. 6 Industrial Separators for Gas Cleaning (Štorch et al.)
- Vol. 7 Twin Screw Extrusion (Janssen)
- Vol. 8 Fault Detection and Diagnosis in Chemical and Petrochemical Processes (Himmelblau)
- Vol. 9 Electrochemical Reactor Design (Pickett)
- Vol. 10 Large Chemical Plants (Froment, editor)
- Vol. 11 Design of Industrial Catalysis (Trimm)
- Vol. 12 Steady-state Flow-sheeting of Chemical Plants (Benedek, editor)
- Vol. 13 Chemical Reactor Design in Practice (Rose)
- Vol. 14 Electrostatic Precipitators (Böhm)
- Vol. 15 Toluene, the Xylenes and their Industrial Derivatives (Hancock, editor)
- Vol. 16 Dense Gas Dispersion (Brunner and Griffiths, editors)
- Vol. 17 Gas Transport in Porous Media: The Dusty Gas Model (Mason and Malinauskas)
- Vol. 18 Principles of Electrochemical Reactor Analysis (Fahidy)
- Vol. 19 The Kinetics of Industrial Crystallization (Nývlt et al.)
- Vol. 20 Heat Pumps in Industry (Moser and Schnitzer)
- Vol. 21 Electrochemical Engineering (Roušar et al.) in 2 volumes: Parts A-C and Parts D-F
- Vol. 22 Heavy Gas Dispersion Trials at Thorney Island (McQuaid, editor)
- Vol. 23 Advanced Design of Ventilation Systems for Contaminant Control (Goodfellow)
- Vol. 24 Ventilation '85 (Goodfellow, editor)
- Vol. 25 Adsorption Engineering (Suzuki)

Preface

I was introduced to adsorption when I spent two years (1969/1971) with Professor J. M. Smith at the University of California, Davis, studying application of chromatographic methods to determine rate processes in adsorption columns. After returning to the Institute of Industrial Science, University of Tokyo, I joined Professor Kunitaro Kawazoe's adsorption research group where pioneering work in adsorption engineering had been conducted, and started research on development of adsorption technology for water pollution control.

Since then I have had many opportunities to acquire valuable ideas on adsorption problems not only from Professor Kawazoe but from numerous other senior colleagues including Professor Toshinaga Kawai of Kanagawa University, Professor Yasushi Takeuchi of Meiji University and the late Professor Hiroshi Takahashi of I.I.S., University of Tokyo.

In the laboratory, I was fortunate to have many good collaborators including Dr. Kazuyuki Chihara, Dr. Dragoslav M. Misić, Professor Byun-Rin Cho, Dr. Akiyoshi Sakoda, Dr. Ki-Sung Ha and other students. The technical assistance of Mr. Toshiro Miyazaki and Mr. Takao Fujii in laboratory work was invaluable. This volume was written based on the work of this group and I am very grateful to these colleagues and to many others not listed here.

In preparing the manuscript, I repeatedly felt that much work remains to be done in this field and that many directions of research are waiting for newcomers to seek out. Because of my imperfect knowledge and experience, many important problems which require discussion are not included. If possible these should be treated in a future edition. It took me far longer than expected at the beginning to prepare the manuscript for this monograph mainly due to idleness. Mr. Ippei Ohta of Kodansha Scientific Ltd. diligently prodded me. Without his energy this book would never have been completed. I also had to spend much time working at home and I am very grateful to my patient and gentle wife, Keiko, to whom I dedicate this volume.

Contents

Preface v

1	Introduction	1
2	Porous Adsorbents.....	5
	2 1 Activated Carbon	8
	2 2 Silica and Alumina	15
	2 3 Zeolite	16
	2 4 Other Adsorbents	21
	2 5 Measurement of Pore-related Properties	22
3	Adsorption Equilibrium	35
	3 1 Equilibrium Relations	35
	3 2 Adsorption Isotherms	37
	3 3 Heat of Adsorption	51
	3 4 Adsorption Isotherms for Multicomponent Systems	56
	3 5 Adsorption Isotherms of Unknown Mixtures	60
4	Diffusion in Porous Particles	63
	4 1 Diffusion Coefficient	63
	4 2 Pore Diffusion	64
	4 3 Surface Diffusion	70
	4 4 Micropore Diffusion	85
5	Kinetics of Adsorption in a Vessel	95
	5 1 Fundamental Relations	95
	5 2 Batch Adsorption with a Constant Concentration of Surrounding	

	Fluid	97
	5 3 Batch Adsorption in a Batch with Finite Volume	106
	5 4 Adsorption in a Vessel with Continuous Flow	117
	5 5 Fluid-to-Particle Mass Transfer in a Vessel	118
6	Kinetics of Adsorption in a Column—Chromatographic Analysis	125
	6 1 Fundamental Relations	126
	6 2 Analysis of Chromatographic Elution Curves	127
	6 3 Method of Moment	128
	6 4 Extension of the Method of Moment to More Complex Systems	135
	6 5 Comparison with Simpler Models	144
	6 6 Other Methods for Handling Chromatographic Curves	148
7	Kinetics of Adsorption in a Column—Breakthrough Curves	151
	7 1 Linear Isotherm Systems—Solution to the General Model	152
	7 2 Linear Isotherm System—Simple Models	156
	7 3 Nonlinear Isotherm Systems—Constant Pattern Adsorption Profile	158
	7 4 Numerical Solutions for Nonlinear Systems	170
	7 5 Breakthrough of Multicomponent Adsorbate Systems	172
	7 6 Dispersion and Mass Transfer Parameters in Packed Beds	179
8	Heat Effect in Adsorption Operation	187
	8 1 Effect of Heat Generation on Adsorption Rate Measurement by a Single Particle Method	187
	8 2 Basic Models of Heat Transfer in Packed Beds	190
	8 3 Heat Transfer Parameters in Packed Beds	193
	8 4 Chromatographic Study of Heat Transfer in Packed Beds of Adsorbents	197
	8 5 Adiabatic Adsorption in a Column	201
	8 6 Adsorption with Heat Transfer Through the Wall	203
9	Regeneration of Spent Adsorbent	205
	9 1 Thermal Desorption in Gas Phase	206
	9 2 Chemical Desorption from a Column	208
	9 3 Thermal Regeneration of Spent Activated Carbon from Water Treatment	214

10	Chromatographic Separation	229
10.1	Basic Relations of Chromatographic Elution Curves in Linear Isotherm Systems	229
10.2	Separation of the Neighboring Peaks	232
10.3	Large Volume Pulses	233
10.4	Elution with Concentration Gradient Carrier	236
10.5	Chromatography for Large-scale Separation	238
11	Pressure Swing Adsorption	245
11.1	General Schema of PSA Operation	246
11.2	Equilibrium Theory for PSA Criteria	250
11.3	Numerical Solution of Nonequilibrium PSA Model	253
11.4	Simplified Solution of Dynamic Steady State Profile from Continuous Countercurrent Flow Model	259
11.5	Mass Transfer Coefficient in Rapid Cyclic Adsorption and Desorption	267
11.6	PSA Based on Difference of Adsorption Rates	271
12	Adsorption for Energy Transport	275
12.1	Principle of Adsorption Cooling	275
12.2	Choice of Adsorbate—Adsorbent System	277
12.3	Analysis of Heat and Mass Transfer in a Small-scale Adsorption Cooling Unit Utilizing Solar Heat	280
12.4	Heat Pump Utilizing Heat of Adsorption	287

Introduction

Understanding of engineering design methods of adsorption systems is an important aspect of process engineering design not only in the chemical industry but also in the fields of environmental pollution control and energy utilization. Moreover, adsorption is coming to be regarded as a practicable separation method for purification or bulk separation in newly developed material production processes of, for example, high-tech materials and biochemical and biomedical products.

Advances in chemical engineering principles such as transfer rate processes and process dynamics and accumulation of quantitative data in the field of adsorption, together with the development of easily accessible microcomputers, have combined to enable the development of an integrated curriculum of adsorption engineering.

The first book on engineering design of adsorption apparatus in Japan, written by Professor Kunitaro Kawazoe (1957), was published as part of the "Advanced Series in Chemical Engineering." The contents included: 1. Adsorbents, 2. Industrial Adsorbers, 3. Adsorption Equilibrium, 4. Adsorption Rate, 5. Contact Filtration Adsorption, 6. Moving Bed Adsorption, 7. Fixed Bed Adsorption, and 8. Fluidized Bed Adsorption. For many adsorption design engineers, this was the only textbook for a long time. Later developments in the field have been published in *Kagaku-kogaku-benran* (Chemical Engineering Handbook edited by the Society of Chemical Engineers, Japan). This is a good contrast with Perry's Chemical Engineers' Handbook up to 6th editions where the works of the school of the late Professor Theodore Vermeulen were introduced.

A number of volumes have been written on adsorbents and adsorption. The one by professor D. M. Ruthven (1985) is a good compilation of the chemical engineering work conducted in this field. Extensive work on diffusion in zeolite by the author and his collaborators are summarized and a complete collection of mathematical analyses in the literature are useful for readers initiating advanced studies in this field. Also Professor R. T. Yang (1986) published a book focusing on gas separation by

adsorption, which is also a good reference for chemical engineers.

The purpose of the present volume is to provide graduate students and chemical process engineers an overall understanding of the chemical engineering principles related to adsorption processes. Balanced rather than detailed discussions are attempted.

Chapter 2 gives brief picture of the adsorbents frequently used in actual processes. Surface characteristics and pore structures of adsorbents are the main properties in determining adsorption equilibrium and rate properties which are needed for plant design. New adsorbents are continuously being developed, introducing new applications for adsorption technology.

Chapter 3 introduces the concepts of adsorption equilibrium with the primary purpose of discussing the applicabilities and limits of some simple expressions which are used in later sections on design of adsorbers. Adsorption equilibrium is the fundamental factor in designing adsorption operations.

Chapter 4 is an attempt to provide an global view of diffusion phenomena in adsorbent particles, another important aspect of adsorption engineering.

Chapter 5 deals mainly with batch adsorption kinetics in a vessel. Determination of intraparticle diffusion parameters should be done with a simple kinetic system where no other rate processes are involved. For this purpose measurement of concentration change in the finite bath where adsorption takes place is the most effective method. Concentration change curves derived for nonlinear isotherm systems as well as for a linear isotherm system are presented for convenient determination of rate parameters. These discussions are also applicable to the analysis and design of adsorption operation in a vessel or differential reactor.

Chapter 6 introduces another powerful technique for determining the rate parameters involved in an adsorption column. The principle of chromatographic measurement implicitly contains many fundamental concepts concerning dynamic performance of a column reactor. The mathematical treatments introduced in this chapter can easily be extended to cover more complicated dynamic operations.

Chapter 7 gives the basic relations used for calculation of breakthrough curves in an adsorption column. The discussion focuses on simpler treatment with overall mass transfer parameter. There are many rigorous solutions to fundamental equations but in most industrial designs, while a quick estimation method is preferable at the same time the effects of many parameters need to be clarified. Constant pattern development is an important characteristic in the case of nonlinear (favorable) isotherm systems simplifying design calculation.

Heat effects in adsorption processes are discussed in Chapter 8. Adsorption is accompanied by heat generation, and adsorption equilibrium and rate are dependent on temperature. This coupling effect brings about complex but interesting problems.

Chapter 9 is devoted to methods for the regeneration of spent adsorbents. Since adsorption separation is a transient technique, regeneration of adsorbents after the period of adsorption is an important part of an adsorption purification or separation system. Recovery of valuable adsorbates will also become increasingly important.

In Chapter 10, chromatographic operations on the industrial scale is considered. Development of this area is especially needed in the area of fine products separation such as required in biotechnological processes. Much improvement of adsorbents and new operation schemes are expected in this field.

Chapter 11 introduces a bulk separation technique, pressure swing adsorption (PSA). This method has become very sophisticated and complex. The chapter attempts to define fundamental ideas in considering these attractive processes.

In Chapter 12, one unique application of adsorption for energy utilization purposes is introduced. For refrigeration, cooling and heat pumping application of adsorption phenomena has been attempted. Fundamental ideas on these application are discussed.

As described above, Chapters 2 through 4 deal with the fundamentals of adsorption phenomena which are necessary to understand the operation and design of basic adsorption operations introduced in Chapters 5 to 7. Chapters 8 and 9 are fundamental topics specific to adsorption operations and Chapters 10, 11 and 12 introduce basic ideas on the practical and rather new applications of adsorption phenomena. The reader can start from any chapter of interest and refer to the fundamentals if necessary.

Porous Adsorbents

Physical adsorption is caused mainly by van der Waals force and electrostatic force between adsorbate molecules and the atoms which compose the adsorbent surface. Thus adsorbents are characterized first by surface properties such as surface area and polarity.

A large specific surface area is preferable for providing large adsorption capacity, but the creation of a large internal surface area in a limited volume inevitably gives rise to large numbers of small sized pores between adsorption surfaces. The size of micropore determines the accessibility of adsorbate molecules to the adsorption surface so the pore size distribution of micropore is another important property for characterizing adsorptivity of adsorbents.

Also some adsorbents have larger pores in addition to micropores which result from granulation of fine powders or fine crystals into pellets or originate in the texture of raw materials. These pores called macropores are several micrometers in size. Macropores function as diffusion paths of adsorbate molecules from outside the granule to the micropores in fine powders and crystals. Adsorbents containing macropores and micropores are often said to have "bi-dispersed" pore structures.

Pore size distributions of typical adsorbents are shown in Fig. 2.1.

Surface polarity corresponds to affinity with polar substances such as water. Polar adsorbents are thus called "hydrophilic" and aluminosilicates such as zeolites, porous alumina, silica gel or silica-alumina are examples of adsorbents of this type.

On the other hand, nonpolar adsorbents are generally "hydrophobic." Carbonaceous adsorbents, polymer adsorbents and silicalite are typical nonpolar adsorbents. These adsorbents have more affinity with oil than water.

Popular adsorbents in commercial use are reviewed in the following sections. Measurement techniques for pore size distributions are also briefly introduced in the later sections of this chapter.

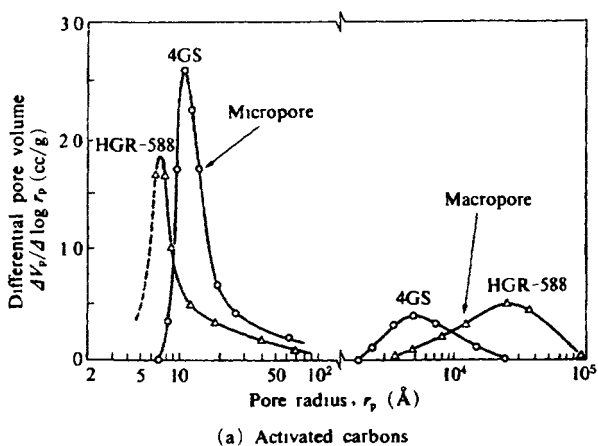


Fig. 2.1.a. Pore size distribution of typical activated carbons.

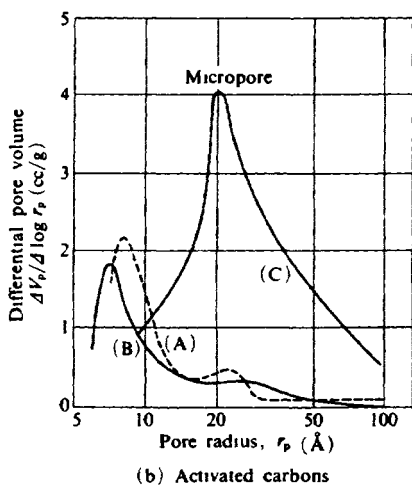


Fig. 2.1.b Pore size distribution of typical activated carbons for solvent recover

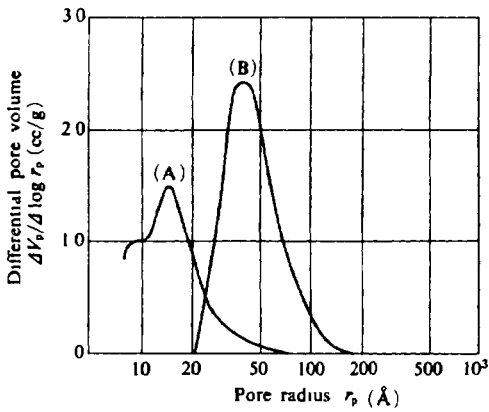


Fig 2 1 c Pore size distributions of Silica gel (A) Type A, (B) Type B

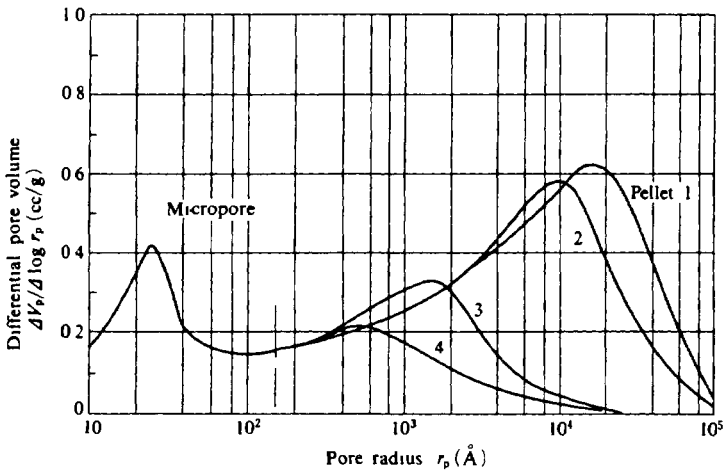


Fig 2 1 d Pore size distributions of Alumina pellets with different pelletizing pressures Pellet density 1 0.58, 2 0.68, 3 0.83, 4 1.02 g/cm³

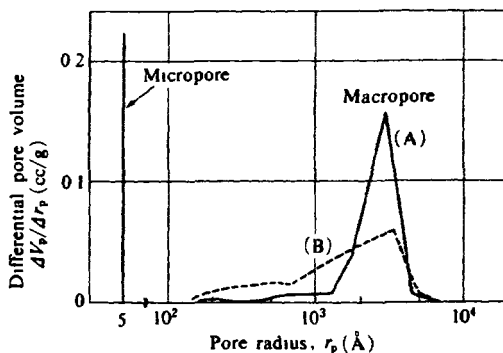


Fig 21e Pore size distributions of Molecular sieve zeolite 5A (A) Davidson Z-100 (Binderless), (B) Davidson Regular.

2.1. Activated Carbon

Activated carbons are the microporous carbonaceous adsorbents whose history can be traced back to 1600 B.C. when wood chars were used for medicinal purposes in Egypt. In Japan, a well for underground water equipped with a charcoal filter at the bottom was found at an old shrine (Kashiwara Jingu, Nara) constructed in the 13th century A. D. In Europe, wood char and later bone char were used for refining beet sugar, a practice started in France because of the blockade against the Continent during the Napoleonic era. In the 20th century, during the World Wars, the need to develop gas masks stimulated rapid growth in adsorption research. Many books have been published on activated carbon and its applications (Araki, 1932; Bailleul *et al.*, 1962; Hassler, 1974; Mantell, 1951; Mattson and Mark, 1971; Tanso Zairyo-Gakkai, 1975).

2.1.1. Preparation of activated carbons

Commercially available activated carbons are prepared from carbon-containing source materials such as coal (anthracite or brown coal), lignite, wood, nut shell, petroleum and sometimes synthetic high polymers

These materials are first pyrolyzed and carbonized at several hundred degrees centigrade. During this process the volatile fraction and low molecular products of pyrolysis are removed and the residual carbon-

ceous material undergo the following activation process by using oxidizing gases, such as steam at above 800°C or carbon dioxide at higher temperatures. Micropores are formed during the activation process. The yield of activated carbon from raw materials is in most cases less than 50% and sometimes below 10%.

Carbonization and activation can also be performed using inorganic chemicals such as zinc chloride or phosphoric acid, which is known to have a catalytic effect on pyrolytic condensation of carbohydrates. Then reaction proceeds at lower temperatures and increases yield of char during carbonization. In this process, precursor of micropore is formed when carbonization takes place around fine crystals of inorganic salt and washing of the salt by acid after carbonization produces micropores which are larger in diameter than those formed by gas phase activation. This method provides the larger micropores preferable for the adsorption of larger molecules.

2.1.2 Features of activated carbons

A. micropores

Micropores, where most adsorption takes place, are in the form of two-dimensional spaces between two graphite-like walls, two-dimensional crystallite planes composed of carbon atoms. The distance between the two neighboring planes of graphite is 3.76 Å (0.376 nm), but in the case of activated carbons which have a rather disordered crystallite structure (turbostratic structure), this figure must be larger since adsorbate molecules are not accessible otherwise (Fig. 2.2).

B. surface oxide groups

Most activated carbons contain some oxygen complexes which arise from either source materials or from chemical adsorption of air (oxidation) during the activation stage or during storage after activation. Surface oxides add a polar nature to activated carbons, e.g. hydrophilicity, acidity and negative ζ -potential.

Oxygen complexes on the surface exist mainly in the form of four different acidic surface oxides: I) strong carboxylic groups, II) weak carboxylic groups which exist as lactone groups combined with the neighboring carbonyl groups, III) phenolic groups and IV) carbonyl groups which form lactone groups with carboxyl groups of Type II (Fig. 2.3).

Distinguishing these acidic oxides is possible by multibasic titration (Boehm *et al.*, 1964), titration with alkaline solutions of different

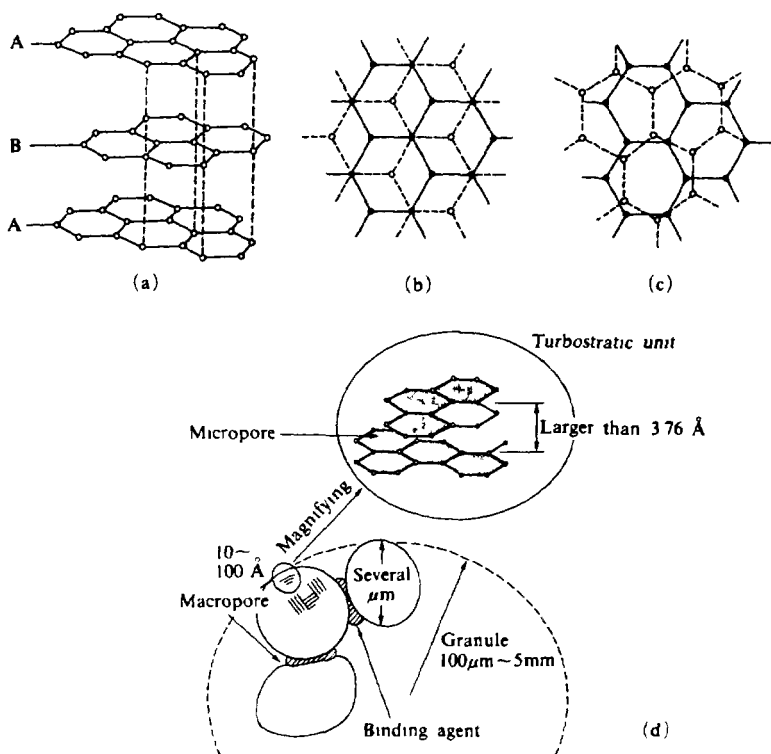


Fig. 2.2. Graphite structure (a,b) and turbostratic structure (c). Conceptual illustration of granular activated carbon (d).

strength. For instance, sodium bicarbonate, NaHCO_3 , whose pK_a value is 6.37, neutralizes surface oxides of group (I). Sodium carbonate, Na_2CO_3 ($pK_a=10.25$), can be used for titration of groups (I) and (II), sodium hydroxide, NaOH ($pK_a=15.74$), for groups (I), (II) and (III) and sodium methoxide, NaOC_2H_5 ($pK_a=20.58$), for groups (I), (II), (III) and (IV). Hence it is possible to determine the amount of each surface oxide group from the difference in titration values.

There are several other forms of oxides including basic groups such as cyclic ether groups. The basic character of activated carbon is emphasized when activation is conducted at higher temperatures.

Surface oxide groups can be removed by heat treatment of carbons in an inert atmosphere or under vacuum (Puri *et al.*, 1962, 1964, 1966). Evolution of CO_2 is observed at temperatures below 600°C and surface acidity is closely related to the amount of the evolved CO_2 .

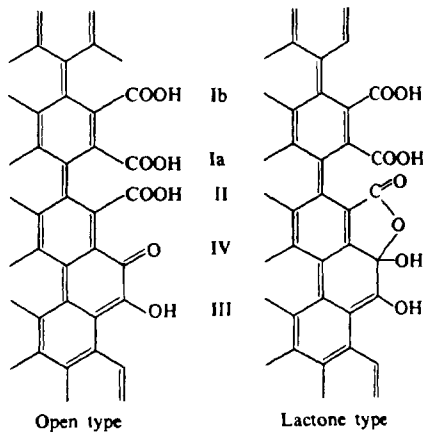


Fig. 2.3. Surface oxides on carbon surface. I : Carboxyl group, a : Removed by 200°C, b : Removed above 325°C, II : Carboxyl group which exists as lactol group, III : Phenolic hydroxyl group, IV : Carbonyl group.

Above 600°C, the evolving CO is considered to correspond to the basic functional groups on the carbon surface.

C. ashes

Activated carbon also contains to some extent ashes derived from starting materials. The amount of ash ranges from 1% to 12%. Ashes consist mainly of silica, alumina, iron, alkaline and alkaline earth metals. The functions of these ashes are not quantitatively clarified but some of them are 1) increasing hydrophilicity of activated carbon, which is advantageous when PAC is used for water treatment, 2) catalytic effects of alkaline, alkaline earth and some other metals such as iron during activation or regeneration step which modifies pore size distribution to larger pore range, and so on. Acid soluble ashes can be removed by washing with weak acid.

2.1.3. Powdered activated carbon (PAC)

Activated carbons in commercial use are mainly in two forms: powder form and granular or pelletized form. Powdered activated carbons (PAC) in most cases are produced from wood in the form of saw dust. The average size of PAC is in the range of 15 to 25 μm and the geometrical standard deviation is between 0.15 to 0.266. This particle size assures that intraparticle diffusion will not be the rate limiting step; thus the adsorption operation is designed from the view point of selection of

contacting apparatus, mixing of PAC with liquid, separation of PAC after contacting and disposal or regeneration if possible after usage.

The major industrial uses of PAC are decolorization in food processes, such as sugar refinery, oil production and sodium glutamate production as well as wine preparation. Recently, considerable PAC is used in water treatment for both drinking water and wastewater treatment.

In the use of PAC in water phase, surface charge of the carbon powder becomes an important factor since it affects ease of coagulation sedimentation or filtration for separation of PAC from the bulk liquid after adsorption. Surface charge can be detected by ζ -potential or colloid titrations. Measurement of ζ -potential for several commercially available PACs showed that it varies considerably by sample and that it is also very dependent on pH of the solution, suggesting that the existence of dissociative functional groups (oxide groups) is playing an important role. The effects of the acid washing for removing soluble ashes and the successive heat treatment to remove surface acidic oxides

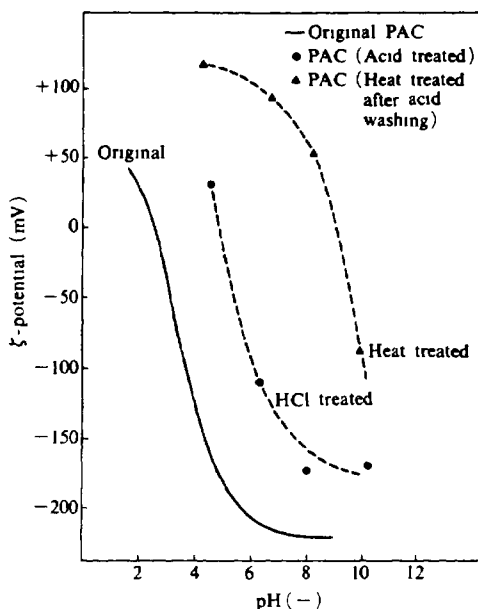


Fig 2.4 Change of ζ -potential of PAC by acid treatment (HCl 1 N) and heat treatment (900°C, N₂ stream) PAC Hokuetsu Tanso, wood char (Reproduced with permission by Suzuki, M and Chihara, K, *Water Res.*, 22, 630 (1988))

on ζ -potential are clearly shown in Fig. 2.4. Powdered activated carbons produced from saw dust are used and ζ -potential calculated from the electromobility of the powders at different levels of pH are illustrated in the figure. Presence of both acid soluble ashes and surface oxides increases the negative charge of the particles; this is not desirable when coagulation of the powders is needed.

When PAC is used, not only is its adsorbability utilized but its surface charge may also cooperate as a coagulant for colloidal fractions in the liquid phase. In this case, however, the regeneration of PAC may become rather difficult. This is one of the reasons why spent PAC is in most cases dumped rather than regenerated for repeated use.

2.1.4. Granular activated carbon (GAC)

Granular activated carbons (GAC) are either in the form of crushed granules (coal or shell) or in the pelletized form prepared by granulation of pulverized powders using binders such as coal tar pitch. GAC produced from petroleum pitch is prepared by activation of the spherical beads prepared from the pitch.

Size of granules differ depending on the application. For gas phase adsorption, cylindrically extruded pellets of between 4 to 6 mm or crushed and sieved granules of 4/8 mesh to 10/20 mesh are often used. The main applications in gas phase are solvent recovery, air purification, gas purification, flue gas desulfurization and bulk gas separation.

In the case of liquid phase adsorption, intraparticle diffusion often becomes the rate determining step of adsorption so smaller particles of for example, 12/42 mesh are advantageous from this point of view, but operational requirements such as ease of handling, low pressure drop in the adsorption bed, little elutriation or abrasion during back washing and so on define the lower limit of the particle size. Decolorization in sugar refinery, removal of organic substances, odor and trace pollutants in drinking water treatment, and advanced wastewater treatment are major applications of liquid phase adsorption.

Spent GAC in most applications is regenerated by a thermal method. Detailed discussions are given in Chapter 9.

2.1.5. Carbon molecular sieves

Size of micropore of the activated carbon is determined during pyrolyzing and activation steps. Thus small and defined micropores that have molecular sieving effects can be prepared by using proper starting materials and selecting conditions such as carbonizing temperature,

activation temperature and time or properties of binders for granulation.

The main applications of activated carbon with molecular sieving ability are separation of nitrogen and oxygen in air on the basis of difference of diffusion rates of these gases in small micropores, and adjustment of fragrance of winery products where only small molecules are removed by adsorption in liquid phase.

Carbon molecular sieve (CMS, or Molecular Sieving Carbon, MSC) is an interesting material as a model of activated carbons since it has a uniform and narrow micropore size distribution. The Dubinin-Astakhov Equation for adsorption isotherms of various gases was tested using MSC (Kawazoe *et al.*, 1974), and later this equation was extended for adsorbents with micropore size distributions (Sakoda and Suzuki, 1983) and for isotherm relation in the low pressure range. Also, chromatographic measurement of Henry's constants and micropore diffusivities were made for MSC (Chihara *et al.*, 1978); these gave clear relations between heat of adsorption and activation energy of diffusion in micropores of MSC.

2.1.6. Activated carbon fiber

Synthetic fibers such as phenolic resin (Kynol R), polyacrylic resin (PAN) and viscose rayon are carbonized at high temperatures in inert atmosphere and activated carbon fiber (ACF) is then prepared by careful activation. Recently the carbon fibers prepared by spinning from mesophase carbon melt derived from coal tar pitch are being further activated to provide ACF at less cost.

Most ACFs have fiber diameter of 7 to 15 μm , which is even smaller than powdered activated carbon. Hence the intrafiber diffusion becomes very fast and the overall adsorption rate is controlled in the case of ACF bed, by longitudinal diffusion rate in the bed (Suzuki and Sohn, 1987).

ACF is supplied in the form of fiber mat, cloth and cut fibrous chip of various sizes. ACF and cellulose composite sheet is also available.

Application of sheet adsorbent is found in the field of air treatment such as solvent recovery. Application in water treatment is under development in several areas such as chlorinated organics and odorous components removal during city water purification from deteriorated water sources such as eutrophicated lake water and polluted underground water (Sakoda *et al.*, 1988).

2.2. Silica and Alumina

2.2.1. Silica gel

Pure silica, SiO_2 , is naturally a chemically inactive non-polar material like quartz but when it has a hydroxyl functional group (silanol group), the surface becomes very polar and hydrophilic (Fig. 2.5).

Silica gel is the adsorbent particle prepared by coagulation of a colloidal solution of silicic acid (3 to 5 nm) followed by controlled

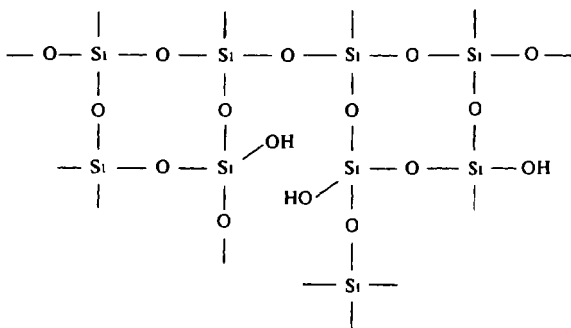


Fig. 2.5. Surface hydroxyl group on silica surface.

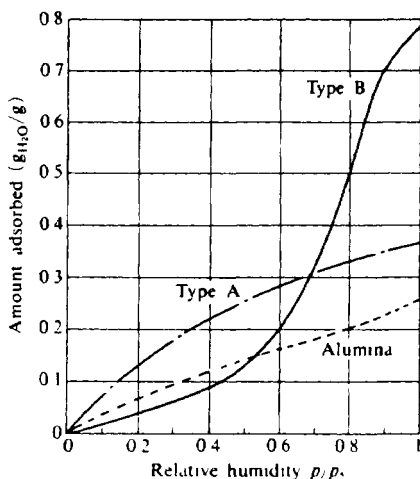


Fig. 2.6 Typical examples of adsorption isotherms of water vapor on Silica gel type A and B and active alumina

dehydration. Liquid sodium silicates are neutralized by sulfuric acid and the mixture is then coagulated to form hydrogel. The gel is washed to remove the sodium sulfate formed during the neutralization reaction. Then it is dried, crushed and sieved. Spherical silica gel particles are prepared by spray drying of the hydrogel in hot air.

Silica gels of two types of pore size distribution are frequently used for commercial purposes. Type A and B have different shapes of adsorption isotherms of water vapor (Fig. 2.6). This difference originates from the fact that type A is controlled to form pores of 2.0/3.0 nm while Type B has larger pores of about 7.0 nm. Internal surface areas are about 650 m²/g (Type A) and 450 m²/g (Type B).

Silica gel contains about 0.04 to 0.06 g_{H₂O}/g of combined water after heating at 350°C and if it loses this water, it is no longer hydrophilic and loses adsorption capacity of water.

The main application is dehumidification of gases such as air and hydrocarbons. Type A is suitable for ordinary drying but Type B is more suitable for use at relative humidity higher than 50%.

2.2.2. Active alumina

Aluminum oxides have several crystal forms. Active alumina (porous alumina) used as an adsorbent is mainly γ -alumina. Specific surface area is in the range of 150 and 500 m²/g with pore radius of 15 to 60 Å (1.5 to 6 nm), depending on how they are prepared. Porosity ranges from 0.4 to 0.76 which gives particle density of 1.8 to 0.8 g/cm³.

Porous alumina particles are produced by dehydration of alumina hydrates, in most cases alumina trihydrate, Al₂O₃·3H₂O, at controlled temperature conditions to about 6% of moisture content.

Active alumina is also used as a drying agent and the typical adsorption isotherm of water vapor is included in Fig. 2.6. It is also employed for removal of polar gases from hydrocarbon streams.

2.3. Zeolite

Zeolite (the word derives from a Greek word *zein* meaning to boil) is an aluminosilicate mineral which swells and evolves steam under the blowpipe. More than 30 kinds of zeolite crystals have been found in natural mines. Many types can be synthesized industrially.

Crystalline structures are composed of tetrahedral units, at the center of which a silicon (Si) atom is located with four oxygen atoms surrounding it. Several units construct secondary units, which are

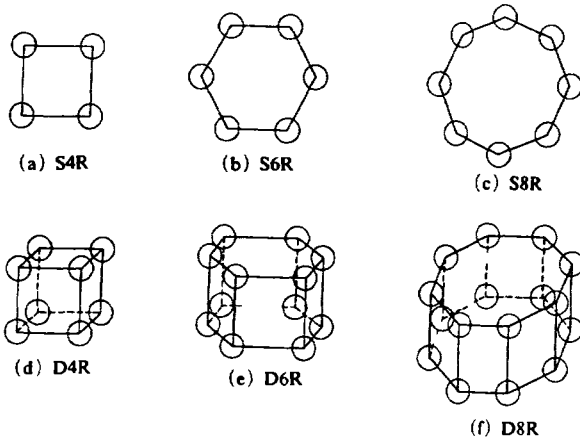


Fig 27 Several fundamental units of Si atoms in Zeolite structures
Neighboring Si atoms are connected through oxygen atom not shown in the figure

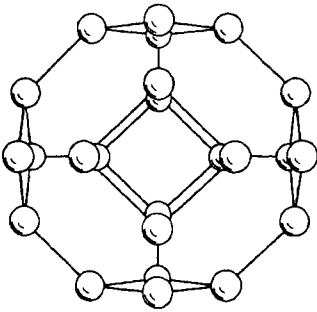
listed in Fig 27 Arrangement of these secondary units forms regular crystalline structures of zeolites

Regular crystalline structures provide unique adsorption characteristics For example, in the case of zeolite type A, eight sodalite units, (a) in Fig 28, form a cubic cell whose unit side is 12.32 \AA and each sodalite unit is located at the corner Neighboring units are connected through the D4R unit (Fig 27 d) in the form of (c) in Fig 28 and the resulting eight-membered ring connecting neighboring cells controls accessibility of adsorbate molecules into the cell where adsorption takes place In the case of zeolite type X or Y sodalite units are connected through D6R (Fig 27 e) units and form the unit structure shown by Fig 28 e A cell in the unit shown by Fig 28 f has four openings composed of 12-membered rings

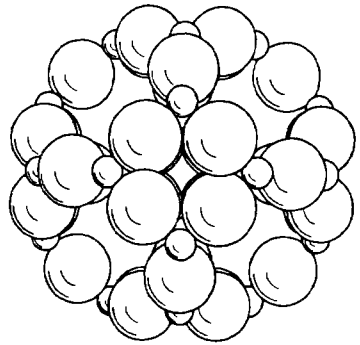
Si atoms in tetrahedral units can be replaced by aluminum (Al) ion which results in a deficit of positive valence, requiring the addition of cations such as alkaline or alkaline earth ions corresponding to the number of Al atoms These cations are easily exchangeable and the size and properties of these ions modify adsorption characteristics of zeolites since they affect the size of the window between the cells

2.3.1 Natural zeolite

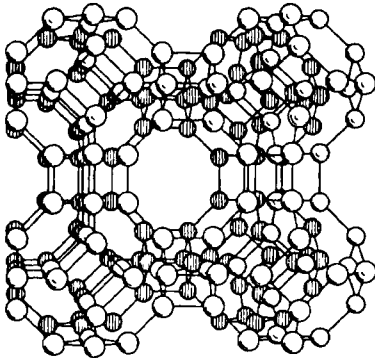
Zeolite mined in Japan and neighboring countries is limited in type and only clinoptilolite and mordenite are now excavated (Minato 1967)



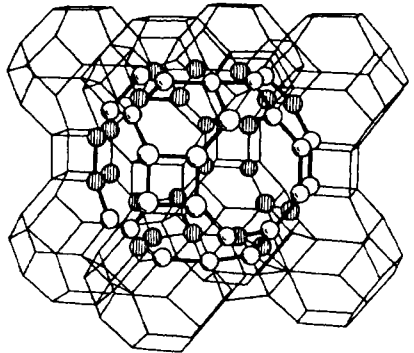
(a) Sodalite unit (β -cage) (Si, Al atoms are shown)



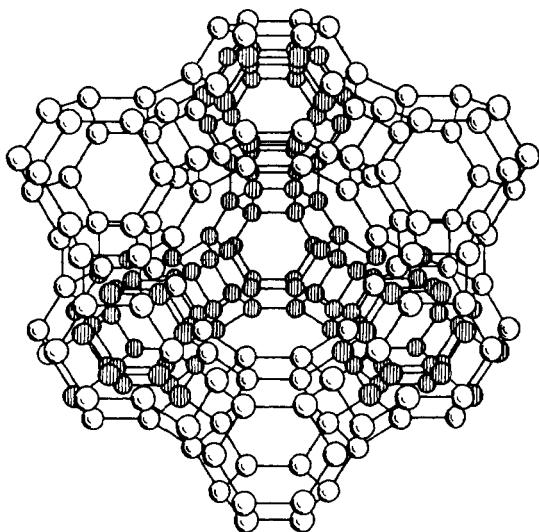
(b) Sodalite unit (with oxygen atoms)



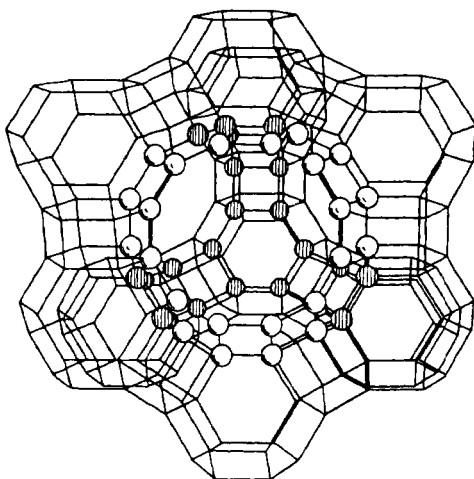
(c) Type A structure unit Composed of eight sodalite units (only Si, Al atoms are shown, black circles are on the back)



(d) Micropore cell in Type A unit- α cage, gas molecules enter through eight-membered rings



(e) Type X and Y structure unit, composed of 10 sodalite units connected by D6R units



(f) Micropore cell in Type X(Y) unit, gas molecules enter through twelve-membered rings

Fig 2 8 Structure unit of sodalite ((a) and (b)), Type A ((c) and (d)), X(Y) ((e) and (f)) Zeolites

The main uses of natural zeolite as adsorbent are as drying agents, deodorants, adsorbents for air separation, ion exchangers for water purification especially for removing ammonium ion and heavy metal ions and for water softening, soil upgrading and so on.

Suzuki and Ha (1985) showed that clinoptilolite has good adsorption selectivity of ammonium ion and obtained the adsorption equilibrium and rate of ammonium exchange.

2.3.3. Synthetic zeolite

Some zeolitic crystal structures can be synthesized by hydrothermal

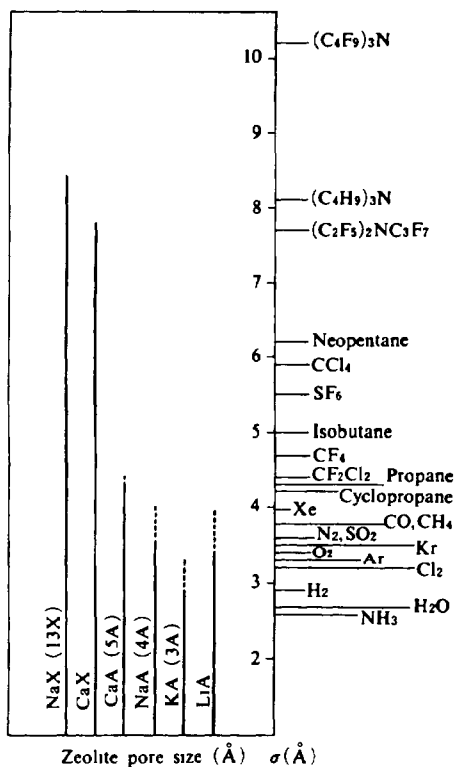


Fig 29 Relations between effective pore size of Zeolites A and X and Lennard-Jones kinetic diameter, σ Reproduced with permission from Breck, D W, *Zeolite Molecular Sieve-structure, Chemistry and Use*, J Wiley and Sons, New York (1974)
(Reproduced with permission by Ruthven, M, *Principles of Adsorption & Ads Processes*, 11, Wiley (1985))

reaction in autoclaves. Much of the literature is devoted to clarifying crystal structure and synthesis (Barrer 1968, Flanigan and Sand 1971, Breck 1973, Meier and Uytterhoeven 1973, Katzer 1977, Barrer 1982, Olson and Bisio 1984, Ramoa *et al.* 1984, Drzaj *et al.* 1985, Murakami *et al.* 1986).

A limited number of synthetic zeolites are currently used as commercial adsorbents i.e., Type A and Type X.

In the crystal structures of Type A, shown in Fig. 2.8, exchangeable cations are located near the window between neighboring cells. The 4A type zeolite contains Na ion at this site, which permits the entry of molecules smaller than 4 Å. This effect is called the molecular sieving effect, and is schematically illustrated in Fig. 2.9. If the K ion, which is larger than the Na ion, is introduced to this position, effective window (aperture) size becomes 3 Å and only H₂O and NH₃ can penetrate through the window. Then this type is called 3A zeolite. On the other hand, if a Ca ion, which has two valences, is introduced, the effective aperture becomes larger. The zeolite of this type is called 5A zeolite.

Type X zeolite has much larger windows made up of 12-membered rings (Fig. 2.8), and is usually called 13X zeolite.

2.4. Other Adsorbents

2.4.1. Bone char

In sugar refineries, bone char has been commonly used as an adsorbent for decolorizing and refining sugar since the 19th century. Bone char is believed to have basically the same adsorption characteristics as activated carbons. But in addition to the ion exchange abilities derived from the main constituent, calcium hydroxy apatite functional groups from animal matter may render superior adsorption ability for removing color, odor and taste.

Dry bones free of flesh together with fat and oil of animals crushed, screened and freed from miscellaneous foreign elements are put in an airtight iron retort and heated at 600–900°C for about 8 h. The volatile gases evolved by this process contain ammonium, tar and non-condensable gas. The remaining char is cooled in inert atmosphere then taken out for further crushing and screening. The yield of bone char is about 60%.

Calcium hydroxyapatite is an interesting adsorbent which collects cations of heavy metals such as lead and cadmium. Suzuki (1985) suggested that hydroxyapatite is capable of ion exchange not only with

cations but also with anions such as fluoride ion. The same effects may be expected in part of the hydroxyapatite composing bone chars.

2.4.2. Metal oxides

Metal oxides appear to be simple inorganic materials having well-defined chemical structures. However, as far as adsorption on oxide surface is concerned, surface properties, which is largely dependent on how the oxide is prepared, reveal very complicated functions. This is well known in the preparation of metal oxide catalysts.

Metal oxides developed for industrial adsorbents include magnesium oxide, titanium oxide, zirconium oxide and cerium oxide. Magnesium oxide (magnesia) is used for removing polar molecules such as color, acids, and sulfide compounds from gasoline and solvent for dry-cleaning purposes. Also it is effective in removing silica from water, and magnesium trisilicate is used as a medicinal adsorbent. Ikari (1978) showed that magnesium hydroxide is a good adsorbent for phosphate removal in the advanced treatment of wastewaters.

Oxides of four valence metals, titanium, zirconium and cerium, sometimes show selective adsorption characteristics in removing anions from water phases. Hydrated titanium oxide is known to be a selective adsorbent for recovering uranium in seawater, which is present in the form of carbonyl complex in concentrations as low as 3.2 ppb.

Zirconium oxide in a monohydrated form is found to adsorb phosphate ion from wastewaters (Suzuki and Fujii, 1987). Cerium oxide is effective in adsorption of fluoride ion in industrial wastewaters.

2.5. Measurement of Pore-related Properties

2.5.1. Porosity

Porosity of adsorbents is determined by several alternative methods. When true solid density, ρ_s (g/cm^3), is known, total porosity, ε_t (-), or specific pore volume, v_p (cm^3/g), is calculated from ρ_s and particle density, ρ_p (g/cm^3), as

$$\varepsilon_t = 1 - \rho_p / \rho_s \quad (2-1)$$

$$v_p = 1 / \rho_p - 1 / \rho_s \quad (2-2)$$

Particle density, ρ_p , can be determined using a mercury pycnometer by assuming that mercury does not enter any pore of the porous sample.

When the sample is first evacuated and the evacuated sample is exposed to mercury at atmospheric pressure, P_a , then mercury can penetrate pores with radius larger than $7.5 \mu\text{m}$. Most porous adsorbents have intraparticle pores smaller than this and one atmosphere is enough to fill the void between particles with mercury. Thus, by comparing the weight of the empty glass pycnometer filled with mercury, W_m , and that of the pycnometer with the sample of weight, W_s , filled with mercury after evacuation, W_p , the particle density, ρ_p , is calculated as

$$\begin{aligned}\rho_p &= \text{particle weight/particle volume} \\ &= W_s / [(W_m - W_p + W_s) / \rho_{\text{Hg}}] \end{aligned} \quad (2-3)$$

where ρ_{Hg} is the density of mercury at the measurement temperature.

True solid densities, ρ_s , are often found in the literature. But some porous bodies are not easy to find in the tables or to make an estimation because they have confined pores which are not accessible from outside. In such cases, the "true" density must be determined by direct measurement.

One practical method is to use the same method as described for measuring particle density using mercury, except that mercury is replaced by a liquid which penetrates pores. Water and organic solvents are often used. The same equation can be used by replacing ρ_{Hg} with the density of the liquid employed.

Another method is to employ a helium densitometer (Fig. 2.10). This method is based on the principle of $PV = \text{constant}$ at constant temperature. A known weight, W_s , of porous sample is put into then evacuated from a closed vessel of volume V_1 . Next nonadsorbable gases such as helium are introduced to pressure P_1 , the valve closed and the volume of the vessel changed by moving the piston in the connected cylinder. From the displacement of the piston, the change in volume, ΔV , and change in pressure, ΔP , are obtained. Then the volume of the sample, V_s , in which helium cannot penetrate is obtained as

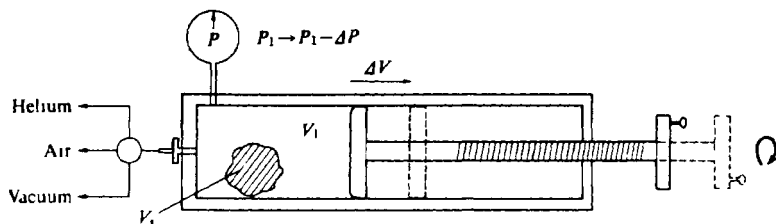


Fig. 2.10 Displacement type pycnometer (helium densitometer)

$$V_s = V_1 - (P_1/\Delta P - 1)\Delta V$$

and true density, ρ_s , is defined as

$$\rho_s = W_s/V_s$$

Obviously, adsorbable or condensable gases cannot be employed in this method.

2.5.2. Pore size distribution

The most common methods to determine pore size distributions are the A. mercury penetration method, B. nitrogen adsorption method, and C. molecular probe method.

A. mercury penetration method

By applying pressure, P , to mercury surrounding a porous body, mercury penetrates into the pores whose radii are larger than r given by the following equation

$$r = - \frac{2\sigma \cos \theta}{P}$$

where σ represents the surface tension of mercury, 470 dyne/cm (298 K), θ is the contact angle between mercury and the sample

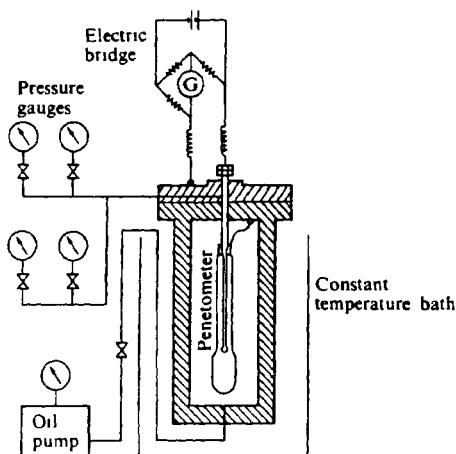


Fig 2 11 Mercury penetration apparatus.

surface, which is usually taken as 140°C. Then

$$\rho_p = 720 \text{ dyne/cm} = 7.34 \times 10^{-4} \text{ kg/cm}^2$$

An example of a mercury porosimeter is illustrated in Fig. 2.11. A small amount of a sample is put in to the penetrometer, then evacuated, after which mercury is introduced from the separate vessel. Then the penetrometer is set in the pressure vessel shown in the figure and high pressure is applied by oil pressure pump. Mercury penetration is detected from displacement of meniscus at the burette of the penetrometer. The pore size distribution is calculated from the pressure-penetration volume relation.

An ordinary mercury porosimeter generates pressure as high as 3000 kg/cm², which makes it possible to determine pore size distributions down to $r=25 \text{ \AA}$. Usually, this method is suitable for determining larger pores such as macropores of activated carbons.

B. nitrogen adsorption method

When nitrogen adsorption is carried out at liquid nitrogen temperature ($-195.8^\circ\text{C}=77.34 \text{ K}$), nitrogen adsorption on the surface and capillary condensation of nitrogen in the pores take place (Fig. 2.12). The thickness of adsorbed layer on the surface, t , and the size of the pore where condensation happens, r_k , depend on the partial pressure of nitrogen. Thus adsorption isotherm can be converted to the pore size distribution by assuming proper relations between both t and r_k and the partial pressure, p .

There are several equations proposed for the relation between t and

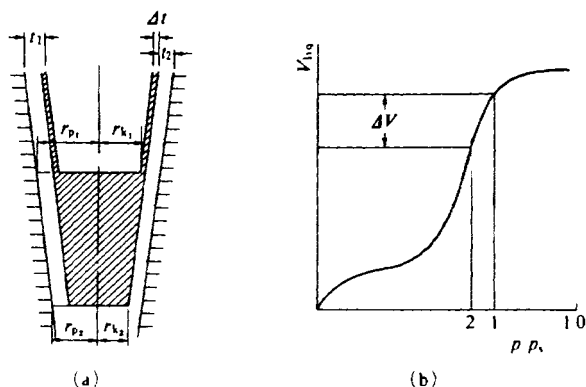


Fig 2.12 Concept of pore size measurement by the adsorption method

the pressure, but Halsey's relation is given here as one of the most fundamental relations.

$$t (\text{\AA}) = 4.3[5/\ln(p_s/p)]^{1/3}$$

where p_s is the saturation pressure, which is the atmospheric pressure in this case.

For the capillary condensation radius, r_k , Kelvin radius is derived as

$$r_k (\text{\AA}) = -9.53/\ln(p/p_s)$$

by assuming the contact angle of nitrogen θ is given as $\cos \theta = 1$ and the surface tension $\sigma = 8.85$ dyne/cm.

Adsorption isotherm of nitrogen at liquid nitrogen temperature is determined by the gravimetric method (Fig. 2.13), or the constant volume method (Fig. 2.14). From the adsorption isotherm of nitrogen shown in Fig. 2.15, the pore size distribution is calculated by Dollimore method (1964) and shown in Fig. 2.16. Cumulative pore size distribution is sometimes preferred when change of pore size distribution is involved, for example during thermal regeneration or activation of activated carbons.

For microporous adsorbents such as carbon molecular sieves, Dollimore's method is not advisable since the Kelvin equation is no

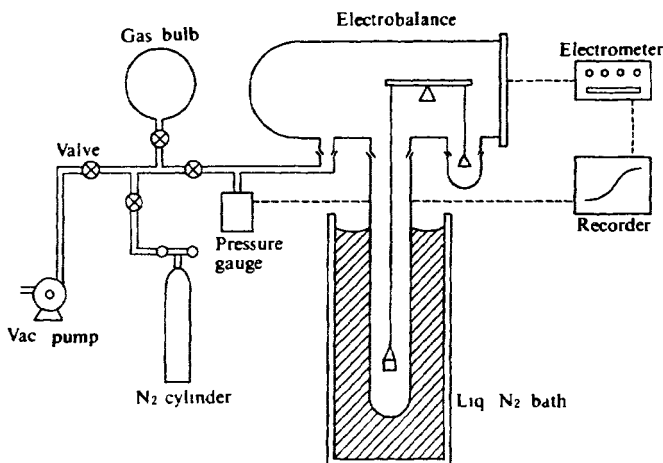


Fig 2.13 Gravimetric measurement of nitrogen adsorption isotherms at liquid nitrogen temperature

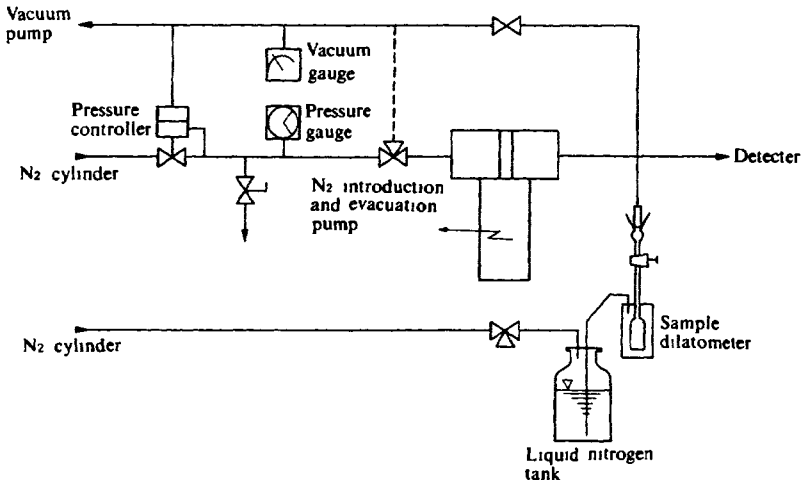


Fig 2 14 Automatic adsorption system for nitrogen (constant volume type), Carlo Erba

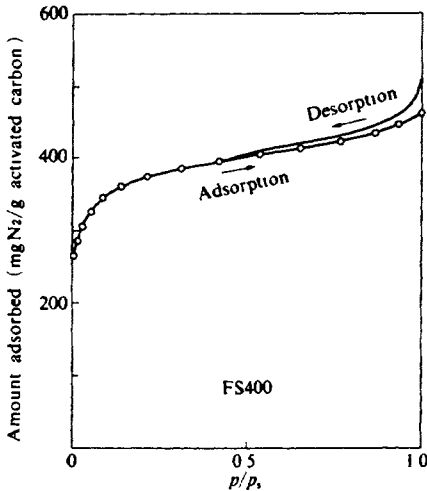


Fig 2 15 Adsorption isotherm of nitrogen at liquid nitrogen temperature (-195.8°C)

longer valid when pore size is close to molecular size of adsorbate (Dollimore and Heal, 1964)

For the purpose of describing pore size distribution in this range, Horvath and Kawazoe (1983) proposed a method based on potential func-

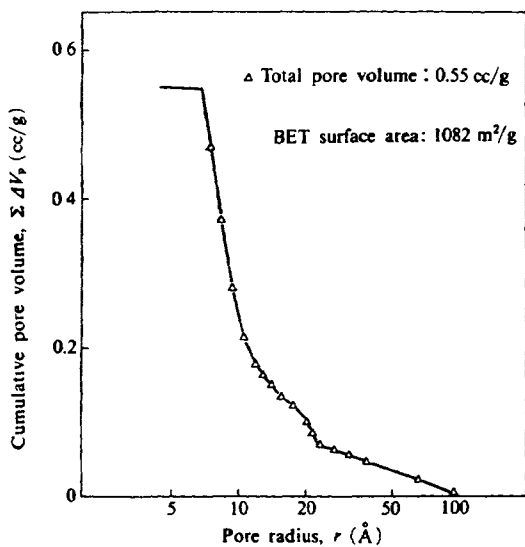


Fig 2.16 a Cumulative pore volume (below 100 Å) FS 400.

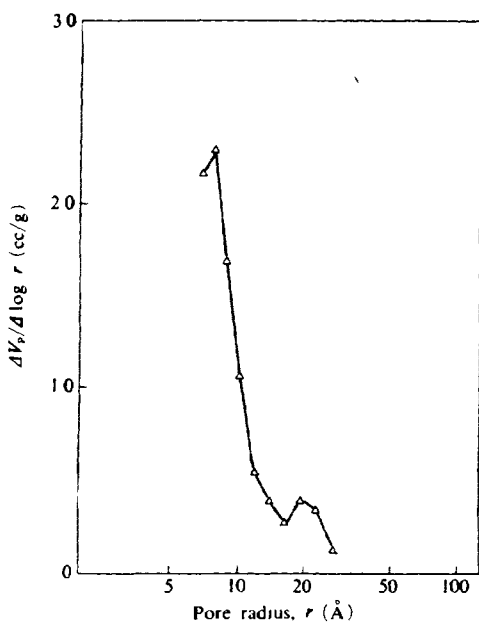


Fig 2.16 b Differential, pore size distribution curve, FS 400.

tion in the pore.

For obtaining an average potential in the slit-like pore between the two layers of carbon, adsorption potential, an expression of adsorbate-adsorbent and adsorbate-adsorbate interactions resulted in the following equation.

$$RT \ln(p/p_s) = K \frac{N_a A_a + N_A A_A}{\sigma^4 (l-d)} \left[\frac{\sigma^4}{3(l-\frac{d}{2})^3} - \frac{\sigma^{10}}{9(l-\frac{d}{2})^9} \right. \\ \left. - \frac{\sigma^4}{3(\frac{d}{2})^3} + \frac{\sigma^{10}}{9(\frac{d}{2})^9} \right]$$

where l represents the distance between the nuclei of the two layers, N_A and N_a , respectively, are the number of molecules per unit area of adsorbate and the number of atoms composing the surface layer per unit area, A_a and A_A are the constants in the Lennard-Jones potential function defined as

$$A_a = 6mc^2 \alpha_a \alpha_A / (\alpha_a / \chi_a + \alpha_A / \chi_A)$$

$$A_A = 3mc^2 \alpha_A \chi_A / 2$$

where m is the mass of electron, c is the velocity of light, α and χ represent the polarizability and the magnetic susceptibility of adsorbent atom (suffix, a) and an adsorbate molecule (suffix, A) and K is the Avogadro number. d is defined as

$$d = d_a + d_A$$

where d_a is the diameter of an adsorbent atom and d_A is that of an adsorbate molecule.

σ is the distance between an adsorbate molecule and adsorbent atom where interaction energy becomes zero and Everett and Powl (1976) gave the equation as follows.

$$\sigma = 0.858d/2$$

By taking proper values for the nitrogen-carbon system as shown in TABLE 2.1, the final form becomes

$$\ln\left(\frac{p}{p_s}\right) = \frac{623.8}{l-6.4} \left[\frac{1.895}{(l-3.2)^3} - \frac{270.87}{(l-3.2)^9} - 0.05014 \right]$$

TABLE 2.1 Physical Properties for Pore Size Distribution Calculation by Horvath-Kawazoe Method(1983)

	Carbon	Nitrogen
Diameter [Å]	3.4	3.0
Liquid density [g/cm ³]	—	0.808
α , Polarizability [cm ³]	1.02×10^{-24}	1.46×10^{-24}
χ , Susceptibility [cm ³]	13.5×10^{-29}	2×10^{-29}
N [mol/cm ²]	3.845×10^{15}	6.7×10^{14}

(Reproduced with permission by Horvath, G and Kawazoe, K, *J Chem Eng Japan* 16, 472 (1983))

TABLE 2.2 Values of Corresponding (p/p_0), ($l-d_a$) Pairs According to Horvath and Kawazoe and Dollimore

Relative pressure p/p_s [-]	Effective pore size [nm]	
	Horvath-Kawazoe model ($l-d_a$)	Dollimore model
1.46×10^{-7}	0.4	—
6.47×10^{-7}	0.43	—
2.39×10^{-6}	0.46	—
1.05×10^{-5}	0.5	—
1.54×10^{-4}	0.6	—
8.86×10^{-4}	0.7	—
2.95×10^{-3}	0.8	—
2.22×10^{-2}	1.1	1.16
4.61×10^{-2}	1.3	1.32
7.59×10^{-2}	1.5	1.46
3.15×10^{-1}	3.0	2.23
7.24×10^{-1}	10.0	5.09

(Reproduced with permission by Horvath, G and Kawazoe, K, *J Chem Eng Japan*, 16, 473 (1983))

where l is in Å

From the equation, the relation between p and l is uniquely defined and thus the relation between the effective pore size ($l-d_a$) and p is also obtained as shown in TABLE 2.2. The relation is also plotted in Fig. 2.17. In the table and figure, the pore size calculated by Dollimore's method is included. Both methods approach pore size of around 13.4 Å and $p/p_s=0.05$, and Horvath and Kawazoe suggested that their method should be applied to measurements below $p/p_s=0.5$ and that Dollimore's method should be used above this relative pressure.

Pore size distributions of carbon molecular sieve determined by this method are shown in Fig. 2.18, where W_∞ is the maximum pore volume determined from the amount adsorbed at $p/p_s=0.9$.

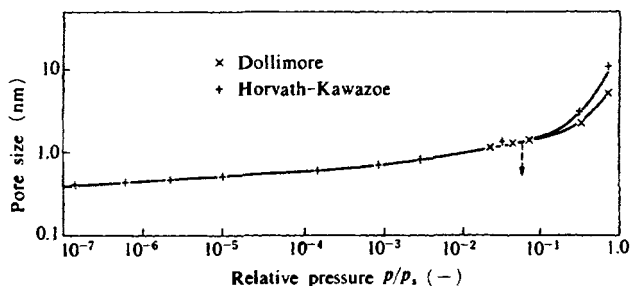


Fig. 2.17. Pore size vs. pressure.
(Reproduced with permission by Horvath, G. and Kawazoe, K., *J. Chem. Eng. Japan*, 16, 473 (1983)).

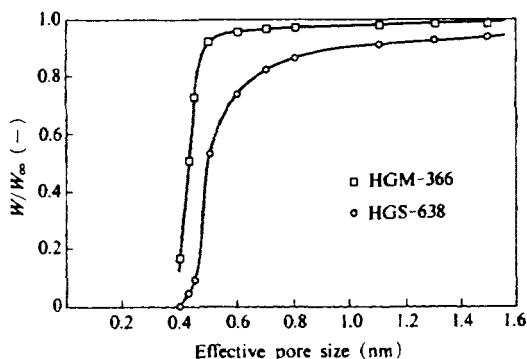


Fig. 2.18. Effective pore size distributions of carbon molecular sieves calculated by Horvath-Kawazoe method.
(Reproduced with permission by Horvath, G. and Kawazoe, K., *J. Chem. Eng. Japan*, 16, 474 (1983)).

C. molecular probe method

As is understood from Fig. 2.9, for small pores which have molecular sieving abilities, it is not possible to determine pore size distribution by nitrogen adsorption method. In these cases, the most direct determination of the effective pore size is the molecular probe method.

For zeolites, size of entering molecules is determined by assuming that the pores are cylindrical. In the case of activated carbons, especially in the case of CMS, thickness of the molecules decides the adsorbability of the molecules to the micropore since the micropores are considered to be two-dimensional.

For several CMS's, this method is applied and comparison of pore

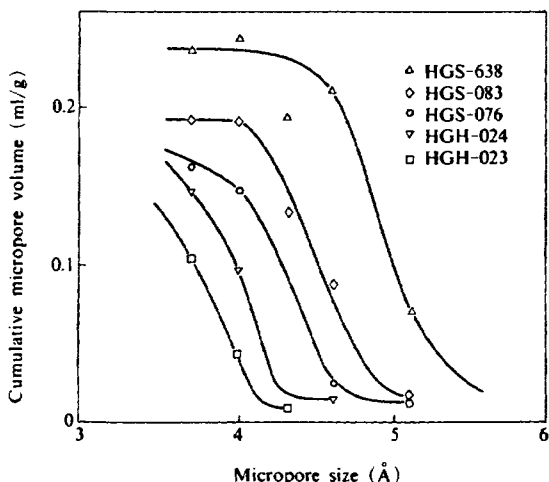


Fig. 2.19. Micropore size distributions of carbon molecular sieve adsorbents determined by the molecular probe method.

sizes is tried (Fig. 2.19). Adsorption from saturated pressures of five organic solvents, carbon disulfide (thickness of 3.7 Å), methylene dichloride (4.0 Å), ethyl iodide (4.3 Å), chloroform (4.6 Å) and cyclohexane (5.1 Å), were tried and from the amount adsorbed of each component, the pore volume for the micropores larger than this size can be determined.

2.5.3. Surface area

Internal surface area of microporous adsorbents is often used as one of the measures to describe the degree of development of pores. The concept of B.E.T. adsorption isotherm (Eq. 3-12), where the amount adsorbed by monomolecular coverage, q_m , is defined, gives the specific surface area by assuming the molecular sectional area of nitrogen to be $16.2 \text{ Å}^2/\text{molecule}$, which corresponds to $9.76 \times 10^4 \text{ m}^2/\text{mol}$ or $4.35 \text{ m}^2/\text{Ncc}$.

To determine q_m from the experimentally obtained data of isotherm, so-called BET plot of $p_r/[q(1-p_r)]$ versus p_r is made as shown in Fig. 3.7. Then from the slope and the intercept of the straight line obtained in the range of $0.35 < p_r < 0.5$, q_m is readily obtained.

In the case of adsorbents with very fine micropores, such as those with molecular sieving effect, it is not easy to make a rigorous definition of the surface area. If BET plot is applied mechanically, "surface area" can

be calculated but the physical meaning and importance may be reduced.

For microporous adsorbents, micropore volumes and size distributions determined by the molecular probe method or the nitrogen adsorption method, if possible, may be more informative than the surface area.

REFERENCES

- Araki, T, *Kassentanso* (Active Carbon), Maruzen, Tokyo (1932) (in Japanese)
- Bailleul, G, K Bratzler, W Herbert and W Vollmer, *Aktive Kohle und Ihre Industrielle Verwendung*, 4th Ed, Ferdinand Enke, Stuttgart (1962)
- Barrer, R M, *Hydrothermal Chemistry of Zeolites*, Academic Press, New York (1982)
- Barrer, R M (ed), *Molecular Sieves, Proc of the 1st Int Zeolite Conference*, Soc Chem Ind (1968)
- Boehm, H P, *Advances in Catalysis*, 16, 179 (1964)
- Boehm, H P, E Diehl, W Heck and R Sappok, *Angew Chem*, Int Ed, 3, 669 (1964)
- Breck, D W, *Zeolite Molecular Sieve-Structure, Chemistry and Use*, John Wiley and Sons, New York (1974)
- Chihara, K, M Suzuki and K Kawazoe, *AIChE Journal*, 24, 279 (1982)
- Dollimore, D and G R Heal, *J Appl Chem*, 14, 109 (1964)
- Drzaj, B, S Hocevar and S Pejovnik (eds), *Zeolites-Synthesis Structure, Technology and Application*, Elsevier, Amsterdam (1985)
- Everett, D H and J C Powl, *J Chem Soc, Faraday Trans*, 1 72, 619 (1976)
- Flanigan, E M and L B Sand (eds), *Molecular Sieve Zeolites-I & II*, Proc of the 2nd Int Zeolite Conference, *Adv in Chemistry Series 101 & 102*, ACS (1971)
- Hassler, J W, *Purification with Activated Carbon*, Chem Pub, New York (1974)
- Horvath, Geza and K Kawazoe, *J Chem Eng Japan*, 16, 470 (1983)
- Hara, N and H Takahashi (eds), *Zeoratto (Zeolites)*, Kodansha, Tokyo (1975) (in Japanese)
- Ikari, Y, *Kagaku to Kogyo*, 31, 4 (1978) (in Japanese)
- Katzer, J R (ed), *Molecular Sieves II*, Proc of the 4th Int Zeolite Conference, ACS Symposium Series, 40, ACS (1977)
- Kawazoe, K, T Kawai, Y Eguchi and K Itoga, *J Chem Eng Japan*, 7, 158 (1974)
- Mantell, C L, *Adsorption*, 2nd Ed, McGraw-Hill, New York (1951)
- Mattson, J S and Mark, Jr, H B, *Activated Carbon*, Marcel Dekker, New York (1971)
- Meier, W M and J B Uytterhoeven(eds), *Molecular Sieves*, Proc of the 3rd Int Zeolite Conference, *Adv in Chemistry Series 121*, ACS (1973)
- Minato, H, *Zeoratto to sono Riyou (Zeolite and its Applications)*, Chapter 2, Gihodo, Tokyo (1967) (in Japanese)
- Murakami, Y, A Iijima and J W Ward (eds), *New Developments in Zeolite Science and Technology*, Proc of the 7th Int Zeolite Conference, Kodansha-Elsevier, Tokyo/Amsterdam (1986)
- Olson, D and A Bisio (eds), *Proceedings of the Sixth International ZEOLITE Conference*, Butterworth, London (1984)
- Puri, B R (ed), *Proceedings of the 5th Conference on Carbon*, vol 1, 165 (1962)
- Puri, B R and R C Bansal, *Carbon*, 1, 451, 457 (1964)
- Puri, B R, *Carbon*, 4, 391 (1966)
- Ramoa, F A E Rodrigues, L D Rollmann and C Naccache(eds), *Zeolites Science and Technology*, NATO ASI Series E-80 Nijhoff Publ The Hague (1984)
- Sakoda, A and M Suzuki, *J Chem Eng Japan*, 15, 279 (1982)
- Sakoda, A, K Kawazoe and M Suzuki, *Water Research* 21, 717 (1987)
- Smisek, M and S Cerny *Active Carbon Manufacture Properties and Applications* Elsevier, London (1970)

- Suzuki, M and K -S Ha, *J. Chem Eng. Japan*, **17**, 139 (1984).
Suzuki, M and J.-E. Sohn, *159th ACS Annual Meeting*, Denver(1987).
Suzuki, M. and T Fujii, *Proc 4th APCChE '87*, 675, Singapore (1987).
Suzuki, M and K Chihara, *Water Research*, **22**, 627 (1988).
Suzuki, T , K. Ishigaki and N. Ayuzawa, *Chem. Eng. Commun.*, **34**,143 (1985).
Tanso-zairyo-gakkai, *Kasseitan, Kiso to Ouyou (Activated Carbon, Fundamentals and Applications)*, Kodansha, Tokyo (1975) (in Japanese)
Zeoraito to sono Riyou Henshuu Iinkai, *Zeoraito to sono Riyou (Zeolite and its Applications)*, Gihodo, Tokyo (1967) (in Japanese).

Adsorption Equilibrium

In practical operations, maximum capacity of adsorbent cannot be fully utilized because of mass transfer effects involved in actual fluid-solid contacting processes. In order to estimate practical or dynamic adsorption capacity, however, it is essential, first of all, to have information on adsorption equilibrium. Then kinetic analyses are conducted based on rate processes depending on types of contacting processes. The most typical of the rate steps in solid adsorbents is the intraparticle diffusion which is treated in the next chapter.

Since adsorption equilibrium is the most fundamental property, a number of studies have been conducted to determine 1) the amount of species adsorbed under a given set of conditions (concentration and temperature) or 2) how selective adsorption takes place when two or more adsorbable components coexist. There are many empirical and theoretical approaches. Only several simple relations, however, can be applied in later treatments on kinetic description of adsorption. These relations are sometimes insufficient for predicting adsorption isotherms under a new set of operating conditions. Thus more sophisticated trials on sound thermodynamics or on substantial models have been proposed by many authors.

A basic review is given here. For more detailed discussions refer to Ross and Olivier (1964) and Ruthven (1984). A recent publication by Myers (1988) also gives adsorption equilibrium data available in the literature.

3.1. Equilibrium Relations

When an adsorbent is in contact with the surrounding fluid of a certain composition, adsorption takes place and after a sufficiently long time, the adsorbent and the surrounding fluid reach equilibrium. In this state the amount of the component adsorbed on the surface mainly of the micropore of the adsorbent is determined as shown in Fig. 3.1. The relation between amount adsorbed, q , and concentration in the fluid phase, C , at

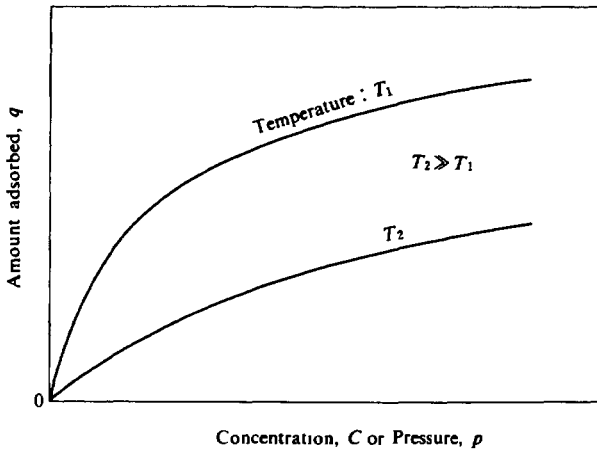


Fig 3 1 Adsorption isotherms

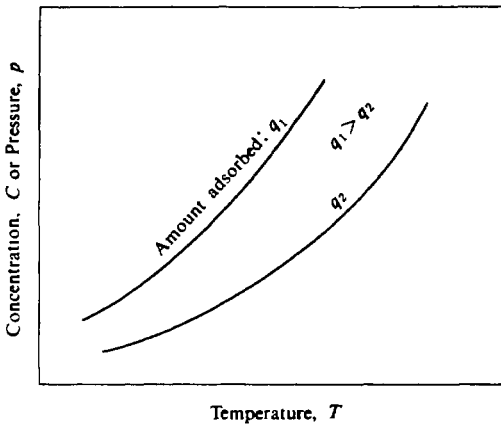


Fig 3 2 Adsorption isosteres.

temperature, T , is called the adsorption isotherm at T .

$$q = q(C) \text{ at } T \tag{3-1}$$

The relation between concentration and temperature yielding a given amount adsorbed, q , is called the adsorption isostere (Fig. 3 2),

$$C = C(T) \text{ for } q \tag{3-2}$$

Adsorption isotherms are described in many mathematical forms, some of which are based on a simplified physical picture of adsorption and desorption, while others are purely empirical and intended to correlate the experimental data in simple equations with two or at most three empirical parameters: the more the number of empirical parameters, the better the fit between experimental data and the empirical equation. But empirical equations unrelated to physical factors do not have practical significance since they do not allow extrapolation beyond the range of variables for which the parameters have been determined.

3.2. Adsorption Isotherms

3.2.1. Surface adsorption

The simplest model of adsorption on a surface is that in which localized adsorption takes place on an energetically uniform surface without any interaction between adsorbed molecules. When surface coverage or fractional filling of the micropore is $\theta (=q/q_0)$ and the partial pressure in the gas phase, p , which is to be replaced by $C(=p/RT)$ when the concentration in the fluid phase is used, the adsorption rate is expressed as $k_a p(1 - \theta)$ assuming first order kinetics with desorption rate given as $k_d \theta$. Then equilibration of adsorption rate and desorption rate gives the equilibrium relation as

$$\theta = Kp/(1 + Kp) \quad (3-3)$$

or

$$p = \frac{1}{K} \left(\frac{\theta}{1 - \theta} \right) \quad (3-4)$$

The above relation is given by Langmuir (1918) and $K = k_a/k_d$ is called the adsorption equilibrium constant.

The above equation is called the Langmuir isotherm. When the amount adsorbed, q , is far smaller compared with the adsorption capacity of the adsorbent, q_0 , Eq. (3-3) is reduced to the Henry type equation;

$$\theta = Kp \quad (3-5)$$

Further, when the concentration is high enough, $p \gg 1/K$, then adsorption sites are saturated and

$$\theta = 1 \quad (3-6)$$

The above equation is modified when interaction between adsorbing molecules are taken into account. Fowler and Guggenheim (1939) gave

$$p = \frac{1}{K} \left(\frac{\theta}{1-\theta} \right) \exp(2u\theta/kT) \quad (3-7)$$

where $2u$ represents pair interaction energy (positive for repulsion and negative for attraction), and k is the Boltzmann constant.

When adsorbed molecules are free to move on the adsorbent surface (mobile adsorption), the Langmuir equation is modified to

$$p = \frac{1}{K} \left(\frac{\theta}{1-\theta} \right) \exp\left(\frac{\theta}{1-\theta}\right)$$

When mobile adsorption with interaction is considered, the following is derived.

$$p = \frac{1}{K} \left(\frac{\theta}{1-\theta} \right) \exp\left[\left(\frac{\theta}{1-\theta}\right) + 2u\theta/kT\right] \quad (3-8)$$

Fig. 3.3 shows deviation of the isotherm relation from the Langmuir

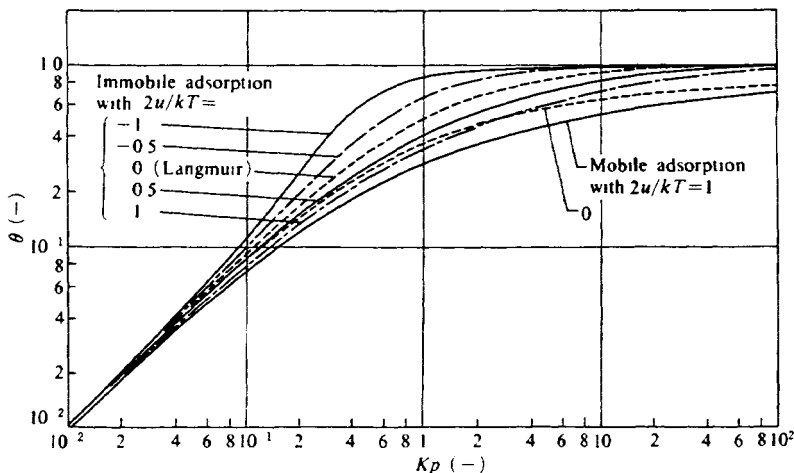


Fig 3.3 Effect of mobile adsorption and interaction of adsorbed molecules on shape of isotherm

equation due to mobile adsorption and interaction between molecules.

Suwanayuen and Danner (1980) introduced the nonideality of adsorbed phase by considering the adsorbed phase as a mixture of adsorbate and vacancies. The activity of vacancies is used to describe the nonideality and the Wilson equation is employed to express activity coefficient involving two parameters for a single component system.

$$P = \frac{1}{K} \frac{\theta}{1-\theta} \left[A_{13} \frac{1 - (1 - A_{31})\theta}{A_{13} + (1 - A_{13})\theta} \right] \exp \left[- \frac{A_{31}(1 - A_{31})\theta}{1 - (1 - A_{31})\theta} - \frac{(1 - A_{13})\theta}{A_{13} + (1 - A_{13})\theta} \right] \quad (3-9)$$

where A_{13} and A_{31} are Wilson's parameters for surface interaction between adsorbate and vacancy.

Another typical example of the isotherms frequently employed is the Freundlich type equation (Freundlich, 1926).

$$q = k_F C^{(1/n_F)} \quad (3-10)$$

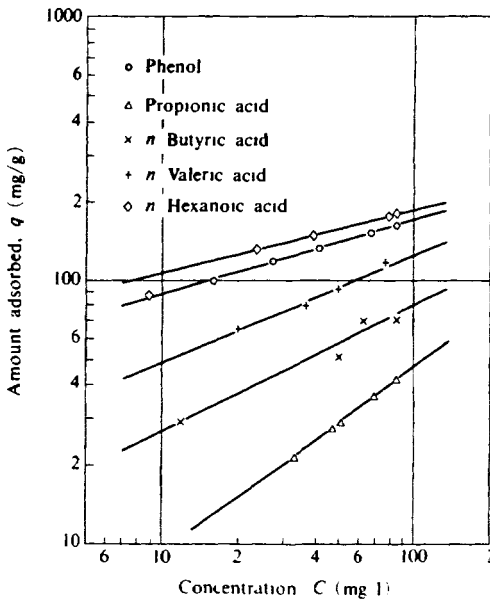


Fig 3.4 Examples of Freundlich plot. Aqueous phase adsorption of single component organic acids on activated carbon, FS-400 at 298 K

This equation is often considered to be an empirical equation. It is possible to interpret this equation theoretically in terms of adsorption on an energetically heterogeneous surface as described below. This form can also be related to the Dubinin-Astakov equation, which is derived for adsorption of the micropore filling type (Dubinin and Astakov, 1970).

Examples of correlation of adsorption data taken in aqueous phase are shown in Fig. 3.4. This equation fits well with the experimental data for a limited range of concentrations.

The Freundlich equation does not satisfy the conditions given by Eqs. (3-5) and (3-6) because it gives no limit of adsorption capacity, making the amount adsorbed go to infinity when concentration increases. It is only applicable below the saturation concentration (solubility or saturation vapor pressure) where condensation or crystallization occurs and adsorption phenomena are no more significant.

At extremely low concentrations, the Henry type equation (Eq. (3-3)) usually becomes valid. Radke and Prausnitz (1972) formulated the following equation, which combines the Freundlich equation with the Henry type equation.

$$q = 1 / \left[\frac{1}{K_H p} + \frac{1}{k_F p^{1/n_F}} \right] \quad (3-11)$$

This equation contains three empirical constants and is useful in

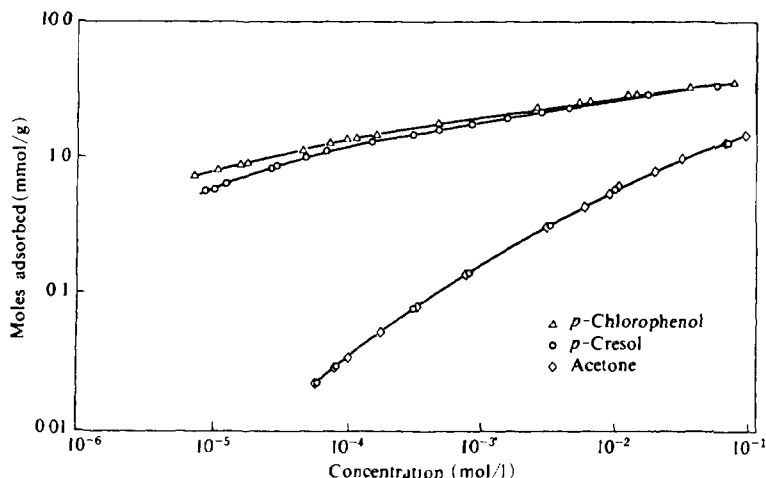


Fig. 3.5. Adsorption from aqueous solution at 25°C. (Reproduced with permission by Radke, C. J. and Prausnitz, J. M., *Ind. Eng. Chem. Fundamentals*, **11**, 447 (1972))

correlating isotherm data obtained in a wide range of concentrations. An example is shown in Fig. 3.5.

Another useful expression is the Toth equation (Toth, 1971) which contains also three parameters.

$$\theta = q/q_0 = [1/(Kp)^t + 1]^{-1/t} \quad (3-12)$$

The equation reduces to the Henry type at low concentrations (pressures)

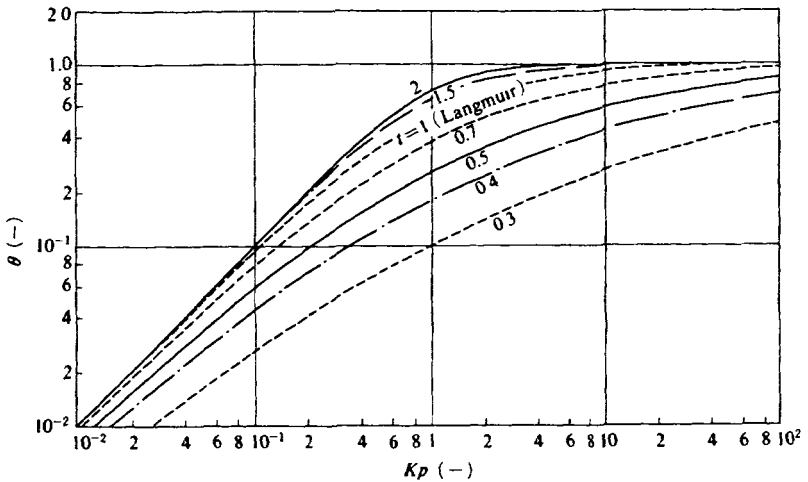


Fig. 3.6. Toth equations for different values of t .

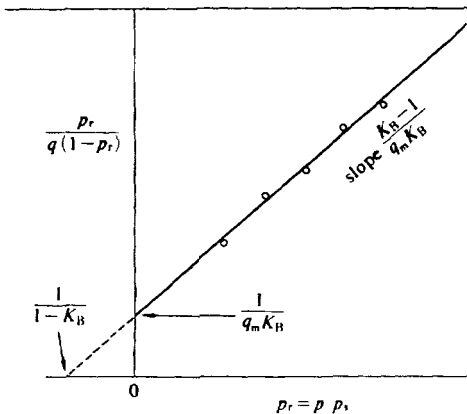


Fig 37 BET plot of gas phase adsorption isotherm.

and approaches saturation limit at high pressures. When the parameter, t , is unity, the above equation is identical to the Langmuir equation. Fig. 3.6 shows the effect of parameter, t , on the shape of the isotherm.

When adsorption takes place in multilayers, adsorption on the adsorbent surface and above the adsorbed molecules is considered to be based on different attractive forces. Monolayer adsorption is formed by the same concept as the Langmuir type adsorption while adsorption above monolayers is equivalent to condensation of the adsorbate molecules, giving rise to the BET (Brunauer, Emmett and Teller, 1938) equation

$$q/q_m = K_B p_r / [(1 - p_r)(1 - p_r + K_B p_r)] \quad (3-13)$$

where p_r is the relative pressure ($= p/p_s$) and q_m represents the amount adsorbed by monomolecular coverage on the surface. From nitrogen adsorption at liquid nitrogen temperature, the surface area of the adsorbent is determined by converting q_m to the surface area. In most cases, q_m is obtained from the BET plot of the adsorption data as shown in Fig. 3.7. It gives a straight line in the range $0.05 < p_r < 0.35$ and q_m is readily determined. Then by multiplying nitrogen surface area of $3480 \text{ m}^2/\text{g}$ with q_m , specific surface area of the adsorbent based on nitrogen adsorption is calculated.

3.2.2. Micropore adsorption

In micropores of size comparable to the size of adsorbate molecule, adsorption takes place by attractive force from the wall surrounding the micropores, and the adsorbate molecules start to fill the micropore volumetrically. This phenomenon is similar to capillary condensation that occurs in large pores at high partial pressure, although the adsorbed phase in micropores is different because of the effect of the force field of the pore wall.

In this type of adsorption, the adsorption equilibrium relation for a given adsorbate-adsorbent combination can be expressed independent of temperature by using the adsorption potential.

$$W = q/\rho = W(A) \quad (3-14)$$

where W is the volume of micropore filled by the adsorbate and ρ is the density of the adsorbed phase. Adsorption potential, A , is defined as the difference in free energy between the adsorbed phase and the saturated liquid.

$$A = -RT \ln(p/p_s) \quad (3-15)$$

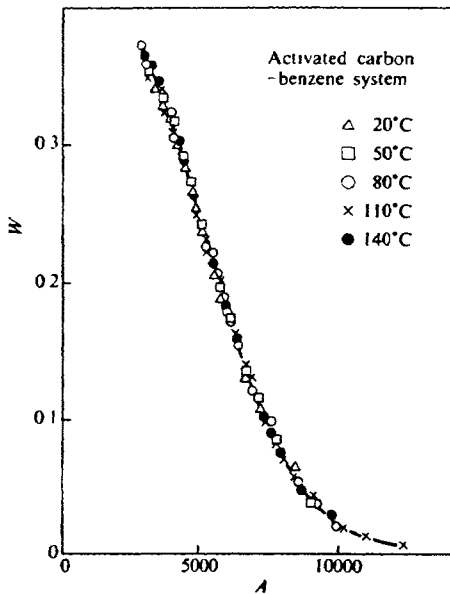


Fig. 3.8. Adsorption characteristic curve.

(Reproduced with permission by Kawai, T., *Ph.D. Theses (Univ of Tokyo, 1976)*, p 34 (1976)).

$W(A)$ is the adsorption characteristic curve originally introduced by Polanyi (1914) and Berenyi (1920). Adsorption of benzene on activated carbon is plotted in Fig. 3.8 in the form of the characteristic curve.

Dubinin (1960) assumed a distribution of the Gaussian type for the characteristic curve and derived the following, which is called Dubinin-Radushkevich equation.

$$W = W_0 \exp[-kA^2] \quad (3-16)$$

Adsorption equilibrium relation of benzene on two types of activated carbon are plotted by the Langmuir plot and the Dubinin plot in Fig. 3.9(a) and (b). Apparently, the Dubinin equation gives a better regression to the data of Hasz (1969).

Later this equation was generalized by Dubinin and Astakhov (1970) to the following form.

$$W = W_0 \exp[-(A/E)^n] \quad (3-17)$$

In this expression E is the characteristic energy of adsorption and obtained from adsorption potential A at $W/W_0 = e^{-1}$. The parameter n in the

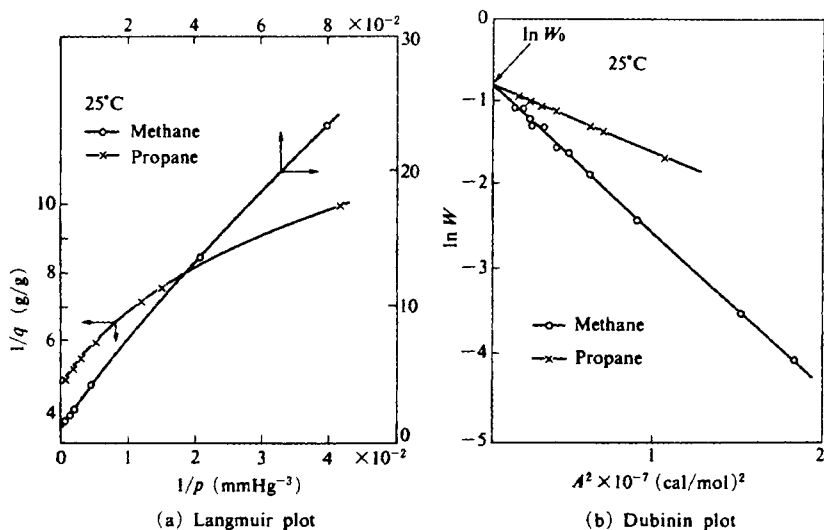


Fig. 3.9. Correlation of equilibrium data on activated carbon (Columbia NXC), data by Hasz, source: Kawai, 1976. (Reproduced with permission by Kawai, T., Seiken Koushukai Text No. 3, 7, Seisan Gijutu Shoureikai (1977)).

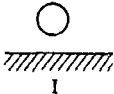
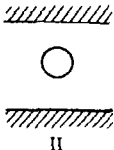
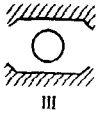
Dubinin-Astakhov equation was originally considered to have integer value, and $n = 1, 2$ and 3 respectively corresponds to adsorption on the surface, in micropores and ultramicropores where adsorbed molecules lose one, two or three degrees of freedom. For nonpolar adsorbates, the simplified estimates given in TABLE 3.1 have been proposed.

Kawazoe and Kawai (1974) tried to examine applicability of the Dubinin-Astakhov (D-A) equation to equilibrium data of molecular sieve carbon (MSC). Since the D-A equation can be written as

$$\ln \ln(W_0/W) = n(\ln A - \ln E) \quad (3-18)$$

It is possible to determine n and E by plotting the left hand side of Eq. (3-18) versus $\ln A$ provided W_0 is known. An example is given in Fig. 3.10 for benzene on MSC 5A (Kawazoe *et al.*, 1971). W_0 can be estimated from the limit of adsorption and is considered to correspond to the micropore volume of the adsorbent. Density of the adsorbed phase, ρ , is necessary to convert the amount adsorbed to the volume filled by adsorbate. For adsorption below critical temperature, liquid density at the same temperature can be used for ρ but above critical temperature, the hypothetical density estimated from the Dubinin-Nikolaev equation is

TABLE 3 1 Parameters of Dubinin-Astakhov Equations in Relation to ratio of pore size, D , and molecular size, d ΔH_0 represents heat of vaporization

Adsorption site	Ratio	n	E	Examples of a adsorption systems	Three types of adsorption sites
(I) Surface	$D/d > 5$	1	$\sim \frac{1}{3} \Delta H_0$	Carbon black-benzene, Silica gel-hydrocarbon	 I
(II) Micropore	$5 > D/d > 3$	2	$\sim \frac{2}{3} \Delta H_0$	Activated carbon-CO ₂ , benzene hydrocarbon, rare gas etc	 II
(III) Ultramicropore	$3 > D/d$	3	$\sim \Delta H_0$	MSC-ethane, Activated carbon (Columbia LC)-saturated hydrocarbon	 III

(Reproduced with permission by Kawazoe, K and Kawai, T, *Seisan Kenkyu*, 22, 493 (1970))

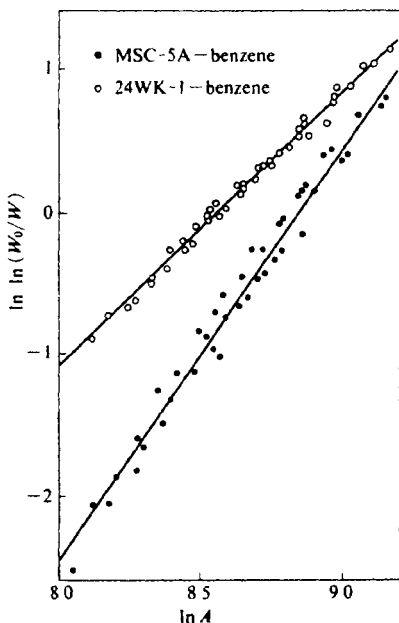


Fig 3.10 $\ln \ln (W_0/W)$ vs $\ln A$ plot according to Eq. (3-18).
(Reproduced with permission by Kawazoe, K., Astakhov, V A., Kawai, T and Eguchi, Y., *Kagaku Kogaku*, 35, 1009 (1971)).

recommended.

$$\left. \begin{aligned} \rho &= \rho_b - \frac{\rho_b - \rho_0}{T_c - T_b} (T - T_b) \\ \rho_0 &= M/b, \quad b = RT_c/8p_c \end{aligned} \right\} \quad (3-19)$$

where ρ_b is the density of liquid at normal boiling point, T_b , and ρ_0 is the density of adsorbed phase at critical temperature, T_c . M and b are molecular weight and van der Waals constant. Characteristic values of the adsorption of various gases on MSC-5A are shown in TABLE 3.2. Characteristic energy of adsorption was correlated by parachor as shown in Fig. 3.11 (Kawai and Kawazoe, 1975).

Also from TABLE 3.2 one can see that a parameter, n , is not necessarily an integer. n may be a function of relative magnitude of adsorbate molecular size and micropore size.

From this point of view, and Suzuki and Sakoda (1982) tried to extend the D-A equation to include adsorbent which has apparent micropore size

TABLE 3.2 Characteristic Values of Adsorption on MSC 5A

Adsorbate	W_0 [cc/g]	n [—]	E [cal/mol]
1 nitrogen	0.170	2.6	2,800
2 carbon dioxide	0.168	2.3	2,700
3 oxygen	0.185	2.3	2,200
4 hydrogen	0.170	2.5	1,300
5 neon	0.159	3.0	970
6 argon	0.175	2.9	2,400
7 krypton	0.168	2.8	2,700
8 xenon	0.175	2.8	3,400
9 methane	0.175	2.8	3,200
10 ethylene	0.175	3.0	3,700
11 ethane	0.175	2.9	4,000
12 propylene	0.175	3.0	5,100
13 <i>n</i> -butane	—	2.9	5,600
14 <i>n</i> -hexane	—	2.8	7,300
15 benzene	—	3.1	6,900
16 ethyl acetate	—	3.1	6,600
17 <i>p</i> -xylene	—	3.3	9,000
18 trichloroethylene	—	3.2	7,500
19 tetrahydrofuran	0.155	3.0	5,800
20 methylene chloride	—	3.0	5,000
21 cyclohexane	0.083	2.8	6,000
22 acetone	—	2.8	5,000
23 carbon disulfide	—	2.6	5,000
24 methanol	—	2.7	2,600
25 ethanol	—	2.7	4,100
26 <i>n</i> -butanol	—	2.6	6,100
27 acetic acid	—	3.0	5,000
28 pyridine	—	3.0	6,800

(Reproduced with permission by Kawazoe, K., Kawai, T., Eguchi, Y. and Itoga, K., *J Chem Eng Japan*, 7, 160 (1974))

distribution. In this case n and E are assumed to be functions of d/D , the ratio of molecule size to pore size, and the adsorption isotherm is given in integral form.

$$W = \int_0^{\infty} W(D) dD = \int_0^{\infty} W_0 f(D) \exp[-\{A/E(d/D)\}^{n(d/D)}] \quad (3-20)$$

where $f(D)$ is the density distribution function of micropore size $n(d/D)$ and $E(d/D)$ were determined using MSC 5A and 7A with xenon, ethylene and ethane as calibration gases. The results are given in Fig. 3.12 (a) and (b). For ordinary activated carbons it is difficult to determine the strict functional form of $f(D)$. Assuming normal distribution for $f(D)$ from the mean pore size \bar{D} and the square root of the variance σ for the density function of pore size, $f(D)$ for the commercial activated carbon was obtained from the adsorption isotherm measurement.

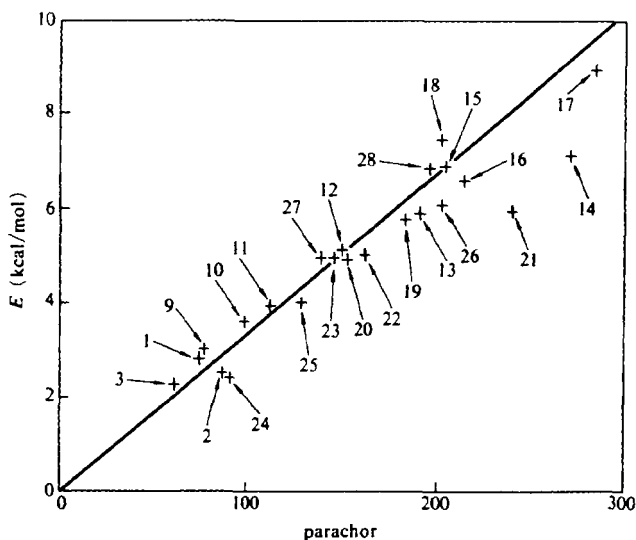


Fig. 3.11. Correlation of characteristic energy of adsorption and parachor (For key refer to TABLE 3.2).

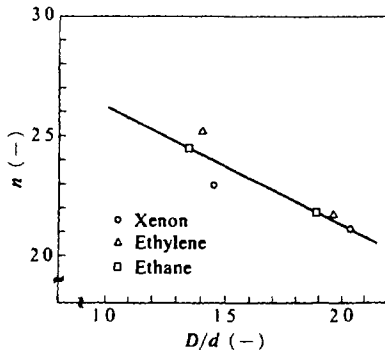
(Reproduced with permission by Kawazoe, K., Kawai, T., Eguchi, Y. and Itoga, K., *J. Chem. Eng. Japan*, 7, 161 (1974)).

$$f(D) = \frac{1}{\sigma\sqrt{2\pi}} \exp\left\{-\frac{1}{2}\left(\frac{D - \bar{D}}{\sigma}\right)^2\right\} \quad (3-21)$$

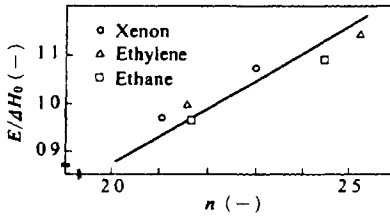
A typical result is shown in Fig. 3.13. Micropore size of ordinary activated carbon for gas phase adsorption is believed to range from 0.5 to 1.5 nm.

One obvious deficiency of the D-A equation is that it does not approach the Henry type equation at lower concentrations. According to chromatographic measurement using helium gas as a carrier (Chihara, Suzuki and Kawazoe, 1978), the adsorption equilibrium coefficient of the Henry type equation, which was assumed to hold at an extreme of $C=0$, could be determined for MSC 5A. The results are shown in Fig. 3.14. In this experiment, since helium gas exists in large excess compared with adsorbable tracer gas, the coadsorption effect of helium may not have been negligible, making it possible to assume the Henry type isotherm for the tracer gases.

Sakoda and Suzuki (1983) measured the adsorption isotherm of xenon on MSC 5A in a wide pressure range (4×10^{-4} – 1×10^2 Torr) in the absence of other components and assumed that below the point where the D-A equation has a tangent that goes through the origin, the Henry equation can be used instead of the D-A equation, as shown in Fig. 3.15. If this



(a) Variation of n with change of D/d from MSC samples



(b) Plots of $E/\Delta H_0$ versus n for MSC samples

Fig. 3 12. Relations among $E/\Delta H_0$, n and ratio of pore size and molecular diameter, D/d
(Reproduced with permission by Suzuki, K. and Sakoda, A., *J Chem. Eng. Japan*, 7, 283 (1982)).

assumption is valid, then the adsorption equilibrium constant of the Henry type equation is related to the constants involved in the D-A equation as

$$K_H = \frac{W_0}{p_s} \exp \left[\frac{n-1}{n} \left\{ \frac{1}{n} \left(\frac{E}{RT} \right)^n \right\}^{\frac{1}{n-1}} \right] \quad (3-22)$$

Transience occurs at

$$p = p_s \exp \left[- \left\{ \frac{1}{n} \left(\frac{E}{RT} \right)^n \right\}^{1/(n-1)} \right] \quad (3-23)$$

and the fractional amount adsorbed at this point is

$$W/W_0 = \exp \left[- \left(A/E \right)^{n/(n-1)} \right] \quad (3-24)$$

For adsorption of xenon on MSC 5A at room temperature, E , and n given

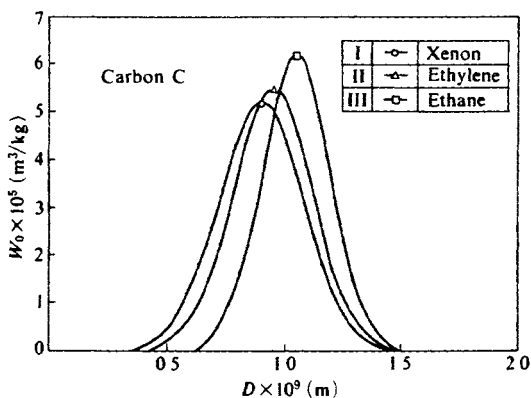


Fig 3 13 Normal distribution curves of carbon C Curve (I) from isotherm of xenon, Curve (II) from isotherm of ethylene, Curve (III) from isotherm of ethane
(Reproduced with permission by Suzuki, M and Sakoda, A, *J Chem Eng Japan*, 15 284 (1982))

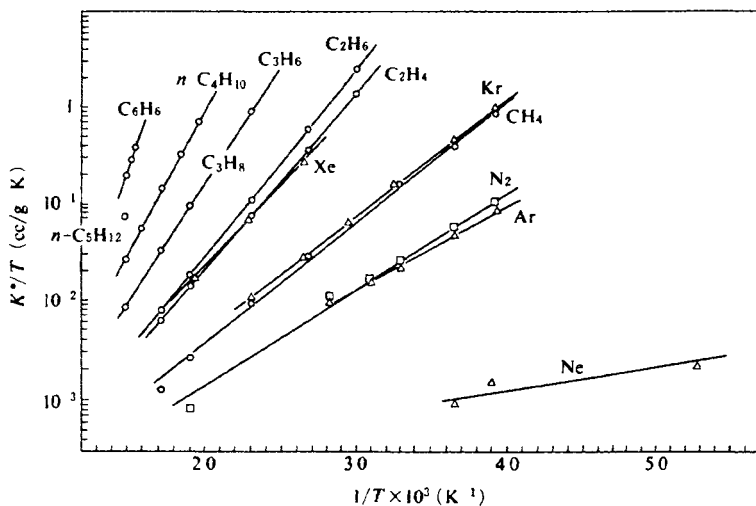


Fig 3 14 van't Hoff's plot of adsorption equilibrium constants
(Reproduced by permission by Chihara, K, Suzuki, M and Kawazoe, K, *AIChE Journal*, 24, 241 (1978))

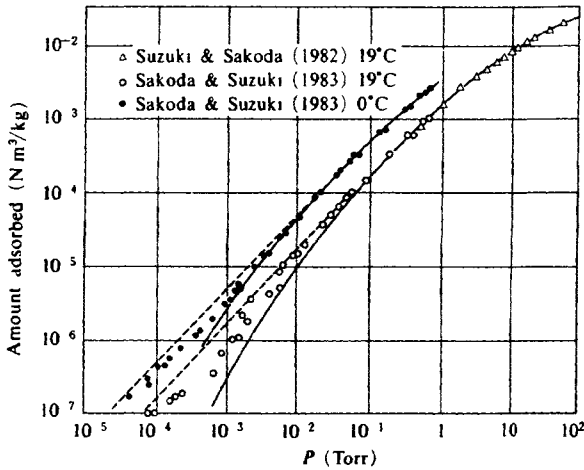


Fig 3.15 Adsorption isotherms of xenon on MSC 5A at 0°C and 19°C. Dotted lines and solid lines correspond to the Henry type equation and the D-A equation, respectively (Reproduced with permission by Sakoda, A. and Suzuki, M., *J Chem Eng Japan* 16, 157 (1982))

in TABLE 3.2 indicate that the transience from the D-A equation to the Henry equation occurs at around $W/W_0 = 0.001$

It should be added that the D-A equation when $n=1$ is reduced to the Freundlich type equation

$$W/W_0 = (p/p_s)^{RT/E} \quad (3-25)$$

Then parameters in Eq (3-10) correspond to the parameters in Eq (3-25) as follows

$$k_F = \rho W_0 (C_s)^{RT/E} \quad (3-26)$$

$$n_F = E/RT \quad (3-27)$$

3.3. Heat of Adsorption

Adsorption is accompanied by evolution of heat since adsorbate molecules are more stabilized on the adsorbent surface than in the bulk phase. Adsorption is accompanied by phase change and thus depending on the occasion it may involve mechanical work. For this reason, the amount of heat evolution by unit adsorption depends on the system adopted

(Ross and Olivier, 1964). From a practical standpoint, the important definitions of heat of adsorption are "differential heat of adsorption" and "isosteric heat of adsorption."

Differential heat of adsorption, Q_{diff} , is defined as heat evolution when unit adsorption takes place in an isolated system. This heat is directly measurable by calorimeter.

Isosteric heat of adsorption, Q_{st} , is defined from isotherms at different temperatures by Eq. (3-29). Q_{st} is bigger than Q_{diff} since it requires work equivalent to $pV(=RT)$.

$$Q_{\text{st}} = Q_{\text{diff}} + RT \quad (3-28)$$

Q_{st} is related to adsorption isotherms at different temperatures by the van't Hoff equation

$$\begin{aligned} Q_{\text{st}} &= RT^2(d \ln P/dT) = R d \ln P/d(1/T) \\ &= RT^2(d \ln c/dT) + RT/2 \end{aligned} \quad (3-29)$$

From experimental isotherms at temperature T_1 and T_2 , Q_{st} is obtained as

$$Q_{\text{st}} = R(\ln p_1 - \ln p_2)/(1/T_1 - 1/T_2) \quad (3-30)$$

For the Henry equation and the Langmuir equation, Q_{st} is related to the equilibrium constant, K , as

$$Q_{\text{st}} = RT^2(d \ln K/dT) = R d \ln K/d(1/T) \quad (3-31)$$

or

$$K = K_0 \exp(Q_{\text{st}}/RT) \quad (3-32)$$

When adsorption sites are energetically homogeneous and when there is no interaction between adsorbed molecules, the heat of adsorption is independent of the amount adsorbed. However, when the adsorbent surface is composed of a number of patches having different energy levels, or when interaction among adsorbed molecules cannot be neglected, the heat of adsorption varies with the surface coverage. Whether variation of heat of adsorption is due to surface heterogeneity or to the interaction among adsorbed molecules is hard to distinguish in some cases. Here no distinction between the two mechanisms is made and only phenomenological variation is considered.

Variation of heat of adsorption can be described two ways. One is by

defining the spectral density of adsorption sites where heat of adsorption is Q , $f(Q)$. Then

$$\int_0^{Q_{\max}} f(Q) dQ = 1 \quad (3-33)$$

Or more directly, it is possible to describe the heat of adsorption as a function of amount adsorbed q , $Q(q)$.

The relation between $f(Q)$ and $Q(q)$ is as follows: $Q(q)$ is converted so that the amount adsorbed, q , is written as an explicit function of Q , $q(Q)$, and then

$$f(Q) = q(Q)/q_0 \quad (3-34)$$

When energy distribution, $f(Q)$, is given, the corresponding form of adsorption isotherm can be estimated by assuming that the heterogeneous surface consists of small homogeneous patches (small areas) and that the adsorption isotherm on homogeneous surface holds on each small patch. For example, Langmuir type isotherm relation (Eq. (3-3) with Eq. (3-32)) can be assumed to hold on each patch.

$$dq = q_0 \frac{Kp}{1 + Kp} f(Q) dQ \quad (3-35)$$

where dq is the amount adsorbed on the patch having the adsorption energy Q . Then the total isotherm equation is given as

$$q = q_0 \int_Q^{Q_{\max}} f(Q) \frac{K_0 \exp(Q/RT)p}{1 + K_0 \exp(Q/RT)p} dQ \quad (3-36)$$

This equation is solved for a given $f(Q)$ using Stieltjes transform. But for the sake of simplicity Roginsky's approximation is attractive, i.e., assumption of the Langmuir type isotherm on each patch is further simplified to a stepwise isotherm as

$$\begin{aligned} \theta &= 0 \text{ for } p < 1/K \\ \theta &\equiv q/q_0 = 1 \text{ for } p \geq 1/K \end{aligned} \quad (3-37)$$

Then the integral in Eq. (3-36) is simplified to

$$q = q_0 \int_Q^{Q_{\max}} f(Q) dQ \quad (3-38)$$

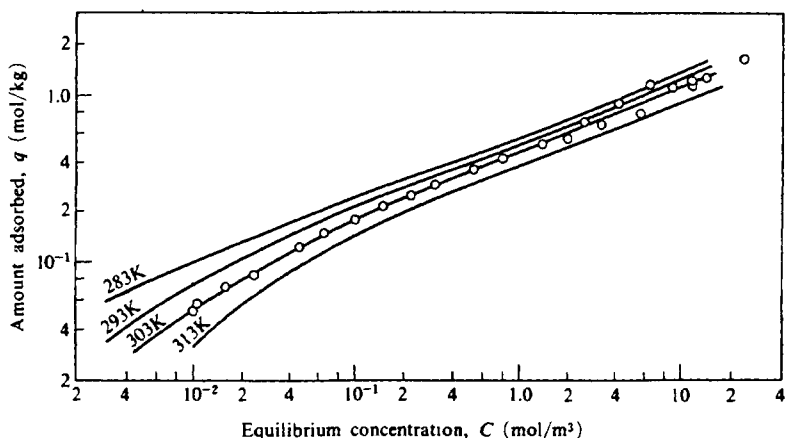


Fig. 3.16. Summary of adsorption isotherms of propionic acid on activated carbon HGR 513 from aqueous solution measured at 283, 293, 303 and 313 K. Hollow circles are measured points at 303 K.

where

$$Q = -RT \ln K_0 p \quad (3-39)$$

Then if $f(Q)$ is given, corresponding adsorption isotherm is easily calculated.

Also from an isotherm relation, $q(p)$, spectral density function, $f(Q)$, can be calculated from the following equation.

$$f(Q) = -(1/RT) dq/d \ln p |_{\tau} \quad (3-40)$$

As a typical example of an adsorption isotherm in aqueous phase, adsorption of propionic acid on activated carbon is shown in Fig. 3.16. At higher concentrations isotherms can be correlated by the Freundlich type equation, but at low coverage ($q < 0.1$ mmol/g), the slope of isotherms becomes steeper and seems to reach Henry's type relation. From isotherms at different temperatures, isosteric heat of adsorption was obtained as a function of the amount adsorbed as shown in Figs. 3.17 and 3.18. At higher coverage, measured isosteric heat of adsorption seems to decrease with increasing amount adsorbed.

$$Q = Q_s - Q_0 \ln q \quad (3-41)$$

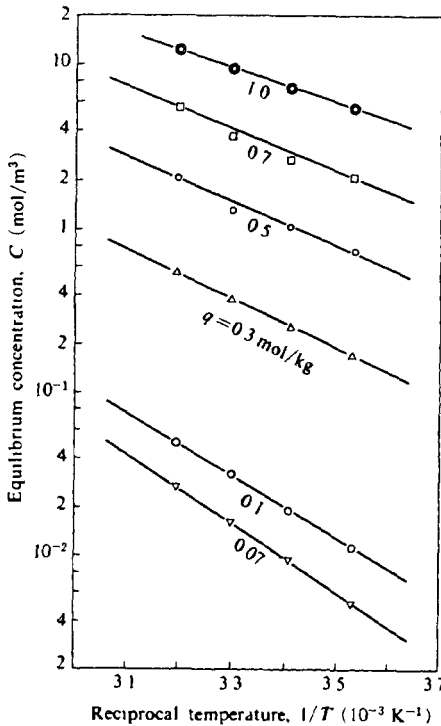


Fig 3.17 Adsorption isotherms for determining isosteric heat of adsorption from Eq 3-30
(Reproduced with permission by Suzuki, M and Fujii, T, *AIChE Journal*, 28, 383 (1982))

This functional form is consistent with the Freundlich isotherm and the Freundlich exponent n_F determined by experiment are compared with Q_0/RT in TABLE 3.3. Agreement between them is reasonable.

At low coverage, the Freundlich isotherm assumes existence of sites with very high heat of adsorption. For measured equilibrium data, the Radke and Prausnitz equation can be used for correlating low coverage data. Temperature dependence of K gives heat of adsorption at initial coverage. This $Q_{s,0}$ was 4.6 J/mol and is shown in Fig. 3.18 by the arrow. From Figs 3.16 and 3.18, transition from Henry type isotherm and Freundlich type isotherm can be said to occur at around 4×10^{-2} mol/kg.

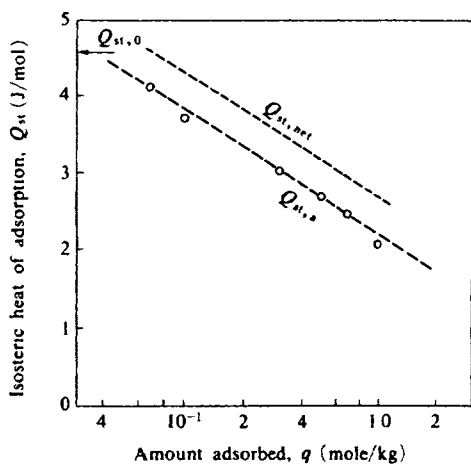


Fig 3.18 Isosteric heat of adsorption $Q_{st,a}$ plotted against amount adsorbed q (Reproduced with permission by Suzuki, M and Fujii, T, *AIChE Journal* 28, 384 (1982))

TABLE 3.3 Constants of Freundlich Type Equation $q = kc^{1/n}$
Applied to the isotherm results for $q > 10^{-1}$ mol/kg

Temperature (K)	k	n	Q_0/RT
283	0.55	2.74	3.00
293	0.49	2.64	
303	0.43	2.52	
313	0.32	2.45	2.71

(Reproduced with permission by Suzuki, M and Fujii, T, *AIChE Journal*, 28, 383 (1982))

3.4. Adsorption Isotherms for Multicomponent Systems

When two or more adsorbable components exist with the possibility of occupying the same adsorption sites, isotherm relationships become more complex. The simplest is extension of the Langmuir type isotherm by assuming no interaction between adsorbing molecules. In the case of two components, the extended Langmuir isotherm (Markham and Benton, 1931) is given as

$$\left. \begin{aligned} q_1 &= q_{01}K_1p_1/(1 + K_1p_1 + K_2p_2) \\ q_2 &= q_{02}K_2p_2/(1 + K_1p_1 + K_2p_2) \end{aligned} \right\} \quad (3-42)$$

This equation enables quick estimation of equilibrium relations of

multicomponent adsorption from Langmuir parameters determined from the single component isotherm of each component. Eq. (3-42) is thermodynamically consistent when $q_{01} = q_{02}$ holds. Furthermore, the equation can be applied without significant error to a combination of different values of q_0 if the components are similar in nature and follow the Langmuir isotherm relation.

From Eq. (3-42), it follows that the separation factor for a mixture of two components can be given directly by the ratio of the equilibrium constants.

$$a_{12} = (x_1/x_2)/(y_1/y_2) = K_1/K_2 \quad (3-43)$$

This relation holds independent of concentration and can naturally be extended to an arbitrary combination of components.

$$a_{ij} = a_{ik} \times a_{kj} = K_i/K_j \quad (3-44)$$

Lewis *et al.* (1950) showed that for adsorption of two components with a constant total pressure of $P = p_1 + p_2$, the following relation holds between the amount adsorbed of each component, q_1 and q_2 .

$$q_1/q^{\circ}_1 + q_2/q^{\circ}_2 = 1 \quad (3-45)$$

where q°_1 and q°_2 are the amounts of pure components adsorbed at pressure $p^{\circ}_1 = P$ and $p^{\circ}_2 = P$. The above relation is derived from Eq. (3-42). For adsorption of mixtures of hydrocarbons, Eq. (3-45) is valid since a_{ij} becomes relatively constant independent of concentration. The examples of measurement by Lewis *et al.* (1950) are shown in Fig. 3.19.

The extended Langmuir (Markham-Benton) isotherm has limited applicability especially for liquid phase adsorption, since even single-component isotherms in liquid phase are rarely explained by the Langmuir equation. There have been several trials to extend the Freundlich type equation to mixture isotherms. Fritz and Schlünder (1974) gave the following equation.

$$q_i = \frac{a_i C_i^{b_i + b_{ij}}}{C_i^{b_{ij}} + a_{ij} C_j^{b_{ij}}} \quad (3-46)$$

These types of frequently found equations involve problems concerning inconsistency with single-component isotherm data and lack of thermodynamic background. However since they employ relatively large numbers of empirical parameters, final fit with the experimental data

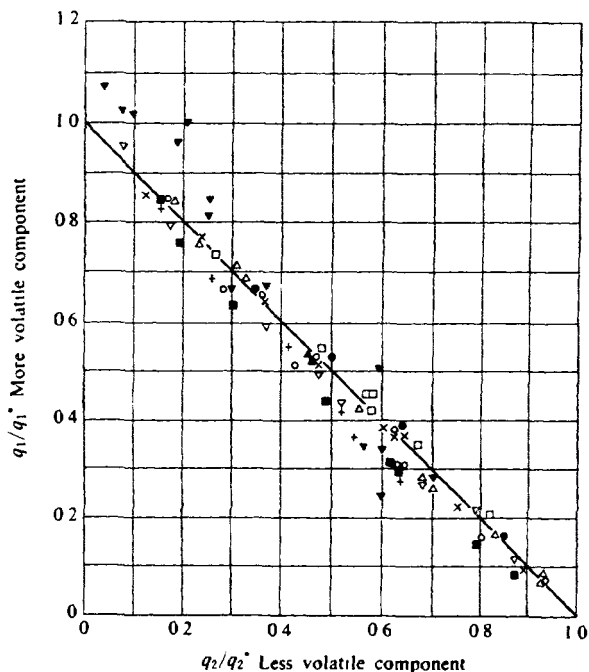


Fig 3 19 Lewis plot of amounts adsorbed for silica gel and activated carbons

PCC Carbon	Silica gel	Columbia G carbon
○ $C_2H_4 + C_2H_6$	▼ $CH_4 + C_2H_4$	▽ $CH_4 + C_2H_4$
△ $C_2H_6 + C_3H_8$	+ $C_2H_6 + C_3H_8$	● $C_2H_4 + C_2H_6$
□ $i-C_4H_{10} + 1-C_4H_{10}$	× $i-C_4H_{10} + 1-C_4H_{10}$	■ $C_2H_4 + C_3H_8$
		▲ $C_3H_8 + C_3H_8$

becomes satisfactory.

A more reliable method for estimating adsorption isotherm of binary components from single-component isotherms is the IAS (Ideal Adsorbed Solution) method of Myers and Prausnitz (1965).

Surface pressure π is determined as a function of pressure p° for each single-component isotherm.

$$\pi(p^\circ) = \frac{RT}{A} \int (d \ln q^\circ / d \ln p^\circ) dq \quad (3-47)$$

Ideal solution assumption is applied to the adsorbed phase and the total amount adsorbed, q_T , is then related to the mole fraction of each component

$$1/q_T = x_1/q^{\circ}_1(\pi) + x_2/q^{\circ}_2(\pi) \quad (3-48)$$

The Raoult law is also applied to the relation between mole fraction in gas phase and adsorbed phase.

$$p_1 = Py_1 = p^{\circ}_1(\pi)x_1, \quad p_2 = Py_2 = p^{\circ}_2(\pi)x_2 \quad (3-49)$$

where y_i and x_i are mole fraction of the i -th component in gas phase and in adsorbed phase, respectively.

$$\sum x_i = 1, \quad \sum y_i = 1 \quad (3-50)$$

To obtain the equilibrium amounts adsorbed which correspond to a given set of gas phase concentrations, first a guess of surface pressure $\pi A/RT$ is made and then p°_1 and p°_2 are obtained. Then from p_1, p_2, p°_1 and p°_2, x_1 and x_2 are obtained by Eq. (3-49). This procedure is repeated until Eq. (3-50) is satisfied. Then from q°_1 and q°_2 determined from p°_1 and p°_2, q_T can be determined by Eq. (3-48), which then gives q_1 and q_2 from x_1 and x_2 previously obtained. The iteration procedure is minimized by employing a small computer. When isotherms for single components can be expressed by analytical equations, the integral of Eq. (3-47) can be determined analytically. For instance, if the Freundlich equation can be applied in a wide range, then the integral becomes

$$\pi A/RT = n_F q^{\circ} \quad (3-51)$$

which greatly simplifies the procedure. But it should be kept in mind that unless single-component isotherms especially for the weaker component are determined in a wide range of amounts adsorbed, this simplified treatment may result in considerable deviation.

The IAS model is practical for predicting binary isotherms from single-component isotherm data. As an example, isotherms of propane and butane on activated carbon are shown in Fig. 3.20. The assumption of ideal adsorbed solution may need careful consideration in some cases where a combination of two components forms an azeotropic mixture in the adsorbed phase as reported by Glessner and Meyers (1969).

The IAS theory is also applicable in the case of adsorption from aqueous solution, as shown by Radke and Prausnitz (1972b).

The vacancy solution model was extended to describe mixture adsorption isotherm (Suwanayuen and Danner, 1980).

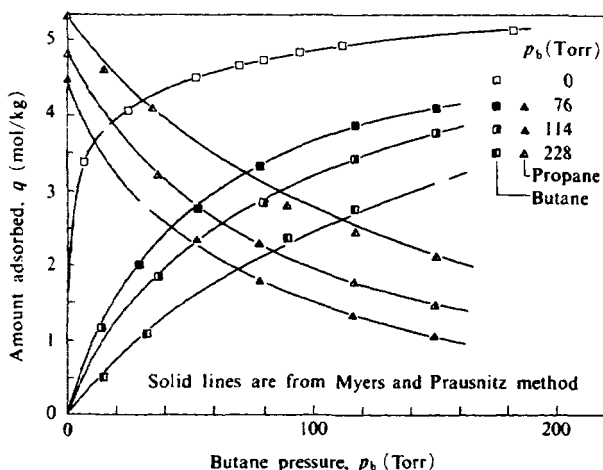


Fig. 3.20. Adsorption isotherms of propane and butane mixture on activated carbon; amount adsorbed of propane and butane for propane pressures 0, 76, 114 and 228 Torr.

(Reproduced with permission by Suzuki, M. *et al.*, *Fundamentals of Adsorption Engineering* Foundation, 622 (1985).

3.5. Adsorption Isotherms of Unknown Mixtures

In the case of water treatment by adsorption, mixtures of organics usually become involved and phenomenological parameters are used to express water qualities. These parameters are COD (chemical oxygen demand), BOD (biochemical oxygen demand) or TOC (total organic carbon), which correspond to the weighted sum of concentrations of component organics. Since each organic component has different adsorbability, the weighted total sometimes appears strange in adsorption characteristics.

For the sake of simplicity, the adsorption of an aqueous solution of COD which consists of two organic components on activated carbon is considered here. One of the components, whose concentration is C_1 , is not adsorbed at all while the other component of concentration C_2 has an adsorption isotherm of the Freundlich type, $q = kC_2^{1/n}$, when it exists as a single component. COD of the mixture, COD_1 , is the weighted sum of C_1 and C_2 .

$$COD_1 = C_1 + C_2$$

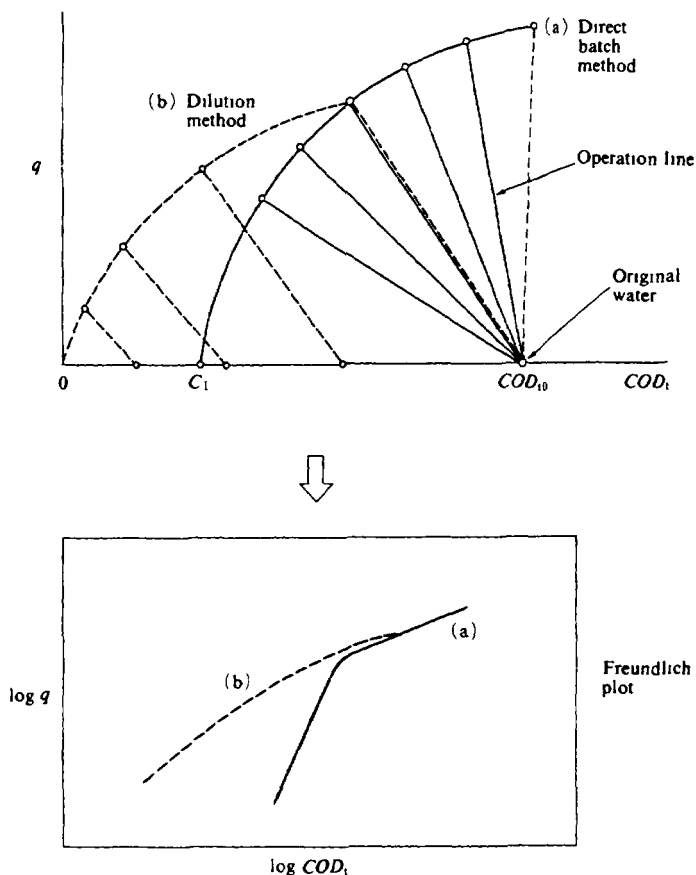


Fig 3.21. Illustration of shape of the isotherms of mixtures measured by different methods

If adsorption isotherm is measured by the batch adsorption technique, i.e. measurement of COD concentration change in vessels with different carbon load, then adsorption equilibrium is attained for Component 2 but coexistence of Component 1 results in an unfamiliar shape of adsorption isotherm with regard to adsorption of COD_t , as shown in Fig. 3.21.

Another method of measurement of isotherm is the dilution method, which is performed by preparing several bottles containing raw water diluted to different levels and adding the same amount of adsorbent in the bottles. Then the amount adsorbed in each flask is determined by comparing the initial concentrations and the final concentrations. By this method the

measured isotherm will become as shown by dotted lines in Fig 3.21.

The difference in isotherms by the two methods which never occurs in single-component measurement is due to the dilution of the unadsorbed component in the latter case. In other words, the existence of an unadsorbable component may be checked by measuring isotherms by these two different methods.

REFERENCES

- Berenyi, M, *Z Physik Chemie*, **94**, 628 (1920), **105**, 55 (1923)
 Brunauer, S, P H. Emmett and E Teller, *J Am Chem Soc*, **60**, 309 (1938)
 Chihara, K, M Suzuki and K Kawazoe, *AIChE Journal*, **24**, 237 (1978)
 Dubinin M M, *Chemistry and Physics of Carbon*, vol 2, p 51 Marcel Dekker, New York (1966)
 Dubinin, M M, *Chem Rev.*, **60**, 265 (1960)
 Dubinin, M M, V A Astakhov, *2nd Int Conf on Molecular-Sieve Zeolite* (1970)
 Fowler, R H and E A Guggenheim, *Statistical Thermodynamics*, Cambridge University Press, Cambridge (1939)
 Freundlich, H, *Colloid and Capillary Chemistry*, Mathuen, London, pp 110-134 (1926)
 Fritz, W and E U Schlunder, *Chem Eng Sci*, **29**, 1279 (1974)
 Glessner A J and A L Myers, *Chem Eng Progr Sympo Ser*, **96**, Vol 65, 73 (1969)
 Hasz, J W and C A Barrere, Jr, *Chem Eng Progr Sympo Ser*, **96**, Vol 65, 48 (1969)
 Kawazoe, K, T Kawai, *Seisan Kenkyu*, **22**, 491 (1970) (in Japanese)
 Kawazoe, K, T Kawai, Y Eguchi and K Itoga, *J Chem Eng Japan*, **7**, 158 (1974)
 Kawazoe, K, V A Astakhov, T Kawai and Y Eguchi, *Kagaku Kogaku*, **35**, 1006 (1971) (in Japanese)
 Langmuir, I, *J Chem Soc*, **40**, 1361 (1918)
 Lewis, W K, E R Gillil and B Chertow and W P Cadogen, *Ind Eng Chem*, **42**, 1319 (1950)
 Markham E C and A F Benton, *J Am Chem Soc*, **53**, 497 (1931)
 Myers, A L, *Database on Adsorption Equilibrium*, in preparation (1988)
 Myers, A L and J M Prausnitz, *AIChE Journal*, **11**, 121 (1965)
 Polanyi, M, *Verh Deut Chem*, **57**, 106 (1914)
 Radke, C J and J M Prausnitz, *Ind Eng Chem. Fundam.*, **11**, 445 (1972a)
 Radke, C J and J M Prausnitz, *AIChE Journal*, **18**, 761 (1972b)
 Ross, S and J P Olivier, *On Physical Adsorption*, Interscience (1964)
 Ruthven, D M, *Principles of Adsorption and Adsorption Processes*, John Wiley & Sons, New York (1984)
 Sakoda, A and M Suzuki, *J Chem Eng Japan*, **16**, 156 (1983)
 Suzuki, M and A Sakoda, *J Chem Eng Japan*, **15**, 279 (1982)
 Suzuki, M, M Horii and K Kawazoe, *Fundamentals of Adsorption*, 619 Eng Foundation, NY (1985)
 Suwanayuen S and R P Danner, *AIChE Journal*, **26**, 68, 76 (1980)
 Suzuki, M and T Fujii, *AIChE Journal*, **28** 380 (1982)
 Toth, J, *Acta Chim Acad Sci Hung*, **69** 311 (1971)

Diffusion in Porous Particles

Most of the adsorbents commercially used are porous particles. For large adsorption capacity, large surface area is preferable, as a result large numbers of fine pores, as fine as possible, are needed. Adsorbate molecules come from outside adsorbent particles and diffuse into the particle to fully utilize the adsorption sites. Depending on the structure of the adsorbent, several different types of diffusion mechanisms become dominant and sometimes two or three of them compete or cooperate. The dominant mechanism also depends on a combination of adsorbate and adsorbent and adsorption conditions such as temperature and concentration range.

In adsorbent particles with bi-dispersed pore structures, such as activated carbon, macropores usually act as a path for the adsorbate molecules to reach the interior of the particle. In this case molecular diffusion or Knudsen diffusion takes place in the macropore; this is called pore diffusion.

When adsorbed molecules are mobile on the surface of the adsorbent, e.g. volatile hydrocarbon on activated carbon, diffusion due to migration of the adsorbed molecules may contribute more than pore diffusion to intraparticle diffusion. This type of diffusion is called surface diffusion.

When the size of an adsorbate molecule is close to the size of the micropore, diffusion of the molecule becomes restricted and the rate of transport in the micropore may have a significant effect in the overall adsorption rate. This type of diffusion in the micropore is an activated process which depends heavily on adsorbate properties.

4.1. Diffusion Coefficient

Diffusion of an adsorbate molecule in the adsorbent particle occurs when there is concentration distribution in the particle. Since the mechanism of diffusion and the real driving force of diffusion may not

be sufficiently clear, diffusion data are described by means of the diffusion coefficient defined by Fick's first law taking a gradient of an appropriate concentration as the driving force.

$$J = -D(C) \frac{dC}{dx} \quad (4-1)$$

Diffusion coefficient $D(C)$ is then a phenomenological coefficient and may be a function of concentration. The concentration may be a concentration in fluid phase or adsorbed phase. The physical meaning of $D(C)$ is dependent on the controlling mechanism in the diffusion concerned. Then only the mathematical problem of solving differential equations will be left.

4.2. Pore Diffusion

Diffusion of molecules to be adsorbed in the macropore of the porous body is easily understood by describing the flux using partial pressure or concentration of the species in the fluid phase in the pore.

$$J = -D_p \frac{dp}{dx} \quad (4-2)$$

D_p is the effective pore diffusion coefficient.

The effective diffusion coefficient in the particle, D_p , is considered to be proportional to the diffusivity in the bulk phase, D_v , when macropore diffusion is dominant and

$$D_p = \eta D_v \quad (4-3)$$

where a proportionality constant, η , is called the diffusibility. Then estimation of the diffusibility and the diffusivity in the fluid phase makes prediction of D_p possible.

4.2.1. Diffusibility

The diffusibility, η , may be determined from a detailed structure or configurations of pore network but actual pore structure is usually quite complicated and in most cases only simplified considerations are made.

One of the simplest models of a porous body is a packed bed of particles. Typical measured diffusibilities for packed beds of particles are shown in Fig. 4.1. The broken line in the figure shows the diffusibility for the system with dispersed inactive particles (spherical) determined from the

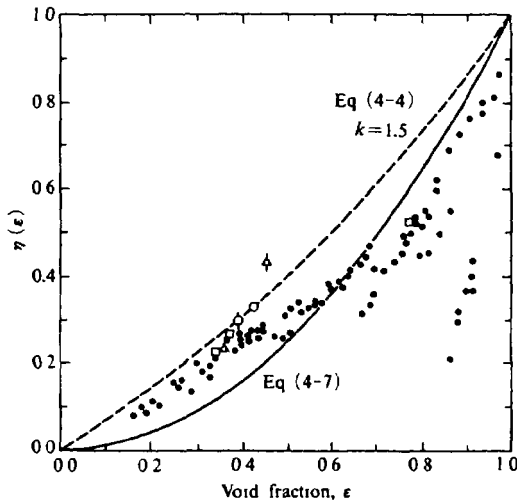


Fig. 4.1 Diffusibility in packed beds as a function of void fraction.

Source ○ Hoogschagen (1955), • Currie (1960), ◊ Suzuki and Smith (1972), △ Porous particle, Suzuki and Smith (1972), △ : Wooding (1959), □ . Evans and Kenney (1966).

analogy of electrical conductivity as cited in Suzuki and Smith (1972).

$$\eta = \varepsilon / \{ \varepsilon + k(1 - \varepsilon) \} \quad (4-4)$$

where k is a function of the shape of the dispersed phase (particle) and given as shown in TABLE 4.1.

In many cases, the diffusibility is customarily divided into two parts, the contribution of porosity ε and that of tortuosity k^2 of the pore.

$$\eta = \varepsilon / k^2 \quad (4-5)$$

or

$$D_p = (\varepsilon / k^2) D_v \quad (4-6)$$

Tortuosity factor of the pore, k^2 , is 3 if the pore direction is random but in most cases falls between 2 and 6, as shown in TABLE 4.2. Tortuosity factor may be a function of pore diameter to length ratio or more complicated parameters describing the configuration of the pore.

TABLE 4.1. Parameter, k , in Eq. (4-4) for Different Particle Shapes.

Particleshape	k
Spherical	1.5
Ellipsoidal with axes $a=b=nC$ $n=5$	2.1
$n=10$	3.1

TABLE 4.2. Comparison of the Effective Diffusivities of K_r in N_2 and Obtained Tortuosity Factor (20°C).

Sample	Macropore	Micropore	$D_{e,exp}$	k^{2*}
Activated carbon	(-)	(-)	(cm^2/s)	(-)
HGR-513	0.29	0.33	10.5×10^{-3}	3.9
HGR-588	0.31	0.32	11.9	3.9
2GS	0.17	0.43	5.2	4.4
3GS	0.20	0.44	6.6	4.0
4GS	0.17	0.49	5.3	4.2
Silica gel D-4	—	0.69	1.01	5.9
Zeolite				
13X (1/8")	0.32	0.28	9.2	3.6
5A (1/8")	0.32	0.24	12.2	3.3

*For bidispersed particles, porosity of macropore was used for deriving tortuosity. Source: Kawazoe *et al.* (1966)

(Reproduced with permission by Kawazoe, K. and Sugiyama, I., *Kagaku Kogyou*, **30**, 1010 (1966)).

Usually tortuosity factor is considered to increase with decreasing porosity, in which case the most simplest correlation may be to assume (Wakao and Smith, 1962).

$$\eta = \varepsilon^2 \quad \text{or} \quad D_p = \varepsilon^2 D_v \quad (4-7)$$

This relation is shown in Fig. 4.1 by a solid line.

When diffusion of large molecules takes place in fine pores whose diameter is close to the size of the diffusing molecules, pore opening must be corrected for the size effect. Satterfield *et al.* (1973) gave a simple experimental correlation which is written in terms of the notations used here as follows,

$$\eta = \frac{\varepsilon}{k^2} \exp\left(-2.0 \frac{d_s}{d_p}\right) \quad (4-8)$$

where d_s and d_p respectively represents the diameter of the diffusing molecule and that of the pore. Fig. 4.2 shows their diffusion measure-

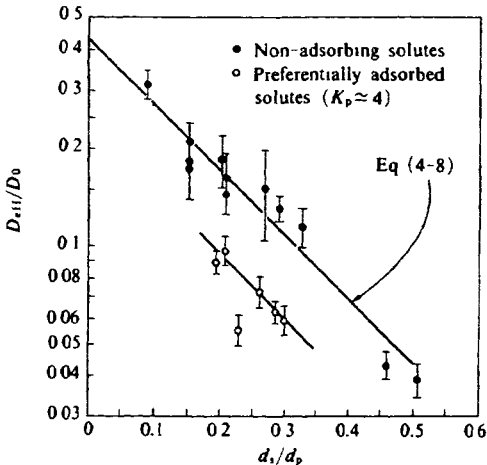


Fig. 4.2. Effect of ratio of solute critical diameter to pore diameter on effective diffusivity in restricted diffusion: solid circles correspond to non adsorbable molecules & open circles show adsorbable molecules in silica-alumina beads (median pore diameter 3.2 nm). (Reproduced with permission by Satterfield, N., Cotton, K. and Pitcher Jr., *AIChE Journal*, 19, 633 (1973)).

ments for thirteen nonadsorbing solutes in silica alumina catalyst particle.

4.2.2. Diffusivity in fluid phase

Diffusion in large size pores can be considered to be molecular diffusion which is controlled by collision of molecules rather than collision between molecules and the atoms constituting the pore walls.

A. molecular diffusivity in gas phase

Molecular diffusivity in gas phase may be estimated by the Chapman-Enskog equation. For a mixture of components 1 and 2,

$$D_m = \frac{0.00158 T^{3/2} (1/M_1 + 1/M_2)^{1/2}}{P \sigma_{12}^2 \Omega(\varepsilon/kT)} \quad (\text{cm}^2/\text{s}) \quad (4-9)$$

where M_1 and M_2 are the molecular weight, P is the total pressure (atm), $\sigma_{12} = (\sigma_1 + \sigma_2)/2$ is the collision diameter (\AA) determined from Lennard-Jones potential, and Ω is a function of ε/kT where $\varepsilon = \sqrt{\varepsilon_1 \varepsilon_2}$ is the Lennard-Jones force constant where k is the Boltzmann constant.

Apparently, molecular diffusivity is inversely proportional to the total pressure, P , and is proportional to roughly 1.7 power of temperature, $T^{1.7}$, which comes from a combined effect of the $T^{3/2}$ factor and temperature effect of Ω in Eq. (4-9).

B. Knudsen diffusion

When the total pressure is very low or pore diameter is small, mean free path of a gas molecule, λ , becomes smaller than the pore diameter, $2R_p$.

$$\lambda = \frac{3\mu}{P\sqrt{M}} \sqrt{\frac{\pi RT}{8}} \quad (P \text{ in dyne/cm}^2) \quad (4-10)$$

$\lambda = 2R_p$ yields the critical pressure to determine diffusion patterns.

$$p_{cr} = \frac{3}{4\sqrt{2}} \sqrt{\frac{\pi RT}{M}} \cdot \frac{1}{R_p} \quad (4-11)$$

If the total pressure, P , is far larger than p_{cr} then molecular diffusion is dominant in the pore of radius R_p .

Then collisions between gas molecules and the pore wall become more dominant than collisions between molecules, which are dominant in molecular diffusion.

In this case, by colliding and bouncing on the wall, a molecule loses its momentum in the direction of the pore and thus the more frequently collision takes place, the smaller the diffusion speed. This type of diffusion is known as the Knudsen diffusion.

The Knudsen diffusivity may be estimated using the following equation.

$$D_K = \left(\frac{2}{3}\right) \sqrt{\frac{8RT}{\pi M}} \cdot R_p = 9700 R_p (T/M)^{1/2} \quad (\text{cm}^2/\text{s}) \quad (4-12)$$

where R_p is the mean pore radius (cm), T is the temperature (K) and M is the molecular weight of the diffusing gas.

From Eq. (4-12) it is clear that when the pressure is far smaller than the critical pressure given by Eq. (4-11), diffusivity is independent of pressure and is proportional to $T^{1/2}$.

C. intermediate region

When the total pressure is around p_{cr} , molecular diffusion and Knudsen diffusion coexist. In this range, overall diffusivity can be

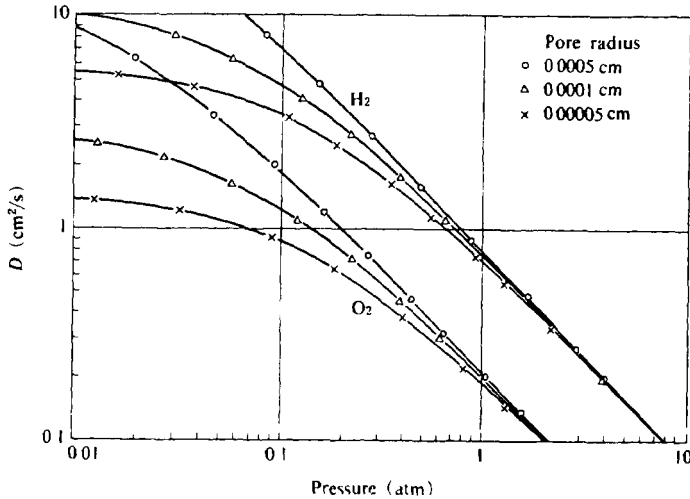


Fig. 4.3. Effect of pressure on diffusivity in a pore : Diffusion of oxygen and hydrogen in nitrogen, calculated by Eq. (4-13).

obtained from Bosanquit's equation.

$$1/D = 1/D_m + 1/D_K \quad (4-13)$$

The above expression implicitly assumes equimolar counterdiffusion, but can be used for other cases as a good approximate.

Equation (4-13) allows pressure dependency of D to be as shown in Fig. 4.3.

D. molecular diffusivity in liquid phase

Molecular diffusion in liquid phases, such as aqueous phase, is rather complicated because of possible dissociation of diffusing molecules or interaction between diffusing molecules and surrounding molecules, e.g. hydration.

In the most ideal case of infinitesimally small concentration of the solute, the Wilke-Chiang equation is sometimes used for estimation of molecular diffusivity.

$$D_v = 7.4 \times 10^{-8} (aM)^{1/2} T / (\mu_2 V_1^{0.6}) \quad (4-14)$$

where a represents the association coefficient given as 2.6 for water, 1.9 for methanol, 1.6 for ethanol and 1.0 for nonassociative solvents such as

benzene. M and μ are molecular weight and viscosity of solvent and V_1 is the molecular volume at boiling point. The above equation may give a rough estimate of D_v with less than 20% accuracy. For higher concentrations there is no reliable estimation method for diffusivity in liquid phase.

Diffusivities of organic molecules of low molecular weight in water are in the range of 10^{-6} to 1.5×10^{-5} cm^2/s while it can be smaller with increasing molecular weight.

4.3. Surface Diffusion

Migration of adsorbed molecules on the surface may contribute to transport of the adsorbates into the particle. This effect is very much dependent on the mobility of the adsorbed species, which is determined by the relative magnitude of the heat of adsorption and the activation energy of migration.

As shown in Fig. 4.4, when the energy barrier, E_s , existing between neighboring sites, is smaller than the heat of adsorption, Q_{st} , then it is easier to hop to the next site than to desorb into the bulk phase.

The effective surface diffusion coefficient is defined by taking the gradient of the amount adsorbed as the driving force of diffusion.

$$J = -D_s \rho_p \frac{dq}{dx} \quad (4-15)$$

The effective surface diffusion coefficient may be written as

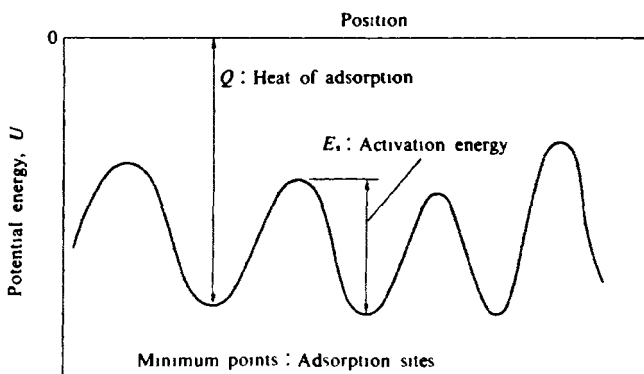


Fig 4 4 Cross sectional view of potential energy distribution of adsorption on solid surface

$$D_s = D_s^*/k_s^2 \quad (4-16)$$

where D_s^* is the surface diffusivity on the adsorption surface and k_s^2 is the tortuosity of surface diffusion. Usually, it is difficult to define k_s^2 in which case D_s rather than D_s^* is taken into account when theoretical interpretation is made.

4.3.1. Random walk concept

Surface diffusion can be related to random walk in the direction of diffusion. When unit step is defined by length, Δx , and time, Δt , as shown in Fig. 4.5, then after n steps (after $n\Delta t$), variation of the position $x = \pm \Delta x \pm \Delta x \pm \dots \pm \Delta x$ (n steps) is given as

$$\bar{x}^2 = n \overline{\Delta x^2} \quad (4-17)$$

For large n , diffusion coefficient D is related to \bar{x}^2 by Einstein's equation.

$$\bar{x}^2 = 2Dn\Delta t \quad (4-18)$$

Then D is given as

$$D = (1/2) (\overline{\Delta x^2} / \Delta t) \quad (4-19)$$

Hence if $\overline{\Delta x^2}$ and Δt are assumed by a proper model, surface diffusivity

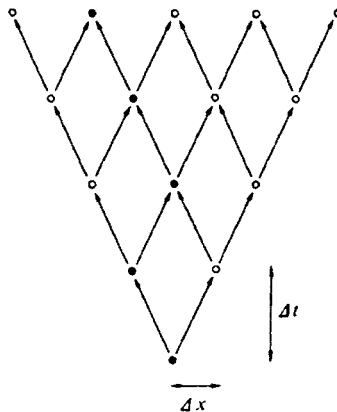


Fig 4 5 Concept of random walk model

can be readily defined.

A. two-dimensional fluid

When thermal energy of adsorbed molecules, RT , is bigger than the energy barrier between the sites, the adsorbed phase is considered to be two-dimensional fluid.

In this case, mean free path of the molecule, λ , is determined by

$$\lambda = 1/(2d\sigma) \quad (4-20)$$

where d is the diameter of molecule and σ represents the amount adsorbed. Velocity of thermal movement, v_t , is given as

$$v_t = (\pi kT/2M)^{1/2} \quad (4-21)$$

where k is the Boltzmann constant, T is the temperature and M denotes the molecular weight of the adsorbed species.

By taking $\Delta x = \lambda$ and $\Delta t = \lambda/v_t$, Eq. (4-19) gives the surface diffusivity as

$$D_s = (1/2) (1/2d\sigma) (\pi kT/2M)^{1/2} \quad (4-22)$$

Reported examples in actual systems are rare. This may be because diffusion of this type does not pose a significant problem in practical operations.

B. hopping model

When the energy barrier between neighboring adsorption sites is not negligible, the hopping of an adsorbed molecule from the site to the nearest vacant site is considered to be a unit step of the random walk.

In the simplest case, the lattice constant of the crystal which constitutes the adsorbent surface is taken as the hopping distance. The hopping frequency, $(1/\Delta t)$, is taken to be a reciprocal of the residence time of the molecule at the site. Then the following equation is derived from absolute rate theory.

$$1/\Delta t = 2\nu_x \exp(-E_s/RT) \quad (4-23)$$

where ν_x is the vibration of the adsorbed molecules and considered to be of the order of $10^{11} - 10^{13} \text{ sec}^{-1}$. E_s is the activation energy of hopping. Then D_s is given as

$$D_s = D_s' \exp(-E_s/RT) \quad (4-24)$$

$$D_s' = (\Delta x)^2 \nu_s \quad (4-25)$$

C. effect of surface coverage

When surface coverage cannot be neglected in considering the unit hopping, then modification of dx or dt becomes necessary. According to Higashi *et al.* (1963), when surface coverage is θ , a hopping molecule has to repeat random hopping until it finds an empty site. The expected number of hopping is a function of surface coverage.

$$n(\theta) = \sum k(1 - \theta) \theta^{k-1} = 1/(1 - \theta) \quad (4-26)$$

Namely, during a unit hopping time τ , n -time random walks will be tried. Since unit step is Δx , corresponding time should be taken as $\Delta t = \tau/n$. Then D_s becomes a simple function of the surface coverage as

$$D_s = D_{s0}/(1 - \theta) \quad (4-27)$$

Several improvements of this equation were tried. Yang *et al.* (1973) considered the effect of residence time of the hopping molecule after landing on the occupied site and before starting the next hopping. Then the effective surface diffusion coefficient is described as

$$D_s = D_{s0} \frac{1}{1 - \theta + \theta \frac{\nu_1}{\nu_2} \exp\{-(E_{s0} - E_{s1})/RT\}} \quad (4-28)$$

where E_{s0} and E_{s1} represent the activation energy of the diffusion of the molecules in the first layer and that in the second layer, respectively. ν_i represents the frequency of oscillation in the perpendicular direction to the surface in i -th layer. The dependence of D_s on the surface coverage θ by Eqs. (4-27) and (4-28) is shown in Fig. 4.6.

Okazaki *et al.* (1981) added the effect of multilayer adsorption. Final equation for the homogeneous surface is given as

$$D_s = D_{s0} \left(\frac{\theta_c}{\theta} \right) \frac{\exp\left(-\frac{E_{s0}}{RT}\right) - \exp\left(-\frac{Q_{st}}{RT}\right)}{\left[1 - \exp\left(-\frac{Q_{st}}{RT}\right)\right] \left[1 - \theta_c \left(1 - \frac{\tau_1}{\tau_0}\right)\right]} \quad (4-29)$$

where θ_c is the fractional coverage of the surface effective to the surface

diffusion and τ_0 and τ_1 represent the residence time of migrating molecule in the first adsorption layer and in the layers the second and above layers. τ_1/τ_0 is given as

$$\frac{\tau_1}{\tau_0} = \frac{\left[\exp\left(-\frac{E_{s0}}{RT}\right) - \exp\left(-\frac{Q_{st}}{RT}\right) \right] \left[1 - \exp\left(-\frac{\lambda_{vap}}{RT}\right) \right]}{\left[\exp\left(-\frac{E_{s1}}{RT}\right) - \exp\left(-\frac{\lambda_{vap}}{RT}\right) \right] \left[1 - \exp\left(-\frac{Q_{st}}{RT}\right) \right]} \quad (4-30)$$

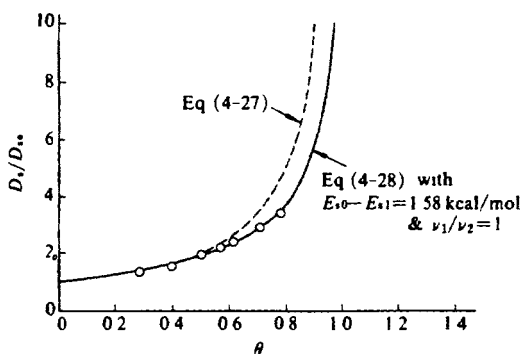


Fig 4.6 Comparison of Eqs (4-27) and (4-28) with the diffusion data of propane on silica glass at 35°C
(Reproduced with permission by Yang, R., *et al*, *AIChE Journal*, 19, 242 (1978))

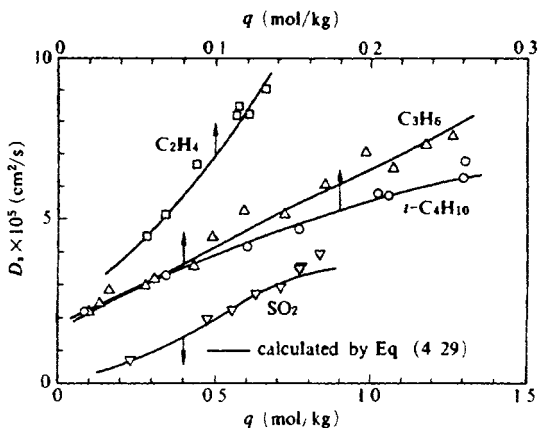


Fig 4.7 Surface diffusion coefficients on porous Vycor glass (30°C)
(Reproduced with permission by Okazaki, M., Tamon, H. and Toei, R., *AIChE Journal*, 27, 267 (1981))

Q_{st} and λ_{vap} are the heat of adsorption and the latent heat of vaporization, and E_{s0} and E_{s1} are the activation energies of transport at the first layer and at the second and above layers. E_{s1} is determined from temperature dependency of liquid viscosity of adsorbate and E_{s0} is considered to be proportional to Q_{st} as discussed in 4.3.3. Further, this model was extended to the case of heterogeneous surface, where energy distribution function is involved. Comparison of the model and the data on vycor glass is shown in Fig. 4.7.

4.3.2. Surface flow induced by surface pressure gradient

A. fundamental relation of surface diffusion

When there is a gradient of surface pressure, two-dimensional flow is expected to occur. Force balance in this case may be written as

$$d\pi = -u C_r dx \quad (4-31)$$

where u represents the average velocity of adsorbed species and C_r is the coefficient of friction between the adsorbed molecules and the adsorbent surface. Surface flow flux is written as

$$J_s = qu \quad (4-32)$$

Surface pressure is related to the partial pressure in gas phase by assuming local equilibrium to be

$$\begin{aligned} A_m d\pi &= (V/n) dp \\ &= RT d \ln p \end{aligned} \quad (4-33)$$

where A_m is an area occupied by unit adsorbed amount.

$$A_m = S/q \quad (4-34)$$

Then by comparing Eq. (4-15) and Eq. (4-32) and by using Eqs. (4-31), (4-33) and (4-34), corresponding surface diffusion coefficient is derived as

$$D_s = (qRT/SC_r) d \ln p / d \ln q \quad (4-35)$$

where S is the surface area of the adsorbent.

B. concentration dependence of D_s in surface pressure driving force model

From Eq. (4-35) it is expected that dependence of D_s on concentration or the amount adsorbed is determined from the adsorption isotherm relation since the following relation is expected provided C_r is independent of concentration.

$$D_s = \text{const. } q \, d \ln p / d \ln q \quad (4-36)$$

For instance, in the case of the Langmuir type isotherm, $d \ln p / d \ln q$ varies from unity at $q = 0$ to infinity at $q = q_0$ and D_s is expected to increase with increase of the amount adsorbed, q .

An example of this relation is given in Fig. 4.8 for gaseous phase adsorption of propane and butane on activated carbon pellets. D_s are well plotted in proportion to $q \, d \ln p / d \ln q$ determined from the isotherm relations.

C. diffusion of two components from surface pressure driving force model

Equilibrium relation for bi-component mixtures can be formulated by the ideal adsorbed solution model using surface pressure. This can be extended to describe the diffusion of bi-component mixtures.

Phenomenological relations of diffusion of component 1 and component 2 are written as

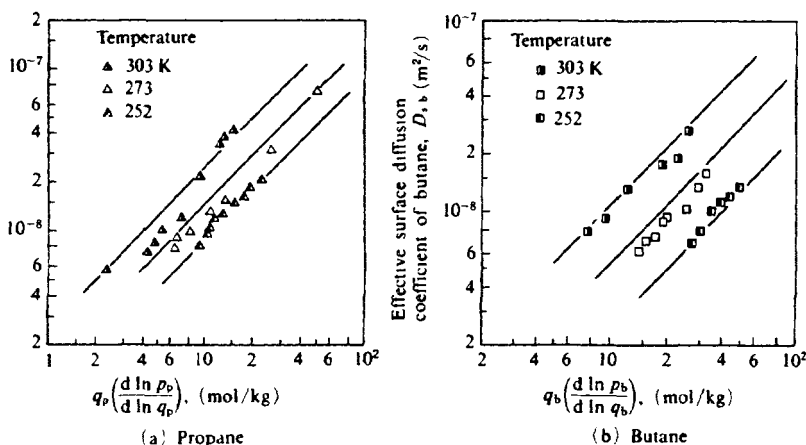


Fig 4.8 Effective surface diffusion coefficients of propane and butane in single component runs (a) Propane, (b) Butane
(Reproduced with permission by Suzuki, M., Hori, M and Kawazoe, K., *Fundamentals of Adsorption*, p 624, Engineering Foundation, NY (1985))

$$J_1 = -\rho_p D_{s,11} dq_1/dx - \rho_p D_{s,12} dq_2/dx \quad (4-37)$$

$$J_2 = -\rho_p D_{s,21} dq_1/dx - \rho_p D_{s,22} dq_2/dx \quad (4-38)$$

Assuming that surface flow of both component 1 and component 2 occurs by the gradient of the total surface pressure determined from the equilibrium relation, the final corresponding equations of J_i ($i=1$ or 2) are derived as

$$J_i = -(\rho_p/C_n) q_i (d\pi/dx) \quad (4-39)$$

$$= -(\rho_p/C_n)(RT/A) \frac{1}{L} \left\{ \int_0^{q_1} q_1 \frac{\partial \ln p_1}{\partial \ln q_1} dq_1 + \int_0^{q_2} q_2 \frac{\partial \ln p_2}{\partial \ln q_2} dq_2 \right\} \quad (4-40)$$

Then $D_{s,n}$ and $D_{s,i}$ are related as

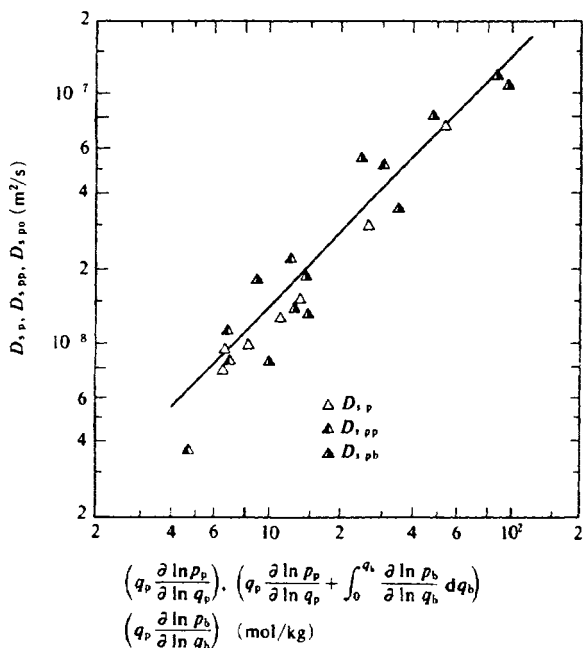


Fig 49(a) Comparison of effective surface diffusion coefficients of propane $D_{s,p}$ for single-component system and $D_{s,pp}$ and $D_{s,pb}$ for two-component system

(Reproduced with permission by Suzuki, M., Hori, M. and Kawazoe, K., *Fundamentals of Adsorption*, Engineering Foundation, 626 (1985))

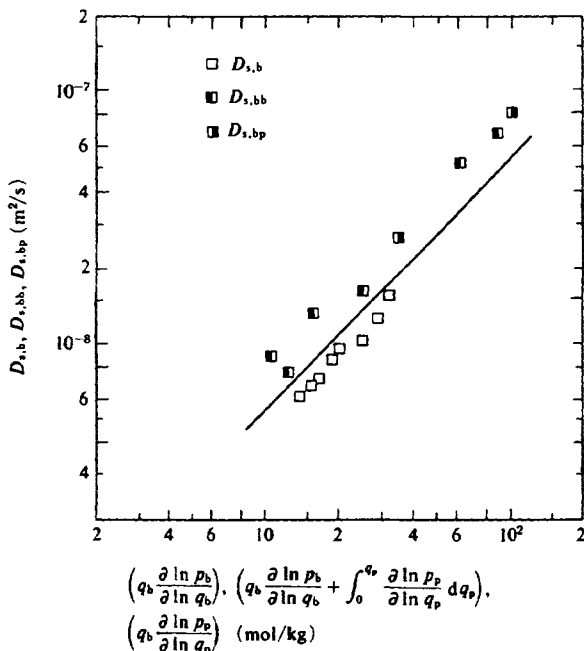


Fig. 4.9.(b) Comparison of effective surface diffusion coefficients of butane, $D_{s,b}$ for single-component system and $D_{s,bb}$ and $D_{s,bp}$ for two-component system.

(Reproduced with permission by Suzuki, M., Hori, M. and Kawazoe, K., *Fundamentals of Adsorption*, Engineering Foundation, 626 (1985).

$$D_{s,i} = \frac{RT}{AC_n} \left\{ q_i \frac{\partial \ln p_i}{\partial \ln q_i} + \int_0^{q_i} \frac{\partial \ln p_j}{\partial \ln q_j} dq_j \right\} \quad (4-41)$$

$$D_{s,ij} = (RT/AC_n)(q_i \partial \ln p_j / \partial \ln q_j) \quad (4-42)$$

The above relations are verified by comparing $D_{s,i}$ and $D_{s,ij}$ with $q_i \frac{\partial \ln p_i}{\partial \ln q_i} + \int_0^{q_i} \frac{\partial \ln p_j}{\partial \ln q_j} dq_j$ and $q_i \partial \ln p_j / \partial \ln q_j$ respectively in Fig. 4.9.

In the figure, D_s from single-component runs are also included. All the results are correlated by a single straight line of slope = 1, suggesting that the surface pressure driving force with the specific resistance coefficient for each component is acceptable in the case of co-diffusion of propane and butane on activated carbons.

4.3.3. Activation energy of surface diffusion

A. activation energy and heat of adsorption

It is natural to consider the activation energy of surface migration as being proportional to the heat of adsorption.

$$E_s = aQ_{st} \quad (4-43)$$

Sladek *et al.* (1974) correlated the data of the surface diffusion coefficient in the literature, as shown in Fig. 4.10. They correlated gas phase data of many combinations of adsorbates and adsorbents including chemical adsorption by defining the proportionality constant a as shown in TABLE 4.3.

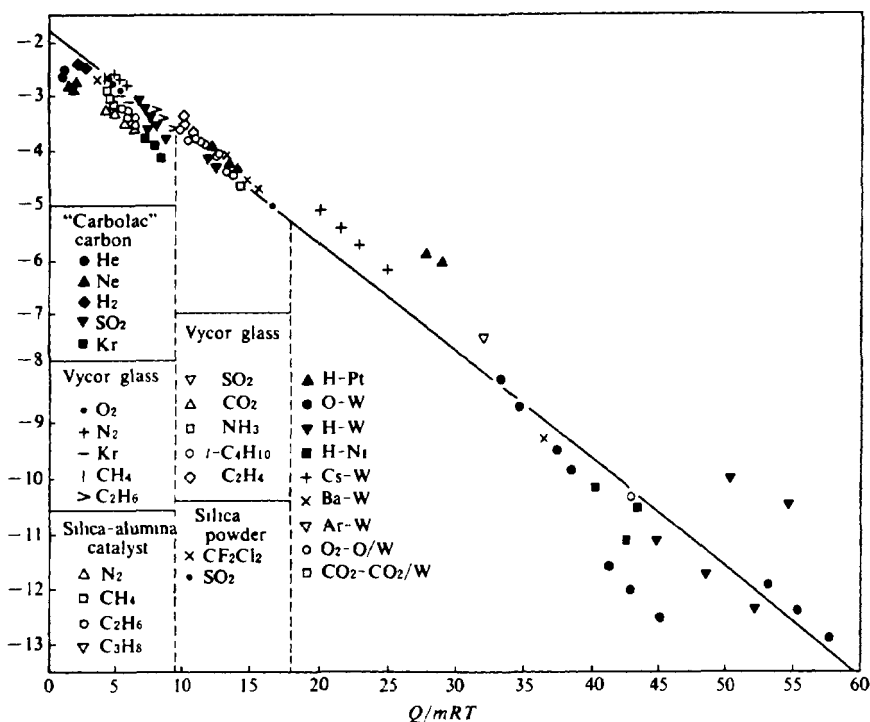


Fig 4.10 Surface diffusion coefficient plotted against heat of adsorption (Reproduced with permission by Sladek, J., Gilliland, R. and Baddour, F., *Ind Eng Chem Fund.* 13, 104 (1974))

Suzuki and Kawazoe (1975) measured the effective surface diffusion coefficients of various volatile organics during aqueous phase adsorption on activated carbon pellets and correlated the data using the boiling

TABLE 4.3 Value of m Determined from Type of Binding Between Molecule and Solid Surface

Binding	Solid	m	Examples
van der Waals			
Polar molecule	{ Conductive	2	SO ₂ -Carbon
	{ Insulative	1	SO ₂ , NH ₃ -Glass
Nonpolar molecule	{ Conductive	1	Ar-W, N ₂ -Carbon
	{ Insulative	1	Kr, C ₂ H ₄ -Glass
Ionic	{ Conductive	2	Cs, Ba-W
	{ Insulative	1	—
Covalent	{ Conductive	3	H-Metal, O-W
	{ Insulative	1	—

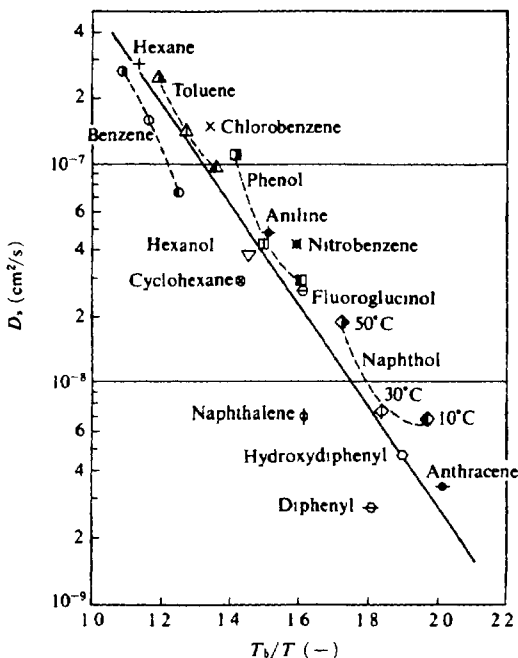


Fig 4 11 Plots of the effective surface diffusion coefficient against T_b/T for fifteen volatile organics. T_b , boiling point of adsorbate (K), T adsorption temperature (K)
(Reproduced with permission by Suzuki, M and Kawazoe, K, *J Chem Eng Japan*, 8, 381 (1975))

point of the organics as representative properties as shown in Fig. 4.11.

$$D_s = D_{s0} \exp(-bT_b/T) \quad (4-44)$$

where

$$D_{s0} = 1.1 \times 10^{-4} \text{ cm}^2/\text{s} \quad (4-45)$$

$$b = 5.38 \quad (4-46)$$

The above equation is related to the conventional Arrhenius form by considering the activation energy E_s as

$$E_s = RbT_b \quad (4-47)$$

By considering Trouton's rule,

$$\lambda_{\text{vap}} = 21T_b \quad (4-48)$$

Eq. (4-47) means that E_s is about half the heat of vaporization.

D_{s0} is related to characteristics of activated carbons if hopping distance, l , is considered to be in a two-dimensional direction and time constant of vibration, τ , is considered to be 5×10^{-14} s. The effective surface diffusion coefficient also includes the tortuosity of diffusing path and $k^2 = 3$ is taken as a first approximate. Then the estimated D_{s0} is given as

$$D_{s0, \text{hop}} = l^2 / (6\tau) / k^2 \approx 1 \times 10^{-4} \text{ cm}^2/\text{s} \quad (4-49)$$

This is in good agreement with Eq. (4-45).

B. surface diffusion on heterogeneous surface

In the case of adsorption on heterogeneous surface, energy distribution may result in change of activation energy with increase of amount adsorbed. Assuming that the local activation energy is proportional to the local heat of adsorption as follows, the dependence of the surface diffusion coefficient on the amount adsorbed can be described.

$$E_s(q) = aQ_s(q) \quad (4-50)$$

$$D_s(q) = D_{s0} \exp(E_s(q)/RT) \quad (4-51)$$

In the case of Freundlich isotherm systems, the heat of adsorption is given as Eq. (3-41) or

$$Q_{st}(q) = -Q_0 \ln(a_0 q) \quad (4-52)$$

Combining Eqs. (4-50)-(4-52) gives

$$D_s = D_{s0} \exp\{-(Q_0/RT) \ln(a_0 q)\} \quad (4-53)$$

or

$$D_s = D_{s0}(a_0 q)^{n_F} \quad (4-54)$$

where n_F is the reciprocal exponent of the Freundlich isotherm and equal to Q_0/RT . The Eq. (4-54) relation is compared with experimental results obtained for surface diffusion measurement of propionic acid aqueous solution on activated carbon pellet in Fig. 4.12.

When decrease of the heat of adsorption is proportional to the

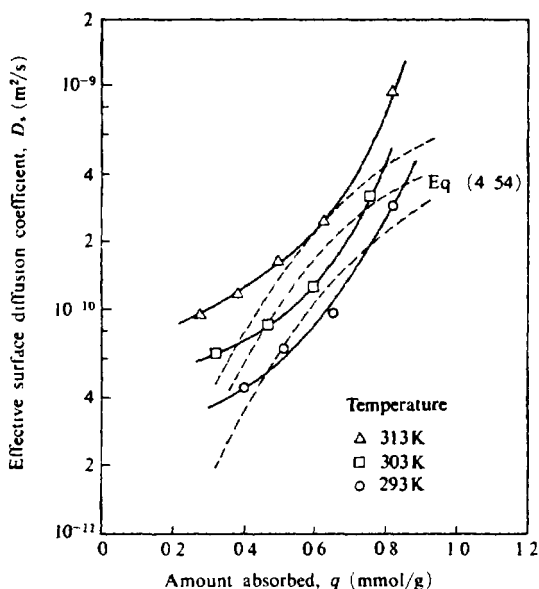


Fig. 4.12 Surface diffusion coefficient of propionic acid on activated carbon plotted against amount adsorbed
(Reproduced with permission by Suzuki, M and Fuzii, T, *AIChE Journal*, 28, 383 (1982))

amount adsorbed as in the case of the Temkin isotherm (Neretnieks, 1976),

$$Q_s(q) = Q_s - Aq \quad (4-55)$$

then the dependence of D_s is formulated as

$$D_s = D_{s0} \exp(aAq) \quad (4-56)$$

This may explain the results obtained by Sudo *et al.* (1978) for aqueous phase adsorption of chlorophenols and two other compounds on activated carbons.

$$D_s = D_{s0} \exp(0.88q) \quad (4-57)$$

The above results are shown in Fig. 4.13 with TABLE 4.4.

4.3.4. Parallel contribution of surface diffusion and pore diffusion

When contributions of both pore diffusion and surface diffusion are of the same order of magnitude, the total flux can be written as

$$J = -(D_p dp/dx + D_s \rho dq/dx) \quad (4-58)$$

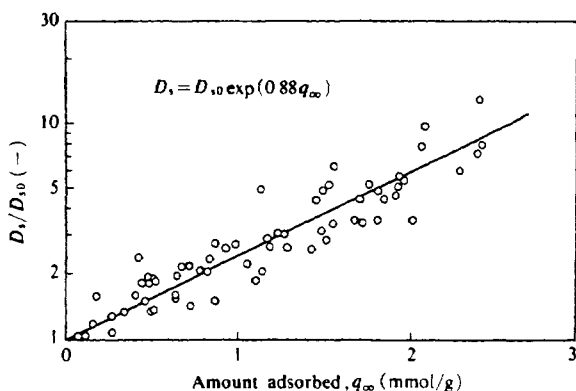


Fig. 4.13. D_s/D_{s0} vs the amount of adsorbed organics, q_{∞}
(Reproduced with permission by Sudo, Y., Misic, M. and Suzuki, M., *Chem Eng Sci*, 33, 1289 (1978))

TABLE 4.4 Equilibrium Constants and Rate Results

Adsorbate	Constants in Eq (3-10) n_F	k_F [(g/g)/(mg/l) ¹⁻ⁿ]	Range of q_m (mmol/g)	D_{s0} (cm ² /s)	D_s estimated from Eq (4-44) (cm ² /s)
<i>o</i> -chlorophenol	5	0.090	0.44-2.40	1.7×10^{-8}	3.4×10^{-8}
<i>m</i> -chlorophenol	5	0.059	0.27-1.85	1.9×10^{-8}	1.7×10^{-8}
<i>p</i> -chlorophenol	5	0.098	0.48-2.40	1.5×10^{-8}	1.6×10^{-8}
dichlorophenol	5.5	0.084	0.47-1.71	1.5×10^{-8}	1.8×10^{-8}
β -chloropropionic acid	3	0.092	0.10-1.10	5.4×10^{-8}	2.0×10^{-8}
benzoic acid	4	0.068	0.44-2.42	1.4×10^{-8}	1.2×10^{-8}

(Reproduced with permission by Sudo, Y, *et al Chem Eng Sci*, 33, 1289 (1978))

where local adsorption equilibrium is assumed and ρ represents the particle density.

For practical purposes, the apparent diffusion coefficient is sometimes defined and used.

$$J = -D_p^* dp/dx \quad (4-59)$$

where D_p^* represents the apparent pore diffusion coefficient defined by taking dp/dx as the imaginary driving force of diffusion.

$$D_p^* = D_p + D_s \rho (dq/dp) \quad (4-60)$$

The apparent pore diffusion coefficient thus depends on pressure or the amount adsorbed since dq/dp is not constant in nonlinear isotherm systems.

Also, if the apparent surface diffusion coefficient D_s^* is defined in terms of dq/dx , then D_s^* is related to D_p and D_s as follows.

$$J = -D_s^* \rho dq/dx \quad (4-61)$$

$$D_s^* = D_s + D_p (1/\rho) (dp/dq) \quad (4-62)$$

Depending on the relative magnitude of D_p and $D_s \rho (dq/dp)$, either D_p^* or D_s^* becomes more independent of concentration in the range of operation conditions concerned, but it is difficult to predict which is more practical for approximate treatment.

4.4. Micropore Diffusion

Diffusion of molecules which are similar in size to the size of the pores is very restricted because of the effect of potential field of the wall atoms. Diffusion in molecular sieve materials is often of this type. Diffusion in this case is accompanied by relatively large activation energy and can be correlated by assuming that the driving force of diffusion is the chemical potential gradient. Ordinarily, diffusion coefficient is defined in terms of amount adsorbed, q , similar to the case of surface diffusion.

Micropore diffusion coefficients, D_c , measured by chromatographic method for many gases in molecular sieving carbon are shown in Fig. 4.14. The activation energies, E_a , are determined from the slopes of the Arrhenius plots of the diffusion coefficients.

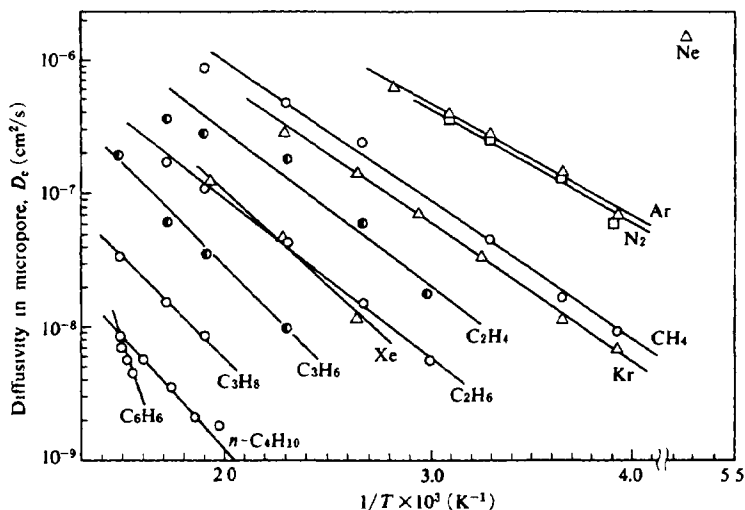


Fig. 4.14. Arrhenius' plot of diffusivities in micropore (Reproduced with permission by Chihara, K., Suzuki, M. and Kawazoe, K., *AIChE Journal*, 24, 243 (1978)).

TABLE 4.5 Parameters of Equilibrium Relations and Diffusion in Molecular Sieving Carbon, MSC 5

Gas	Q_{st} [kcal/mol]	$(K^0/T)_{1/T \rightarrow 0}$ [cm ³ /g·K]	E_a [kcal/mol]	D_{c0} [cm ² /s]
CH ₄	5.7	1.1×10^{-5}	4.8	1.3×10^{-4}
C ₂ H ₄	8.5	3.9×10^{-6}	5.3	6.4×10^{-5}
C ₂ H ₆	9.0	3.0×10^{-6}	5.5	2.3×10^{-5}
C ₃ H ₆	11.4	1.6×10^{-6}	7.0	3.4×10^{-5}
C ₃ H ₈	11.7	1.2×10^{-6}	7.0	6.8×10^{-6}
n-C ₄ H ₁₀	13.9	7.1×10^{-7}	7.8	3.0×10^{-6}
C ₆ H ₆	21.8	1.3×10^{-8}	21.4	8.4×10^{-2}
Ne	1.1	1.1×10^{-4}	—	—
Ar	4.0	3.0×10^{-5}	3.9	1.7×10^{-4}
Kr	5.6	1.5×10^{-5}	4.8	8.4×10^{-5}
Xe	7.8	8.3×10^{-6}	6.5	7.2×10^{-5}
N ₂	4.5	1.3×10^{-5}	3.9	1.5×10^{-4}
He				

(Reproduced with permission by Chihara, K., Suzuki, M. and Kawazoe, K., *AIChE Journal*, 24, 242 (1978))

$$D_c = D_{c0} \exp(-E_a/RT) \quad (4-63)$$

These values are listed in TABLE 4.5 together with the equilibrium

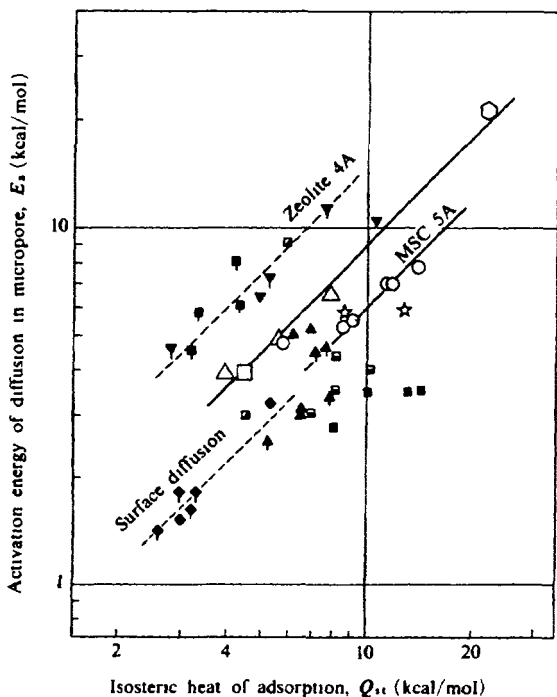


Fig 4.15 Correlation of activation energy of the micropore diffusion with isosteric heat of adsorption
(Reproduced with permission by Chuhara, K. *et al.*, *AIChE Journal*, 24, 243 (1978))

parameters.

4.4.1. Activation energy of micropore diffusion

The activation energy thus determined is compared with the heat of adsorption for each gas obtained by van't Hoff plot (Fig. 3.12) in Fig. 4.15. The activation energy for rare gases, methane and benzene and for hydrocarbons except methane have different proportionality constants to the isosteric heat of adsorption, Q_{st} .

In the figure, the measurement for zeolite 4A where more restricted micropore diffusion is expected is included and the relation for the case of surface diffusion is also shown. For the latter, a becomes about 0.5 while a larger than unity value for a is observed for the former.

For molecular sieving materials such as molecular sieving carbon, zeolite 4A and 5A, Ruthven compared the activation energy of diffusion

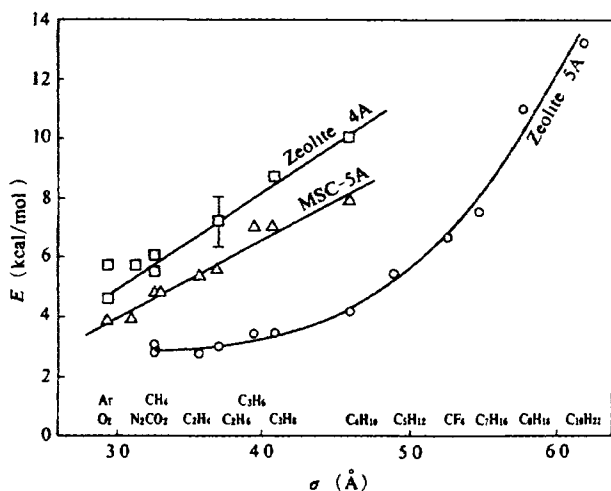


Fig 4.16 Variation of diffusional activation energy with van der Waals diameter for diffusion in 4 Å and 5 Å zeolites and 5 Å molecular sieve carbon (Reproduced with permission by Ruthven, M, *Principles of Adsorption and Adsorption Processes*, p 148, John Wiley and Sons, New York (1985))

of various gases with the van der Waals diameters of the gases as shown in Fig. 4.16.

4.4.2. Physical interpretation of D_c

Adsorbate molecules in the micropores are considered to be on the adsorption sites. These molecules move from site to site across the potential energy barrier. Diffusivity for the activated diffusion can be interpreted by means of the absolute rate theory (Hill, 1960).

$$D_c = Ca^2/\tau \quad (4-64)$$

$$1/\tau = (M^*/M)\nu_x \exp(-V_0/kT) \quad (4-65)$$

where C is a constant depending on the lattice configuration and the tortuosity of the pore, a is the distance between nearest neighboring sites, τ is the mean time a molecule spends at a site between successive jumps, M^*/M represents the ratio of the number of activated states to the number of sites which depends on the lattice type, ν_x is the frequency of vibration of a molecule at a site parallel to the surface. V_0 is the activation energy per unit molecule, k is the Boltzmann constant and T

is the absolute temperature.

The potential energy distribution function in the micropore of activated carbon can be assumed to be two-dimensional sinusoidal as follows:

$$U_0(x, y) = U_\infty + \frac{1}{2}V_0\left(1 - \cos \frac{2\pi x}{a}\right) + \frac{1}{2}V_0\left(1 - \cos \frac{2\pi y}{a}\right) \quad (4-66)$$

where $U_0(x, y)$ is the potential energy at position (x, y) and U_∞ is the minimum potential energy. Then the molecules vibrate around the minima in $U_0(x, y)$ with frequency

$$\nu_x = \nu_y = (V_0/2ma^2)^{1/2} \quad (4-67)$$

where m denotes the mass of a molecule. By comparing Eqs. (4-64, 65, 67) with Eq. (4-63), the pre-exponential factor D_{e0} is derived as

$$D_{e0} = Ca^2(M^*/M)(V_0/2ma^2)^{1/2} \quad (4-68)$$

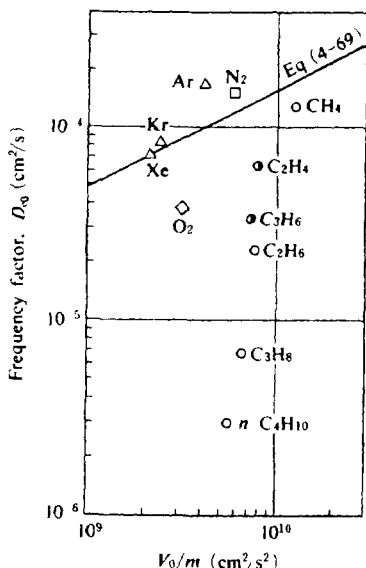


Fig. 4-17 Dependence of the frequency factor, D_0 , on the activation energy per unit mass of molecule (V_0/m). D_{e0} are from Table 4.5. (Reproduced with permission by Chihara, K. and Suzuki, M., *J. Colloid. Int. Sci.*, 64, 585 (1978))

The above equation suggests that D_{e0} is directly determined from the activation energy provided lattice structure constants are given.

By taking $C = (1/3)/3$, $a = 1.34 \text{ \AA}$ and $M^*/M = 3/2$ and by considering the tortuosity factor for micropores as 3, D_{e0} is written as

$$D_{e0} = 3.23 \times 10^{-4} (E_s/M)^{1/2} \quad (4-69)$$

where D_{e0} is given in cm^2/s if E_s is given in kcal/mol and M in g/mol . Fig. 4.17 compares D_{e0} determined from chromatographic measurement with the theoretical calculation by using Eq. (4-69) where the activation energy is given on the basis of unit mass of molecule. Apparently agreement is satisfactory for Ar, Kr, Xe, N_2 and CH_4 . The other gases especially hydrocarbons with carbon number larger than two show poor coincidence probably because they do not behave like a solid sphere in micropores, which is implicitly assumed in deriving Eq. (4-68).

4.4.3. Interpretation of concentration dependence of micropore diffusion coefficient in terms of chemical potential driving force model

When the driving force of diffusion is taken as the slope of the chemical potential, then by using mobility, B , flux can be described as

$$J = -Bq d\mu/dx \quad (4-70)$$

chemical potential μ is

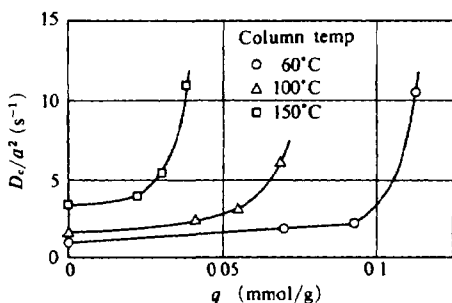


Fig 4 18. (a) Dependence of diffusivity on amount adsorbed at 60, 100 and 150°C (Reproduced with permission by Kawazoe, K. *et al.*, *J Chem. Eng Japan*, 7, 151 (1974))

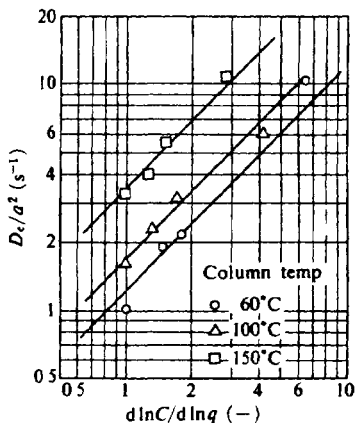


Fig 4 18 (b) Plots of D_c/a^2 versus $d \ln C/d \ln q$
 (Reproduced with permission by Chihara, K *et al*, *J Chem Eng Japan*, 11, 155 (1978))

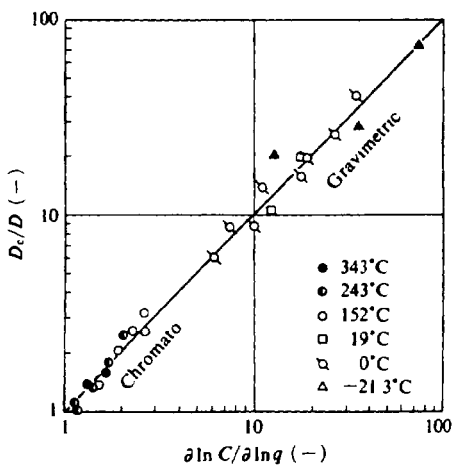


Fig. 4 18 (c) Correlation of micropore diffusivity with $\partial \ln C/\partial \ln q$ Source Chihara and Suzuki, *J Chem Eng Japan*, 11, 153 (1978)

$$\mu = \mu' \pm RT \ln a = \mu'' \pm RT \ln p \quad (4-71)$$

Thus

$$J = -BRTq \frac{d \ln p}{dx} \quad (4-72)$$

Then by comparison with Fick's law

$$D_c(q) = D_0 \frac{d \ln p/d \ln q}{d \ln q} \quad (4-73)$$

where $D_0 = BRT$. At lower coverage where Henry's law is expected, $d \ln p/d \ln q = 1$ holds and then $D_c = D_0$ is expected

Eq. (4-73) looks similar to Eq. (4-36) except that surface pressure driving force assumption gives larger dependence of amount adsorbed, since $d \ln p/d \ln q$ usually increases with increasing amount adsorbed, q .

Concentration dependence of micropore diffusion coefficient of propylene on molecular sieving carbon was obtained by Chihara and Suzuki (1978). The results are well interpreted by this concept as shown in Fig. 4.18.

For diffusion in other microporous adsorbents, such as zeolites, concentration dependence is often successfully explained by this model (Ruthven, 1985)

REFERENCES

- Bosanquet, C H, *British TA Report BR 507*, Sept 27 (1944)
- Burger, H C, cited in D A de Vries, *Trans IVth Congress Intern Assoc Soil Science*, Vol II, 41 (1950)
- Carman, P C and F A Raal, *Proc Roy Soc*, **201a**, 38 (1951)
- Chihara, K and M Suzuki, *Carbon*, **17**, 339 (1979)
- Chihara, K and M Suzuki, *J Chem Eng Japan*, **11**, 153 (1978)
- Chihara, K and M Suzuki, *J Colloid Interfacial Sci*, **64**, 584 (1978)
- Chihara, K, M Suzuki and K Kawazoe, *AIChE Journal*, **24**, 237 (1978)
- Currie, J A, *Brit Appl Phys*, **11**, 314 (1960)
- Edwards, M. F and J F Richardson, *Chem Eng Sci*, **23**, 109 (1968)
- Evans, E V and C N Kenney, *Trans Inst Chem Engrs*, **44**, T189 (1966)
- Gilliland, E R, R F Baddour and J L Russell, *AIChE Journal*, **4**, 90 (1958)
- Higashi, K, H Ito and J Oishi, *J Atomic Energy Soc Japan*, **5**, 846 (1963)
- Hill, T L, *Introduction to Statistical Thermodynamics*, p 198-200, Addison-Wesley Reading, Mass (1960)
- Hirschfelder, J O, C F Curtiss and R B Bird, *Molecular Theory of Gases and Liquids* John Wiley and Sons New York (1964)
- Hoogschagen, J, *Ind Eng Chem*, **47**, 906 (1955)
- Kawazoe, K, I Sugiyama and Y Fukuda, *Kagaku Kogaku*, **30**, 1008 (1966) (in Japanese)

- Kawazoe, K, M Suzuki and K Chihara, *J Chem Eng Japan*, 7, 151 (1974)
Neretnieks, I, *Chem Eng Sci*, 31, 1029 (1976)
Okazaki, M, H Tamon and R Toei, *AIChE Journal*, 27, 262 (1981)
Ruthven, D M, *Principles of Adsorption & Adsorption Processes*, John Wiley and Sons, New York (1984)
Satterfield, C N, C K Colton and W N Pitcher Jr, *AIChE Journal*, 19, 628 (1973)
Sladek, K J, E R Gilliland and R F Baddour, *Ind Eng Chem Fundamentals*, 13, 100 (1974)
Sudo, Y, D M Mistic and M Suzuki, *Chem. Eng Sci*, 33, 1287 (1978)
Suzuki, M and T Fujii, *AIChE Journal*, 28, 380 (1982)
Suzuki, M and K Kawazoe, *J Chem. Eng Japan*, 8 (1975)
Suzuki, M and K Kawazoe, *J Chem Eng Japan*, 7, 346 (1974)
Suzuki, M and J M Smith, *The Chemical Engineering Journal*, 3, 256 (1972)
Suzuki, M, T Kawai and K Kawazoe, *J Chem Eng Japan*, 8, 203 (1975)
Suzuki, M, M Horii and K Kawazoe, *Fundamentals of Adsorption*, p 624, Eng Foundation, NY (1985)
Wakao, N and J M Smith, *Chem Eng Sci*, 17, 825 (1962)
Wooding, R A, *Proc Roy Soc A* 252, 120 (1959)
Yang, R T, J B Fenn and G L Haller, *AIChE Journal*, 19, 1052 (1973)

Kinetics of Adsorption in a Vessel

When adsorption takes place with suspended adsorbent particles in a vessel, adsorbate is transported from the bulk fluid phase to the adsorption sites in the adsorbent particle. In this type of situation, changes in the amount adsorbed or concentration in the fluid phase can be predicted by solving the set of differential equations describing the mass balances in the particle, at the outer surface and between the particle and the fluid phase.

In this chapter the adsorption uptake relations are shown for several typical situations. These are applicable to batch adsorption in a liquid stirred tank, batch measurement of gas adsorption by gravity method or by pressure method as shown in Fig 5.1. Also adsorption in a shallow bed is a typical example of application of the treatment for batch adsorption with continuous flow (Fig 5.2).

5.1 Fundamental Relations

Basic equations to describe adsorption uptake phenomena in vessels consist of a set of the following mass balance equations. a diffusion equation to describe the mass balance in a particle, mass balance at the surface of the particle, global mass balance in a vessel.

Mass balance at a point in the particle is given as

$$\rho_p D_s \nabla^2 q + D_p \nabla^2 c = \rho_p \partial q / \partial t \quad (5-1)$$

where D_s and D_p respectively denote the effective surface diffusion coefficient and the effective pore diffusion coefficient in the particle. ρ_p represents the particle density. The amount adsorbed, q , and the concentration in the pore, c , are considered to be in local equilibrium

$$q = q(c) \quad (5-2)$$

Mass balance at the surface of the particle is given by introducing mass

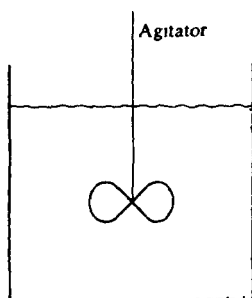


Fig 5 1 Batch adsorption in an agitated tank

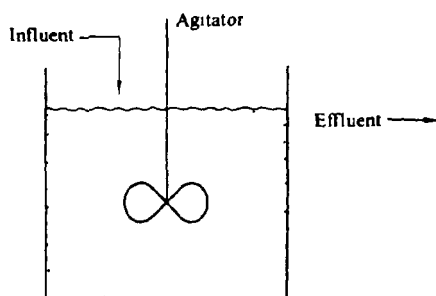


Fig 5 2 Continuous flow adsorption in an agitated tank

transfer resistance of the diffusion boundary layer developing on the particle surface

$$N_s = k_f(C - c_s) = D_s \rho_p \frac{\partial q}{\partial r} + D_p \frac{\partial c}{\partial r} \quad (5-3)$$

where N_s is the mass flux per unit surface area of the particle, which corresponds to the increase of the amount adsorbed in the particle when multiplied by the total external surface area of the particles

$$N_s A_s = W_s \frac{\partial q_{av}}{\partial t} \quad (5-4)$$

where W_s represents the weight of the adsorbent and A_s is the external surface area of the adsorbents. The amount adsorbed expressed by q_{av} is the integral average of the amount adsorbed in the particle

$$q_{av} = \frac{\int_0^R (4\pi r^2 q) dr}{4\pi R^3 / 3} \quad (5-5)$$

Fluid to particle mass transfer coefficient k_f is determined from fluid dynamic conditions as well as diffusion property of the fluid.

Mass balance in the vessel of the volume, V , is given as

$$VdC/dt = -W_s dq_{av}/dt \quad (5-6)$$

for a batch adsorption.

When adsorption occurs in the vessel with continuous flow of fluid, then the mass balance equation becomes

$$VdC/dt = F(C_{in} - C) - W_s dq_{av}/dt \quad (5-7)$$

Adsorption equilibrium equation relates the amount adsorbed, q , and the concentration, c , in the particle. F represents the flow rate of fluid.

In the following discussion, the Freundlich equation is adopted as an example of nonlinear adsorption equilibrium relation.

$$q(c) = k_{FC}^{1/n} \quad (5-8)$$

Employing a two-parameter equation such as this may be justified for two reasons: 1) it is enough to describe a nonlinear isotherm in a limited concentration range for practical purposes, and 2) mathematical simplicity.

5.2. Batch Adsorption with a Constant Concentration of Surrounding Fluid

When adsorption takes place in a large vessel, the concentration in the vessel is regarded as being constant throughout the progress of adsorption so the solution of Eqs. (5-1)-(5-3) with constant concentration in the fluid phase, C , can be obtained rather easily.

The rate processes involved in this case are mass transfer between fluid and particle and intraparticle diffusion. First cases involving a single rate-determining step are considered followed by cases in which both steps must be accounted for.

5.2.1. Intraparticle diffusion controlling—Pore diffusion

When pore diffusion is the only rate controlling step, the governing equations for batch kinetics in the infinite vessel (constant surface concentration) is Eq (5-1), where surface diffusion terms are neglected.

$$D_p \nabla c = \rho_p \partial q / \partial t \quad (5-9)$$

with the boundary condition

$$c = C_0 \quad \text{at} \quad r = R_p \quad (5-10)$$

when the Freundlich isotherm is adopted, the above equations are to be solved numerically. First, the basic equation is written in a dimensionless form as follows.

$$\partial^2 X / \partial \rho^2 + (2/\rho) \partial X / \partial \rho = \partial Y / \partial \tau \quad (5-11)$$

where

$$X = c / C_0 \quad (5-12)$$

$$Y = q / q_0 \quad (5-13)$$

$$\rho = r / R_p \quad (5-14)$$

$$\tau = (D_p t / R_p^2) (C_0 / \rho q_0) \quad (5-15)$$

with the initial and boundary conditions as

$$X = 0 \quad \text{and} \quad Y = 0 \quad \text{at} \quad \tau = 0 \quad (5-16)$$

$$X = 1 \quad \text{at} \quad \rho = 1 \quad \text{for} \quad \tau > 0 \quad (5-17)$$

For deriving dimensionless parameters, the amount adsorbed in equilibrium with C_0 , q_0 is introduced as a reference value.

$$q_0 = k_F C_0^{1/n} \quad (5-18)$$

Then the uptake curve q/q_0 versus dimensionless adsorption time τ is obtained as shown in Fig. 5.3, where the Freundlich constant n is a parameter.

In the case of a linear isotherm (the Freundlich isotherm with $n=1$), the analytical solution (Crank, 1975) is given as

$$q/q_0 = 1 - 6/\pi^2 \sum_{n=1}^{\infty} (1/n^2) \exp(-n^2 \pi^2 \tau) \quad (5-19)$$

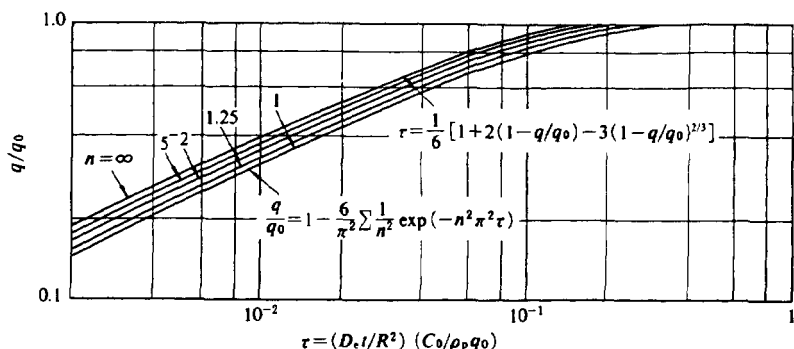


Fig. 5.3. Uptake curve q/q_0 versus $\tau = (D_e t / R^2)(C_0 / \rho_p q_0)$ pore diffusion controlling in infinite bath.

(Reproduced with permission by Suzuki, M. and Chihara, K., *Seisan Kenkyu*, 34, 152 (1982)).

Also, for the case of the irreversible isotherm which is considered to be the Freundlich isotherm with the constant $n = \infty$, the analytical solution of the shell model (Yagi and Kunii, 1953) can be applied as shown by Suzuki and Kawazoe (1974).

$$\tau = (1/6)(1 + 2(1 - q/q_0) - 3(1 - q/q_0)^{2/3}) \quad (5-20)$$

These equations are included in Fig. 5.3.

Apparently, the uptake curves in the range of q/q_0 below 0.3, can be approximated by the equation of the form

$$q/q_0 = A \cdot \sqrt{\tau} \quad (5-21)$$

As a matter of fact, Eqs. (5-19) and (5-20) respectively reduce to

$$q/q_0 = (6/\sqrt{\pi}) \cdot \sqrt{\tau}, \text{ for a linear isotherm } (n=1) \quad (5-22)$$

$$q/q_0 = \sqrt{18} \cdot \sqrt{\tau}, \text{ for a rectangular isotherm } (n=\infty) \quad (5-23)$$

For intermediate values of n , A is given as a function of the Freundlich constant n as shown by Suzuki and Chihara (1982) in Fig. 5.4. The interpolation may be possible as

$$A = (1 - 1/n)\sqrt{18} + 6/(n\sqrt{\pi}) \quad (5-24)$$

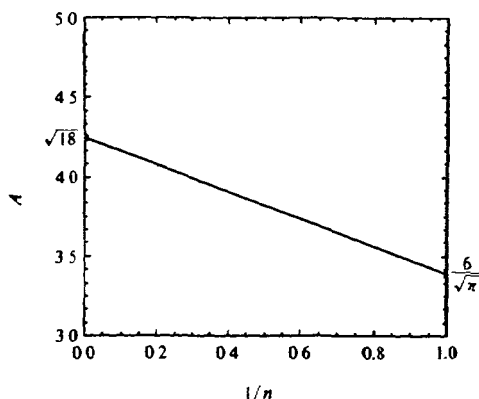


Fig. 5.4. Illustration of Eq. (5-24).

5.2.2. Intraparticle diffusion controlling—Surface diffusion

When surface diffusion is dominant in the particle, the governing equation becomes

$$D_s \rho_p \nabla^2 q = \rho_p \frac{\partial q}{\partial t} \quad (5-25)$$

with the boundary condition as

$$q = q_0 \quad \text{at} \quad r = R_p \quad (5-26)$$

where q_0 is given by Eq. (5-18).

By defining dimensionless time, τ_s , as

$$\tau_s = D_s t / R_p^2 \quad (5-27)$$

dimensionless form of the above equations become

$$\frac{\partial^2 Y}{\partial \rho^2} + \frac{2}{\rho} \frac{\partial Y}{\partial \rho} = \frac{\partial Y}{\partial \tau_s} \quad (5-28)$$

with the initial and boundary conditions as

$$Y = 0 \quad \text{at} \quad \tau_s = 0 \quad (5-29)$$

$$Y = 1 \quad \text{at} \quad \rho = 1 \quad \text{for} \quad \tau_s > 0 \quad (5-30)$$

In this case the analytical solution is possible regardless of nonlinearity of the isotherm relations. The solution becomes identical to Eq. (5-19) except that nondimensional adsorption time, τ_s , defined by Eq. (5-27), should be used instead of τ .

5.2.3. External mass transfer controlling

When fluid-to-particle mass transfer is a rate-determining step, the basic equations are greatly simplified, since concentration in the particle is assumed to be uniform.

$$k_f A (C - c_s) = W_s dq/dt \quad (5-31)$$

where the amount adsorbed on solid phase, q , is in equilibrium with the surface concentration, c_s , as

$$q = k_F c_s^{1/n} \quad (5-32)$$

and the initial conditions are

$$q = 0, \quad c_s = 0 \quad \text{at} \quad t = 0 \quad (5-33)$$

$$C = C_0 \quad \text{for} \quad t > 0 \quad (5-34)$$

Dimensionless form of the above equation becomes

$$3dY/d\tau_f = 1 - X^* \quad (5-35)$$

with the initial condition

$$X = 0, \quad Y = 0 \quad \text{at} \quad \tau_f = 0 \quad (5-36)$$

where

$$\tau_f = (k_f t / R_p)(C_0 / \rho_p q_0) \quad (5-37)$$

and q_0 is given by Eq. (5-18).

In the case of a linear isotherm, the analytical solution is easily obtained as

$$q/q_0 = 1 - \exp(-3\tau_f) \quad (5-38)$$

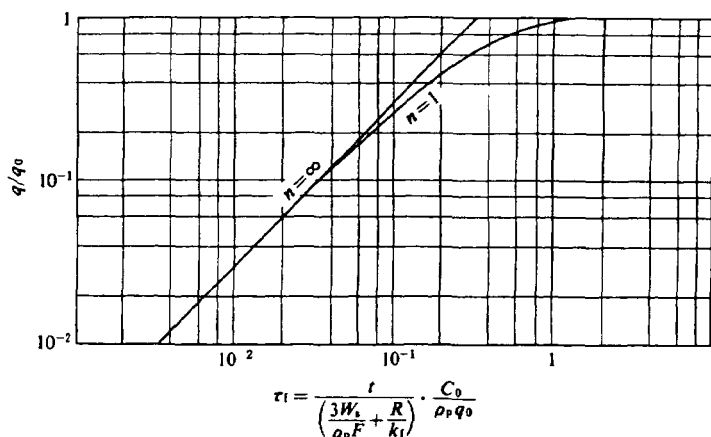


Fig 5.5 Uptake curve, q/q_0 versus $\tau_t = \frac{t}{(3W_s/\rho_p F + R/k_i)} \cdot (C_0/\rho_p q_0)$
 particle-to-fluid mass transfer controlling
 (Reproduced with permission by Suzuki, M and Chihara, K., *Seisan Kenkyu*
 34, 151 (1982))

For the rectangular isotherm ($n=\infty$ of the Freundlich isotherm), the solution becomes

$$q/q_0 = 3\tau_t \quad \text{for } \tau_t < 1/3 \quad (5-39)$$

$$q/q_0 = 1 \quad \text{for } \tau_t \geq 1/3 \quad (5-40)$$

Adsorption uptake curves for these cases are shown in Fig 5.4.

Numerical solutions can be obtained for an arbitrary Freundlich constant, n , the uptake curves for which may be located between the two curves given in Fig. 5.5.

5.2.4. Both particle-to-fluid mass transfer and intraparticle diffusion controlling

Dimensionless forms of the basic equations in this case for pore diffusion kinetics in the particle are given as follows:

$$Bi(X_L - X|_{\rho=1}) = \partial X / \partial \rho \quad (5-41)$$

$$\partial^2 X / \partial \rho^2 + (2/\rho) \partial X / \partial \rho = \partial Y / \partial \tau \quad (5-42)$$

$$Y = X^{1/n} \quad (5-43)$$

$$Y = X = 0 \quad \text{at} \quad \tau = 0 \quad (5-44)$$

$$X_L = 1 \quad \text{for} \quad \tau > 0 \quad (5-45)$$

where Biot's number in Eq. (5-41) represents the relative importance of the intraparticle diffusion resistance and fluid-to-particle mass transfer resistance and is given as

$$Bi = k_t R_p / D_p \quad (5-46)$$

Analytical solution for the above equations is derived for a linear isotherm ($n=1$), as follows (Crank, 1975):

$$\frac{q}{q_0} = 1 - \sum_{n=1}^{\infty} \frac{6Bi^2 \exp(-\beta_n^2 \tau)}{\beta_n^2 \{\beta_n^2 + Bi(Bi - 1)\}} \quad (5-47)$$

where the β_n 's are the n -th positive roots of

$$\beta_n \cot \beta_n + Bi - 1 = 0 \quad (5-48)$$

The uptake curves according to Eq. (5-47) are given in Fig. 5.6.a with Biot's number as a parameter (Suzuki and Chihara, 1982).

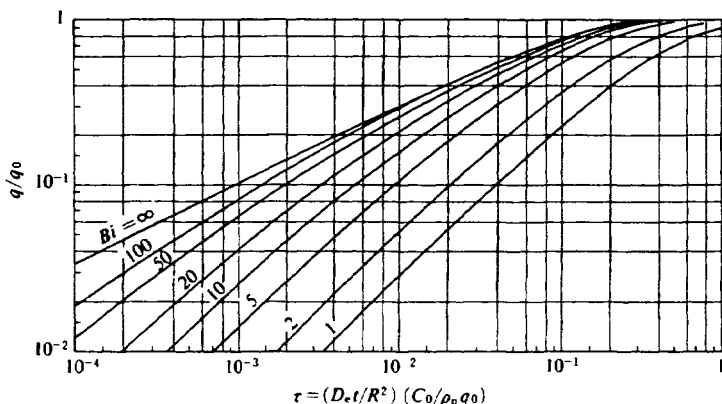


Fig 5.6 a. Uptake curve, q/q_0 versus $\tau = (D_e t / R^2) (C_0 / \rho_p q_0)$ both particle-to-fluid mass transfer and pore diffusion controlling, for $n=1$ Eq (5-47) (Reproduced with permission by Suzuki, M and Chihara, K., *Seisan Kenkyu*, 34, 150 (1982))

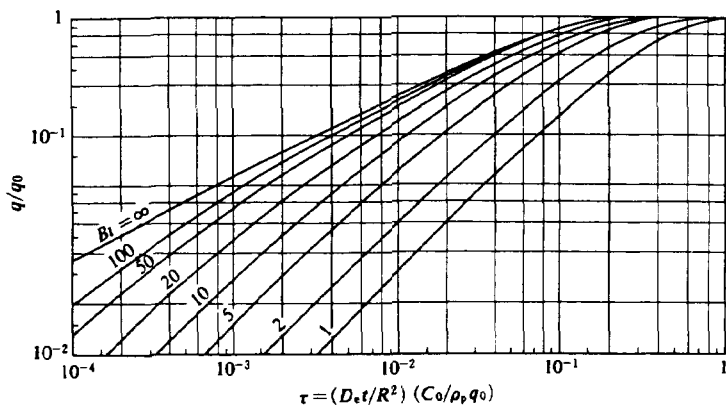


Fig 5.6 c Uptake curve, q/q_0 versus $\tau = (D_e t / R^2) (C_0 / \rho_p q_0)$ both particle-to-fluid mass transfer and pore diffusion controlling for $n=2$
(Reproduced with permission by Suzuki, M and Chihara, K, *Seisan Kenkyu* 34, 150 (1982))

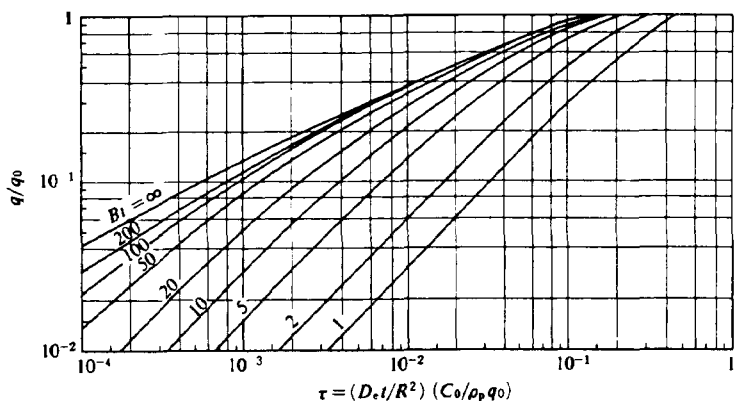


Fig 5.6 b Uptake curve, q/q_0 versus $\tau = (D_e t / R^2) (C_0 / \rho_p q_0)$ both particle-to-fluid mass transfer and pore diffusion controlling, for $n=\infty$
(Reproduced with permission by Suzuki, M and Chihara, K, *Seisan Kenkyu*, 34, 150 (1982))

In the case of the rectangular isotherm ($n=\infty$), adsorption takes place at a sharp adsorption front where concentration in the pore, c , is zero while the amount adsorbed, q , increases from zero to the adsorption capacity, q_0 . In this case, the basic equations for diffusion in the particle are described according to the shell model as follows

$$D_p \left(\frac{\partial^2 c}{\partial r^2} + \frac{2\partial c}{r\partial r} \right) = 0 \quad \text{for } r_1 < r < R \quad (5-49)$$

$$-\rho_p q_0 \partial r_1 / \partial t = D_p \partial c / \partial r \quad \text{at } r = r_1 \quad (5-50)$$

$$c = 0 \quad \text{for } r \leq r_1 \quad (5-51)$$

$$r_1 = R_p \quad \text{at } t = 0 \quad (5-52)$$

where r_1 represents the location of the adsorption front in the particle and it is assumed that the quasi-steady diffusion through the shell part outside of the front determines the moving speed of the adsorption front into the interior of the particle. At particle surface, Eq. (5-41) is used as a boundary condition.

By introducing dimensionless location of the adsorption front, ξ , as

$$\xi = r_1 / R_p \quad (5-53)$$

which naturally corresponds to the fractional uptake, q_{av}/q_0 , as

$$\xi = (1 - q_{av}/q_0)^{1/3} \quad (5-54)$$

Then the basic equation describing the moving speed of the adsorption front reduces to

$$-d\xi/d\tau = [Bi/\{1 + Bi(1/\xi - 1)\}]/\xi^2 \quad (5-55)$$

with the initial condition being

$$\xi = 1 \quad \text{at } \tau = 0 \quad (5-56)$$

where τ is defined by Eq. (5-15) and Bi is given by Eq. (5-46).

Analytical solution can be obtained for the above set of equations as follows (Suzuki and Kawazoe, 1974a).

$$\tau = (1/Bi)(1 - \xi^3)/3 - (\xi^2/6)(3 - 2\xi) + 1/6 \quad (5-57)$$

The uptake curves obtained from Eq. (5-57) are shown in Fig. 5.6.b.

For an arbitrary value of the Freundlich constant, n , numerical computations of Eqs. (5-49) to (5-50) are necessary. A typical example of the calculation for $n=2$ is given in Fig. 5.6.c.

5.3. Batch Adsorption in a Bath with Finite Volume

When batch adsorption takes place in a vessel with finite volume, concentration of the fluid in the vessel decreases with progress of adsorption. In this case, the mass balance (Eq. (5-7)) in the vessel must be accounted for; this is expressed in the following form when $C=C_0$ and $q=0$ are considered at initial stage, $t=0$.

$$V(C_0 - C) = W_s q_n \quad (5-58)$$

where C_0 is the initial concentration in the vessel. In liquid phase adsorption, it is difficult to follow directly the change of the amount adsorbed but the progress of adsorption may be traced by observing the concentration changes in the liquid phase. Concentration changes of the adsorbable component in the liquid phase is also concerned in the purification of liquid products.

Again rate processes involved in the system are the fluid-to-particle mass transfer and the intraparticle diffusion where pore diffusion or surface diffusion may be dominant. Concentration change in the fluid phase is presented here according to the controlling rate process in the system.

5.3.1. Intraparticle diffusion controlling—Pore diffusion

The basic equations are Eq. (5-9) and Eq. (5-58).

For a linear isotherm system ($n=1$), the analytical solution has been given by Crank (1975).

$$\frac{C}{C_0} = 1 - \frac{1}{1 + \alpha} \left\{ 1 - \sum_{n=1}^{\infty} \frac{6\alpha(\alpha + 1)\exp(-q_n^2\tau)}{9 + 9\alpha + q_n^2\alpha^2} \right\} \quad (5-59)$$

where q_n 's are n -th non-zero positive roots of

$$\tan q_n = 3q_n/(3 + \alpha q_n^2) \quad (5-60)$$

where α represents the adsorbent load factor:

$$\alpha = V/W_s K \quad (5-61)$$

K denotes the adsorption equilibrium constant of the linear isotherm relation. Then the final equilibrium concentration C_∞ in the vessel is given as

$$C_{\infty}/C_0 = \alpha/(1 + \alpha) \tag{5-62}$$

For the irreversible adsorption, the isotherm becomes rectangular ($n=\infty$). Suzuki and Kawazoe (1974a) presented the solution for this case as

$$\begin{aligned} \tau = \frac{1 + \beta^3}{3\beta} \left[\beta \ln \frac{\xi^3 + \beta^3}{1 + \beta^3} + \ln \frac{\xi + \beta}{1 + \beta} - \frac{1}{2} \ln \frac{\xi^2 - \beta\xi + \beta^2}{1 - \beta + \beta^2} \right. \\ \left. + \sqrt{3} \left\{ \tan^{-1} \frac{2 - \beta}{\sqrt{3}} - \tan^{-1} \frac{2\xi - \beta}{\sqrt{3}} \right\} \right] \end{aligned} \tag{5-63}$$

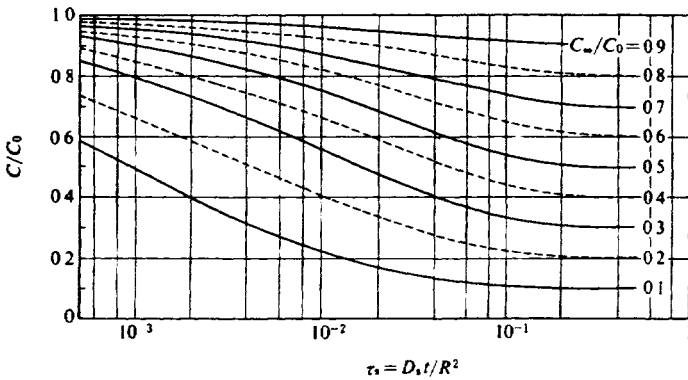


Fig 57 a Diagrams of C/C_0 versus τ , for linear isotherm ($D_s = D_c / \rho_p K_d$) (Reproduced with permission by Suzuki, M and Kawazoe, K, *J Chem Eng Japan*, 7, 347, 348 (1974))

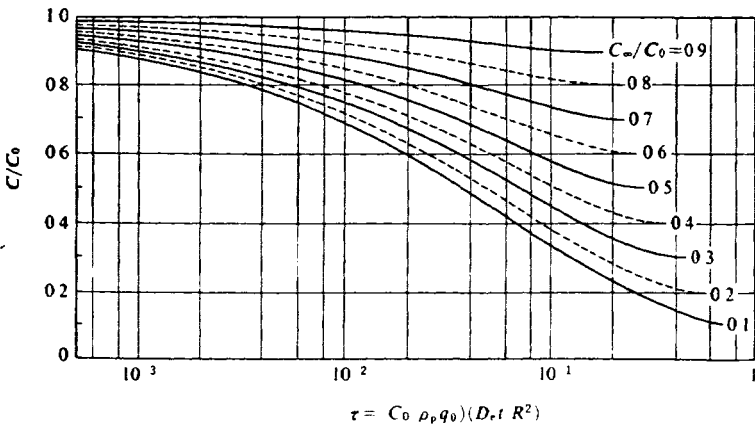


Fig 57 b Diagrams of C/C_0 versus τ for irreversible adsorption with pore diffusion kinetics (Reproduced with permission by Suzuki, M and Kawazoe, K, *J Chem Eng Japan*, 7, 347, 348 (1974))

where $\beta = [C_\infty / (C_0 - C_\infty)]^{1/3}$ and $\xi = [(C - C_\infty) / (C_0 - C_\infty)]^{1/3}$.

Concentration curves calculated from Eqs. (5-59) and (5-63) are given in Fig. 5.7.a and 5.7.b, where C_∞ / C_0 is chosen as a parameter.

For an arbitrary value of the Freundlich constant, n , numerical calculation of the basic equations (Suzuki and Kawazoe, 1974c) gave

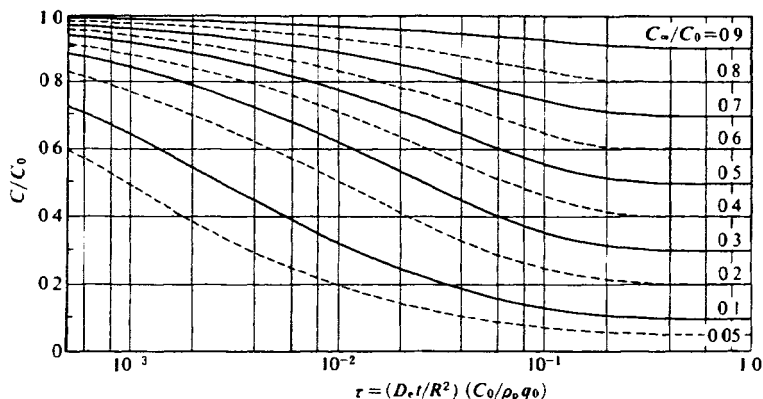


Fig 5.7 c Concentration decay C/C_0 versus $\tau = (D_e t / R^2) (C_0 / \rho_p q_0)$ for $n=1.5$ (Reproduced with permission by Suzuki, M and Kawazoe, K, *Seisan Kenkyu*, 26, 297, 298 (1974))

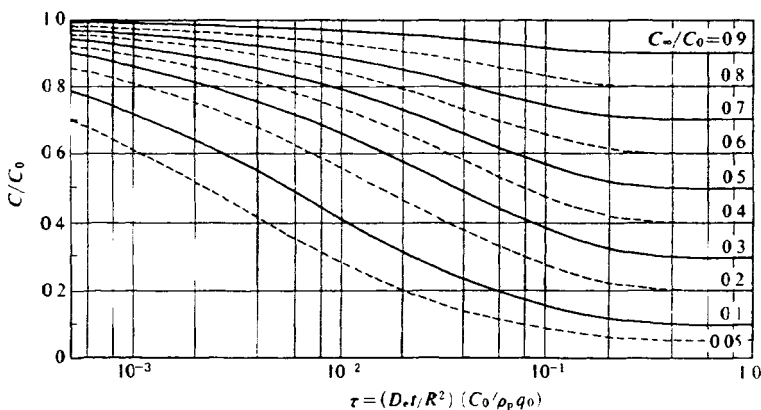


Fig 5.7 d Concentration decay C/C_0 versus $\tau = (D_e t / R^2) (C_0 / \rho_p q_0)$ for $n=2$ (Reproduced with permission by Suzuki, M and Kawazoe K, *Seisan Kenkyu*, 26, 297, 298 (1974))

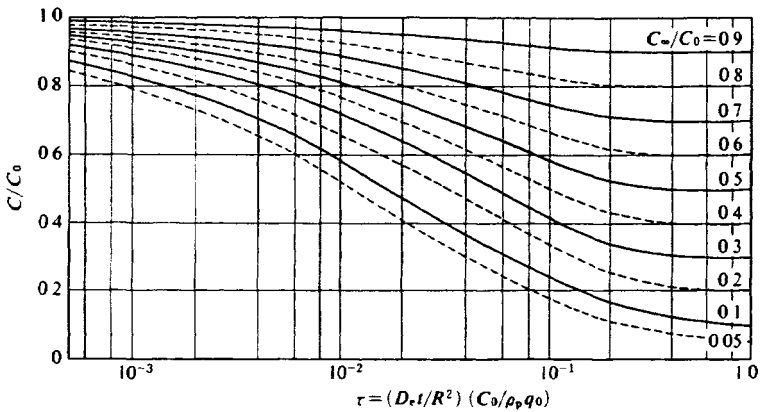


Fig 5.7.e. Concentration decay C/C_0 versus $\tau = (D_e t / R^2) (C_0 / \rho_p q_0)$ for $n=5$. (Reproduced with permission by Suzuki, M and Kawazoe, K, *Seisan Kenkyu*, 26, 297, 298 (1974)).

similar concentration curves. Curves for $n=1.5, 2$ and 5 are shown in Fig. 5.7.c-5.7.e in the same manner as Fig. 5.7.a and 5.7.b.

Final equilibrium concentration C_∞/C_0 which is related to the adsorbent loading ratio, α , as

$$\begin{aligned} \alpha &= W_s q_0 / V C_0 \\ &= \{1 - C_\infty / C_0\} / (C_\infty / C_0)^{1/n} \end{aligned} \quad (5-64)$$

is again a parameter in Fig. 5.7.c-5.7.e.

5.3.2. Intraparticle diffusion controlling—Surface diffusion

Similar calculation is possible for surface diffusion controlling in the particle.

For a linear isotherm system, Eq. (5-59) is applicable since no distinction between the effect of pore diffusion and that of surface diffusion is possible in the case of a linear isotherm. For dimensionless time τ_s , Eq. (5-27) must be employed.

Concentration curves in this case are the same as given in Fig. 5.7.a.

In the case of the irreversible isotherm, the amount adsorbed at the external surface of the particle is considered to be constant regardless of the decrease of liquid phase concentration, and then Eq. (5-19) can be modified to give the concentration change in the vessel

$$\frac{C}{C_0} = 1 - \frac{W_s q_0}{V C_0} \left\{ 1 - \frac{6}{\pi^2} \sum_{n=1}^{\infty} \frac{1}{n^2} \exp(-n^2 \pi^2 \tau_s) \right\} \quad (5-65)$$

Concentration decrease in this case is calculated and given in Fig. 5.8.a.

For an arbitrary value of the Freundlich constant, n , numerical calculation of the set of basic equations is necessary. Typical examples are given in Fig. 5.8.b-5.8.d for $n=1.5, 2, 5$ (Suzuki and Kawazoe, 1974b).

5.3.3. Fluid-to-particle mass transfer controlling

Concentration curves in this case can be readily obtained by combining

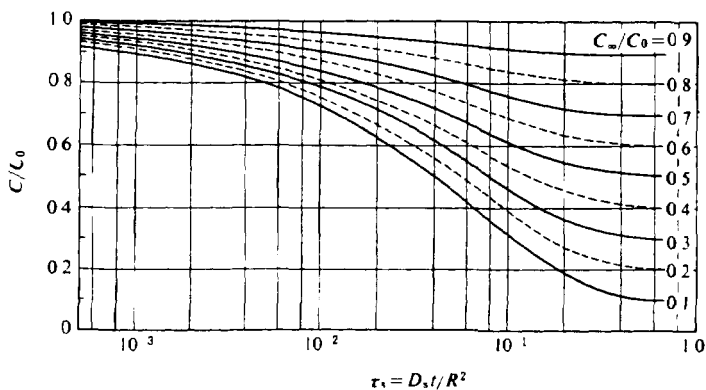


Fig 5.8 a Diagrams of C/C_0 versus τ , for irreversible adsorption with surface diffusion kinetics
(Reproduced with permission by Suzuki, M and Kawazoe, K., *J Chem Eng Japan*, 7, 348 (1974))

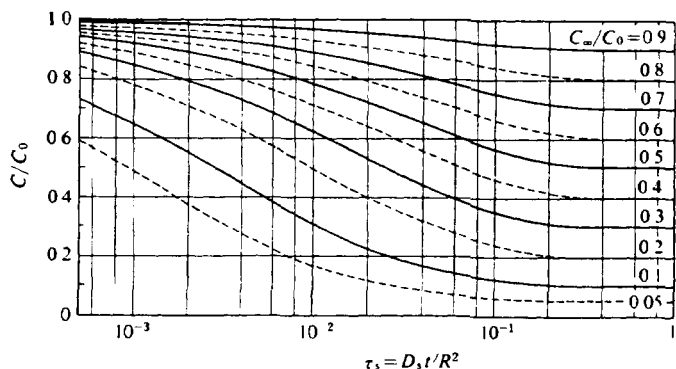


Fig 5.8 b C/C_0 versus $\tau = D_s t / R^2$ for $n=1.5$.
(Reproduced with permission by Suzuki, M and Kawazoe, K., *Seisan Kenkyu*, 26 276, 277 (1974))

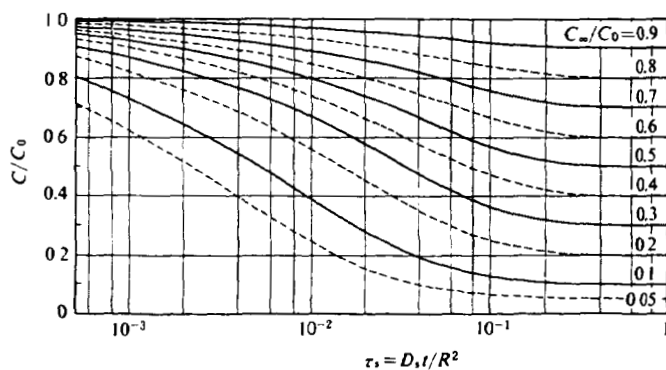


Fig. 5.8.c. C/C_0 versus $\tau = D_s t / R^2$ for $n=2.0$.
(Reproduced with permission by Suzuki, M. and Kawazoe, K., *Seisan Kenkyu*, 26, 276, 277 (1974))

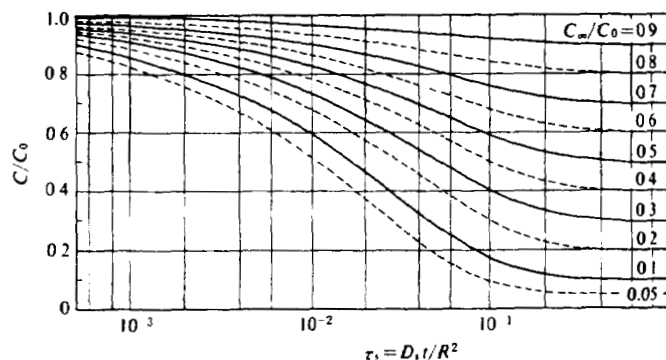


Fig. 5.8.d. C/C_0 versus $\tau = D_s t / R^2$ for $n=5.0$.
(Reproduced with permission by Suzuki, M. and Kawazoe, K., *Seisan Kenkyu*, 26, 276, 277 (1974))

the mass balance equation (Eq. (5-31)) with Eq. (5-58). Naturally q is equal to q_{av} in this case.

For a linear isotherm system, C/C_0 is given as

$$C/C_0 = \frac{1 + \alpha \exp\{-3(1 + \alpha)\tau\}}{1 + \alpha} \quad (5-66)$$

For a rectangular isotherm, the following solution is obtained.

$$C/C_0 = \exp(-3\alpha\tau) \quad \text{for } C/C_0 \geq C_\infty/C_0 = 1 - \alpha \quad (5-67)$$

Concentration decrease curves obtained by the above equations are given in Fig. 5.9.a and b

For intermediate values of the Freundlich constant, n , some diagrams obtained from numerical calculations (Suzuki and Kawazoe, 1975c) are shown in Fig. 5.9.c-5.9.e.

5.3.4. Both fluid-to-particle mass transfer and intraparticle diffusion controlling

When both fluid-to-particle mass transfer resistance and intraparticle

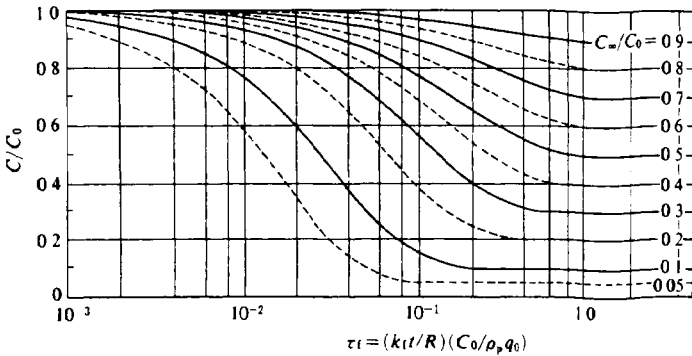


Fig 5.9 a C/C_0 versus $\tau_t = (k_f t/R)(C_0/\rho_p q_0)$ for $n=1$ obtained from Eq (5-66) (Reproduced with permission by Suzuki, M and Kawazoe, K, *Seisan Kenkyu*, 27, 384-386 (1975))

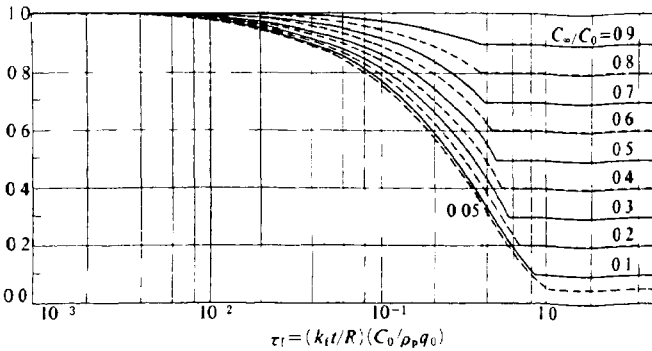


Fig 5.9 b C/C_0 versus $\tau_t = (k_f t/R)(C_0/\rho_p q_0)$ for irreversible isotherm system Eq (5-67) (Reproduced with permission by Suzuki, M and Kawazoe K *Seisan Kenkyu*, 27, 384-386 (1975))

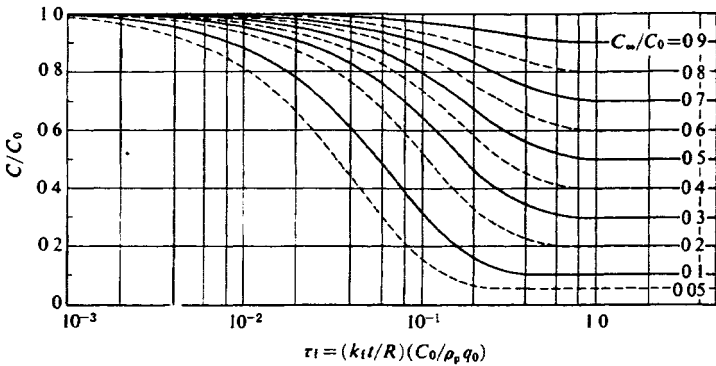


Fig 5 9 c C/C_0 versus $\tau_t = (k_f t/R)(C_0/\rho_p q_0)$ for $n=1.5$
 (Reproduced with permission by Suzuki, M and Kawazoe, K, *Seisan Kenkyu*,
 27, 384-386 (1975))

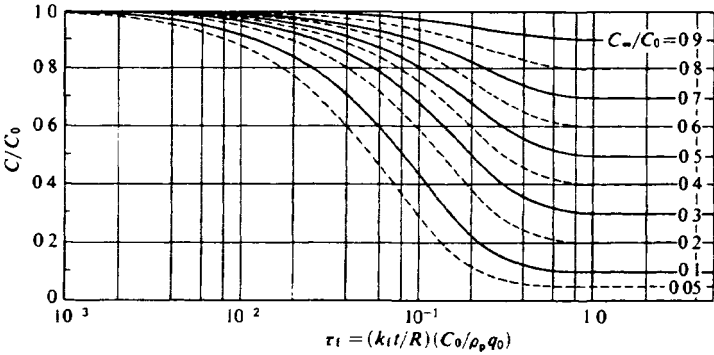


Fig 5 9 d C/C_0 versus $\tau_t = (k_f t/R)(C_0/\rho_p q_0)$ for $n=2$
 (Reproduced with permission by Suzuki, M and Kawazoe, K, *Seisan Kenkyu*,
 27, 384-386 (1975))

diffusion resistance play significant roles in a finite bath batch adsorption, two rate parameters, k_f and D_p , and two equilibrium parameters, adsorbent loading ratio and the Freundlich constant, n , are involved.

For a linear isotherm system, the analytical solution has been obtained by Huang and Li (1973)

$$\frac{C}{C_0} = 1 - \frac{1}{1 + \alpha} \left[1 - \sum_{n=1}^{\infty} \frac{6Bt^2(1 + \alpha)\exp(-\beta_n^2 \tau)}{\left(\frac{9}{\alpha} + \alpha\beta_n^2 + 9\right)Bt^2 - (6 + \alpha)\beta_n^2 Bt + \alpha\beta_n^4} \right]$$

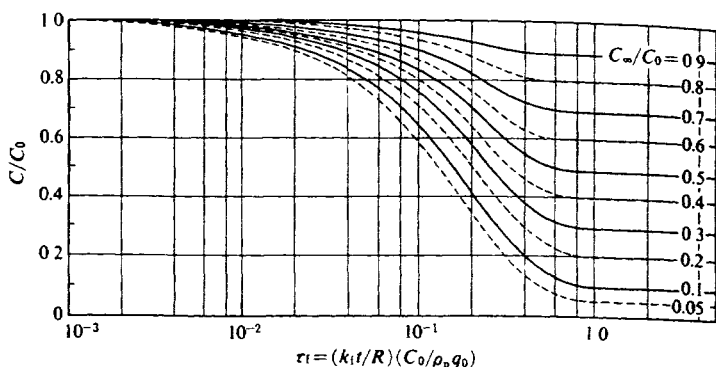


Fig. 5.9 c. C/C_0 versus $\tau_i = (k_f t / R)(C_0 / \rho_p q_0)$ for $n=5$.
(Reproduced with permission by Suzuki, M. and Kawazoe, K., *Seisan Kenkyu*,
27, 384-386 (1975)).

where β_n is the n -th nonzero root of the equation.

$$\frac{\tan \beta_n}{\beta_n} = \frac{3Bi - \alpha\beta_n^2}{(Bi - 1)\alpha\beta_n^2 + 3Bi} \quad (5-69)$$

where $Bi = k_f R / D_p$ and $\alpha = W_p q_0 / VC_0$. Final equilibrium concentration is related to α by Eq. (5-64) where $n=1$ is valid for this case.

In the case of a rectangular isotherm system, the analytical solution given by Suzuki and Kawazoe (1974a) is as follows.

$$\begin{aligned} \tau = & \frac{(1 + \beta^3)(1 - \beta i^{-1})}{3} \ln \frac{\xi^3 + \beta^3}{1 + \beta^3} + \frac{1 + \beta^3}{3\beta} \ln \frac{\xi + \beta}{1 + \beta} \\ & - \frac{1 + \beta^3}{6\beta} \ln \frac{\xi^2 - \beta\xi + \beta^2}{1 - \beta + \beta^2} \\ & + \frac{1 + \beta^3}{\sqrt{3}\beta} \left\{ \tan^{-1} \frac{2 - \beta}{\sqrt{3}\beta} - \tan^{-1} \frac{2\xi - \beta}{\sqrt{3}\beta} \right\} \end{aligned} \quad (5-70)$$

where $Bi = k_f R_p / D_p$, $\beta = [C_\infty / (C_0 - C_\infty)]^{1/3}$ and $\xi = [(C - C_\infty) / (C_0 - C_\infty)]^{1/3}$.

Concentration decrease curves are given only for the case of $C_\infty / C_0 = 0.5$ in Fig. 5.10.a for the linear isotherm and 5.10.b for the rectangular isotherm with Bi as a parameter.

For an arbitrary value of the Freundlich parameter, numerical calculation is involved. Kawai and Suzuki (1984) presented similar diagrams of concentration decrease for this case. Typical calculation results are given

in Fig. 5.10.c-5.10.e. To utilize these diagrams, the experimental conditions of the batch adsorption must be chosen so the final equilibrium concentration satisfies $C_{\infty}/C_0=0.5$.

It must be added that a similar calculation is possible for a combination of the fluid-to-particle mass transfer and the dominant surface diffusion in

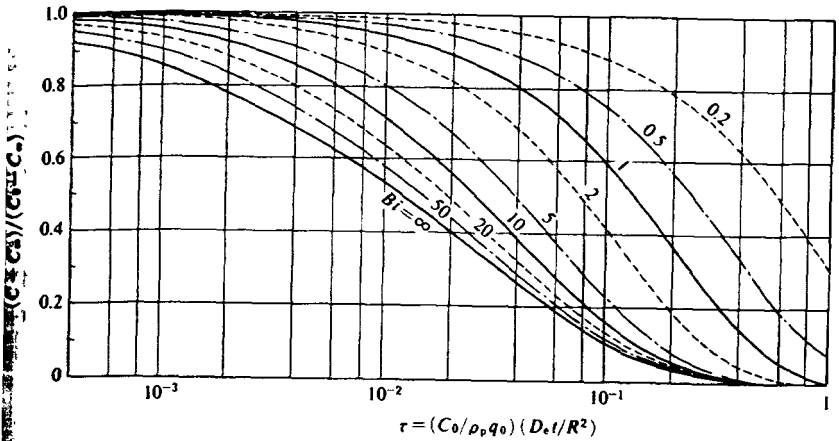


Fig. 5.10.a. $(C - C_{\infty}) / (C_0 - C_{\infty})$ versus τ for a linear isotherm system. Effect of external mass transfer resistance. ($C_{\infty}/C_0=0.5$). (Reproduced with permission by Kawai, T. and Suzuki, M., *Kanagawa Daigaku Houkoku (in Japanese)*, 7, 347 (1984)).

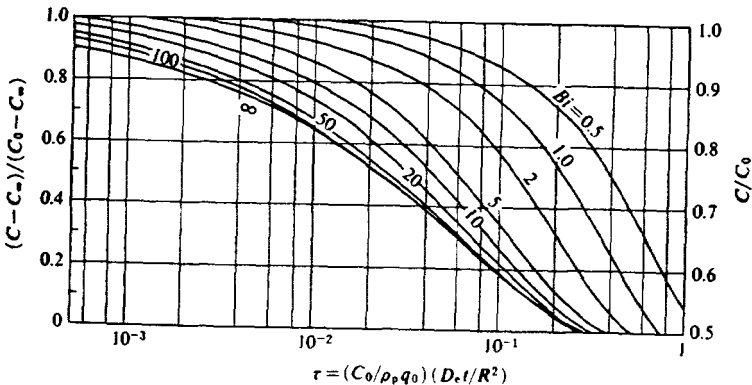


Fig. 5.10.b. Effect of external mass transfer resistance for $n=\infty$ and $C_{\infty}/C_0=0.5$. (Reproduced with permission by Suzuki, M. and Kawazoe, K., *J. Chem. Eng. Japan*, 7, 347 (1974)).

the particle The result of calculation is also shown in Kawai and Suzuki (1984)

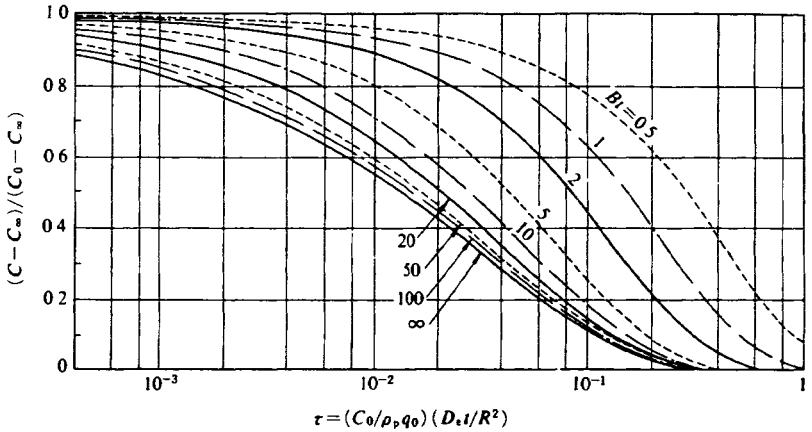


Fig 5 10 c $(C - C_\infty)/(C_0 - C_\infty)$ versus τ for $n=1.5$, $C_\infty/C_0=0.5$ with pore diffusion kinetics
(Reproduced with permission by Kawai, T and Suzuki, M, *Kanagawa Daigaku Houkoku (in Japanese)*, 7, 347 (1984))

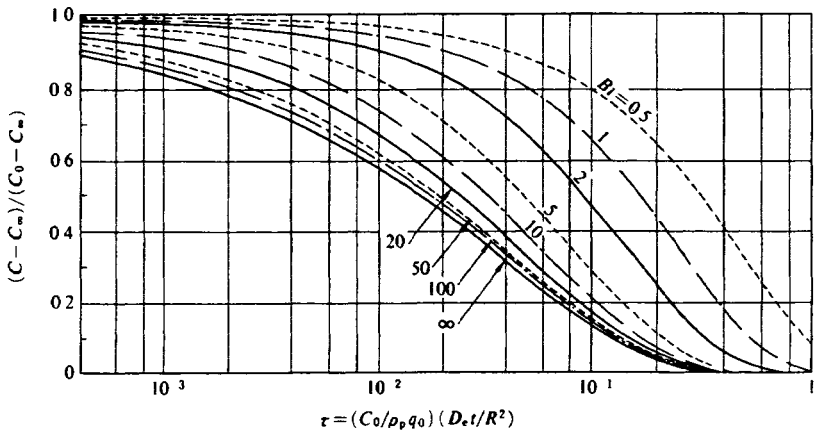


Fig 5 10 d $(C - C_\infty)/(C_0 - C_\infty)$ versus τ for $n=2$, $C_\infty/C_0=0.5$ with pore diffusion kinetics
(Reproduced with permission by Kawai, T and Suzuki, M, *Kanagawa Daigaku Houkoku (in Japanese)* 7 347 (1984))

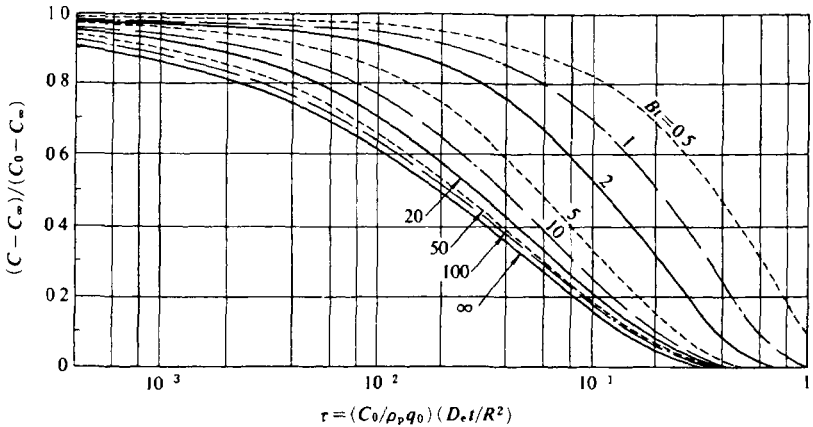


Fig 5.10 e $(C - C_\infty)/(C_0 - C_\infty)$ versus τ for $n=5$, $C_\infty/C_0=0.5$ with pore diffusion kinetics
 (Reproduced with permission by Kawai, T and Suzuki, M, *Kanagawa Daigaku Houkoku (in Japanese)*, 7, 347 (1984))

5.4. Adsorption in a Vessel with Continuous Flow

When adsorption occurs in a vessel where adsorbents are in contact with a flowing fluid, the basic equations must be modified so that Eq. (5-5) is involved. Suzuki and Chihara (1982) provide a detailed discussion on the topic; the results are summarized as follows: When the concentration of the inlet fluid, C_{in} , is constant, then the solutions obtained in Section 5.2.3 and 5.2.4 are applicable by equating

$$C_0 = C_{in} \tag{5-71}$$

and

$$Bi = (R_p^2/D_p)/[(3W_s/\rho_p F) + (R_p/k_i)] \tag{5-72}$$

This modification is understood since mass flux to the surface of the adsorbent particle may be limited both by mass flow into the vessel and by mass transfer from fluid to particle, in series.

5.5. Fluid-to-Particle Mass Transfer in a Vessel

In many cases of liquid phase adsorption by adsorbents of small particle size in a vessel, fluid-to-particle mass transfer becomes an important rate controlling step. This is mainly because molecular diffusivities in liquid phase are small and the relative importance of fluid-to-particle contact efficiency may be more pronounced.

For a system with multiparticles in a moving fluid, the mass transfer coefficient between fluid and particle, k_f , may be defined as follows:

$$k_f = k_{f,\text{stagnant}} + k_{f,\text{motion}} \quad (5-73)$$

where $k_{f,\text{stagnant}}$ represents the mass transfer coefficient when the fluid is stagnant and $k_{f,\text{motion}}$ corresponds to the effect of fluid motion to the mass transfer between fluid and particle.

5.5.1. Mass transfer coefficient of a multiparticle system with stagnant fluid

The mass transfer between particles and stagnant fluid is a well established problem when a single particle and the infinite surrounding fluid are involved. As a matter of fact, when mass transfer takes place from a single spherical particle to an infinite body of fluid, the basic differential equation to describe diffusion around the particle is:

$$D\{\partial^2 C/\partial r^2 + (N/r)\partial C/\partial r\} = \partial C/\partial t \quad (5-74)$$

where $N=2$ holds for a three-dimensional diffusion from a spherical particle. The equation must be solved with the boundary condition

$$C = C_0 \quad \text{at} \quad r = R_p \quad (5-75)$$

$$C = 0 \quad \text{at} \quad r = \infty \quad (5-76)$$

and the initial condition

$$C = 0 \quad \text{for} \quad R_p < r < \infty \quad \text{at} \quad t = 0 \quad (5-77)$$

Then the steady state solution is obtained as

$$C/C_0 = R_p/r \quad (5-78)$$

and the definition of the mass transfer coefficient k_f derives from the steady state concentration profile as

$$k_f(C_0 - 0) = -DdC/dr|_{r=R_p} \quad (5-79)$$

which becomes

$$k_f = DC_0/R_p \quad (5-80)$$

This corresponds to the traditional Ranz and Marshall relation as

$$Sh = k_f d_p / D = 2k_f R_p / D = 2.0 \quad (5-81)$$

where d_p is the particle diameter ($2R_p$). Sh represents a dimensionless parameter called the Sherwood number.

This relation, as stated earlier, follows from the existence of the steady state concentration profile around a single spherical particle. When two-dimensional or one-dimensional diffusion is considered, such as diffusion from a single long filament or diffusion from a plane, no steady state concentration profile can be obtained. Then mass transfer coefficient in the same sense as in the case of a single particle, cannot be defined.

In the multiparticle system, the situation is similar and there may not be steady concentration profiles in the same sense. In this case, the basic equation is Eq. (5-74), but the following equation is used instead of Eq. (5-76) as the boundary condition.

$$dC/dr = 0 \text{ at } r = R_0 \quad (5-82)$$

This is based on the same concept as the free surface model. R_0 represents the outer radius of the concentric shell within which one particle is responsible. R_0 is related to the void fraction defined from the multiparticle arrangement.

$$(R_0^3 - R_p^3)/R_p^3 = \epsilon/(1 - \epsilon) \quad (5-83)$$

where ϵ is the void fraction of the multiparticle phase.

For this case, the steady state solution becomes $C=C_0$ for $R_p < r < R_0$ and then it is not possible to define the mass transfer coefficient in the same manner as in the case of diffusion from a single particle. The transient concentration distribution around the particle can be obtained and used to define the mass transfer coefficient for a multiparticle system.

$$\frac{C}{C_0} = 1 - \sum_{n=1}^{\infty} \left[2 \left\{ \beta_n^2 + \left(\frac{\rho_0 - 1}{\rho_0} \right)^2 \right\} \sin \left(\beta_n \frac{\rho - 1}{\rho_0 - 1} \right) \right] \times \left[\beta_n \rho \left(\frac{1 - \rho_0}{\rho_0^2} + \beta_n^2 \right) \right]^{-1} e^{-\beta_n \tau / (\rho - 1)} \quad (5-84)$$

where β_n is the n -th nonzero root of the equation

$$\beta_n \cot \beta_n = 1 - (1/\rho_0) \quad (5-85)$$

and $\rho = r/R_p$, $\tau = Dt/R_p^2$ and

$$\rho_0 = R_0/R_p \quad (5-86)$$

By defining the mass transfer coefficient as

$$k_t = \frac{\frac{4}{3} \pi (R_0^3 - R_p^3) \frac{dC_{av}}{dt}}{4\pi R_p^2 (C_0 - C_{av})} \quad (5-87)$$

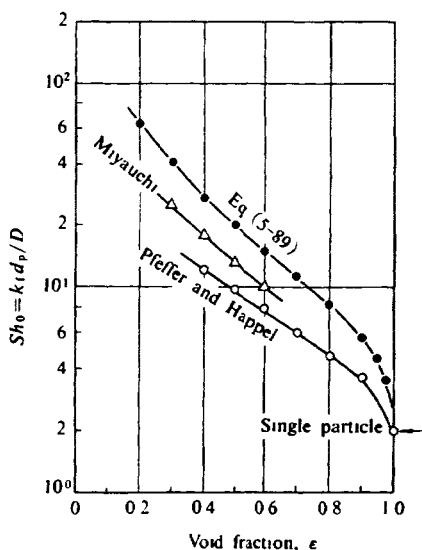


Fig. 5.11 Limiting Sherwood number as a function of void fraction in beds of active spheres
(Reproduced with permission by Suzuki, M, *J Chem Eng Japan*, 8, 164 (1975))

where

$$C_{av} = 3 \int_1^{\rho_0} \rho^2 C d\rho / (\rho_0^3 - 1) \quad (5-88)$$

By taking the limit of τ to infinity

$$Sh = k_r d_p / D = \frac{2}{3} \frac{\rho_0^2 + \rho_0 + 1}{\rho_0 - 1} \beta_1^2 \quad (5-89)$$

The Sherwood number for the stagnant fluid Sh_0 calculated from Eq. (5-89) is plotted in Fig. 5.11 (Suzuki, 1975). In the figure, the solutions of Miyauchi (1971) and Pfeffer and Happel (1964), who used different boundary conditions in order to obtain the steady state concentration profile for multiparticle systems, are included.

5.4.2 Mass transfer coefficient in agitated vessels

Fluid-to-particle mass transfer is accelerated by the motion of the surrounding fluid. Increase of the mass transfer coefficient in this case, $k_{f, \text{motion}}$ can be correlated with the energy dissipation in the fluid phase, ϵ , since the thickness of the concentration boundary layer which develops on the particle surface is considered to correspond to the size of the smallest eddy in the turbulent field.

The energy dissipation, ϵ , is defined as the power input or the energy consumed in the unit mass of the fluid (m^2/s^3).

$$\epsilon = Pg_c / \rho V \quad (5-90)$$

where P ($\text{kg}\cdot\text{m}/\text{s}$) is the input power to the fluid of volume V and the density ρ . g_c denotes the gravity conversion coefficient ($\text{kg}\cdot\text{m}/\text{kg}\cdot\text{s}^2$). When homogeneous agitation is attained in a turbulent agitated vessel with baffles, Pg_c is a function of the revolution speed and the size of the impeller as

$$Pg_c = N_p \rho n^3 d^5 \quad (5-91)$$

where n and d , respectively, represent the rotation speed (1/s) and the sweeping diameter of the impeller. N_p is the power number ranging from 0.35 for propeller to about 6 for six blade flat turbin. These numbers are decreased for the agitator without baffles.

Misic *et al.* (1982) applied the diagrams presented in Fig. 5.3.c for the adsorption of phenol and β -naphthol on powdered activated carbon and

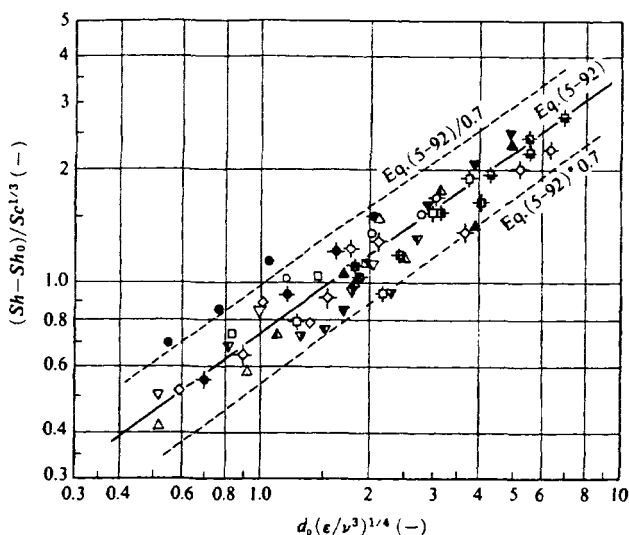


Fig. 5.12. Correlation of Sherwood number, $Sh = k_f d_p / D_L$, against nondimensional energy dissipation in the vessel. Sh_0 is obtained from Eq. (5-89). (Reproduced with permission by Misić, D. M. *et al.*, *J. Chem. Eng. Japan*, 15, 67 (1982)).

correlated the data as shown in Fig. 5.12. The correlation presented is

$$Sh = Sh_0 + 0.74 Sc^{1/3} (d_p / d_{\text{eddy}})^{0.4} \quad (5-92)$$

where Sc is the Schmidt number defined as $Sc = \nu / D$. d_{eddy} is the size of the minimum eddy which is obtained by assuming isotropic turbulence as

$$d_{\text{eddy}} = (\nu^3 / \epsilon)^{1/4} \quad (5-93)$$

The ratio d_p / d_{eddy} indicates the Reynolds number of the fluid boundary layer on the particle of the diameter d_p . Sh_0 is the Sherwood number presented by Eq. (5-89).

When good contact between the particle and fluid is necessary, high speed agitation of the suspended system is often tried. But high speed agitation of fluid does not necessarily assure good contact between the suspended particles and the fluid, because particles move together with the moving fluid, reducing the relative velocity between them.

In order to obtain maximum contact between particle and fluid, several types of contactors have been tried. Suzuki and Kawazoe (1975) used a basket impeller in which adsorbent particles were held. Since maximum

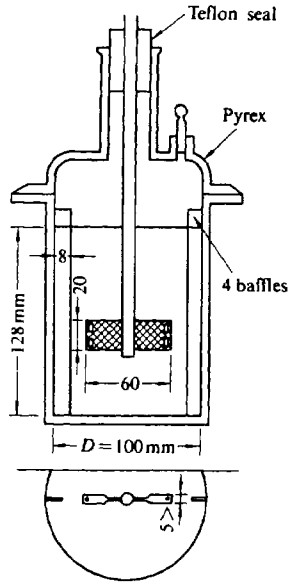


Fig 5.13 Schematic illustration of the reactor
(Reproduced with permission by Suzuki, M and Kawazoe, K, *J Chem Eng Japan*, 8, 80 (1975))

turbulence is attained in the fluid around the impeller, maximum contact or the highest relative velocity between the particles and the fluid is expected. This type of contactor is shown in Fig. 5.13 and the mass transfer coefficient obtained from dissolution of naphthalene particles is observed to be four times bigger than in a suspended system with the same revolution speed. Hence this contactor is effective when negligible mass transfer resistance between fluid and the particle surface is desirable, a condition which is met when the intraparticle diffusion rate is involved.

REFERENCES

- Crank, J, *Mathematics of Diffusion*, 2nd ed, Clarendon Press (1975)
 Huang, T C and K Y Li, *Ind Eng Chem, Fundamentals*, 12, 50 (1973)
 Kawai, T and M Suzuki, *Reports of Fac Eng Kanagawa Univ.*, 22, 31 (1984) (in Japanese)
 Mistic, D M, Y Sudo, M Suzuki and K Kawazoe, *J Chem Eng Japan*, 15, 67 (1982)
 Miyauchi, T, *J Chem Eng Japan*, 4, 238 (1971)
 Pfeffer, R and J Happel, *AIChE Journal*, 10, 605 (1964)

- Suzuki, M , *J Chem Eng Japan*, **8**, 163 (1975)
Suzuki, M and K Chihara, *Seisan Kenkyu*, **34**, 149 (1982) (in Japanese)
Suzuki, M and K Kawazoe, *J Chem Eng Japan*, **8**, 79 (1975a)
Suzuki, M and K Kawazoe, *J Chem Eng Japan*, **8**, 379 (1975b)
Suzuki, M and K Kawazoe, *Seisan Kenkyu*, **27**, 383 (1975c) (in Japanese)
Suzuki, M and K Kawazoe, *J Chem Eng Japan*, **7**, 346 (1974a)
Suzuki, M and K Kawazoe, *Seisan Kenkyu*, **26**, 275 (1974b) (in Japanese)
Suzuki, M and K Kawazoe, *Seisan Kenkyu*, **26**, 296 (1974c) (in Japanese)
Yagi, S and D Kuni, *Kogyokagaku Zasshi*, **56**, 131, 134 (1953) (in Japanese)

Kinetics of Adsorption in a Column— Chromatographic Analysis

Chromatography originated as an analytical method. Mathematical theory to describe elution characteristics of chromatography was later developed for linear isotherm systems making it possible to apply the chromatographic method to the measurement of transport processes which accompany adsorption in adsorbent beds. The theory itself is very clear-cut, making it easy to understand the effects of unit transfer processes not only on chromatographic elution curves but also on breakthrough curves and other transient responses of the column.

Using this theory, equilibrium and rate parameters of the system can be determined from laboratory experiments, and most of the parameters are independent of the dimensions of the equipment, so the results from the laboratory-scale apparatus are generally applicable to the commercial design of the adsorbers. In this case, the nature and operation of the laboratory apparatus are the same as for conventional chromatographic experiments. However rigorous treatment of the effluent peak becomes necessary for the extraction of the parameters from the response data.

The purpose of this chapter is to summarize theoretical development regarding the analysis of the elution curves. There are two general methods of analyzing data, one of which is known as the plate theory (Glueckauf, 1955; Giddings, 1965; Klinkenberg and Colleagues, 1956, 1961), while the other is based on the differential equations describing the mass balance and the rate processes in the adsorbent bed. This latter approach has been developed over a long period (Nusselt, 1911; Anzelius, 1926; Thomas, 1944; Rosen, 1952; Kubin, 1965; Kucera, 1965). The treatment here follows this approach initiated by Kubin (1965); the relation to other methods of analysis including the plate theory is given in Section 6.6.

In a fixed bed of adsorbent particles, the adsorbate-containing input pulse is influenced by several mass transport steps both in the gas in the porous adsorbent particles. It is difficult to extract reliable values for the rate parameters for all of these steps from the shape of a single effluent peak. Therefore, pulse-response experiments at different values

of operating conditions such as gas velocity, particle size, and temperature are desirable. Data for conditions that enlarge the influence of the rate parameter specifically desired are particularly helpful.

First, the general theory is presented for a bed of monodisperse particles, followed by illustrations of the use of specific data in evaluating particular rate parameters. Application of the method to more complex systems such as a bed of bi-disperse particles and a bed of catalyst particles where surface reaction occurs is also discussed.

Reference is made as well to application of the theory developed for linear systems to non-linear isotherm systems.

6.1. Fundamental Relations

In the simplest case of a fixed bed of adsorbent particles, the following mass transport processes are considered: axial dispersion in the interparticle fluid phase, fluid-to-particle mass transfer, intraparticle diffusion, and a first-order, reversible adsorption in the interior of the particle. The last step corresponds to a linear adsorption isotherm with a finite adsorption rate. This assumption includes the case of infinitely fast adsorption rate.

In this model, a mass balance equation for the adsorbable component in the interparticle space is given as

$$E_z \frac{\partial^2 C}{\partial z^2} - u \frac{\partial C}{\partial z} - \frac{3(1-\varepsilon)}{\varepsilon R} N_o = \frac{\partial C}{\partial t} \quad (6-1)$$

where E_z is the axial dispersion coefficient based on the cross sectional area of the bed, u is the interstitial velocity of the fluid in the bed, ε is the void fraction and N_o represents the mass flux of the component from fluid to outer surface of the particles. This flux may be described in terms of the fluid-to-particle mass transfer coefficient k_f or the intraparticle diffusion coefficient D_e :

$$\begin{aligned} N_o &= k_f(C - c_{i|R}) \\ &= D_e \partial c_i / \partial r |_{r=R} \end{aligned} \quad (6-2)$$

where r is the radial coordinate in the particle and R is the radius. For the particles, the mass balance equation is

$$D_e \{ \partial^2 c_i / \partial r^2 + (2/r) \partial c_i / \partial r \} - N_i = c_p \partial c_i / \partial t \quad (6-3)$$

where N_i denotes the rate of disappearance of the tracer per unit volume of the particle, and c_i is the concentration in the pores. For a linear isotherm system, N_i is expressed as

$$N_i = \rho_p k_a (c_i - q_i / K_a) = \rho_p \partial q_i / \partial t \quad (6-4)$$

The coefficients k_a and K_a represent the adsorption rate constant and adsorption equilibrium constant, respectively. In the above equations, ρ_p and ε_p are the particle density and porosity of the particle, and C , c_i and q_i denote concentrations of the component in the fluid phase, in the pores of the particle, and adsorbed on the particle, respectively.

Pore diffusion kinetics is assumed to be dominant in Eqs. (6-2) and (6-3) but it is easily extended to the case of dominant surface diffusion kinetics by taking $\rho_p K_a D_s$ instead of D_c in these equations, since a linear isotherm relation is assumed here.

6.2. Analysis of Chromatographic Elution Curves

The chromatographic experiment, based on introducing a pulse of adsorbable tracer of concentration C_0 and duration time τ into the entrance of the bed, is illustrated in Fig. 6.1. For quantitative analysis of the effluent peak $C_e(t)$, there are several alternative techniques to determine model parameters by comparing the mathematical solution of the fundamental equations and the experimental results. These are: 1) fitting the solution of the fundamental equations in the time domain directly with $C_e(t)$ obtained experimentally, 2) fitting the solution in the Laplace or Fourier domain with the experimental effluent curve transformed into the imaginary domain, and 3) comparison of the characteristics of the elution curve such as the moments, with the theoretically derived moment equations. Each of the techniques has its advantages as well as disadvantages.

Since curve fitting methods both in time domain and in imaginary

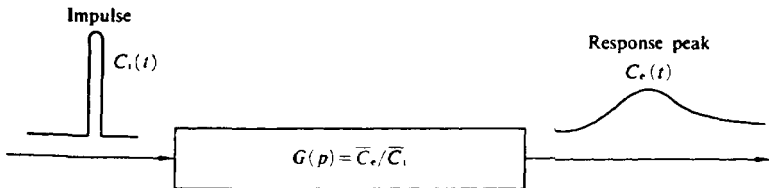


Fig 6 1 Chromatographic experiment.

domain need rather bulky computation, the sensitivity of each of the parameters is not necessarily clear. The moment method described in the next section, on the other hand, makes possible an intuitive understanding of the effect of each transport process.

6.3. Method of Moment

Moments of the chromatographic elution curve are defined as

$$m_n = \int_0^{\infty} C_c(t) \cdot t^n dt \quad (6-5)$$

Then the n -th absolute moment is given as

$$\mu_n = m_n / m_0 = \int_0^{\infty} C_c \cdot t^n dt / \int_0^{\infty} C_c dt \quad (6-6)$$

The n -th central moment is defined as

$$\begin{aligned} \mu'_n &= \int C_c(t - \mu_1)^n dt / \int C_c dt \\ &= \sum_{i=0}^n \binom{n}{i} (-\mu_1)^i \mu_{n-i} \end{aligned} \quad (6-7)$$

Usually the first absolute and second central moments are the most significant, since higher moments are subject to large errors when computing from experimental elution curves.

Moments can be related directly to the solution for C_c in the Laplace domain.

If the Laplace transform of $C(t)$ is $\bar{C}(p)$, where

$$\bar{C}(p) = \int_0^{\infty} \exp(pt) C(t) dt \quad (6-8)$$

The set of partial differential equations (6-1) to (6-4) can be transformed to the set of ordinary differential equations. If the input is a square pulse of injection time τ , that is,

$$\left. \begin{aligned} z = 0; \quad C = 0 \quad \text{for } t < 0 \text{ and } t > \tau \\ C = C_0 \quad \text{for } 0 \leq t \leq \tau \end{aligned} \right\} \quad (6-9)$$

the set of differential equations can be solved in the Laplace domain to give

$$\bar{C}_c(p) = \frac{C_0}{p} \{1 - \exp(-p\tau)\} \exp(-\lambda z) \quad (6-10)$$

$$\lambda = (u/2E_z) \left[\sqrt{1 + (4E_z/u^2)G(p)} - 1 \right] \quad (6-11)$$

$$G(p) = p + \frac{3(1-\varepsilon)Bi}{\varepsilon R^2/D_c} \left\{ 1 - \frac{Bi}{A_0(p) + Bi} \right\} \quad (6-12)$$

$$A_0(p) = R \sqrt{\varepsilon_p K(p)/D_c} \quad (6-13)$$

$$K(p) = p + \frac{1}{\varepsilon_p \left(\frac{1}{k_a} + \frac{1}{pK_a} \right)} \quad (6-14)$$

where Bi is the Biot number ($k_f R/D_c$) (Kubin, 1965).

The moments of the chromatographic elution curve are related to the solution in the Laplace domain as follows:

$$m_n = (-1)^n \lim_{p \rightarrow \infty} [(d/dp)^n \bar{C}_c(p)] \quad (6-15)$$

By applying Eq. (6-15) to Eq. (6-10) and by using Eqs. (6-5) to (6-7), the first absolute moment and the second central moment are expressed as follows:

$$\mu_1 = (z/u)[1 + \delta_0] + (\mu_1)_{\text{pulse}} \quad (6-16)$$

$$\begin{aligned} \mu_2' &= \mu_2 - \mu_1^2 \\ &= (2z/u)[\delta_{ax} + \delta_t + \delta_d + \delta_{ad}] + (\mu_2')_{\text{pulse}} \end{aligned} \quad (6-17)$$

where

$$\delta_0 = [(1-\varepsilon)/\varepsilon] (\varepsilon_p + \rho_p K_a) \quad (6-18)$$

and

$$\delta_{ax} = \frac{E_z}{u^2} (1 + \delta_0)^2 \quad (6-19)$$

$$\delta_t = \frac{1-\varepsilon}{\varepsilon} \frac{R}{3k_f} (\varepsilon_p + \rho_p K_a)^2 \quad (6-20)$$

$$\delta_d = \frac{1-\varepsilon}{\varepsilon} \frac{R^2}{15D_c} (\varepsilon_p + \rho_p K_a)^2 \quad (6-21)$$

$$\delta_{ad} = \frac{1-\varepsilon}{\varepsilon} \frac{\rho_p K_a^2}{k_a} \quad (6-22)$$

Eqs. (6-16) and (6-18) show that the first moment expression includes only equilibrium parameters and Eqs. (6-17) and (6-19) to (6-22) mean that the contributions of axial dispersion, fluid-to-particle mass transfer, intraparticle diffusion, and adsorption rate to the second central moment are additive.

$(\mu_1)_{\text{pulse}}$ and $(\mu_2')_{\text{pulse}}$ respectively denote the first moment and the second central moment of the pulse introduced at the inlet of the column. In the case of a square pulse as shown by Eq. (6-9), the moments are given as

$$(\mu_1)_{\text{pulse}} = \tau/2 \quad (6-23)$$

and

$$(\mu_2')_{\text{pulse}} = \tau^2/12 \quad (6-24)$$

6.3.1. First moment analysis

For linear isotherm systems, first moment data give reasonably accurate adsorption equilibrium constants. Typical plots of μ_1 versus

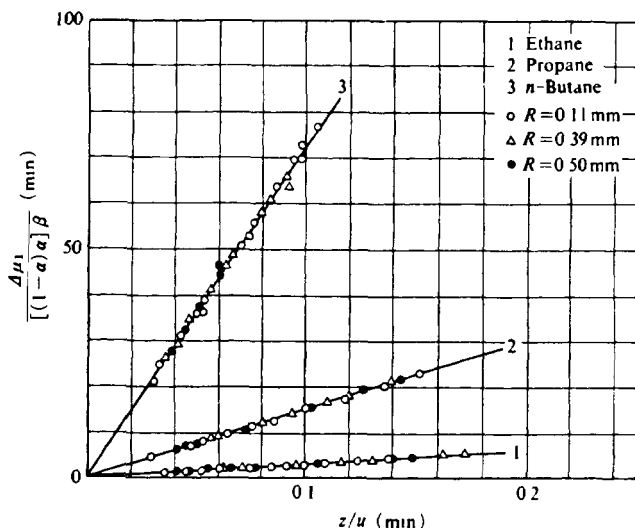


Fig 6.2 Chromatography of hydrocarbons on silica gel (50°C) Dependence of the reduced first absolute moment on z/u (Reproduced with permission by Schneider, P and Smith, M, *AIChE Journal*, 14, 767 (1968))

z/u are shown in Fig. 6.2 for low concentration pulses of hydrocarbon in helium carrier passed through a bed of silica gel (Schneider and Smith, 1968).

For an inert (nonadsorbable) tracer, the first moment becomes

$$(\mu_1)_{\text{inert}} = [1 + \varepsilon_p(1 - \varepsilon)/\varepsilon]z/u \quad (6-25)$$

This inert moment can be evaluated from measurable properties of the bed and the velocity. Subtracting Eq. (6-25) from the counterpart expression for the adsorbable tracer (Eqs. (6-16) and (6-18)) gives

$$\Delta\mu_1 = \frac{1 - \varepsilon}{\varepsilon} \rho_p K_a \quad (6-26)$$

The ordinate of Fig. 6.2 represents this magnitude and the slopes of the straight lines in the figure can then be used to determine K_a . Results obtained from Fig. 6.2 are compared with direct measurement by constant volume method in TABLE 6.1.

6.3.2. Second moment analysis

It is evident from Eq. (6-17) or (6-19) that each transport step gives a separate and additive contribution to the second moment. Then, for instance, from second moments for different gas velocities, the contribution of axial dispersion can be separated from the contribution of the other transport steps. Similarly, from the data for different particle sizes, the contribution of intraparticle diffusion can be separated from the contribution of adsorption. By choosing proper operating conditions, the contribution of the particular step can be maximized so that the rate parameter may be determined with good accuracy.

To simplify data reduction and minimize calculation error, the

TABLE 6.1 Adsorption Coefficients on Silica Gel at 50°C

Hydrocarbon	Adsorption coefficient, K_a (ml/g SiO ₂)	
	From equilibrium adsorption measurements	From evaluation of chromatographic peaks
Ethane	14.5	14.6
Propane	63	65.4
<i>n</i> -Butane	308	311

(Reproduced with permission by Schneider, P. and Smith, M., *AIChE Journal*, 14, 766 (1968))

following parameter, H , is introduced.

$$H = \frac{\Delta\mu_2'(2z/u)}{\{\Delta\mu_1/(z/u)\}^2} \quad (6-27)$$

Then H is given as

$$H = H_0 + E_z/u^2 \quad (6-28)$$

where

$$H_0 = \frac{\delta_r + \delta_d + \delta_{ad}}{(1 + \delta_0)^2} \quad (6-29)$$

as is clear from Eq. (6-27), dependence of H on the fluid velocity is interpreted to be the effect of axial dispersion and when $\rho_p K_a/\epsilon_p \gg 1$ then H_0 reduces to

$$H_0 = \frac{\epsilon}{1 - \epsilon} \left(\frac{R}{3k_f} + \frac{R^2}{15D_e} + \frac{1}{\rho_p k_a} \right) \quad (6-30)$$

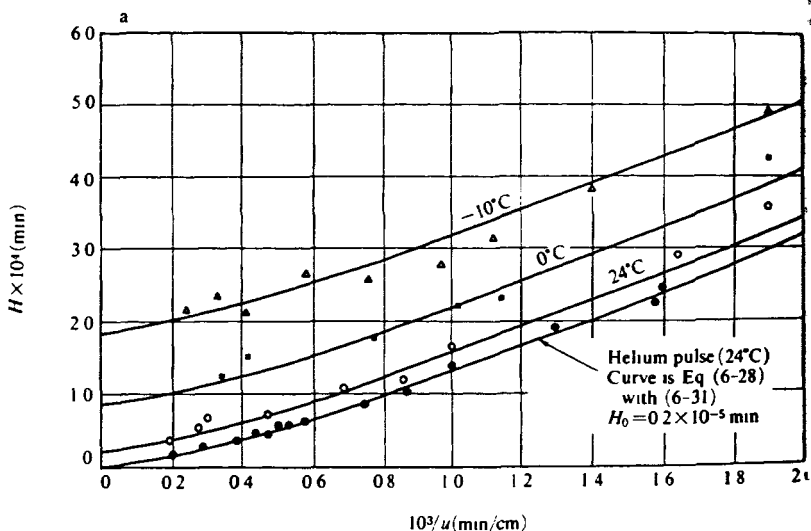


Fig 6.3 Plot of H against $1/u$ for hydrogen-deuterium exchange on nickel catalyst (D_2 pulse in pure H_2) (Reproduced with permission Suzuki, M and Smith, J M, *J Catalysis*, 23, 327 (1971))

A. effect of axial dispersion

When H is plotted against $1/u$ the effect of axial dispersion is clearly demonstrated. As shown in a later section, the axial dispersion coefficient, E_z , is dependent on fluid velocity, u , and the functional form is

$$E_z = \eta D_v + \lambda u \quad (6-31)$$

Then, the plot of H versus $1/u$ gives the effect of axial dispersion as shown in Fig. 6.3. The intercept gives H_0 , while the dependence of H on $1/u$ mainly shows the contribution of axial dispersion. η and λ in Eq. (6-31) can be determined from the curves shown in Fig. 6.3.

B. effect of intraparticle diffusion and fluid-to-particle mass transfer

For relatively large particles and runs at high velocity, the contribution of fluid-to-particle mass transfer (δ_f) to the second moment is usually small for gaseous systems (Schneider and Smith, 1968). Small contribution of fluid-to-particle mass transfer can be corrected by using correlations for k_f in packed beds. First, δ_f is calculated, and from Eq. (6-29), $\delta_d + \delta_{ad}$ are obtained. By plotting $\delta_d + \delta_{ad}$ of the same system for different particle sizes versus the square of the particle radius, a linear relation is expected, and from the slope, the intraparticle diffusivity can be obtained. A typical example of this type of plot is shown in Fig. 6.4.

For linear isotherm systems, contribution of surface diffusion and pore diffusion cannot be separated since the driving forces of the two diffusion mechanisms are proportional. In this case, surface diffusion coefficient can be determined as follows: First estimation of the diffusibility or the tortuosity of pore diffusion by measuring the intraparticle diffusion coefficients at higher temperature or with adsorbates of lower molecular weight are made where the effect of surface diffusion becomes negligible. Then from the obtained intraparticle diffusion coefficients at lower temperatures or with adsorbates of higher adsorbability, the surface diffusion coefficients, D_s , can be determined by subtracting the estimated contribution of the pore diffusion which is calculated by using the diffusibility previously determined, since the intraparticle diffusion coefficient, D_e , is divided into the sum of the contributions of the pore diffusion and the surface diffusion as follows.

$$D_e = \varepsilon_p/k^2 D_v + \rho_p K_a D_s \quad (6-32)$$

From the intercepts at $R^2 = 0$ in plots such as Fig. 6.4, δ_{ad} can be determined, which should make possible estimation of the adsorption rate constant at the adsorption site.

C. adsorption rate constant

For physical adsorption the rate at an adsorption site is likely to be high. Hence the contribution of δ_{ad} to the second moments is very small.

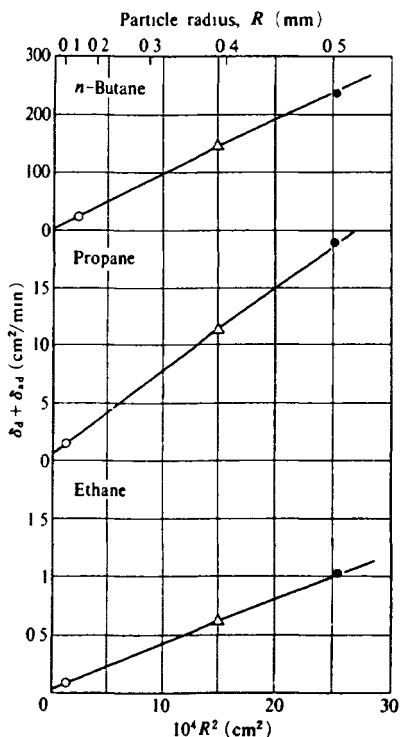


Fig 6.4. Dependence of $\delta_d + \delta_{ad}$ on R
(Reproduced with permission by Schneider, P., *AIChE Journal*, 14, 768 (1968)).

TABLE 6.2 Adsorption rate constants determined from intercepts in Fig 6.4

Substance	k_{ads} (50°C) ml/g SiO ₂
ethane	167
propane	255
n-butane	1500

Schneider and Smith (1968), however, succeeded in applying the moment analysis for making rough estimates of adsorption rate coefficients of low molecular weight hydrocarbons on silica gel. From the intercepts in Fig. 6.4, the rate constants of adsorption were given as shown in TABLE 6.2.

6.4. Extension of the Method of Moment to More Complex Systems

6.4.1 Adsorbents with bidisperse pore structures

Adsorbents can have bidisperse pore structures when they are produced by combining primary particles which themselves are porous (Fig 6.5). The resulting particle has two pore systems micropores within the small particles and macropores corresponding to the space between primary particles. Generally, inadequate diffusivities may result if diffusion data in bidisperse adsorbents are not analyzed by models which account for both micro- and macropores.

Diffusion path in microparticles is far smaller than that in macroparticles. Hence, unless diffusion rate in microparticles is far slower compared with the rate in macropores, it may not be necessary to take into consideration the contribution of the diffusion in micropores to the second moments since the time constant of diffusion is proportional to the square of the particle size. Then the diffusion in microparticles is considered to be solid diffusion or activated diffusion. This becomes the case for most adsorbates in zeolites or molecular sieve carbon.

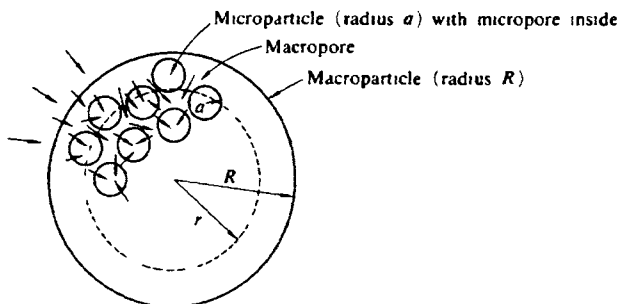


Fig 6.5 Concept of diffusion in a particle of bi-dispersed pore structure

Chihara *et al.* (1978) showed the moment solutions for this case. The basic equations for a particle of monodisperse pore structure are used for material balances in the column and a macroparticle (Eqs. (6-1) to (6-3)), but the following relations are introduced instead of Eq. (6-4) to take into account the diffusion in microparticles of the radius, a .

Material balance at the surface of microparticles

$$N_i = \rho_p D \frac{\partial q}{\partial r_i} \Big|_{r_i=a} \quad (6-33)$$

Adsorption equilibrium at the surface of microparticle

$$q = K_a c_i \quad (6-34)$$

Material balance in the interior of a microparticle

$$D \left\{ \frac{\partial^2 q}{\partial r_i^2} + \left(\frac{2}{r_i} \right) \frac{\partial q}{\partial r_i} \right\} = \frac{\partial q}{\partial t} \quad (6-35)$$

The solution of Eqs. (6-1) to (6-3) and Eqs. (6-33) to (6-35) with the

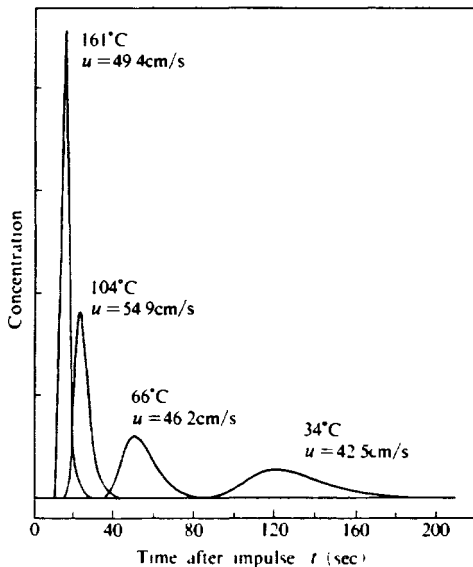


Fig 6.6 Typical chromatographic peaks for krypton on MSC 5A (Reproduced with permission by Chihara, K., Suzuki, M. and Kawazoe, K., *AIChE Journal* 24, 240 (1978))

boundary conditions of a pulse response gives the moment equations by neglecting the moments of the inlet pulse as follows:

$$\mu_1 = (z/u)(1 + \delta_0) \quad (6-36)$$

$$\mu'_2 = (2z/u)[\delta_{ax} + \delta_f + \delta_d + \delta_i] \quad (6-37)$$

where δ_0 , δ_{ax} , δ_f and δ_d are expressed in the same form as Eqs. (6-18) to (6-21) and the contribution of the diffusion in a micropore, δ_i , is given as

$$\delta_i = \frac{1 - \varepsilon_p}{\varepsilon_p} \cdot \frac{\rho_p K_a}{15D} \quad (6-38)$$

This method was applied to evaluate the micropore diffusion rate of various gases in molecular sieving carbon 5A (Chihara, Suzuki and Kawazoe, 1967). Typical chromatographic elution curves for krypton pulse are shown in Fig. 6.6. Micropore diffusivities thus determined are given in Fig. 4.14.

6.4.2. Moments expression for particles with size distributions

When there is a size distribution in the particles packed in a chromatographic column, the distribution does not change the first moment of the elution peak while it may affect peak broadening through the contribution not only of intraparticle diffusion but also of other transport processes such as axial dispersion. The evaluation of the latter effect is not clear but it is possible to make a prediction of the effect of particle size distribution on the intraparticle diffusion contribution, δ_d . This was done by Chihara, Suzuki and Kawazoe (1977) for several typical distribution functions. The effect of the particle size distribution can be accounted for by introducing a correction factor, F , into the expression of δ_d .

$$\delta_d = \frac{1 - \varepsilon}{\varepsilon} \cdot \frac{(\varepsilon_p + \rho_p K_a)^2 R_{av}^2}{15D_c} F \quad (6-39)$$

R_{av} represents the average particle radius. The correction factor, F , is given for a distribution function $f(R)$ as

$$F = \frac{1}{R_{av}^2} \int R^2 f(R) dR \quad (6-40)$$

$$R_{av} = \int Rf(R)dR \quad (6-41)$$

Then F can be easily obtained for typical distribution functions as:

(1) Normal distribution

$$f(R) = \frac{1}{\sigma\sqrt{2\pi}} \exp[-(R - R_{av})^2/2\sigma^2] \quad (6-42)$$

$$F = 1 + (\sigma/R_{av})^2 \quad (6-43)$$

(2) Log normal distribution

$$f(R) = \frac{1}{R} \frac{1}{\sigma_L\sqrt{2\pi}} \exp\left[-\frac{(\ln R - \ln R_{Lo})^2}{2\sigma_L^2}\right] \quad (6-44)$$

$$F = \exp(\sigma_L^2) \quad (6-45)$$

(3) Rectangular distribution

$$f(R) = 1/2R_w \quad \text{for } R_{av} - R_w \leq R \leq R_{av} + R_w \quad (6-46)$$

$$f(R) = 0 \quad \text{for } R < R_{av} - R_w \text{ and } R_{av} + R_w < R$$

$$F = 1 + (R_w/R_{av})^2/3 \quad (6-47)$$

(4) Rosin-Rammler distribution

$$f(R) = -\frac{d}{dR} [\exp(-bR^n)] \quad (6-48)$$

$$F = 2n\Gamma(2/n)/[\Gamma(1/n)]^2 \quad (6-49)$$

The same concept applies to the size distribution of microparticles in the case of adsorbents with bidisperse structures.

6.4.3. Chromatographic measurement in nonlinear isotherm systems

Since the theory of chromatography in linear isotherm systems is simple and useful, there have been several trials to apply the theory to the systems where a "global" isotherm is not linear. Two typical methods are discussed here: A. perturbation chromatography or local linearization technique, and B. isotope chromatography.

A. perturbation chromatography

Even when the isotherm relation is nonlinear, chromatographic technique involves very small concentration change and the isotherm relation governing a small pulse may be considered to be locally linear (Fig. 6.7). Then, by utilizing the local slope of the isotherm as an apparent equilibrium constant, the theory developed for linear isotherm systems can be applied to the analysis of the behavior of the small concentration pulse introduced to the column kept at this point of the equilibrium relation. With this in mind, chromatographic measurement was made by introducing a small adsorbable tracer into the carrier streams which contain the same adsorbable components of different concentration levels. The detection of concentration perturbation at the outlet of a column is sometimes accompanied by fluctuation of a base

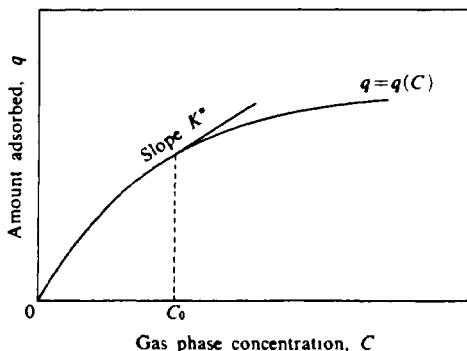


Fig 6.7 Adsorption isotherm and apparent equilibrium constant of local linearization

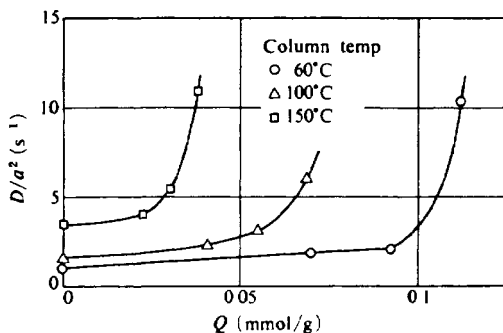


Fig 6.8 Dependence of diffusivity of nitrogen in MSC on amount adsorbed at 60, 100 and 150°C
(Reproduced with permission by Kawazoe, K., Suzuki, M. and Chihara, K., *J Chem Eng Japan*, 7, 156 (1974))

line, which may limit the accuracy of the moment calculations. But this technique is attractive since it provides information regarding concentration dependence of micropore diffusivities as well as the local slopes of an isotherm relation.

Adsorption of nitrogen (Kawazoe, Suzuki and Chihara, 1974) and propylene (Chihara and Suzuki, 1978) on molecular sieving carbon were measured by this technique. The micropore diffusivities of nitrogen in molecular sieving carbon are shown in Fig. 6.8, where dependence of D/a^2 on the amount adsorbed is clearly demonstrated.

B. isotope chromatography

In the case of highly nonlinear isotherm systems, such as chemical adsorption (chemisorption) systems, application of the theory developed for linear systems may seem unfeasible. However nonlinearity of the isotherm relation of chemisorption of hydrogen on nickel catalyst extends to a very low concentration. In such a case, it may be useful if hydrogen exchange rates on catalyst surface can be understood at moderate concentration levels. Employment of isotope technique may provide an answer to this type of need.

Consider a steady flow of an adsorbable gas in an inert carrier stream through a bed of adsorbents at constant temperature and pressure. Under these equilibrium conditions, the surface of the adsorbents is in dynamic equilibrium with the flowing stream. The surface coverage is constant and the fluxes (designated as ϕ) of an adsorbable component from gas phase to adsorbent surface and from adsorbent surface to gas phase are equal. Suppose the isotope of an adsorbable component is introduced as a tracer to the adsorbable component at the inlet of the column, maintaining the total pressure of adsorbable isotopes constant. If the isotope effect is neglected, the total rates will not change, but it is possible to distinguish isotopes from each other in the detector set at the outlet of the column. The rate of adsorption of the isotope is equal to ϕ multiplied by the mole fraction of the isotope in the gas phase. Similarly, the rate of desorption of the isotope will be ϕ multiplied by the fraction of the adsorbed isotope on the surface. Therefore, the net rate of adsorption of the isotope tracer is given by

$$\begin{aligned}\phi_{\text{iso}} &= \phi (C_{\text{iso}}/C_1) - \phi (q_{\text{iso}}/q_1) \\ &= (\phi/C_1) [C_{\text{iso}} - q_{\text{iso}}/(q_1/C_1)]\end{aligned}\quad (6-50)$$

The above equation is in the form

$$\phi_{\text{iso}} = k^*(C_{\text{iso}} - q_{\text{iso}}/K^*)\quad (6-51)$$

where

$$k^* = \phi / C_i \tag{6-52}$$

and

$$K^* = q_i / C_i \tag{6-53}$$

Once k^* and K^* are determined, ϕ can be calculated from Eq. (6-52). K^* is not the adsorption equilibrium constant in the usual sense, but simply the ratio of the amount adsorbed, q_i , and the concentration, C_i , of the adsorbable component concerned at a single point on the non-linear isotherm. This concept is illustrated in Fig. 6.9. Experiments at different total concentrations (partial pressures) and temperatures give different values of k^* and K^* . Hence such measurements determine the effect of pressure and temperature on the rate and the adsorption isotherm.

By setting

$$N_i = \rho_p \phi_{iso} \tag{6-54}$$

Eqs. (6-1) to (6-3) and (6-51) give the same moment equations as Eqs. (6-16) and (6-17) except that k_a and K_a are replaced by k^* and K^* . Therefore, moment method of analysis introduced in 6-3 can be used for isotope chromatography.

Suzuki and Smith (1971a, b) applied this technique to the exchange of hydrogen on copper-zinc oxide catalyst and on nickel-kieselguhr catalyst. Introducing deuterium pulse into hydrogen stream by maintaining the total hydrogen and deuterium concentration in helium carrier constant, deuterium chromatogram was detected at the exit of the column by a thermal conductivity cell. Thus, the exchange

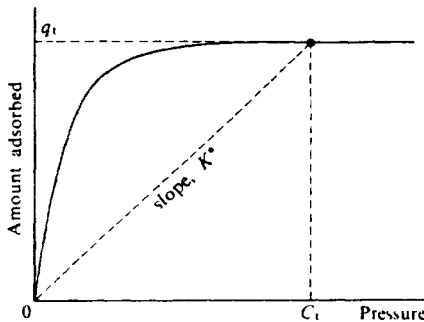


Fig 6.9. Concept of isotope chromatography linearized isotherm

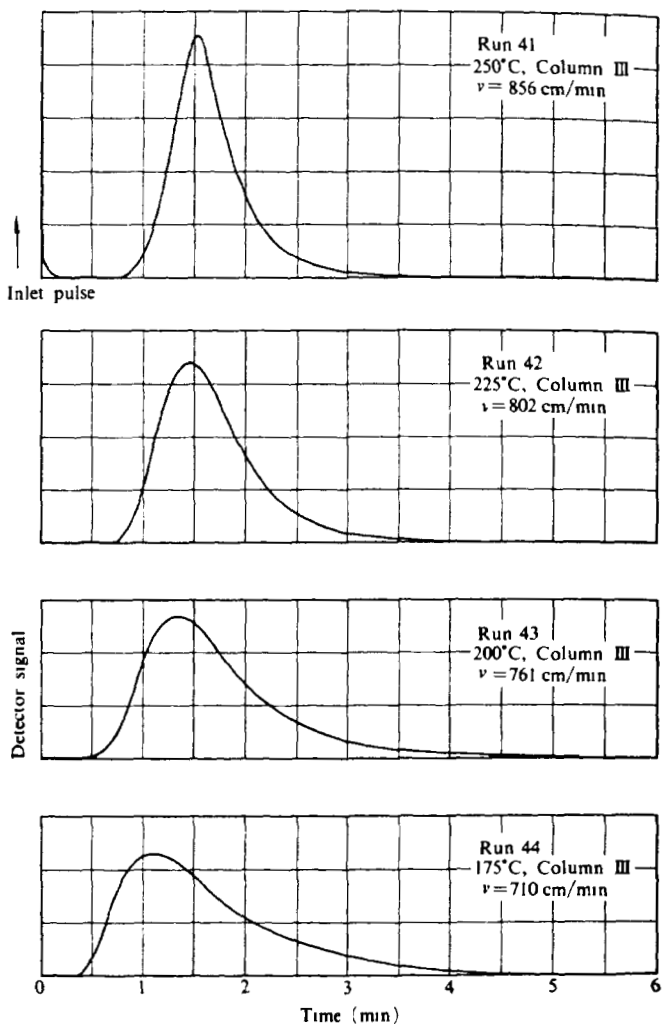


Fig. 6.10. Deuterium chromatographs on Cu-ZnO particles at various temperatures
(Reproduced with permission by Suzuki, M and Smith, M, *J Catal.*, 21, 342 (1971))

equilibrium and the exchange rate were determined at the dynamic equilibrium state with regard to the exchange of total hydrogen ($\text{H}_2 + \text{D}_2$) between catalyst surface and gas phase. Typical chromatograms for deuterium pulses on a similar catalyst are illustrated in Fig. 6.10.

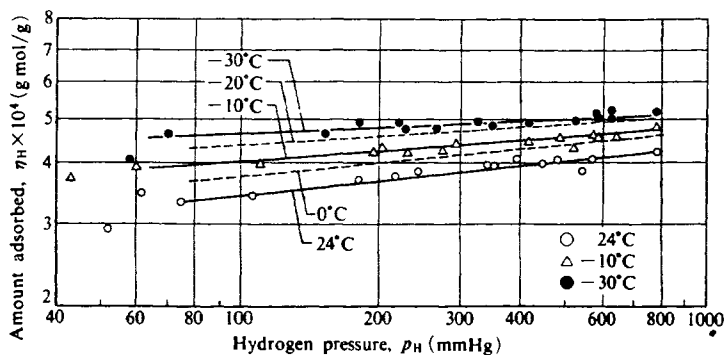


Fig. 6.11. Hydrogen isotherm on nickel-kieselguhr catalyst obtained from deuterium chromatography. Note : Data points of 0°C and -20°C not shown. (Reproduced with permission by Suzuki, M. and Smith, M., *J. Catal.*, 23, 325 (1971)).

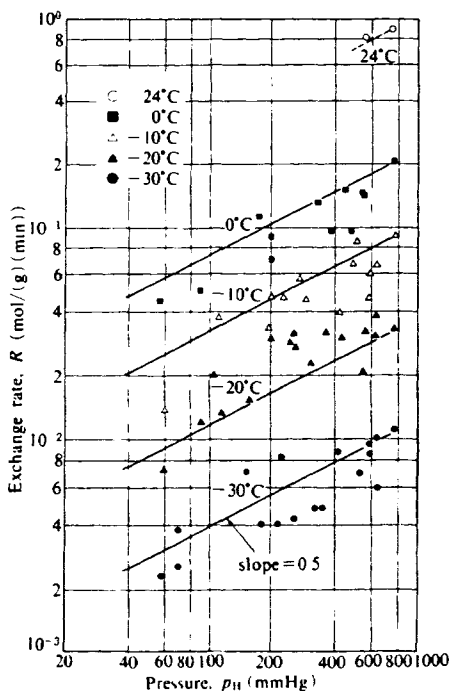


Fig. 6.12. Effect of hydrogen pressure on exchange rate on nickel-kieselguhr catalyst. (Reproduced with permission by Suzuki, M. and Smith, M., *J. Catal.*, 23, 328 (1971)).

From the first moment, the apparent adsorption equilibrium constant, K^* , is obtained and by correcting the effects of axial dispersion and intraparticle diffusion, the apparent adsorption rate constant, k^* , is determined from the second central moment. Then from measurements at different hydrogen concentrations, the amount of hydrogen adsorbed and the exchange rate of hydrogen on nickel catalyst can be determined as a function of hydrogen pressure. Figs. 6.11 and 6.12 show the adsorption equilibrium relation and the exchange rate thus determined at different temperature levels. From the dependence of the amount adsorbed and the exchange rate on hydrogen pressure, discussion of the exchange mechanism is possible. For instance, from the results given in Figs. 6.11 and 6.12, Suzuki and Smith (1971 b) suggested that the Rideal-Eley dual site exchange mechanism might be dominant in the exchange of hydrogen on nickel catalyst.

6.4.3. Chromatography in reacting systems

When reaction and adsorption take place in porous particles, chromatographic measurement may give surface intrinsic reaction rate properties separately from adsorption properties. The theoretical development based on this idea was proposed by Suzuki and Smith (1971 d). The treatment is rather complex but may become useful by selecting a system where the effects of some of the transport processes may be negligible.

6.5. Comparison with Simpler Models

Model described by Eqs. (6-1) to (6-4) for adsorbents of monodisperse structure or additional Eqs. (6-33) to (6-35) are too complicated for analytical use. As a matter of fact, the model can include four rate parameters in addition to the adsorption equilibrium constant. Those equations finally give the solutions for the first absolute moment, μ_1 , and the second central moment, μ_2' . These two moments are only utilized in actual experiments. Therefore, it might be helpful if comparison is made between this model and the models which include only two parameters including the equilibrium constant. As two-parameter models, typical are 1) a dispersion model that includes axial dispersion coefficient as a sole rate parameter and 2) a two-phase exchange model which has a mass transfer coefficient as an only rate parameter. These two models are considered to be the two extremes of the complicated model used in the earlier section, hence the results of

the complicated model may fall between the results derived from the two models.

The relation between the parameters of these models and the first absolute moment and the second central moment of the pulse response of these models is given first; then from the analytical solutions of these models, comparison of the shape of the elution curves are made.

6.5.1. Dispersion model

The basic equation is described by using the axial dispersion coefficient, E_z , as

$$(E_z/u)\partial^2 C/\partial z^2 - \partial C/\partial z - (\alpha/u)\partial C/\partial t = 0 \quad (6-55)$$

where u denotes fluid velocity and α represents the adsorption capacity ratio of the bed. For the sake of simplicity, the impulse response is considered. Then the boundary conditions are:

$$\left. \begin{array}{l} z = 0 \quad C = M\delta(t) \\ z = \infty \quad C = 0 \end{array} \right\} \quad (6-56)$$

Laplace transforms of the above equations are

$$\frac{E_z}{u} \frac{d^2 \bar{C}}{dz^2} - \frac{d\bar{C}}{dz} - \frac{\alpha}{u} p \bar{C} = 0 \quad (6-57)$$

$$\left. \begin{array}{l} z = 0 \quad C = M \\ z = \infty \quad \bar{C} = 0 \end{array} \right\} \quad (6-58)$$

Then the solution in the Laplace domain is given as

$$G(p) = \bar{C}(p)/M = \exp[-Pe/2(\sqrt{1 + 4\tau_p/Pe} - 1)] \quad (6-59)$$

where $Pe = uZ/E_z$ and $\tau = \alpha Z/u$. Z is the column length.

The moments are given by applying Eq. (6-15) to (6-59).

$$\mu_1 = \alpha Z/u = \tau \quad (6-60)$$

$$\mu_2' = \mu_2 - \mu_1^2 = 2\alpha^2 E_z Z/u^2 = 2\tau^2/Pe \quad (6-61)$$

On the other hand the analytical solution to Eq. (6-55) (Levenspiel and Smith, 1957) has been shown as

$$C(t)/M = (\sqrt{Pe} / 2\sqrt{\pi t \tau}) \exp[-Pe/4(t - \tau)^2/t\tau] \quad (6-62)$$

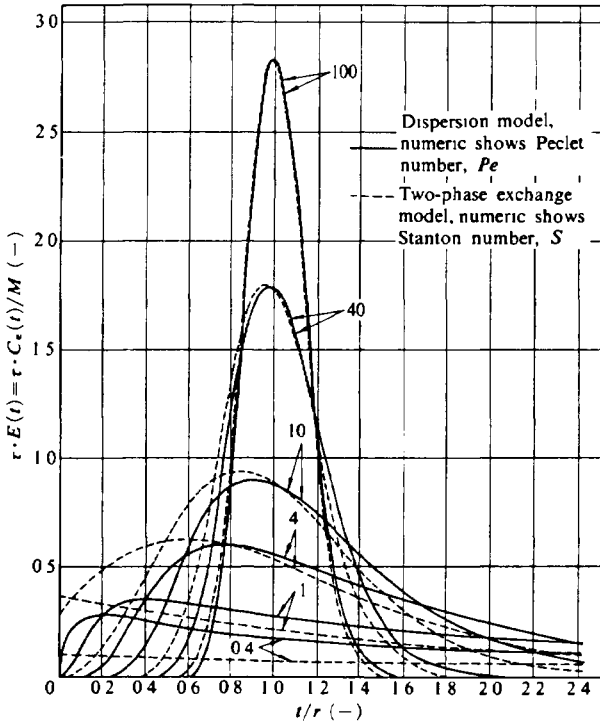


Fig 6.13 Comparison of dispersion model and two-phase exchange model.

The curves derived from Eq. (6-62) for $Pe = 0.4, 1, 4, 10, 40, 100$ are illustrated in Fig. 6.13.

6.5.2. Two-phase exchange model

When there is a mass exchange between the fluid phase and the stagnant phase which has an adsorption capacity, the basic equation is given as

$$-u(\partial C / \partial z) = k(C - c_s) = \alpha(\partial c_s / \partial t) \tag{6-63}$$

The boundary conditions are given by Eq. (6-56). Eq (6-63) is transformed into the Laplace domain and by eliminating concentration in the stagnant phase, c_s , the resultant equation for $\bar{C}(p)$ is obtained as

$$u d\bar{C} / dz + k\alpha_p \bar{C} / (k + \alpha p) = 0 \tag{6-64}$$

Finally $\bar{C}(p)$ is given as

$$G(p) = \bar{C}(p)/M = \exp[1/\{(1/S) + (1/\tau p)\}] \quad (6-65)$$

where $S = kZ/u$ and $\tau = \alpha Z/u$.

The moments are obtained from Eq. (6-65) as

$$\mu_1 = \alpha Z/u = \tau \quad (6-66)$$

$$\mu_2' = 2Z\alpha^2/uk = 2\tau^2/S \quad (6-67)$$

Also the solution in the time domain, $C(t)$, can be obtained by the inverse Laplace transform of $\bar{C}(p)$.

$$C(t)/M = \exp(-S)[\delta(t) + \exp(-St/\tau)(S/\sqrt{t\tau})I_1(2S\sqrt{t/\tau})] \quad (6-68)$$

where $I_1(x)$ is the modified Bessel function of first order. $C(t)$ obtained from the above equation for $S = 0.4, 1, 4, 10, 40, 100$ are shown by dotted lines in Fig. 6.13.

6.5.3. Utilization of the simple models

As is apparent from Fig. 6.13, the two extreme models give similar results when Pe in the dispersion model and S in the two-phase exchange model become large, that is, over 40. As stated above, the result of the rigorous model is expected to fall in between the two curves drawn for the same magnitudes of the first and second central moments.

From Eqs. (6-60), (6-61), (6-66) and (6-67), the two parameters of the simple models are related to the first and the second moments as

$$\tau = \mu_1 \quad (6-69)$$

$$Pe(\text{ or } S) = 2\mu_1^2/\mu_2' \quad (6-70)$$

Therefore, to describe column performance, either of the simple models instead of the rigorous complete model may be used when $2\mu_1^2/\mu_2'$ is large enough (larger than 40), in which case the model parameter can be found by Eqs. (6-69) and (6-70).

6.6. Other Methods for Handling Chromatographic Curves

Problems often arise when the moment method is applied to the analysis of chromatographic curves. When elution peaks are highly nonsymmetrical and accompanied by long tails, estimation of second moments involves large experimental errors. Long tailing is usually brought about by selecting high velocity or a short column which results in smaller first moment compared with the time constants of the rate process such as time constant of intrinsic adsorption rate, intraparticle diffusion time or time constant of axial dispersion, involved in the system. Thus, it is in principle rather difficult to deduct useful information from chromatographic curves with long tails.

Several trials have been made nevertheless to overcome the ambiguity of employing the second moment. Some of the trials discussed here are 1) fitting of the model equation and the experimental elution curves in the Laplace domain, and 2) fitting in the time domain which has often been used for testing the validity of the parameters determined from sophisticated methods. Other methods include Fourier analysis of response curves (Gangwal *et al.*, 1971) and the weighted moment method introduced by Anderssen and White (1971). Comparison of these methods have been made by Anderssen and White (1970), Wakao and Tanisho (1974) and Boersma-Klein and Moulin (1979).

6.6.1. Fitting in Laplace domain

This method was applied to estimation of parameters in simpler models by Hopkins *et al.* (1969), Ostergaard and Michelsen (1969), Michelson and Ostergaard (1970) and Middoux and Charpentier (1970).

In the case of a dispersion model, for instance, transfer function $G(p)$ is given as Eq. (6-59). Transfer function is defined as the ratio of the Laplace transform of the elution concentration curve and that of the input concentration curve, the latter of which is a constant in the case of impulse input. Laplace parameter, p , is a complex variable but if a response curve, $C(t)$, is transformed by using Eq. (6-8) by assuming p as a real parameter, then the resultant $\bar{C}(p)$ gives a transfer function $G(p)$ by dividing by the size of pulse, M , in a real plane. $G(p)$ is then compared with the solution of basic equations obtained in a Laplace domain.

For comparison with the dispersion model, Eq. (6-59) gives the

following relation.

$$F(p) = \ln(G(p)) = (Pe/2)(1 - \sqrt{1 + 4\tau p/Pe}) \quad (6-71)$$

Then

$$1/F(p) = 1/Pe - \tau p/(F(p))^2 \quad (6-72)$$

Thus, if $G(p)$ is determined from elution curve for several values of parameter, p , $F(p)$ is obtained, and by plotting $1/F(p)$ versus $p/(F(p))^2$, τ and Pe are determined from the slope and the intercept of a straight regression line.

Also for comparison with the two-phase exchange model, $F(p) = \ln(G(p))$ is given from Eq. (6-65) as

$$-1/F(p) = 1/S + 1/\tau p \quad (6-73)$$

Thus plots of $1/F(p)$ versus $1/p$ for various p should become a straight line whose intercept and slope should give S and τ .

This method is rather difficult for applying to more complicated models since simple linear plots like Eqs. (6-72) and (6-73) are in most cases unobtainable.

In principle, the moment method compares the slope and curvature of a transfer function equation at $p = 0$ as is obvious from the relation given by Eq. (6-15). But the fitting in Laplace domain corresponds to the fitting at the finite values of p arbitrarily selected for comparison. Fitting by the curvature of $G(p)$ may sometimes give better results but the physical meaning of the fitting is not quite clear. On the other hand, the point $p = 0$ where the moment method is based, corresponds to the integral characteristics of the transfer function as is understood from the fact that the unit of p is 1/sec.

6.6.2. Fitting in the time domain

Another method more intuitively understandable is the fitting in the time domain. Obviously in the cases when it is possible to obtain an analytical solution for the basic equations to describe a model, the comparison with the response curve is easily made. When a numerical solution is to be employed, the effect of each parameter on the calculated concentration curve cannot be easily visualized so the comparison needs repeated calculations for optimum parameter search. Anderssen and White (1970) introduced the error map method to show the deviation of the calculated curves and the response curves, which was later utilized by Wakao *et al.* (1979, 1981).

Obviously, time domain fitting should give the best fit by comparison in the same domain. However, it should be kept in mind that important information may not be easily seen in the main part of the response curve but may be hiding behind the curve. Thus it is necessary to evaluate the validity of the estimated model parameter by repeating response measurements in a series of experimental conditions or by comparing with independent measurements as well as by often reconsidering the appropriateness of the model employed.

REFERENCES

- Adrian, J C and J M Smith, *J Catalysis*, **18**, 578 (1970)
 Anderssen, A S and E T White, *Chem Eng Sci*, **25**, 1015 (1970)
 Anderssen, A S and E T White, *Chem Eng Sci*, **26**, 1203 (1971)
 Anzelius, A, *Z Angew Math Mech*, **6**, 291 (1926)
 Boersma-Klein, W and J A Moulin, *Chem Eng Sci*, **34**, 959 (1979)
 Chihara K and M Suzuki, *J Chem Eng Japan*, **11**, 153 (1978)
 Chihara, K, M Suzuki and K Kawazoe, *AIChE Journal*, **24**, 237 (1978)
 Chihara, K M Suzuki and K Kawazoe *Seisan Kenkyu* **29** 263 (1977) (in Japanese)
 Van Deemter, J J, F J Zuderweg and A Klinkenberg, *Chem Eng Sci*, **5**, 271 (1956)
 Gangwal, S K R R Hudgins, A W Bryson and P L Silveston, *Can J Chem Eng.* **49** 113 (1971)
 Giddings, J C, *Dynamics of Chromatography*, part 1, Chapt 4, Marcel Dekker, New York, 1965
 Glueckauf, E *Trans Faraday Soc.*, **51** 1540 (1955)
 Hashimoto N and J M Smith, *Ind Eng Chem Fundamentals*, **12**, 353 (1973)
 Hashimoto, N and J M Smith, *Ind Eng Chem Fundamentals*, **13**, 115 (1974)
 Hopkins, M J, A J Sheppard and P Eisenklam, *Chem Eng Sci*, **24**, 1131 (1969)
 Kawazoe, K, M Suzuki and K Chihara, *J Chem Eng Japan*, **7**, 151 (1974)
 Klinkenberg A and F Sjenitzer *Chem Eng Sci*, **5**, 258 (1961)
 Kubin, M, *Collection Czechoslov Chem Commun*, **30**, 1104 (1965)
 Kubin, M, *Collection Czechoslov Chem Commun*, **30**, 2900 (1965)
 Kucera, E, *J Chromatogr*, **19**, 237 (1965)
 Lee, D-I, S Kaguet and N Wakao, *J Chem Eng Japan*, **14**, 161 (1981)
 Levenspiel, O and J M Smith, *Chem Eng Sci*, **6**, 227 (1957)
 Michelsen, M L and K Ostergaard, *Chem Eng Sci*, **25**, 1015 (1970)
 Midoux, N and J C Charpentier, *The Chem Eng Journal*, **1**, 163 (1970)
 Nusselt, W, *Tech Mech Thermodynam.*, **1**, 417 (1930)
 Ostergaard, K and M L Michelsen, *Can J Chem Eng*, **47**, 107 (1969)
 Padberg, G and J M Smith, *J Catalysis*, **12**, 172 (1968)
 Rosen, J B, *J Chem Phys*, **20**, 383 (1952)
 Schneider, P and J M Smith, *AIChE Journal*, **14**, 762 (1968)
 Suzuki, M, *Kagaku Souti*, No 6, 21 (1973) (in Japanese)
 Suzuki, M and J M Smith, *J Catalysis*, **21**, 336 (1971a)
 Suzuki, M and J M Smith, *J Catalysis*, **23**, 321 (1971b)
 Suzuki, M and J M Smith, *Chem Eng Journal*, **3**, 256 (1971c)
 Suzuki, M and J M Smith, *Chem Eng Sci*, **26**, 211 (1971d)
 Thomas H C, *J Am Chem Soc* **66** 1664 (1944)
 Wakao, N S Kaguet and J M Smith *J Chem Eng Japan*, **12**, 481 (1979)
 Wakao N and S Tanisho, *Chem Eng Sci*, **29** 1991 (1974)

Kinetics of Adsorption in a Column— Breakthrough Curves

Actual adsorption processes are in many cases associated with adsorption in a column. Adsorbent particles are packed in a column and fluid that contains one or more components of adsorbates flows in the bed. Adsorption takes place from the inlet of the column and proceeds to the exit. In the course of adsorption, a saturated zone is formed near the inlet of the column and a zone with increasing concentration is observed at the frontal part. Mass transfer from fluid to adsorbent occurs in this region called the "mass transfer zone." If concentrations in the effluent stream are measured continuously, seepage of the adsorbable components are observed when the mass transfer zone approaches the exit of the bed and the so-called "breakthrough curve" will be obtained (Fig. 7.1). When and how this breakthrough occurs is the focus of this chapter.

The fundamental equations employed are essentially the same as those used in the previous chapter. Namely, when rigorous treatment is necessary, the model described by Eqs. (6-1) to (6-4) is employed whereas for a quick estimation of the breakthrough behavior of an adsorption column, simplified treatment with a single transfer rate parameter can be used as shown in Section 6.5.

Mathematical treatment of breakthrough curves in a linear isotherm system is quite similar to the case of the chromatographic elution curve, since in this case step response (breakthrough curve) of an adsorption column is an integration of impulse response (chromatographic elution curve) over elapsed time. For reduction of chromatographic data, moments of the elution curves are involved, but when considering breakthrough curves, an analytical solution is desirable, or more simply, so-called dynamic adsorption capacity or break time can be estimated. It is possible to obtain analytical solutions in linear systems, but general solutions for a set of equations are somewhat complicated and in many cases simplified models are used when analytical solutions are necessary.

Analytical solutions to nonlinear isotherms are limited to special cases. For favorable isotherm relations such as those of the Langmuir or

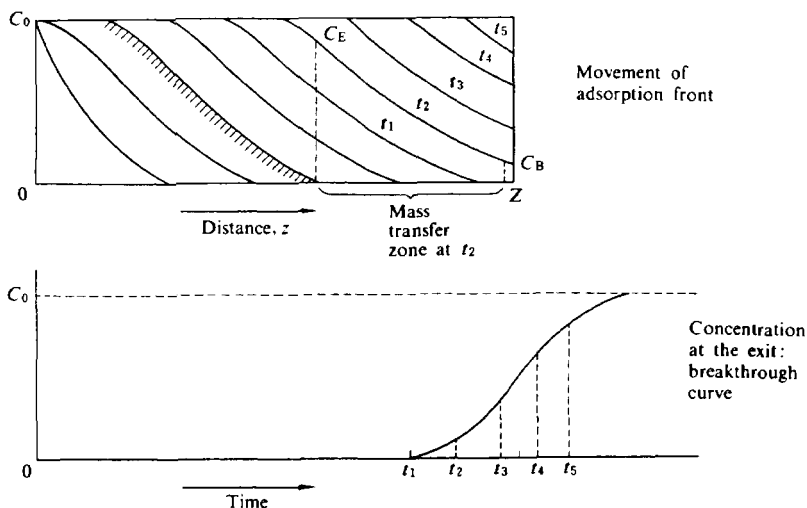


Fig. 7.1. Movement of adsorption front (mass transfer zone) and breakthrough curve.

Freundlich type where $n > 1$, concentration profiles become constant as they move along the column and solutions for these cases have long been discussed. Simple treatment methods are given first in Section 7.3 followed by numerical calculation methods.

7.1. Linear Isotherm Systems—Solution to the General Model

For a packed bed of porous uniform adsorbents, the basic equations for mass balance and transfer rates are the same as those given in the previous chapter.

$$E_z \frac{\partial^2 C}{\partial z^2} - u \frac{\partial C}{\partial z} - N_0 a_v = \frac{\partial C}{\partial t} \quad (7-1)$$

$$N_0 = k_f (C - c_{i|R}) = D_p \frac{\partial c_i}{\partial r} \Big|_{r=R} \quad (7-2)$$

$$D_p \left\{ \frac{\partial^2 c_i}{\partial r^2} + \left(\frac{2}{r} \right) \frac{\partial c_i}{\partial r} \right\} - N_i = \varepsilon_p \frac{\partial c_i}{\partial t} \quad (7-3)$$

$$N_i = \rho_p k_s (c_i - q_i / K_a) = \rho_p \frac{\partial q_i}{\partial t} \quad (7-4)$$

When surface diffusion is a dominant process in intraparticle diffusion,

the right-hand side of Eq. (7-4) is replaced by the following equation.

$$N_i = \rho_p \partial q_i / \partial t - D_s \rho_p \{ \partial^2 q_i / \partial r^2 + (2/r) \partial q_i / \partial r \} \quad (7-5)$$

In most cases of surface diffusion kinetics, adsorption rate at the active sites is considered to be rapid enough to assume the attainment of local adsorption equilibrium. Furthermore, when the adsorption isotherm is linear, Eqs. (7-3) and (7-5) are combined to give the following.

$$(D_p + D_s \rho_p K_a) \{ \partial^2 c_i / \partial r^2 + (2/r) \partial c_i / \partial r \} = (\varepsilon_p + \rho_p K_a) \partial c_i / \partial t \quad (7-6)$$

This means that pore diffusion kinetics and surface diffusion kinetics cannot be distinguished in the mathematical treatment so detailed discussion must be added for an understanding of which of the two mechanisms is controlling the actual phenomena.

For analysis of breakthrough behavior, step input should be considered as a boundary condition at the inlet of the bed.

$$\left. \begin{array}{l} t < 0 : \\ t > 0 \text{ and } z = 0 : \end{array} \right\} \begin{array}{l} C = c_i = q = 0 \\ C = C_0 \end{array} \quad (7-7)$$

The solution to Eqs. (7-1) to (7-4), for example, can be obtained in the Laplace domain as

$$\bar{C}(p) / C_0 = (1/p) \exp(-\lambda z) \quad (7-8)$$

where

$$\lambda = \frac{u}{2E_z} \left[\sqrt{1 + \frac{4E_z}{u^2} G(p)} - 1 \right] \quad (7-9)$$

$$G(p) = p + \frac{3(1-\varepsilon)}{\varepsilon} \frac{Bi}{R^2/D_c} \left[1 - \frac{Bi}{A_0(p) + Bi} \right] \quad (7-10)$$

$$A_0(p) = R \sqrt{\frac{\varepsilon K(p)}{D_c}} \quad (7-11)$$

$$K(p) = p + \rho_p \frac{1}{\varepsilon_p \left(\frac{1}{pK_a} + \frac{1}{k_a} \right)} \quad (7-12)$$

where p is the Laplace parameter.

Then inverse Laplace transform of Eq. (7-8) should give the breakthrough curve in the time domain.

$$\frac{C(t)}{C_0} = \frac{1}{2\pi i} \int_{\alpha-\infty}^{\alpha+\infty} e^{pt} \frac{\bar{C}(p)}{C_0} dp \quad (7-13)$$

The above integration, however, is rather complicated, since Eq. (7-8) includes a number of parameters. There have been many trials to obtain analytical solutions for similar but simpler cases including the pioneering work of Rosen (1952), which used Duhamel's theorem to include intraparticle diffusion kinetics.

Rasmuson and Neretnieks (1980) showed an analytical solution for the case where adsorption equilibrium holds inside the particle (infinite k_a in Eq. (7-4)). Their solution is shown below as an example.

$$\begin{aligned} \frac{C(z, t)}{C_0} = & \frac{1}{2} + \frac{2}{\pi} \int_0^\infty \exp\left(\frac{u}{2E_\tau} - z \sqrt{\frac{\alpha_1(\lambda)^2 + \alpha_2(\lambda)^2 + \alpha_1(\lambda)}{2}}\right) \\ & \cdot \sin\left(\frac{2D_s}{R^2} \lambda^2 t - z \sqrt{\frac{\alpha_1(\lambda)^2 + \alpha_2(\lambda)^2 + \alpha_1(\lambda)}{2}}\right) \frac{d\lambda}{\lambda} \quad (7-14) \end{aligned}$$

with

$$\alpha_1(\lambda) = \frac{u^2}{4E_\tau^2} + \frac{3D_s K}{R^2 \{\varepsilon/(1-\varepsilon)\} E_\tau} H_1 \quad (7-15)$$

$$\alpha_2(\lambda) = \frac{2D_s \lambda^2}{E_\tau} + \frac{3D_s K}{R^2 \{\varepsilon/(1-\varepsilon)\} E_\tau} H_2 \quad (7-16)$$

where H_1 and H_2 are hyperbolic functions of 1 and Bi

$$H_i(\lambda, Bi) = \frac{H_{D_i} + \frac{1}{Bi} (H_{D_i}^2 + H_{D_i}^2)}{\left(1 + \frac{H_{D_i}}{Bi}\right)^2 + \left(\frac{H_{D_i}}{Bi}\right)^2} \quad (7-17)$$

$$H_2(\lambda, Bi) = \frac{H_{D_1}}{\left(1 + \frac{H_{D_1}}{Bi}\right)^2 + \left(\frac{H_{D_1}}{Bi}\right)^2} \quad (7-18)$$

$H_{D_1}(1)$ and $H_{D_1}(\lambda)$ are defined as

$$H_{D_1}(\lambda) = \lambda \left(\frac{\sinh 2\lambda + \sin 2\lambda}{\cosh 2\lambda - \cos 2\lambda} \right) - 1 \quad (7-19)$$

$$H_{D_1}(\lambda) = \lambda \left(\frac{\sinh 2\lambda - \sin 2\lambda}{\cosh 2\lambda - \cos 2\lambda} \right) \quad (7-20)$$

When contribution of axial dispersion are negligible ($E_r = 0$), Eq. (7-14) should coincide with the limiting solution derived by Rosen (1952).

$$\begin{aligned} \frac{C}{C_0} = & \frac{1}{2} + \frac{2}{\pi} \int_0^\infty e^{-\frac{3D_c(1-\epsilon)}{R} \left(\frac{x}{u}\right) H_2(\lambda, Bi)} \\ & \cdot \sin \left[\frac{2}{R^2} \frac{D_c}{\rho_b K_a} \left(t - \frac{x}{u/\epsilon}\right) \cdot \lambda^2 \right. \\ & \left. - \frac{3D_c(1-\epsilon)}{R^2} \left(\frac{x}{u}\right) \cdot H_2(\lambda, Bi) \right] \frac{d\lambda}{\lambda} \quad (7-21) \end{aligned}$$

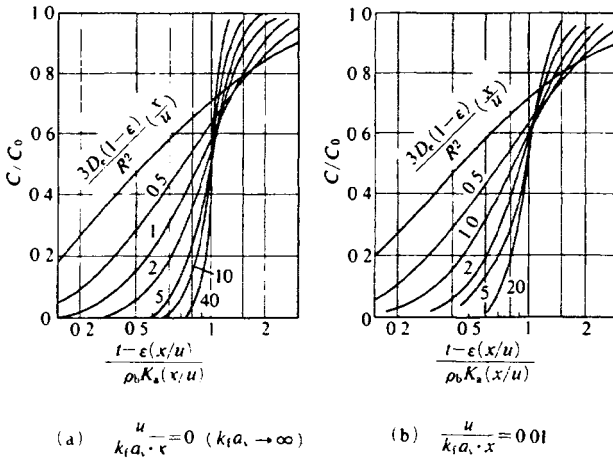


Fig 7.2 Breakthrough curves for linear isotherm systems based on Rose's solution
 (Reproduced with permission by Kawazoe, K., *Kagaku-Kogaku-Benran*, p 866 Maruzen (1978))

where H_1 and H_2 are given by Eqs. (7-17) and (7-18). Similar solutions have been obtained for the case where the rate of adsorption at the adsorption site is taken into account (Masamune and Smith, 1965) and for bi-dispersed porous particles where diffusion resistance in micropore is accounted for in series to the macropore diffusion resistance (Kawazoe and Sugiyama, 1967).

These solutions include two to three rate parameters, which makes it difficult to examine the effect of each rate step on the overall breakthrough curves. As an example calculated breakthrough curves based on Rosen's solution are shown in Fig. 7.2.

As is seen from the figure, breakthrough curves for larger values of column length parameter become rather similar to each other. This suggests that a more simple model may be used for breakthrough characteristics in this range.

7.2. Linear Isotherm System—Simple Models

One of the simple models used to describe adsorption in a column is the two-phase exchange model.

$$-u \frac{\partial C}{\partial z} = k(C - c_s) = \alpha \frac{\partial c_s}{\partial t} \quad (7-22)$$

Analytical solution of the chromatographic elution curve of this model is given by Eq. (6-68).

$$\frac{C(t)}{M} = \exp(-S) \left[\delta(t) + \exp(-St/\tau) \cdot \frac{S}{\sqrt{t\tau}} \cdot I_1(2S\sqrt{t/\tau}) \right] \quad (6-68)$$

where $S = kZ/u$ and $\tau = \alpha Z/u$. This equation is integrated along time to yield step response of the model.

$$C/C_0 = \exp(-S - St/\tau) I_0(2S\sqrt{t/\tau}) + \int_0^t \exp[-S(1 + t/\tau)] I_0[2S\sqrt{t/\tau}] S dt/\tau \quad (7-23)$$

This equation can be approximated in terms of error function for the range $S > 40$ as

$$C/C_0 = (1/2) \{1 + \operatorname{erf} E\} \tag{7-24}$$

where

$$E = \frac{1}{2} \frac{\sqrt{S}}{\tau} (t - \tau) \tag{7-25}$$

and the error function is defined as

$$\operatorname{erf} x = \frac{2}{\sqrt{\pi}} \int_0^x \exp(-x^2) dx \tag{7-26}$$

By equating the second moments of the chromatographic elution curves obtained from the general model and the simple model, k in the two-phase exchange model is replaced by the overall mass transfer coefficient, $K_F a_v$, which is defined as

$$\frac{1}{K_F a_v} = \frac{R^2}{15(1 - \epsilon)D_c} + \frac{1}{k_i a_v} + \frac{d_p}{Pe_u} \tag{7-27}$$

Hence, by using the estimated rate parameters of adsorption in a column, a rough estimation of the breakthrough curve is possible by means of the simple model, provided the column is long enough to

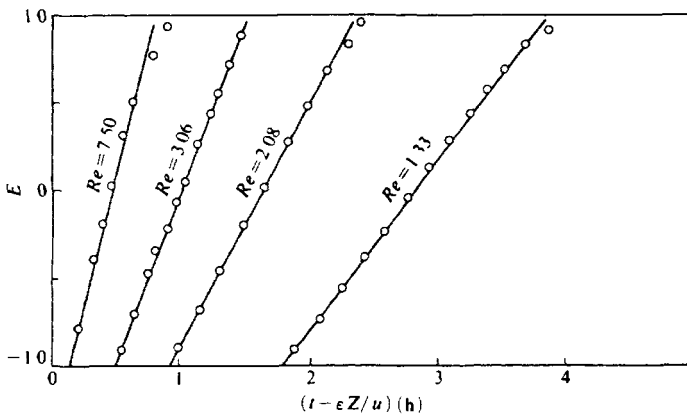


Fig 7.3 Examples of error function plot for breakthrough curves from linear isotherm systems. E is obtained from concentration change, C/C_0 , using Eq (7-24), slope determines $\sqrt{S}/(2\tau)$
 (Reproduced with permission by Kawazoe, K and Takeuchi, Y, *Kagaku Kogaku*, 31, 51 (1967))

satisfy the condition of $S > 40$, which is for the most part met in cases of gas phase adsorption.

Also by applying Eqs. (7-24) and (7-25), determination of K_{Fa_v} is possible provided S is large enough. From experimental observation of the breakthrough curve (C/C_0 versus elapsed time, t), a relation between E and t can be determined by using Eq. (7-24). Then a plot of E versus t according to Eq. (7-25) gives K_{Fa_v} from the slope of the regression line, S ($= K_{Fa_v}Z/u$). An illustration of the plot of E versus t is shown in Fig. 7.3.

It should be noted from Eq. (7-26) that the length of the mass transfer zone increases proportionally to the square root of the adsorption time. This corresponds to linear increase of the second moment of chromatographic response with increase of the column length as shown, for instance, by Eq. (6-17).

7.3. Nonlinear Isotherm Systems—Constant Pattern Adsorption Profile

Adsorption isotherms are in most cases nonlinear and favorable, that is, concave to the direction of the axis of the amount adsorbed

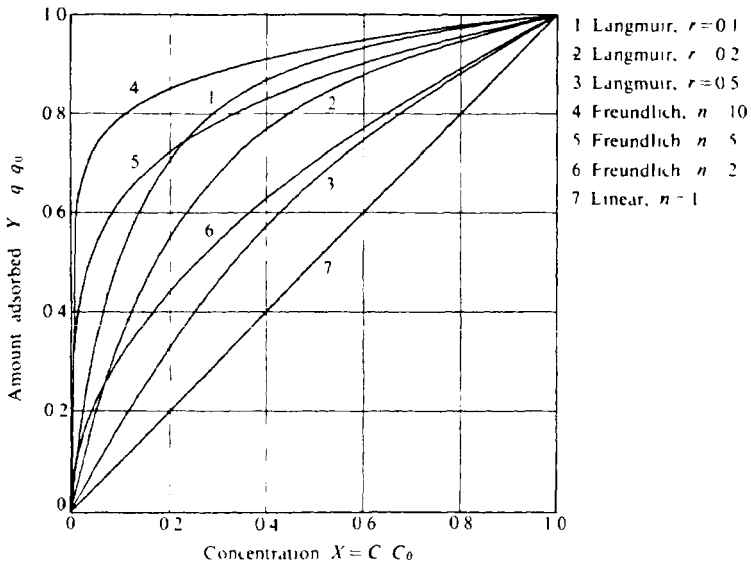


Fig. 7.4 Examples of isotherms

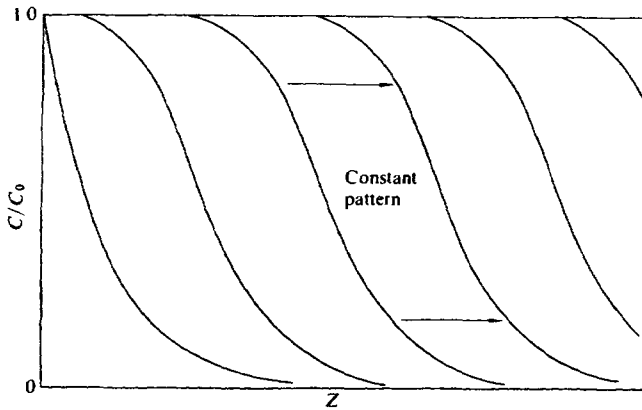


Fig 7.5 Establishment of Constant Pattern

(Fig 7.4), which corresponds to the Langmuir equilibrium with separation factor $r < 1$ or $n > 1$ in the Freundlich isotherm system

In these cases, a constant profile of mass transfer zone is established while adsorption proceeds in a column (Fig 7.5). This is in contrast to linear isotherm systems where mass transfer zone continues to spread with increase of traveling time. The reason for the formation of a constant pattern is explained as follows:

The speed of movement of the point on the mass transfer zone whose concentration is C , $V(C)$, can be related to the equilibrium through the basic equation

$$u dC/dz + \rho_b d\bar{q}/dt = 0 \quad (7-28)$$

as

$$V(C) = |dz/dt|_C = (u/\rho_b) |dC/d\bar{q}|_C \quad (7-29)$$

where \bar{q} is the average amount adsorbed. C and \bar{q} are related to each other by a mass transfer equation and the equilibrium relation.

When equilibrium adsorption takes place, $\bar{q} = q(C)$ holds and $V(C)_{\text{equil}}$ can be written as

$$V(C)_{\text{equil}} = (u/\rho_b) |dC/dq|_C \quad (7-30)$$

For favorable adsorption isotherm systems, the higher the concentration, C , the smaller $|dq/dC|_C$ becomes, thus enlarging $|dC/dq|_C$. This

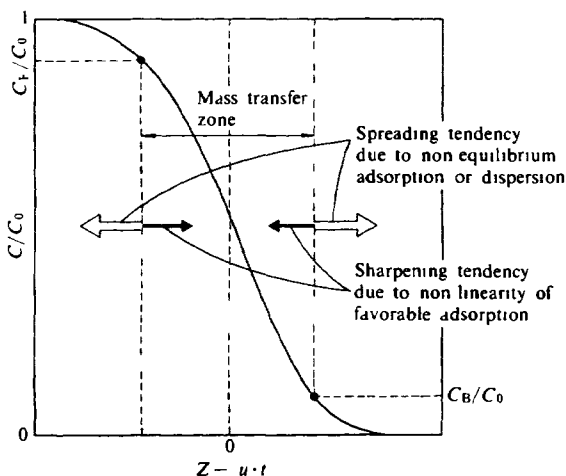


Fig 7.6 Spreading tendency due to the nonequilibrium nature (mass transfer resistance) of adsorption or dispersion in the column is balanced with sharpening tendency due to nonlinearity of favorable isotherm when a constant pattern profile is established

means that a point with a higher concentration on the adsorption front should proceed faster than a point at a lower concentration. This cannot happen in real systems so adsorption front forms a step shape. This imaginary relation caused by a favorable equilibrium relation should be considered rather to play the role of a driving force to narrow the adsorption front (mass transfer zone) once spread by mass transfer resistance and dispersion effects (Fig. 7.6). Therefore, the mass transfer zone proceeds in a constant shape after these two counteracting effects are balanced

When constant pattern profile is established, $V(C)$ is constant regardless of concentration, and then from Eq. (7-28) the following equation is derived as a condition of the constant pattern.

$$x \equiv C/C_0 = y \equiv \bar{q}/q_0 \quad (7-31)$$

7.3.1. Solution of constant pattern profile from LDF models

A LDFC model

Simple models often employ two-phase exchange models. The model introduced in Section 6.5.2 is expressed as Eq. (7-28) with

$$\rho_b d\bar{q}/dt = K_F a_v (C - C^*) \quad (7-32)$$

where C^* is an equilibrium concentration with \bar{q} . This model is based on the idea that mass transfer rate is expressed by using the overall mass transfer coefficient, $K_F a_v$, based on the fluid phase concentration difference as the driving force. This model is referred to as LDFC (linear driving force model based on concentration difference).

Obviously this model is suitable for those cases where fluid-to-particle mass transfer is a dominant mass transfer resistance. In such cases $K_F a_v$ can be replaced by fluid-to-particle mass transfer coefficient, $k_f a_v$.

B. LDFQ model

Another model often used is one similar to the above except that mass transfer is expressed on the basis of particle phase concentration difference. Instead of Eq. (7-32), the following form is introduced.

$$\rho_b d\bar{q}/dt = K_s a_v (q^* - \bar{q}) \quad (7-33)$$

This model is referred to as LDFQ. LDFC and LDFQ models are identical when the adsorption isotherm is linear ($q = KC$), by setting $K_s a_v = K_F a_v / K$. For nonlinear equilibrium systems, however, the two models indicate individual behavior, that is, considerably different concentration profiles, especially when nonlinearity is large.

Compared with a more rigorous model, this model gives better approximation when intraparticle diffusion plays a dominant role in mass transfer. When intraparticle diffusion is the only rate determining step of mass transfer, $K_s a_v$ can be replaced by particle phase mass transfer coefficient, $k_s a_v$, which is related to the intraparticle diffusion parameters as

$$k_s a_v = \rho_b \cdot 15 \phi_s D_s / R^2 \quad (7-34)$$

or

$$k_s a_v = \frac{15 \phi_s D_p / R^2}{q_0 / C_0} \quad (7-35)$$

Selection of the above equations depends on the dominant mechanism of intraparticle diffusion. When surface diffusion kinetics are controlling, then Eq. (7-34) is used, while Eq. (7-35) should be used for dominant pore diffusion kinetics. The parameter, ϕ_s , is introduced to account for the deviation of the approximation from linear equilibrium cases where ϕ_s is taken as unity, as can be understood from the second

moment expression of a chromatographic peak discussed in Chapter 6.

For the Langmuir isotherm system ($y = x/[r + (1 - r)x]$), the following correlation for ϕ_s is given by Miura and Hashimoto (1977).

$$\phi_s = 1 - 0.192(1 - r)^3 \quad (7-36)$$

Also, in the case of Freundlich isotherm systems ($y = x^{1/n}$), ϕ_s is correlated as a function of n as follows.

$$\phi_s = 0.808 + 0.192/n \quad (7-37)$$

C. LDF series model

Better approximation is possible by considering that LDFC model and LDFQ model are valid, respectively, at fluid-to-particle mass transfer and at intraparticle diffusion. In this case, adsorption equilibrium is considered to hold at the particle surface as $q_s = q_s(c_s)$. The basic equations for mass transfer rate expression are as follows.

$$\rho_b d\bar{q}/dt = k_f a_v (C - c_s) = k_s a_v (q_s - \bar{q}) \quad (7-38)$$

This equation is transformed by using constant pattern condition (Eq. (7-31)) and the dimensionless form becomes

$$\frac{1}{1 + \zeta} \cdot \frac{d\bar{y}}{d\theta_T} = x - x_s = (1/\zeta)(y_s - y) \quad (7-39)$$

where

$$\zeta = \left(\frac{k_f a_v}{k_s a_v} \right) \left(\frac{C_0}{q_0} \right), \quad \theta = \frac{t - \varepsilon z/u}{\frac{1}{k_f a_v} + \frac{1}{k_s a_v (q_0/C_0)}}$$

$$x = C/C_0 \quad \text{and} \quad y = q/q_0$$

The solution to Eq. (7-39) was shown by Kawazoe and Fukuda (1965) for the Langmuir isotherm, and Miura and Hashimoto (1976) gave analytical forms for the Langmuir and Freundlich isotherm systems. Eq. (7-39) can be solved in terms of x_s , which is then converted to x and \bar{y} .

For the Langmuir isotherm ($y = x/[r + (1 - r)x]$),

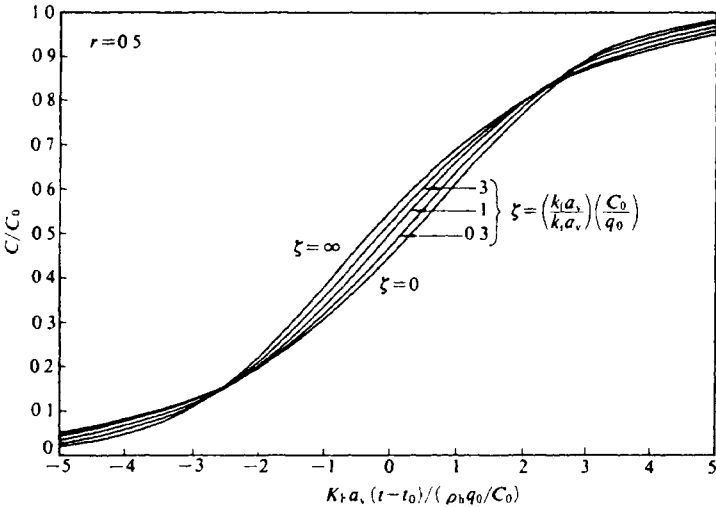
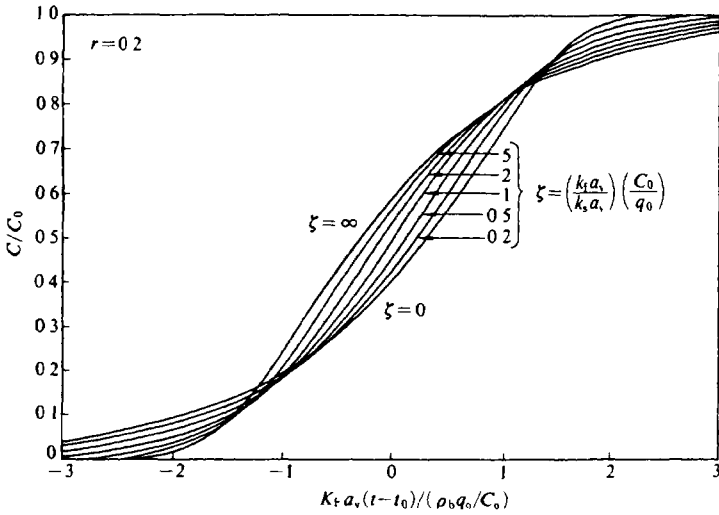


Fig 77 Constant pattern profiles calculated from LDF-series model with Langmuir isotherm

$$\begin{aligned} \frac{(K_s a_v)}{\rho_b}(t - t_0) &= \frac{1}{1 + \zeta} \left[\frac{1}{1 - r} \ln x_s - \frac{r}{1 - r} \ln(1 - x_s) \right. \\ &\quad \left. - \ln\{r + (1 - r)x_s\} - \frac{r}{1 - r} \ln r + 1 \right] \\ &\quad + \frac{\zeta}{1 + \zeta} \left\{ \frac{r}{1 - r} \ln x_s - \frac{r}{1 - r} \ln(1 - x_s) - 1 \right\} \quad (7-40) \end{aligned}$$

where

$$\frac{1}{(K_s a_v)_0} = \frac{q_0/C_0}{k_f a_v} + \frac{1}{k_s a_v} \quad (7-41)$$

$$t_0 = (z/u)[\varepsilon + \rho_b q_0/C_0] \quad (7-42)$$

From x_s , x is obtained as

$$x = [(\zeta r + 1)x_s + \zeta(1 - r)x_s] / (\zeta + 1)[r + (1 - r)x_s] \quad (7-43)$$

The above solution reduces to more simpler forms when external mass transfer is controlling the rate of adsorption (LDFC model) or intraparticle diffusion is the sole rate-determining step (LDFQ model).

a. LDFC model

$$\frac{k_f a_v}{\rho_b q_0/C_0}(t - t_0) = 1 - \frac{r \ln(1 - x) - \ln x}{1 - r} \quad (7-44)$$

which coincides with the results obtained by Michaels (1952).

b. LDFQ model

$$k_s a_v / \rho_b (t - t_0) = \frac{r}{1 - r} \ln x - \frac{1}{1 - r} \ln(1 - x) - 1 \quad (7-45)$$

This equation was obtained by Hall *et al.* (1966).

The effect of ζ on constant pattern profiles for the Langmuir isotherm systems are examined from Eqs. (7-42) and (7-43) and is illustrated in Fig. 7.7 for $r = 0.2$ and 0.5 . Naturally, difference of dominant mass transfer mechanisms is more pronounced at smaller r .

For the Freundlich isotherm ($\gamma = x^{1/n}$), a similar solution was obtained by Miura and Hashimoto (1977) as

$$\begin{aligned}
 (K_s a_v)_0 / \rho_b(t - t_0) = & \\
 & \frac{1}{1 + \zeta} \left\{ \frac{1}{1 - n} \ln(x_s^{1/n} - 1) + 1 + \frac{1}{\zeta + 1} \cdot \frac{1}{n(1 - n)} I_A \right\} \\
 & + \frac{\zeta}{1 + \zeta} \left\{ \frac{1}{1 - n} \ln(1 - x_s^{1 - 1/n}) + \frac{\zeta}{\zeta + 1} \cdot \frac{n}{1 - n} I_B \right\} \\
 & + \frac{\zeta}{(1 + \zeta)^2} \left\{ \frac{1}{n} - 1 + \frac{1}{1 - n} (I_A + I_B) \right\} \tag{7-46}
 \end{aligned}$$

where

$$I_A = - \int_0^1 x^{1/n - 1} \ln(1 - x^{1 - 1/n}) dx \tag{7-47}$$

$$I_B = - \int_0^1 \ln(1 - x^{1 - 1/n}) dx \tag{7-48}$$

These integrals are given by infinite series of two different forms.

$$I_A = \frac{n}{n - 1} \left[1 + \sum_{k=1}^{\infty} (-1)^k \frac{(\frac{2}{n} - 1)(\frac{3}{n} - 2) \dots (\frac{k+1}{n} - k)}{k!(k + 1)^2 (\frac{n-1}{n})^k} \right] \tag{7-49}$$

$$I_B = \frac{n}{n - 1} \left[1 + \sum_{k=1}^{\infty} (-1)^k \frac{\frac{1}{n}(\frac{2}{n} - 1)(\frac{3}{n} - 2) \dots (\frac{k}{n} - k + 1)}{k!(k + 1)^2 (\frac{n-1}{n})^k} \right] \tag{7-50}$$

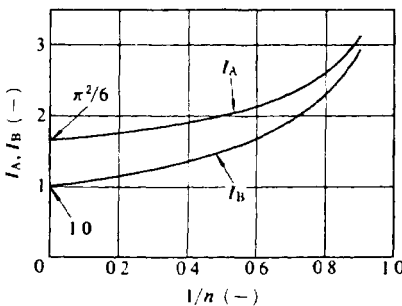


Fig 7 8 Graph representation of I_A and I_B versus reciprocal Freundlich constant n
 (Reproduced with permission by Miura *J Chem Eng Japan* 10, 492 (1977))

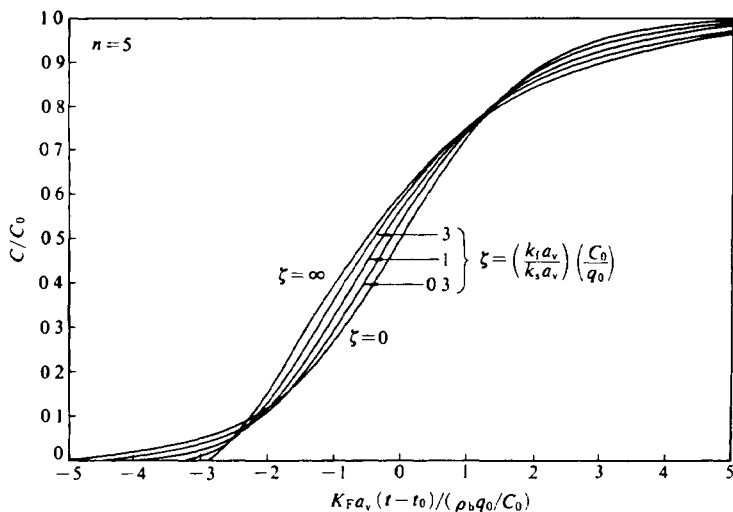
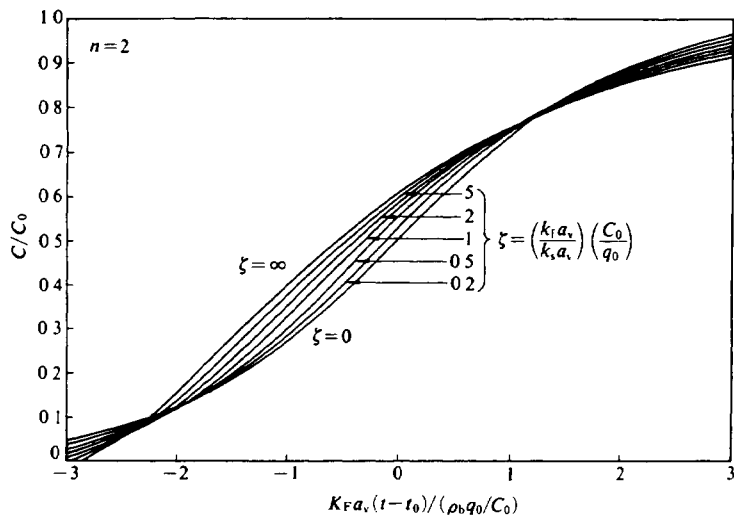


Fig 79 Constant pattern breakthrough curves calculated from LDF-series model with Freundlich isotherm ($Y=X^{1/n}$)

or

$$I_A = \sum_{k=1}^{\infty} \frac{1}{k(k\frac{n-1}{n} + \frac{1}{n})} \quad (7-51)$$

$$I_B = \sum_{k=1}^{\infty} \frac{1}{k(k\frac{n-1}{n} + 1)} \quad (7-52)$$

Eqs (7-49) and (7-50) over Eqs. (7-51) and (7-52) are recommended because of faster convergence. I_A and I_B in graph form are shown in Fig. 7.8.

$(K_s a_v)_0$ and t_0 defined above (Eqs. (7-41) and (7-42)) are valid here, and again x_s can be converted to x by the equilibrium relation at the interface, which is in this case the following equation.

$$x = (\zeta x_s + x_s^{1/n}) / (\zeta + 1) \quad (7-53)$$

The general solution (Eq (7-46)) is simplified when mass transfer rate is expressed in terms of either $k_t a_v$ only (LDFC model) or $k_s a_v$ only (LDFQ model).

a LDFQ model

$$\begin{aligned} \frac{k_t a_v}{\rho_b q_0 / C_0} (t - t_0) = & 1 + \ln x - \frac{1}{n-1} \ln(1 - x^{n-1}) \\ & - \frac{1}{n(n-1)} I_A \end{aligned} \quad (7-54)$$

b LDFC model

$$\frac{k_s a_v}{\rho_b} (t - t_0) = \frac{n}{1-n} [\ln(1 - x^{(n-1)/n}) + I_B] \quad (7-55)$$

The effect of ζ on constant pattern profiles is shown by Fig. 7.9 for Freundlich constant $n = 2$ and 5

7.3.2. Solution of constant pattern profile from dispersion model

For another typical case of simple models, i.e. dispersion model, the basic equation is written instead of Eq (7-28) and (7-32) as follows

$$E_t \partial^2 c / \partial z^2 - u \partial c / \partial z = \rho_b \partial \bar{q} / \partial t \quad (7-56)$$

or, in dimensionless form,

$$(1/Pe) \partial^2 x / \partial z^2 - \partial x / \partial z = \partial \bar{y} / \partial \theta \quad (7-57)$$

where $Pe = uZ/E_z$, $\theta = (tu/Z)(C_0/\rho_b q_0)$, $x = C/C_0$ and $\bar{y} = \bar{q}/q_0$.

By assuming \bar{q} is in equilibrium with C , analytical solutions are given for the Langmuir and Freundlich isotherm systems (Coppola and LeVan, 1981).

Langmuir isotherm:

$$N(1 - T) = \frac{1}{1 - r} \ln \left[\frac{1 - x}{x^r} \right] \quad (7-58)$$

Freundlich isotherm:

$$N(1 - T) = \frac{n}{n - 1} [\ln(1 - x^{(n-1)/n}) + \gamma + \psi[n/(n - 1)]] \quad (7-59)$$

where number of transfer units is $N = Zu/E_z = Pe$, throughput parameter is $T = tu/Z(\rho_b q_0/C_0)$, γ is the Euler constant and $\psi(x)$ is the psi function.

For models with two or more rate parameters, similar solutions have been obtained and discussed (Vermeulen, 1984). For exact treatment, however, recent developments in computers make it easier to directly solve complex basic equations.

7.3.3. Length of mass transfer zone

In the practical designing of adsorption columns or prediction of adsorber performance, it is often necessary to make a quick estimate of the length of mass transfer zone, which is readily calculated from the constant pattern profiles. If we define a length of mass transfer zone as the longitudinal distance between the two arbitrary points where concentrations in the bed are C_E and C_B ($C_0 < C_E < C_B < 0$), the length of mass transfer zone is given if LDFC model is employed as

$$Z_a = (V/K_{fa}) N_{OF} \quad (7-60)$$

$$N_{OF} = \int_{x_B}^{x_E} dC/(C - C^*) \quad (7-61)$$

where V is the propagation speed of the mass transfer zone, which is

obviously

$$V = uC_0 / (\rho_b q_0 + \varepsilon C_0) \tag{7-62}$$

Elution time of mass transfer zone is naturally determined from

$$t_E - t_B = Z_a / V \tag{7-63}$$

Usually $x_B = C_B / C_0$ and $x_E = C_E / C_0$ are taken as 0.05 and 0.95 or 0.1 and 0.9. N_{OF} can be calculated easily from adsorption isotherms.

For the Langmuir isotherm ($r = (1 - y)x / (1 - x)y$), N_{OF} for $x_B = 0.1$ and $x_E = 0.9$ is given as

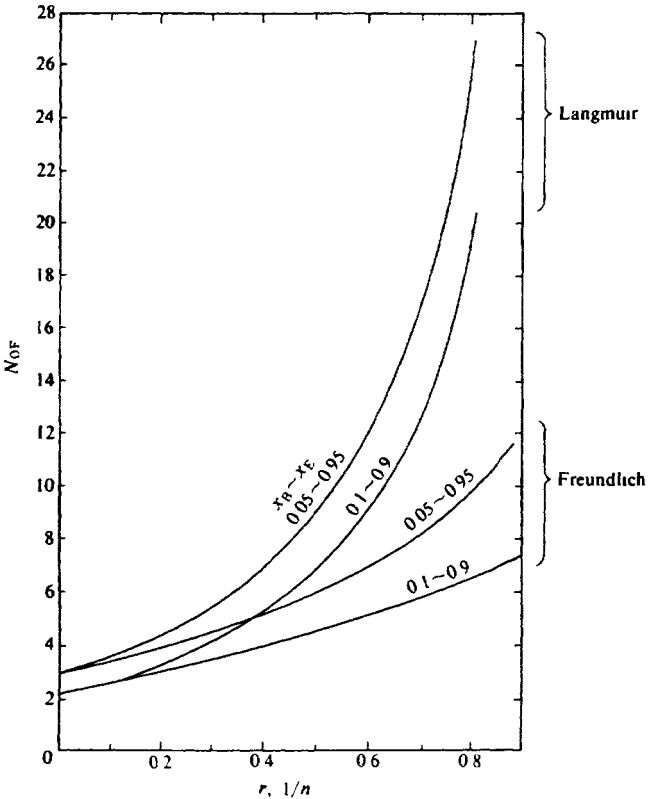


Fig 7 10 N_{OF} for the Langmuir and Freundlich isotherms

$$\begin{aligned}
 N_{OF} &= \int_{x_B}^{x_E} dx / [x - rx / \{1 + (r-1)x\}] \\
 &= \frac{1}{1-r} \ln \frac{x_B(1-x_E)}{x_E(1-x_B)} + \ln \frac{1-x_E}{1-x_B} \\
 &= \frac{1+r}{1-r} \ln 9
 \end{aligned} \tag{7-64}$$

For the Freundlich isotherm ($y = x^{1/n}$),

$$\begin{aligned}
 N_{OF} &= \int_{x_B}^{x_E} dx / (x - x^n) \\
 &= \ln \frac{x_E}{x_B} + \frac{1}{n-1} \ln \frac{1-x_E^{n-1}}{1-x_B^{n-1}} \\
 &= \ln 9 + \frac{1}{n-1} \ln \frac{1-0.1^{n-1}}{1-0.9^{n-1}}
 \end{aligned} \tag{7-65}$$

Fig. 7.10 illustrates N_{OF} defined by taking C_B and C_E as 0.1 and 0.9 or 0.05 and 0.95 as a function of the separation factor r of the Langmuir isotherm or the Freundlich exponent $1/n$. N_{OF} for other isotherm relations can be easily calculated by Eq. (7-61).

7.4. Numerical Solutions for Nonlinear Systems

Breakthrough curves may be calculated directly from basic equations with nonlinear isotherms by numerical computation. The literature includes many works on more rigorous models such as intraparticle diffusion models (Tien and Thodos, 1959; Antonson and Dranoff, 1969; Carter and Husain, 1972; Kyte, 1973; Garg and Ruthven, 1973; 1974; Hashimoto *et al.*, 1977) with or without fluid-to-particle mass transfer resistance. Although these authors assumed negligible axial dispersion effect, numerical computation is bulky. Computation is greatly minimized when constant pattern assumption is employed (Hall *et al.*, 1966; Fleck *et al.*, 1973; Garg and Ruthven, 1975; Miura and Hashimoto, 1976), or linear driving force (LDF) model is employed (Zwiebel *et al.*, 1972; Garg and Ruthven, 1973; Miura and Hashimoto, 1977).

The advantage of numerical solutions is obviously that they provide more rigorous results because of less simplification involved in the model. However, when a model is more complicated and numerical

processing is included, it becomes rather difficult to see the effect of each parameter constituting the model. Then in order to clarify the behavior of the model, many repeated computations using various sets of parameters become necessary, making for bulkier computation.

The simplest advantage of numerical calculation may be its use for examining the validity of simpler models such as LDF models or constant pattern model. As a matter of fact, the correction factor, ϕ_s ,

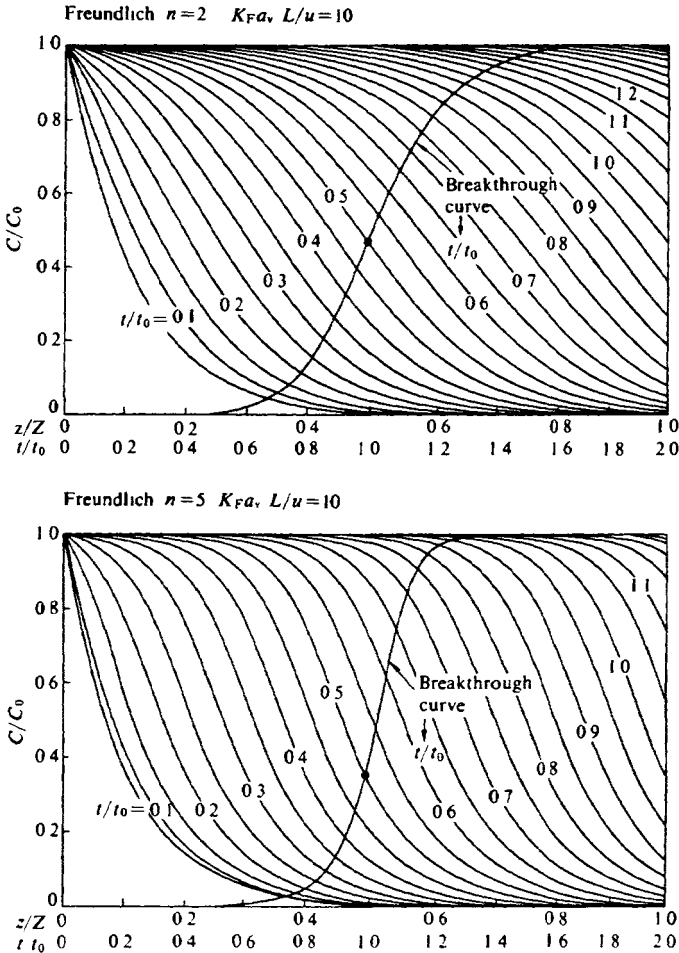


Fig 7.11 Development of concentration profile in an adsorption column, LDFC model with the Freundlich isotherms

TABLE 7.1 Minimum column length needed to establish constant pattern profile, Z_{\min} , in terms of length of mass transfer zone, Z_a

$1/n_F$ in Freundlich equation	Z_{\min}/Z_a
0.3 >	1 >
> 0.5	> 1
0.7	≈ 2

(Reproduced with permission by Hashimoto, K., *Kagaku Kogaku*, 40, 14 (1976))

r in Langmuir equation	Z_{\min}/Z_a
0.83	≈ 5
0.71	≈ 2
0.56	1.1
0.33	0.74

(Reproduced with permission by Garg, D. G. and Ruthven, D. R., *AIChE Journal*, 21, 200 (1975))

introduced for $K_s a_v$ (Eqs. (7-34) to (7-37)) was determined by calibrating an LDFQ model with an intraparticle diffusion model.

The bed length needed to approach constant pattern profile is also discussed using a numerical calculation without constant pattern assumption. According to Hashimoto *et al.* (1976) and Garg and Ruthven (1975), minimum column length needed to establish the constant pattern profiles are obtained relative to the mass transfer zone length as shown in TABLE 7.1. Propagation of the mass transfer zone obtained using the LDFC model is illustrated in Fig. 7.11 for the Freundlich isotherms with $n = 2$ and 5.

7.5. Breakthrough of Multicomponent Adsorbate Systems

When multicomponent adsorbates are contained in the fluid entering an adsorbent bed, breakthrough behavior becomes more complicated than in single component systems. Analysis of multicomponent adsorption is necessary in many cases but two typical situations may be of concern. One situation is related to the separation of mixtures. When separation of two or more components is necessary, the behavior of each component in the column must be described as precisely as possible. The other situation is encountered in the purification of water or air which contains many unknown pollutants. In this case, prediction of the global behavior of the column may be necessary.

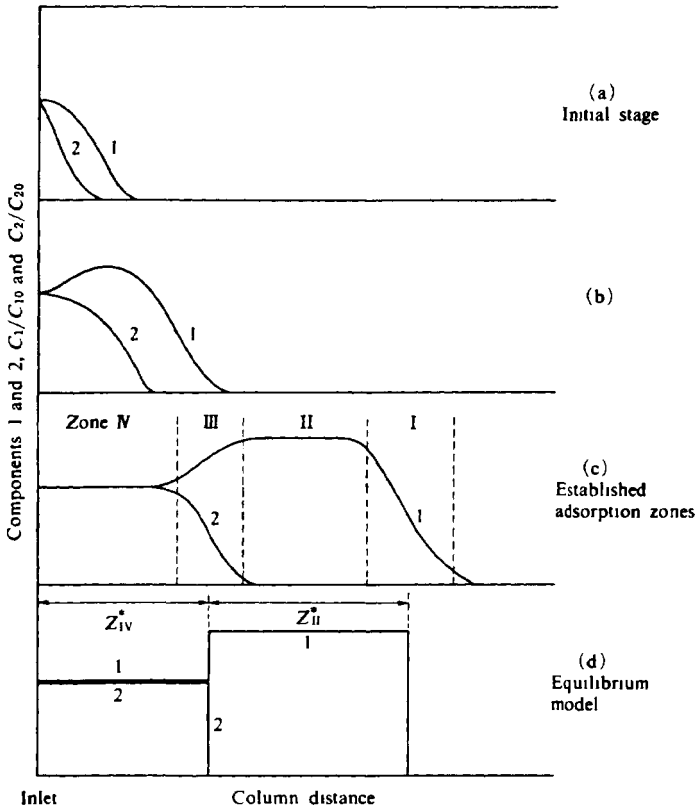


Fig 7.12 Development of adsorption zones in bi component adsorption.

7.5.1. Breakthrough of known bicomponent adsorbates

When weakly adsorbed Component 1 and strongly adsorbed Component 2 are contained in the fluid entering an adsorbent column, Component 1 weakly adsorbed is replaced by the stronger Component 2; then Component 1 proceeds in the column faster than Component 2. In this case, after a certain length of traveling path, the concentration profiles of the two components are established as shown in Fig. 7.12.a-c. The established profiles of the concentrations are discussed by division into four zones.

In Zone IV, the amounts of both components adsorbed on adsorbent are in equilibrium with the concentrations of both components in the

entering fluid. Since the fraction of the amount adsorbed of Component 2 becomes bigger than that in the fluid phase, the weaker component (Component 1) will become in excess in the fluid phase and then is pushed to the front of the column. Single-component adsorption of Component 1 takes place at the frontal part of the adsorption zones (Zones I and II) which is then partly replaced by Component 2 in Zone III.

Mass balance in Zone III determines the concentration level of Component 1 in Zone II. Also, zone length of Zone III can be determined from the equilibrium relation of replacement of Component 1 by Component 2 and mass transfer rate during replacement. Length of Zone I can be determined from the method of estimating the single-component adsorption breakthrough curve stated above. Lengths of Zones II and IV are calculated from mass balances of Components 1 and 2 and the lengths of Zones I and III.

The concentration levels at Zones II and IV and the length of each zone can be obtained as follows.

A. equilibrium consideration of bicomponent breakthrough curves

When adsorption is assumed to take place in equilibrium mode, concentration profiles in the bed may become as shown in Fig. 7.12.d, where the lengths of Zones I and III become infinitesimally small.

The amounts adsorbed of both components in Zone IV are determined from the inlet concentrations, C_{10} and C_{20} , by using the adsorption equilibrium relation for the mixture, e.g. the IAS model proposed by Myers and Prausnitz (1965) or the classical Markham-Benton equation (1931). When the Markham-Benton equation is applicable, the amounts adsorbed of both components, q_{10} and q_{20} in equilibrium with C_{10} and C_{20} are obtained as

$$q_{10} = q_{1\infty} K_1 C_{10} / (1 + K_1 C_{10} + K_2 C_{20}) \quad (7-66)$$

$$q_{20} = q_{2\infty} K_2 C_{20} / (1 + K_1 C_{10} + K_2 C_{20}) \quad (7-67)$$

where $q_{1\infty}$ and $q_{2\infty}$ are the saturation amounts adsorbed of Components 1 and 2 and K_1 and K_2 are the equilibrium constants of both species. These parameters are determined from single-component Langmuir equations.

In the replacement zone (Zone III), if stoichiometric replacement is assumed, the concentration and the amount adsorbed of Component 1 at Zone II, C_{1e} and q_{1e} are related to C_{10} , C_{20} , q_{10} and q_{20} by the following equation.

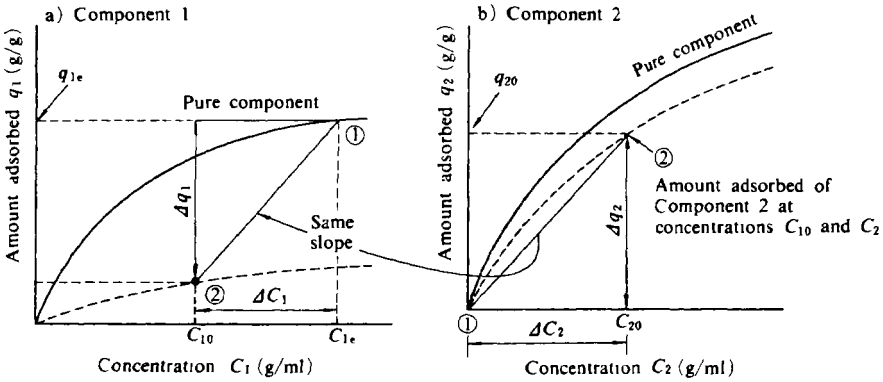


Fig. 7.13. Determination of q_{1e} from pure component and bicomponent isotherms.

$$dq/dC = q_{20}/C_{20} = (q_{1e} - q_{10})/(C_{1e} - C_{10}) \quad (7-68)$$

Also, q_{1e} and C_{1e} are related by the single-component isotherm relation, which is, in this case,

$$q_{1e} = q_{1\infty} K_1 C_{1e} / (1 + K_1 C_{1e}) \quad (7-69)$$

Then by solving Eqs. (7-68) and (7-69), C_{1e} and q_{1e} can be determined.

For arbitrary isotherm relations, determination of C_{1e} and q_{1e} can be made graphically as shown in Fig. 7.13 (Takeuchi *et al.*, 1978). From the bicomponent isotherm relation of Component 2 in Fig. 7.13.a, the slope dq/dC is determined by connecting the point (C_{20}, q_{20}) with the origin with the straight line. Then the cross point of the straight line of the same slope, dq/dC , from the point representing (C_{10}, q_{10}) and the single component isotherm of Component 1 gives C_{1e} and q_{1e} .

In the case of the Markham-Benton isotherm, the analytical solution to Eqs. (7-68) and (7-69) gives C_{1e} as follows.

$$C_{1e} = 1/2K_1 [p + \sqrt{p^2 + 4(1-d)^2}] \quad (7-70)$$

where

$$p = 1 - g_1 + d(1 + g_2) \quad (7-71)$$

$$g_1 = K_1 C_{10}, \quad g_2 = K_2 C_{20} \quad (7-72)$$

$$d = K_1 q_{1\infty} / K_2 q_{2\infty} \quad (7-73)$$

The equilibrium amount adsorbed in Zone II can then be obtained from Eq. (7-69).

From q_{20} , q_{10} and q_{1e} , equilibrium zone length Z_{IV}^* and Z_{II}^* can be readily obtained from the mass balances as

$$Z_{IV}^*(t) = u_0 t C_{20} / \rho_b q_{20} \quad (7-74)$$

$$Z_{II}^*(t) = (u_0 t C_{10} - \rho_b q_{10} Z_{IV}^*) / \rho_b q_{1e} \quad (7-75)$$

B. description of replacement zone, Zone III

When Component 1 previously adsorbed is replaced by Component 2 at Zone III, zone length will be determined from replacement equilibrium relation and mass transfer rates involved in the replacement process.

The simplest treatment is application of the method for estimating a single-component breakthrough curve to the propagation of the replacement front of the stronger component (Component 2). In this case the equilibrium relation for replacement must be composed from bicomponent equilibrium relations by assuming a linear relation between the concentration of Component 1 and that of Component 2 on the surface of the adsorbent.

$$(C_1 - C_{10}) / (C_{1e} - C_{10}) = (C_{20} - C_2) / C_{20} \quad (7-76)$$

The replacement equilibrium relation can be derived by combining the above relation with bicomponent equilibrium relations.

In the case of the Markham-Benton equation, combining Eqs. (7-66), (7-67) and (7-76) gives the following relation.

$$q_2 = q_{20} K_2 C_2 / (1 + K_1 C_{1e} + K^* C_2) \quad (7-77)$$

where

$$K^* = K_2 - K_1 (C_{1e} - C_{10}) / C_{20} \quad (7-78)$$

Obviously, when Component 2 is "stronger", $K^* > 0$ or

$$K_2 C_{20} > K_1 (C_{1e} - C_{10}) \quad (7-79)$$

should hold and then the equilibrium relation described by Eq. (7-77) becomes concave to the q_2 axis or replacement is considered favorable. In this case a constant pattern profile will be established in Zone III.

When K^*C_2 is smaller than $1 + K_1C_{1e}$, the relation expressed by Eq. (7-77) is approximated by the linear relation and the replacement zone does not form a constant pattern profile.

With regard to mass transfer rate in replacement, available information is limited. Whether resistance to the exchange of both components at the adsorption site is negligible and whether counter diffusion of adsorbing component and desorbing component interfere with each other are among the problems not yet solved.

For the sake of simplicity, however, a linear driving force model may be used with reasonable accuracy. As the overall mass transfer coefficient, K_{Fav} , estimated for the more slowly diffusing component, which might be assumed to coincide with the stronger component, may be used for representing the overall characteristics of the replacement. Then, the length of Zone III can easily be estimated by applying the relations shown for the cases of single-component adsorption systems.

The propagation speed of Zone III is apparent from the relation given by Eq. (7-74), which gives

$$V_{III} = u_0 C_{20} / \rho_b q_{20} \quad (7-80)$$

C. description of Zone I

When the concentration of Component 1 in Zone II, C_{1e} , is given, the length of Zone I is readily obtained by the method used for the estimation of a single-component breakthrough curve.

The propagation speed of Zone I is obtained from Eq. (7-75) as

$$V_I = u_0 C_{10} / \rho_b q_{1e} \quad (7-81)$$

7.5.2. Breakthrough of unknown multicomponent adsorbates

When a number of adsorbable components are contained, as for instance, in the case of water treatment, it is difficult and in most cases unnecessary to follow the breakthrough of each component. What is important is to understand the overall characteristics of the breakthrough of total pollutant concentration, e.g. total organic carbon (TOC) or chemical oxygen demand (COD).

Assuming that n adsorbable components are involved and adsorption of the i -th component is stronger than the $(i - 1)$ -th component, then, considering equilibrium, adsorption zones in the column are believed to proceed as shown in Fig. 7.14.a. The weakest component (Component 1) is pushed forward by all the rest and Component 2 follows. This way,

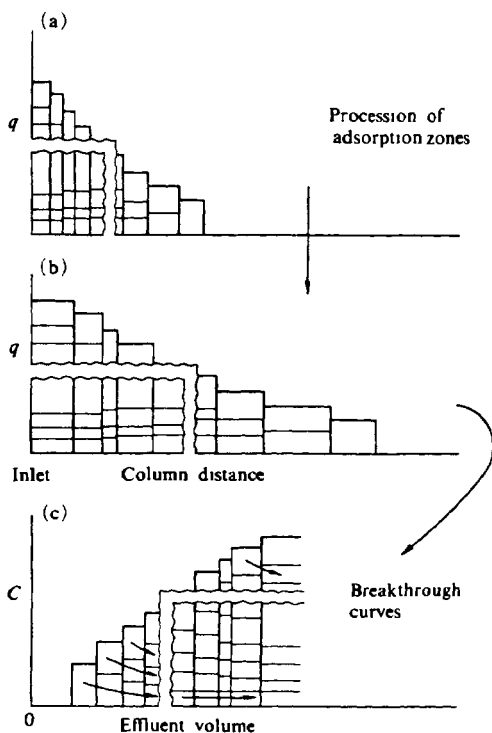


Fig 7 14 Adsorption of multicomponent adsorbates in a column

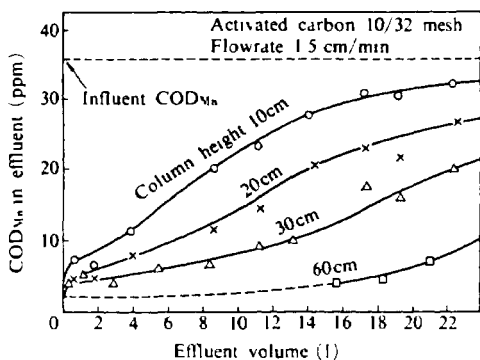


Fig 7 15 Typical breakthrough curves for wastewater containing unknown multicomponent adsorbates
(Reproduced with permission by Kawazoe, K., *Kagaku Kogaku*, 39, 415 (1975))

n equilibrium zones are formed in the bed and the length of each zone increases in proportion to the amount of influent fluid (Fig. 7.14.b).

The breakthrough curve may become as shown in Fig. 7.14.c. In this case, curves of different space velocity can be correlated by plotting exit concentration versus influent volume per unit mass (volume) of adsorbent in the bed.

More rigorous treatment is possible by taking into account the replacement zones which are expected to form between the two neighboring equilibrium zones. Actual overall breakthrough performance is in fact given by a smooth curve rather than a step-like curve as shown in Fig. 7.14.c, which is probably caused by the nonequilibrium nature of adsorption. However, measured COD breakthrough curves for the adsorption of real wastewater from a petrochemical plant (Fig. 7.15) show that except at the initial part, SV (flow rate based on column volume) little affects the shape of the curve, if the data are replotted against effluent volume per column volume for each column length, suggesting that consideration assuming equilibrium can give a rough estimate of the breakthrough curve of a large treatment plant from a rapid measurement using (in this case) a small column.

7.6. Dispersion and Mass Transfer Parameters in Packed Beds

In packed beds, the main parameters of transport of adsorbates are the axial dispersion coefficient and the fluid-to-particle mass transfer coefficient. The other important parameter, the intraparticle diffusion coefficient, is not dependent on type of adsorption contactor and the treatment described in Chapter 4 can be applied.

7.6.1. Axial dispersion coefficient

Axial dispersion contributes to the broadening of the adsorption front due to flow in the void spaces between particles. Similar to diffusion phenomena, dispersion effect in the bed is expressed in terms of the following dispersion model:

$$E_z \partial^2 C / \partial z^2 - u \partial C / \partial z = \partial C / \partial t + (\rho_b / \epsilon) \partial q / \partial t \quad (7-82)$$

or in dimensionless form as

$$(1 / PeB) \partial^2 C / \partial Z^2 - \partial C / \partial Z = \partial C / \partial \tau + (\rho_b / \epsilon) \partial q / \partial \tau \quad (7-83)$$

where E_z represents the axial dispersion coefficient, Pe is the Peclet number ($=d_p\mu/E_z$), $B = L/d_p$ and $Z = z/L$ and $\tau = ut/L$. L is the bed length.

Usually E_z is considered to consist of contribution of molecular diffusion and the dispersion caused by fluid flow.

$$E_z = E_{z,\text{molecular}} + E_{z,\text{flow}} \quad (7-84)$$

A. dispersion caused by molecular diffusion

Dispersion due to molecular diffusion in the interparticle void spaces is described by the void fraction of the bed, ϵ , and the tortuosity of the diffusion path in the void space. Unlike the diffusion in porous particles reviewed in Chapter 4, the latter is considered close to unity for diffusion in packed beds. Then,

$$E_{z,\text{molecular}} = D_v \text{ or } Pe = d_p\mu/D_v \quad (7-85)$$

where D_v is the molecular diffusion coefficient. The contribution of molecular diffusion in addition to fluid dispersion is differs considerably in the gas and liquid phases because of a difference of more than 10^4 times in molecular diffusivity between the two phases.

Generally, the contribution of molecular diffusion becomes dominant in the range of $ScRe_p < 10$. However, in a packed bed of particles smaller than 2 mm, attention should be paid since a higher contribution of dispersion due to fluid flow is often observed (See below).

B. dispersion in turbulent flow regime

Mechanisms of dispersion due to fluid flow differ in laminar flow regime and in turbulent flow regime.

In turbulent flow regime ($Re_p > 100$), the fluid entering each void is considered to be fully mixed and overall dispersion phenomenon can be well described by a tanks-in-series model, where the residence time in a tank is equated with the residence time of flowing fluid in a void of the length $\beta_1 d_p$, $\beta_2 d_p/u$. Then the tanks-in-series model gives the residence time distribution of the Poisson type (Aris and Amundson, 1957), which can be approximated by the impulse response of the dispersion model by equating

$$Pe = ud_p/E_z = 2/\beta_2 \quad (7-86)$$

The perfect mixing assumption in a void is well understood for gas phase turbulent flow. In the liquid phase, however, a small number of diffusivities may retard complete mixing in the void and a higher Re_p of

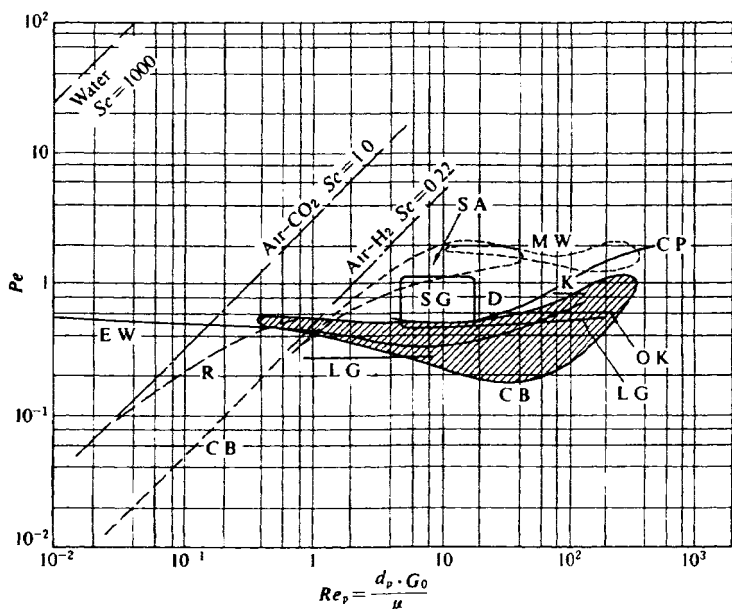


Fig 7.16 Axial dispersion in packed beds Peclet number $= D_p \cdot u / E_z$
 E W, L G, S G, C B, L G, O K, K, C P, D correspond to liquid phase

about 1000 may be necessary to achieve the relation given by Eq. (7-86). This situation can be read from Fig. 7.16

C. dispersion in laminar flow regime

In laminar flow regime ($Re_p = d_p u_0 / \nu < 100$), axial dispersion in a packed column is expected due to the local velocity distribution of fluid in void spaces. In this case, variance of the residence time of the fluid passing one layer of particles, σ^2 , is considered to be proportional to $(d_p/u)^2$ with a proportionality constant of 2λ .

$$\sigma^2 = 2\lambda(d_p/u)^2 \quad (7-87)$$

Then, by applying the Einstein equation, $\sigma^2 = 2E_z t$, the following form is derived.

$$E_z = \lambda d_p u \quad (7-88)$$

which yields

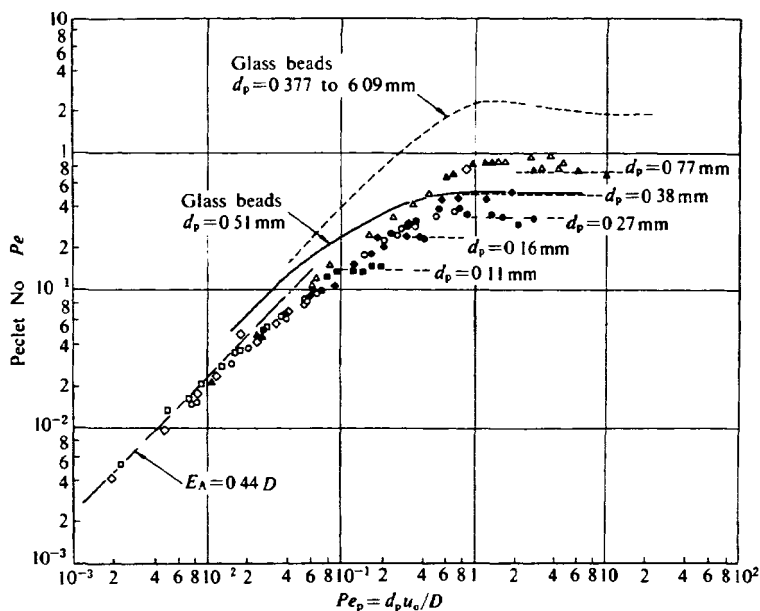


Fig 7.17 Peclet numbers for packed beds of small particles
(Reproduced with permission by Suzuki M and Smith, M, *Chem Eng J* 3, 261 (1972))

$$Pe = 1/\lambda \quad (7-89)$$

In the packed beds of commercial size adsorbents, $\lambda = 1 - 1/2$ can be assumed

Consideration of dispersion in the laminar flow regime may not be necessary for the gaseous phase, since molecular diffusion becomes more significant for small Sc systems

D. dispersion in packed beds of small particles

When the size of packed particles is smaller than a critical value of 1–2 mm, velocity distribution of the scale larger than particle size may become dominant, resulting in a larger contribution of the axial dispersion effect than that expected from the relation established in the previous section. This is likely to be due to the channeling of flow induced by the local irregularity of packing conditions.

Suzuki and Smith (1972) and Moulijn and van Swaay (1976) showed that when particle size of the packing becomes smaller Pe reaches a limiting value at $ScRe_p$ far smaller than 10 as illustrated in

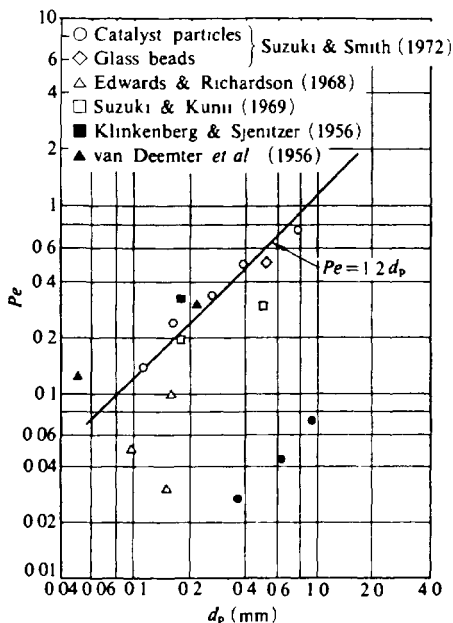


Fig. 7.18 Peclet number (in the high-velocity region) versus particle diameter (Reproduced with permission by Suzuki, M and Smith, M, *Chem Eng J*, 3, 262 (1972))

Fig. 7.17. The measured limiting value of Pe is a function of particle size as shown in Fig. 7.18.

7.6.2. Fluid-to-particle mass transfer coefficient

Regarding mass transfer between fluid and particle, many correlations have been proposed for both gaseous and liquid phase mass transfer. Usually the contribution of molecular diffusion and that of fluid flow are considered to be additive as in the case of mass transfer in agitated vessels.

$$Sh = k_t d_p / D = Sh_{\text{stag}} + Sh_{\text{flow}} \quad (7-90)$$

For the mass transfer coefficient in a stagnant fluid system, $Sh_{\text{stag}} = 2$ is used in the case of mass transfer from a single particle. In multi-particle systems such as packed beds, however, Sh_{stag} takes a different value for the reason noted in Chapter 5, and Sh_{stag} is given as a function of void fraction in the packed bed, ϵ , as shown in Fig. 5.11 (Suzuki,

1975). However, in most cases of adsorption in packed beds, it is rare for mass transfer resistance at low flow rate to become a rate-controlling step. The criteria for this situation are shown by Kunii and Suzuki (1967) roughly as $ScRe_p < 10$ where fluid flowing in void spaces reaches equilibrium with the surrounding particle surface during the contact time with one layer of particles.

Many correlations have been proposed for the effect of fluid flow on the mass transfer coefficient, Sh_{flow} . Some of the equations easily used are given below.

In the turbulent flow regime ($Re_p > 100$) in packed beds, regardless of gaseous or liquid phase, the laminar boundary layer develops on the surface of particles, acting as a shield against the effect of neighboring particles. Then mass transfer between bulk stream and the surface of the particle is described by the ordinary laminar boundary layer equation and the following form can be derived by Carberry (1960).

$$Sh = (1.15/\varepsilon^{1/2})Sc^{1/3}Re_p^{1/2} \quad (7-91)$$

where the Schmidt number, Sc , is defined as $\mu/\rho D$ and the Reynolds number, Re_p , is based on particle diameter as $d_p \rho u_o/\mu$. In deriving Eq. (7-91), velocity distribution in the laminar boundary layer was assumed to be proportional to the square root of the distance from the surface.

Wakao and Funazkri (1978) correlated the published data by correcting the effect of axial dispersion and gave

$$Sh = 1.1Sc^{1/3}Re_p^{0.6} \quad (7-92)$$

In the laminar flow regime ($Re_p < 100$), boundary layer treatment does not hold. In gaseous phase, mass transfer resistance is not an important step, since, as discussed before, $ScRe_p$ becomes rather small and fluid phase is considered to be in equilibrium with the surface of the particles in this range. In liquid phase mass transfer, however, because of the magnitude of the Sc number, $ScRe_p$ becomes larger than 10 even though Re_p is small and concentration boundary layer on the surface of the particle must be considered.

For mass transfer at low Re_p in liquid phase, theoretical treatment based on free surface model (Pfeffer, 1964) or hydraulic radius model (Kataoka *et al.*, 1972) gave similar results. For instance, the free surface model assumes a concentric annular cell of fluid around a particle as mentioned in Section 5.4.1 and concentration profile was obtained assuming potential flow in the cell at a low Re_p number region, in which

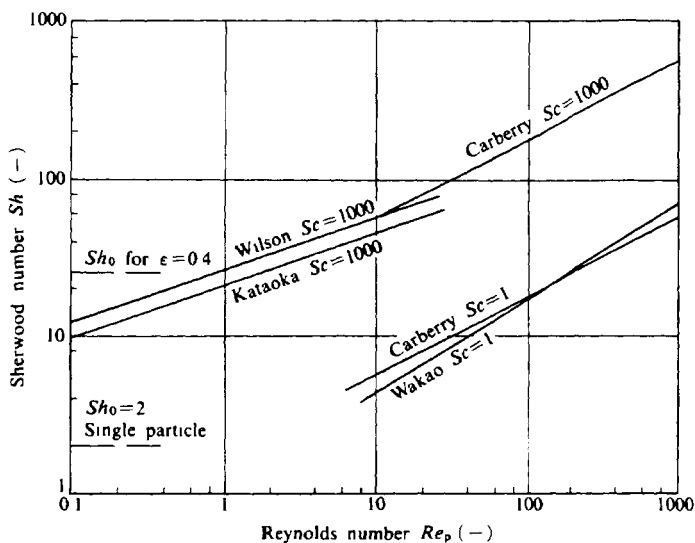


Fig 7.19 Sherwood number correlations for packed beds

case the results are as follows

$$Sh = 1.20[(1 - \gamma^5)/(2 - 3\gamma + 5\gamma^5 - 6\gamma^6)]Sc^{1/3}Re_p^{1/3} \quad (7-93)$$

$$\gamma = (1 - \varepsilon)^{1/3} \quad (7-94)$$

A hydraulic radius model assumes the fluid path in the void spaces in a packed bed to be equivalent to an assembly of the tubes whose radius is taken as the hydraulic radius of the void spaces. Then the resultant relation of mass transfer coefficient is given as

$$Sh = 1.85[(1 - \varepsilon)/\varepsilon]^{1/3}Sc^{1/3}Re_p^{1/3} \quad (7-95)$$

Correlation of the experimental data in this region is given by Wilson and Geankoplis (1966) as

$$Sh = (1.09/\varepsilon)Sc^{1/3}Re_p^{1/3} \quad \text{for } 0.0015 < Re_p < 55 \quad (7-96)$$

Comparison of these equations are made in Fig. 7.19

In the case of aqueous phase adsorption of volatile organics on activated carbon, due to the rapid diffusion inside the carbon particle, mass transfer between fluid and particle can play a significant role in the

overall mass transfer rate process.

REFERENCES

- Antonson, C R and J S Dranoff, *AIChE Symp*, Ser 65 (96), 20 and 27 (1969)
- Aris, R and N R Amundson, *AIChE Journal*, 3, 280 (1957)
- Carberry, J J, *AIChE Journal*, 6, 460 (1960)
- Carberry, J J, *AIChE Journal*, 4, 13M (1958)
- Carter, J W and H Husain, *Chem Eng Sci*, 29 267 (1974)
- Carter, J W and H Husain, *Trans I Chem Eng*, 50, 69 (1972)
- Cooney, D O and N Lightfoot, *Ind Eng Chem Fund*, 4, 233 (1965)
- Coppola, A P and D LeVan, *Chem Eng Sci*, 36 967 (1981)
- Edwards, M F and J F Richardson, *Chem Eng Sci*, 23, 109 (1968)
- Fleck, R D, Jr, D J Kirwan and K R Hall, *Ind Eng Chem Fund*, 12, 95 (1973)
- Garg, D R and D M Ruthven, *Chem Eng Sci*, 30, 1192 (1975)
- Garg, D R and D M Ruthven, *Chem Eng Sci*, 29, 571 (1974)
- Garg, D R and D M Ruthven, *Chem Eng Sci*, 29, 1961 (1974)
- Garg, D R and D M Ruthven, *Chem Eng Sci*, 28, 791, 799 (1973)
- Glueckauf, E, *Trans Faraday Soc*, 51, 1540 (1955)
- Hall K R L C Eagleton, A Acrivos and T Vermeulen, *Ind Eng Chem Fund* 5, 212 (1966)
- Hashimoto, K K Miura and M Tsukano, *J Chem Eng Japan*, 10, 27 (1977)
- Kataoka, T, H Yoshida and K Ueyama *J Chem Eng Japan*, 5, 132 (1972)
- Kawazoe, K and Y Fukuda, *Kagaku Kogaku*, 29 374 (1965) (in Japanese)
- Kawazoe, K and I Sugiyama, *Seisan Kenkyu* 21, 563 (1967) (in Japanese)
- Kawazoe, K and Y Takeuchi, *J Chem Eng Japan*, 7, 431 (1974)
- Klinkenberg A, *Ind Eng Chem*, 46, 2285 (1954)
- Klinkenberg A and F Sjenitzer, *Chem Eng Sci* 5, 258 (1956)
- Kunii, D and M Suzuki *Int J Heat Mass Transfer* 10, 845 (1967)
- Kyte W S, *Chem Eng Sci* 28, 1853 (1973)
- Markham, E C and A F Benton, *J Am Chem Soc*, 53, 497 (1931)
- Masamune, S and J M Smith, *AIChE Journal* 11 35 (1965)
- Michaels A S *Ind Eng Chem* 44 1922 (1952)
- Miura, K and K Hashimoto, *J Chem Eng Japan*, 10, 490 (1977)
- Moulijn and van S Waaj (1976)
- Myers A L and J M Prausnitz, *AIChE Journal* 11, 121 (1965)
- Pfeffer R *Ind Eng Chem Fund* 3 380 (1964)
- Rasmuson, A, *Chem Eng Sci*, 37, 787 (1982)
- Rasmuson, A and I Neretnieks, *AIChE Journal*, 26, 686 (1980)
- Rosen, J B, *Ind Eng Chem* 46 1590 (1954)
- Rosen, J B, *J Chem Phys* 20 387 (1952)
- Suzuki, M *Kagaku Kogaku*, 29, 253 (1965) (in Japanese)
- Suzuki, M and D Kunii, *34th Annual Mtg J Soc Chem Engrs* (1969)
- Suzuki, M *J Chem Eng Japan* 8, 163 (1975)
- Suzuki, M and J M Smith, *Chem Eng J* 3 256 (1972)
- Takeuchi, Y, E Furuya and Y Suzuki *Kogyo Yosui* (Industrial Water), 233, 30 (1978) (in Japanese)
- Tien, C and G Thodos *AIChE Journal* 5, 373 (1959)
- van Deemter J J F J Zuiderweg and A Klinkenberg, *Chem Eng Sci* 5 271 (1956)
- Vermeulen T *Perry's Chem Eng Handbook*, 6th ed (eds R H Perry & D Green), McGraw-Hill, New York (1984)
- Wakao N and T Funazkri, *Chem Eng Sci* 33 1375 (1978)
- Wilson E J and C J Geankoplis *Ind Eng Chem Fund* 5 9 (1966)
- Zwiebel I R L Garipey and J J Schnitzer *AIChE Journal* 18 1139 (1972)

Heat Effect in Adsorption Operation

Adsorption is accompanied by the evolution of heat, and temperature changes affect the adsorption equilibrium relation and, in some cases, adsorption rate. Thus, especially in gas phase adsorption, the effects of heat generation and heat transfer in adsorbent beds must be taken into account. This is essential in the case of thermal regeneration of exhausted adsorbent using steam or hot inert gases, a topic which is discussed in Chapter 9.

Heat generation also affects measurement of adsorption rate by batch techniques such as the gravimetric method. First, the effect of heat transfer rate on measurement of adsorption rate by a batch method is shown using a simple model as an example of nonisothermal effect. Then fundamental equations for heat transfer in packed beds are shown and simplified models presented. Estimation methods for heat transfer rate parameters in packed beds are introduced followed by a discussion of heat transfer in an adsorbent bed in adsorption equilibrium to show the coupling effect of heat and mass dispersion. Finally, the effect of heat transfer on adsorption dynamics in a column is illustrated using simple models.

8.1. Effect of Heat Generation on Adsorption Rate Measurement by a Single Particle Method

A single particle gravimetric method, for example, is often used to determine adsorption rate. In most cases analysis is based on isothermal adsorption neglecting heat generation due to adsorption. Depending on the system employed and experimental conditions, this assumption may become critical.

The effect of heat generation can be checked and the critical conditions for negligible heat effect derived (Chihara and Suzuki, 1976) employing a simple model of mass and heat transfer.

Heat balance and mass balance equations for an adsorbent particle in

response to a step change of gas phase concentration from C_0 to C_∞ are as follows.

$$\rho_p C_p \frac{d\Delta T}{dt} = \rho_p Q_{st} \frac{d\Delta q}{dt} - \frac{3}{R} h_p \Delta T \quad (8-1)$$

$$\rho_p \frac{d\Delta q}{dt} = -\frac{3}{R} k_t \Delta C \quad (8-2)$$

where Q_{st} is the heat of adsorption, ρ_p , C_p and R represent the density, the specific heat and radius of the adsorbent particle. h_p and k_t denote, respectively, heat transfer coefficient between particle and the wall and mass transfer coefficient between particle and fluid. In Eqs. (8-1) and (8-2), ΔT , Δq and ΔC are defined as deviations from the final equilibrium states, and then $\Delta T = T - T_w$, $\Delta q = q - q_\infty$, $\Delta C = C^*(q, T) - C_\infty$, where T_w represents the wall temperature and q_∞ is the amount adsorbed in equilibrium with the concentration, C_∞ .

Initial and final conditions are:

$$\left. \begin{aligned} t = 0 : \Delta q = \Delta q_0 = q_0(C_0, T_w) - q_\infty \text{ and } \Delta T = 0 \\ t = \infty : \Delta q = 0 \text{ and } \Delta T = 0 \end{aligned} \right\} \quad (8-3)$$

By assuming that $\Delta C_0 = C_0 - C_\infty$ is small enough so that Eq. (8-2) can be linearized for the perturbation as

$$\rho_p \frac{d\Delta q}{dt} = -\frac{3}{R} k_t \left\{ \frac{\Delta q}{K} + \frac{\Delta T}{H} \right\} \quad (8-4)$$

where $K = \frac{1}{[\partial C^*/\partial q]_{q_\infty, T_w}}$, $H = \frac{1}{[\partial C^*/\partial T]_{q_\infty, T_w}}$.

Eqs. (8-1) and (8-4) are solved to give

$$\Delta q/\Delta q_0 = \alpha \exp(-t/t_1) + \beta \exp(-t/t_2) \quad (8-5)$$

$$-(C_p \Delta T)/(Q_{st} \Delta q_0) = \lambda [\exp(-t/t_1) - \exp(-t/t_2)] \quad (8-6)$$

where $t_1 > t_2$ and

$$t_{1,2} = (t_m/2)(\gamma \pm \eta) \quad (8-7)$$

$$\alpha = (-t_2/t_m + 1 + \tau_h \tau_a)/\eta \quad (8-8)$$

$$\beta = (t_1/t_m - 1 - \tau_h \tau_a) / \eta \tag{8-9}$$

$$\lambda = \tau_h / \eta \tag{8-10}$$

with $\gamma = 1 + \tau_h(1 + \tau_a)$, $\eta = \sqrt{\gamma^2 - 4\tau_h}$ and $t_m = \rho_p K(q_\infty, T_w) \cdot R / (3k_i)$.
 The parameters τ_a and τ_h are defined as

$$\tau_a = [Q_s K(q_\infty, T_w) / H(q_\infty, T_w)] / C_p \tag{8-11}$$

$$\tau_h = (\rho_p C_p R / 3h_p) / [\rho_p K(q_\infty, T_w) R / 3k_i] \tag{8-12}$$

These parameters mean

$$\tau_a = \frac{\text{apparent heat capacity due to adsorption-desorption effect}}{\text{heat capacity of adsorbent}}$$

$$\tau_h = \frac{\text{time constant of heat transfer}}{\text{time constant of mass transfer}}$$

Obviously, when $\tau_a=0$ (negligible heat generation or temperature effect on equilibrium) or $\tau_h=0$ (rapid thermal equilibrium attainment) holds, Eq. (8-5) reduces to

$$\Delta q / \Delta q_0 = \exp(-t/t_m) \tag{8-13}$$

which is the solution for an isothermal case.

The effects of τ_a and τ_h are readily shown by comparing Eqs. (8-5) and

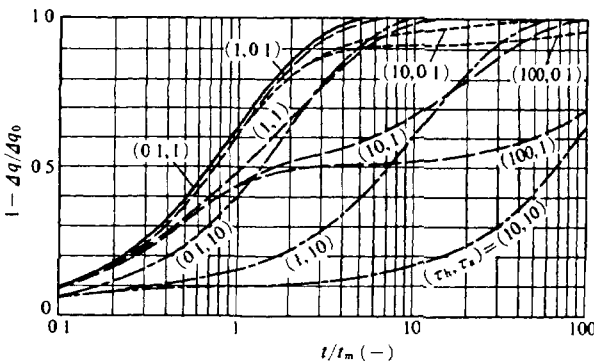


Fig. 8.1 Adsorption uptakes considering heat generation effect
 (Reproduced with permission by Chihara, K. and Suzuki, M., *Chem. Eng. Sci.*, 31, 506 (1976))

(8-13). This is done in Fig. 8.1 in the form of adsorption uptake curves. For the range $\tau_h \tau_a < 0.1$ the isothermal assumption is reasonable, while uptake curves deviate from Eq. (8-13) for larger $\tau_h \tau_a$.

A more detailed discussion based on a diffusional model for mass transfer is given by Ruthven et al. (1980) and is consistent with the above results.

8.2. Basic Models of Heat Transfer in Packed Beds

A packed bed of solid particles usually has poorer heat transfer ability compared with heat transfer in solid. This is true in the case of adsorbent particles. Heat transfer in packed beds of adsorbents can be described by models of varying degrees of simplicity.

One rigorous model is shown in Fig. 8.2, where temperature difference between fluid and particle is taken into account and temperature distribution in the radial direction in the bed occurs due to heat exchange through the column wall. In such cases a set of equations for heat transfer is given as follows.

For fluid phase:

$$k_{cz,f} \frac{\partial^2 T_f}{\partial z^2} + k_{er,f} \frac{\partial}{\partial r} \left(r \frac{\partial T_f}{\partial r} \right) - C_{pf} \rho_f u_0 \frac{\partial T_f}{\partial z} + h_p a_v (T_f - T_s) = C_{pf} \rho_f \varepsilon \frac{\partial T_f}{\partial t} \quad (8-14)$$

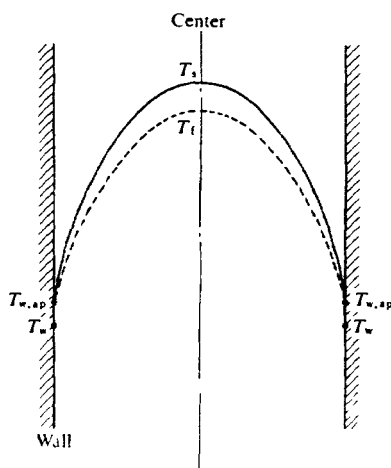


Fig. 8.2. Temperature distributions in a radial direction of the bed

And for solid phase:

$$k_{e0} \left\{ \frac{\partial^2 T_s}{\partial z^2} + \frac{\partial}{\partial r} \left(r \frac{\partial T_s}{\partial r} \right) \right\} + h_p a_v (T_f - T_s) + Q_{ad} = C_{ps} \rho_b \frac{\partial T_s}{\partial t} \quad (8-15)$$

In the above equations, C_{pf} and C_{ps} denote heat capacities of the fluid and solid phases, ρ_b is the bed density and h_p is the heat transfer coefficient between fluid and particles. Transport of heat through the fluid phase in the axial direction and in the radial direction of the bed by conduction are described by the effective thermal conductivities, $k_{cz,f}$ and $k_{cr,f}$, while in the solid phase thermal conduction can be assumed to be isotropic and the effective thermal conductivity k_{e0} can be used to express this effect. Q_{ad} represents the heat evolution/absorption by adsorption or desorption on the basis of bed volume. This model neglects the temperature distribution in the radial position of each particle, which may seem contradictory to the case of mass transfer, where intraparticle mass transfer plays a significant role in the overall adsorption rate. Usually in the case of adsorption, the time constant of heat transfer in the particle is smaller than the time constant of intraparticle diffusion, and the temperature in the particle may be assumed to be constant.

The above model is often too complicated hence several simplified versions are given below.

8.2.1. Homogeneous bed model

When temperature difference between fluid and particle is neglected, bed temperature, $T (= T_f = T_s)$ is described by the summation of Eqs. (8-14) and (8-15) as follows.

$$k_{cz} \frac{\partial^2 T}{\partial z^2} + k_{cr} \frac{\partial}{\partial r} \left(r \frac{\partial T}{\partial r} \right) - C_{pf} \rho_f u_0 \frac{\partial T}{\partial z} + Q_{ad} = (C_{pf} \rho_f \epsilon + C_{ps} \rho_b) \frac{\partial T}{\partial t} \quad (8-16)$$

where k_{cz} and k_{cr} represent the effective thermal conductivities in the axial and radial directions in the packed bed, which are given as follows

$$k_{cz} = k_{e0} + k_{cz,f} \quad (8-17)$$

$$k_{cr} = k_{e0} + k_{cr,f} \quad (8-18)$$

These parameters can be calculated from the theoretical equations given below.

Heat exchange through the column wall is expressed by the boundary

condition as follows.

$$h_w (T_w - T|_{r=R_w}) = k_{er} \left. \frac{\partial T}{\partial r} \right|_{r=R_w} \quad (8-19)$$

where h_w is the apparent wall heat transfer coefficient.

When heat exchange through the column wall is dominant, heat conduction in the direction of column length can be neglected in most cases. In such cases k_{er} in Eq. (8-16) may be deleted.

8.2.2. Overall heat transfer model

To simplify heat transfer expression, the cross-sectional average temperature of the bed, \bar{T} , is often used as the representative temperature.

$$-C_{pf}\rho_f u_0 \frac{\partial \bar{T}}{\partial z} + h_0(2/R_w)(\bar{T} - T_w) + Q_{ad} = (C_{pf}\rho_f \varepsilon + C_{ps}\rho_b) \frac{\partial \bar{T}}{\partial t} \quad (8-20)$$

where h_0 denotes the overall heat transfer coefficient between wall and bed, calculated from k_{er} and h_w and T_w is the temperature of the wall.

8.2.3. Particle-to-fluid heat transfer model

Temperature difference between particle and fluid can sometimes play an important role in the overall heat transfer. This may happen at high flow rates in the adiabatic operations. In such cases, the basic equations of heat transfer are given below.

$$\left. \begin{aligned} C_{pf}\rho_f u_0 \frac{\partial T_f}{\partial z} + h_p a_v (T_f - T_s) &= -C_{pf}\rho_f \varepsilon \frac{\partial T_f}{\partial t} \\ h_p a_v (T_f - T_s) &= C_{ps}\rho_b \frac{\partial T_s}{\partial t} \end{aligned} \right\} \quad (8-21)$$

8.2.4. Axial heat conduction model

In most adiabatic operations, except when flow rate is very high, heat transfer in the axial direction by effective conduction may be a dominant step. Then the temperature in the bed, T , can be given as

$$k_{ez} \frac{\partial^2 T}{\partial z^2} - C_{pf}\rho_f u_0 \frac{\partial T}{\partial z} + Q_{ad} = (C_{pf}\rho_f \varepsilon + C_{ps}\rho_b) \frac{\partial T}{\partial t} \quad (8-22)$$

8.3. Heat Transfer Parameters in Packed Beds

8.3.1. Effective thermal conductivities, k_e

As shown by Eqs. (8-17) and (8-18), the effective thermal conductivities in the radial and axial directions are considered to be composed of the effective thermal conductivity with stagnant fluid, k_{e0} , and the contribution of fluid flow.

A. k_e with stagnant fluid, k_{e0}

Kunii and Smith (1960) presented theoretical equations for estimating k_{e0} . In most adsorption operations, temperature ranges suggest that contribution of radiant heat transfer is negligible, so k_{e0} can be calculated when thermal conductivity of the particle, k_s , is given.

$$k_{e0}/k_f = \varepsilon + (1 - \varepsilon)/[\phi + (2/3)(k_f/k_s)] \quad (8-23)$$

where k_f is the thermal conductivity of fluid and ϕ represents the contribution of solid to solid heat transfer through thin fluid film around a contacting point of neighboring particles. ϕ is given by the following equations where ϕ_1 and ϕ_2 are shown as a function of k_s/k_f in

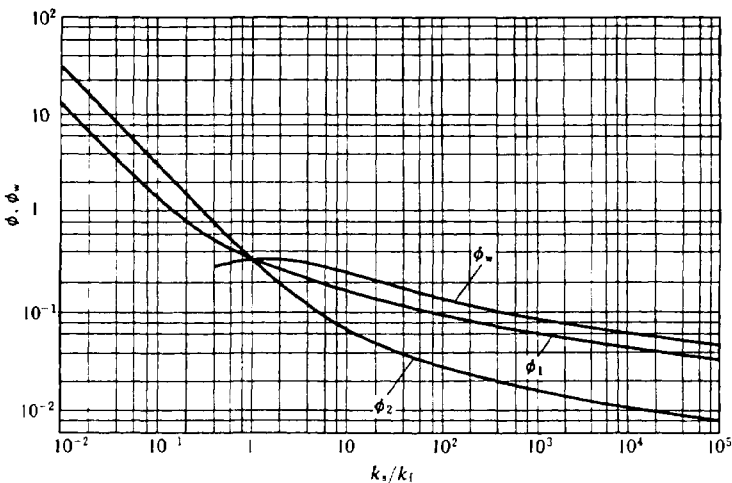


Fig 8.3 ϕ -values for calculation of k_{e0} as a function of k_s/k_f
(Reproduced with permission by Suzuki, M., *Kagaku-Kogaku-Benran*, p 290 (1978))

TABLE 8 1 Effective Thermal Conductivities of Adsorbent Packed Beds

Adsorbents	Gas	k_{e0}^*	k_{e0}/k_f
Alumina	Air	0.2~0.29	7~10.4
Silica gel	Air	0.15~0.22	5.4~8
Activated carbon	Air	0.19~0.27	6.8~9.7
Activated carbon	Steam (373 K)	0.23	9.4

* unit W/mK , Temperature 298 K unless otherwise specified

Fig 8 3

$$\left. \begin{aligned} \phi &= \phi_2 + (\phi_1 - \phi_2)[(\varepsilon - 0.26)/0.216] \\ &\quad \text{for } 0.476 \geq \varepsilon \geq 0.26 \\ \phi &= \phi_1 \text{ for } \varepsilon > 0.476 \\ \phi &= \phi_2 \text{ for } \varepsilon < 0.26 \end{aligned} \right\} \quad (8-24)$$

Several examples of k_{e0} calculated from this equation are given in TABLE 8 1

B contribution of fluid flow to k_e

Dispersion of fluid in packed beds in the radial and axial directions contribute to the effective thermal conductivity as an additive term to k_{e0} as shown by Eqs (8-17) and (8-18)

For the effective thermal conductivity in the radial direction, consideration of packing structure gives (Baron, 1952)

$$C_p(\rho_f u_0)/k_{ef} = Pe_H = 8-10 \quad (8-25)$$

Then Eq (8-18) becomes (Yagi and Kunii, 1957)

$$k_{er}/k_f = k_{e0}/k_f + (\alpha\beta)PrRe_p \quad (8-26)$$

where $\alpha\beta = 1/Pe_H = 0.1-0.15$ and $Pr = C_p\mu/k_f$ and $Re_p = D_p\rho_f u_0/\mu$

Regarding the effective thermal conductivity in the axial direction, a similar consideration gives (Yagi, Kunii and Wakao, 1960),

$$k_{er}/k_f = k_{e0}/k_f + \delta PrRe_p \quad (8-27)$$

where $\delta = 0.5-1.0$

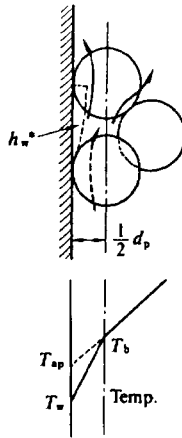


Fig. 8.4. Heat transfer model in the vicinity of the wall.

8.3.2. Apparent heat transfer coefficient between wall surface and packed bed, h_w

Particles near the column wall are arranged in differently from those inside the column. This increases heat transfer resistance near the wall surface, an effect accounted for by introducing an apparent heat transfer coefficient, h_w , as shown in Fig. 8.4.

The effective thermal conductivity in the wall layer of thickness $R_p = d_p/2$, k_{cw} , is defined and h_w is considered as a correction factor based on the difference between k_{cr} and k_{cw} (Kunii and Suzuki, 1966).

$$\frac{1}{h_w R_p / k_f} = \frac{1}{k_{cw} / k_f} - \frac{1}{k_{cr} / k_f} \quad (8-28)$$

where R_p is the radius of particle.

The effective thermal conductivity in the wall layer, k_{cw} , can be estimated by introducing a treatment similar to that for k_{cr} .

$$\frac{k_{cw}}{k_f} = \frac{k_{cw0}}{k_f} + \frac{1}{\frac{1}{\alpha_w P_r Re_p} + \frac{1}{h_w^* R_p / k_f}} \quad (8-29)$$

where α_w denotes the contribution of fluid mixing in the wall layer and in several cases $\alpha_w = 0.2$ are obtained. h_w^* represents the heat transfer

coefficient of the thermal boundary layer which develops on the wall surface. This becomes dominant at high Re_p and is given by a Blasius-type equation as

$$h_w * d_p / k_f = C(Pr^{1/3})Re_p^{3/4} \quad (8-30)$$

where C is an experimental coefficient with a value of 0.1 to 0.2 (Kunii, Suzuki and Ono, 1968).

k_{cw0} is obtained by the following equation similarly to Eq. (8-23).

$$k_{cw0} / k_f = \varepsilon_w + (1 - \varepsilon_w) / [\phi_w + (2/3)(k_f / k_s)] \quad (8-31)$$

where effect of radiant heat transfer is again negligible and ε_w denotes void fraction in the wall layer of about 0.7. ϕ_w can be obtained from Fig. 8.3.

8.3.3. Overall heat transfer coefficient, h_o

For heat transfer in packed beds with constant wall temperature, the overall heat transfer coefficient defined by taking the difference between wall temperature and the average temperature of the flowing fluid as the driving force of heat transfer, h_o , is obtained as follows.

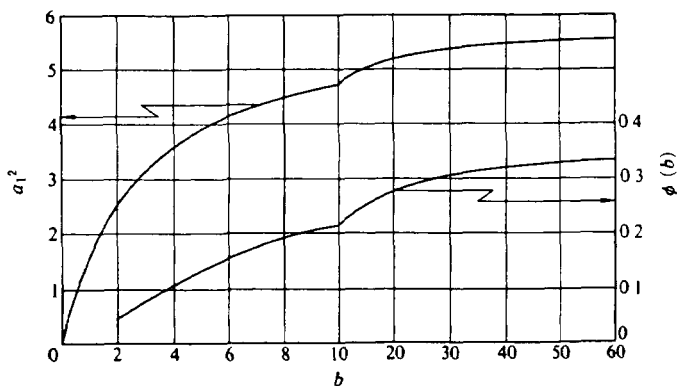


Fig 8.5 a_1^2 and $\phi(b)$ for calculation of h_o against a parameter, b (Reproduced with permission by Yagi and Kunii, *Int Devel Heat Transfer IV*, p 754 (1961))

$$\left. \begin{aligned} h_0 D_T / k_f &= (k_{cr} / k_f) [a_1^2 + \phi(b) / \xi] \\ \xi &= 4k_{cr} Z / \rho_f C_{pf} u_0 D_T^2 \\ b &= h_w D_T / 2k_{cr} \end{aligned} \right\} \quad (8-32)$$

a_1^2 and $\phi(b)$ can be obtained from Fig. 8.5. For extreme cases, the above equation is readily simplified.

For $b < 0.4$

$$h_0 = h_w \quad (8-33)$$

and for $b > 20$ and $\xi > 0.64$

$$h_0 = 5.78 k_{cr} / D_T \quad (8-34)$$

8.3.4. Fluid-to-particle heat transfer coefficient, h_p

Similar to the case of mass transfer between fluid and particle, the Carberry equation may be used to estimate the heat transfer coefficient between particle and fluid.

$$Nu_p = h_p d_p / k_f = Nu_0 + (1.15 / \varepsilon^{1/2}) Pr^{1/3} Re_p^{1/2} \quad (8-35)$$

Nu_0 can be obtained from Fig. 5.11 as a function of void fraction but at low $Pr Re_p$, it is not necessary to employ the model that considers temperature difference between fluid and particle.

8.4. Chromatographic Study of Heat Transfer in Packed Beds of Adsorbents

To understand the coupling effect of adsorption and heat transfer, a chromatographic study (thermal pulse response) was performed by Sakoda and Suzuki (1984).

The fundamental relations for chromatographic methods are introduced in Chapter 5 for mass transfer studies. These can be modified to handle heat transfer problems. In fact, method of moment was used to determine thermal pulse response in packed beds of inert particles (Sagara, Schneider and Smith, 1970). From analogy between Eq. (8-22) without Q_{ad} and Eq. (6-55), the first absolute moment and the second central moment for thermal pulse in an inert bed are given as

$$\mu_1 = (z/u_0)[(C_{pf}\rho_f\varepsilon + C_{ps}\rho_b)/(C_{pf}\rho_f)] \quad (8-36)$$

$$H = (1/u_0^2)k_{ez}/(C_{pf}\rho_f) \quad (8-37)$$

where H is defined as $[\mu_2'/(2z/u_0)]/[\mu_1/(z/u_0)]^2$.

When a packed bed of adsorbents is in equilibrium with flowing fluid which contains an adsorbable component, then Q_{nd} in Eq. (8-22) should be considered together with the mass balance equations. In this case, Q_{nd} is defined as

$$Q_{nd} = Q_{st} \rho_b \partial q / \partial t \quad (8-38)$$

where $\partial q / \partial t$ is connected to the mass balance equations as follows.

$$\rho_b \partial q / \partial t = k_s a_s (q^* - q) \quad (8-39)$$

$$E_z \partial^2 C / \partial z^2 - u_0 \partial C / \partial z - k_s a_s (q^* - q) = \varepsilon \partial C / \partial t \quad (8-40)$$

where $q^* = q^*(C, T)$ denotes the amount adsorbed in equilibrium with C at temperature T .

When a small fluctuation of temperature is introduced to the bed which is in a dynamic steady state of concentration C_0 , temperature T_0 and the amount adsorbed $q_0 = q_0(C_0, T_0)$, then by linearizing the equilibrium relation for a small fluctuation around the steady state condition, the basic equations for fluctuations of concentration ($C' = C - C_0$), temperature ($T' = T - T_0$) and amount adsorbed ($q' = q - q_0$), together with the equilibrium amount adsorbed ($q^{*'} = q^* - q_0$) can be derived.

$$E_z \partial^2 C' / \partial z^2 - u_0 \partial C' / \partial z - k_s a_s (q^{*'} - q') = \varepsilon \partial C' / \partial t \quad (8-41)$$

$$\rho_b \partial q' / \partial t = k_s a_s (q^{*'} - q') \quad (8-42)$$

$$\begin{aligned} k_{ez} \partial^2 T' / \partial z^2 - C_{pf} \rho_f u_0 \partial T' / \partial z + Q_{st} \rho_b \partial q' / \partial t \\ = (C_{pf} \rho_f \varepsilon + C_{ps} \rho_b) \partial T' / \partial t \end{aligned} \quad (8-43)$$

and

$$q^{*'} = K^*(C' + T' / H^*) \quad (8-44)$$

where

$$K^* = \partial q^* / \partial C|_{T_0, C_0} \text{ and } H^* = 1 / (\partial C / \partial T)|_{T_0, C_0} \quad (8-45)$$

Also, C_{ps} is modified to C'_{ps} by taking into account the heat capacity of the adsorbed phase.

$$C'_{ps} = C_{ps} + C_{ads}q_0 \quad (8-46)$$

The above set of equations are combined to give a differential equation for T' , whose solution for moments are derived by applying an approximate method by Suzuki (1973) (Sakoda and Suzuki, 1984).

$$\mu_1 = (z/u_0)(C_{pf}\rho_f\varepsilon + C'_{ps}\rho_b) / [C_{pf}\rho_f + Q_{st}/H^*] \quad (8-47)$$

$$H = (1/u_0^2)(k_{ex} + E_r Q_{st}/H^*) / (C_{pf}\rho_f + Q_{st}/H^*) + (Q_{st}/H^*) / [k_s a_v K^* (C_{pf}\rho_f + Q_{st}/H^*)] \quad (8-48)$$

Comparing Eqs. (8-36) and (8-47) for the first moment and Eqs. (8-37) and (8-48) for H , it is interesting to note that for an adsorption equilibrium system, simple heat transfer relations of Eqs. (8-36) and (8-37) can be used by replacing C_{ps} , C_{pf} and k_{ex} by defining the apparent parameters as follows.

$$(C_{ps})_{app} = C_{ps} + C_{ads}q_0 \quad (8-49)$$

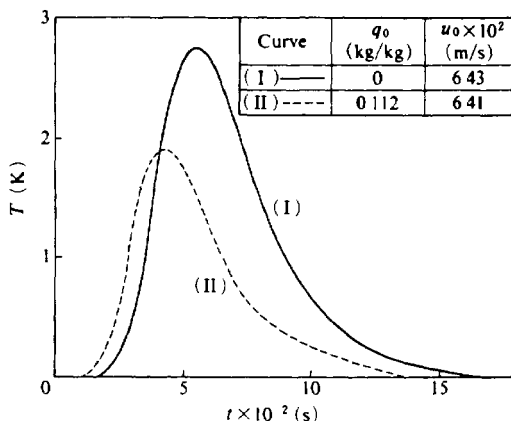


Fig 8.6 Typical heat pulse response curves for dry bed (I) and the bed in adsorption equilibrium (II)
(Reproduced with permission by Sakoda, A and Suzuki, M, *J Chem Eng Japan*, 17, 316, 317 (1984))

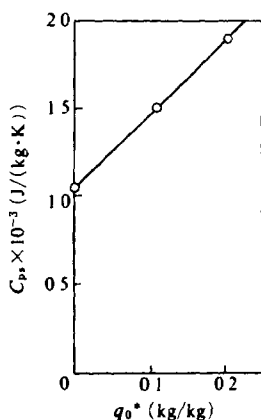


Fig 8.7 Dependency of C'_{ps} on the amount adsorbed, q_0^*
(Reproduced with permission by Sakoda, A. and Suzuki, M., *J Chem, Eng Japan*, 17, 316 (1984))

$$(C_{pt}\rho t)_{app} = C_{pt}\rho t + Q_{st}/H^* \quad (8-50)$$

$$(k_{cz})_{app} = k_{cz} + [E_z + u_0^2/(k_{sa}K^*)](Q_{st}/H^*) \quad (8-51)$$

From the relations given above, it may be understood that besides the apparent increases of the heat capacities of solid phase and gas phase, the apparent transport of heat by dispersion of adsorbable species in gas phase which carries latent heat through dynamic equilibrium between gas phase and adsorbed phase should be added to the effective conduction through the otherwise inert packed bed of adsorbents.

For a simple equilibrium relation such as $q = K_0 \exp(Q_{st}/RT)C$, K^* and H^* are given as

$$K^* = K_0 \exp(Q_{st}/RT_0) \quad (8-52)$$

$$H^* = RT_0^2/(Q_{st}C_0) \quad (8-53)$$

Experimental measurement in a water vapor-silica gel system (Sakoda and Suzuki, 1984) supports the above results. Fig. 8.6 shows a typical example of adsorption effect. Obviously, the increase of heat capacity of fluid due to adsorption/desorption effect (Eq. (8-50)) is stronger than the effect of existence of adsorbed phase on increase of heat capacity, which is shown in Fig. 8.7, and the resultant first moment becomes smaller when the amount adsorbed increases.

8.5. Adiabatic Adsorption in a Column

When gas phase adsorption takes place in a large column, heat generated due to adsorption cannot be removed from the bed wall and accumulated in the bed because of poor heat transfer characteristics in packed beds of particles. A typical model of this situation is an adiabatic adsorption. The fundamental relations for this case are Eqs. (8-22), (8-38), (8-39) and (8-40), which are essentially similar to those employed by Pan and Basmadjian (1970). Thermal equilibrium between particle and fluid is assumed and only axial dispersion of heat is taken into account while mass transfer resistance between fluid phase and particle as well as axial dispersion is considered. This situation is identical with the model employed in the previous section. For further simplification, axial dispersion effect may be involved in the overall mass transfer coefficient of the linear driving force model as discussed in Chapter 5. In this case, after further justifiable simplifications such as negligible heat capacity and accumulation of adsorbate in void spaces, a set of basic equations to describe heat and mass balances can be given as follows.

$$k_{cz}\partial^2 T/\partial z^2 - C_{pf}\rho_f u_0 \partial T/\partial z + Q_{st}\rho_b \partial q/\partial t = C_{ps}\rho_b \partial T/\partial t \quad (8-54)$$

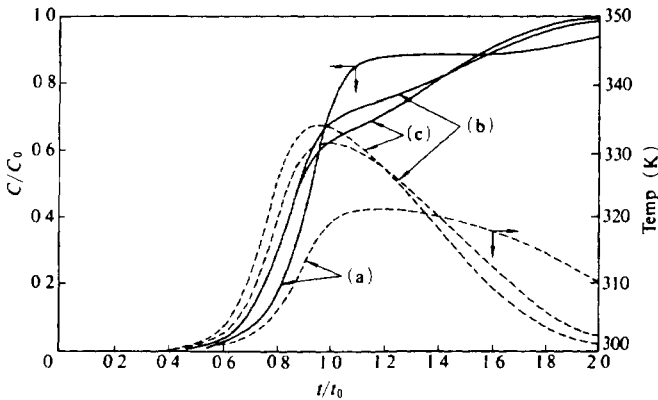


Fig 8.8 Typical examples of concentration and temperature changes of effluent stream from adiabatic adsorption column

Langmuir isotherm $r = 0.2$, $Q_{st} = 33 \text{ kJ/mol}$, $Z = 0.6 \text{ m}$, $u_0 = 0.04 \text{ m/s}$, $K_{j-a}L/u = 10$ Adsorbent $C_{ps} = 1050 \text{ J/kg K}$, $\rho_b = 481 \text{ kg/m}^3$, $k_{cz} = 0.29 \text{ W/mK}$ Gas $C_{pf} = 1138 \text{ J/kg K}$, $\rho_f = 1.21 \text{ kg/m}^3$, $C_0 = 1.0 \text{ mol/m}^3$, $q_0 = 1.0 \text{ mol/kg}$ (a), 3.8 mol/kg (b), 10 mol/kg (c)

$$u_0 \partial C / \partial z + k_s a_s (q^* - q) = 0 \quad (8-55)$$

$$k_s a_s (q^* - q) = \rho_b \partial q / \partial t \quad (8-56)$$

where adsorption equilibrium relation holds between q^* , C and T .

$$q^* = q^*(C, T) \quad (8-57)$$

Several works assume that heat transfer between fluid and particle is a major heat transfer parameter (Carter, 1966–1973; Meyer and Weber, 1967–1969; Raghavan and Ruthven, 1983). This situation may become more likely when operation is carried out at high flow rate ($Re_p > 100$).

Examples of calculation for adiabatic adsorption by means of the above set of equations are given in Fig. 8.8 for adsorption of hydrocarbon gas on activated carbon columns. Effect of heat generation on the shape of adsorption front is clearly shown. By assuming that the equilibrium constant varies with keeping the other parameters constant, changes in thermal waves are also illustrated, i.e. when velocity of adsorption front is slower than that of the thermal wave which is generated at the adsorption front, the thermal wave proceeds in front of the adsorption front while in the opposite case the formation of adsorption front is greatly affected by the temperature increase in the bed.

Analogous to Eq. (8-36), propagation speed of heat wave in packed beds, V_H , is given from Eq. (8-54) as

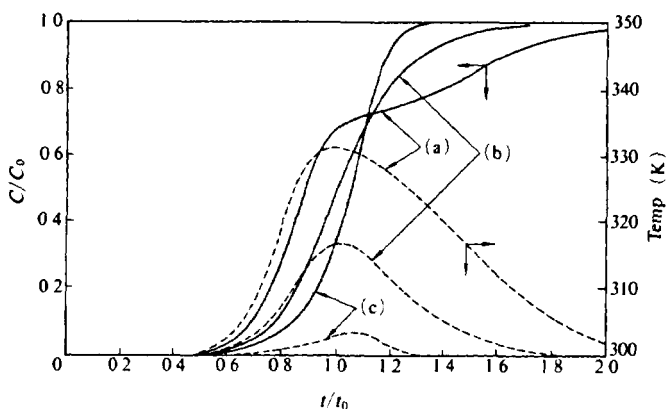


Fig 8.9 Effect of heat exchange through the wall on breakthrough curve and temperature change of effluent stream

Overall heat transfer parameter, $h_0 D_T / k_f = 0$ (adiabatic) (a), 10 (b) and 100 (c) $q_0 = 3.8$ mol/kg and other parameters refer to Fig 8.8

$$V_R = \{(C_{pt}\rho_t)/(C_{ps}\rho_b)\} u_0 \quad (8-58)$$

Also for isothermal adsorption, propagation speed of adsorption front, V_M , is given similar to Eq. (7-62) as

$$V_M = \{C_0/\rho_b q_0\} u_0 \quad (8-59)$$

where q_0 is the amount adsorbed in equilibrium with C_0 at inlet temperature, T_0 . In Eqs. (8-58) and (8-59) accumulation of heat and mass in void spaces can be considered negligible compared with accumulation in the particle phase for the sake of simplicity.

8.6. Adsorption with Heat Transfer Through the Wall

In an adsorbent bed of relatively small diameter, heat exchange through the column wall becomes appreciable. In this case, the overall heat transfer model introduced in 8.2(ii) can replace Eq. (8-54). Then similar calculations are possible by taking the overall heat transfer coefficient h_0 and/or the radius of the column R_w as a parameter to examine this effect. Calculation using the same example considering this effect is shown in Fig. 8.9. Obviously the heat transfer parameter, $(h_0/R_w)(C_{pt}\rho_t u_0/L)$, which is derived from the dimensionless form of the heat balance equation, determines the effect of heat transfer through the wall.

REFERENCES

- Baron, T, *Chem Eng Progr*, **48**, 118 (1952)
 Carter, J W, *Trans Inst Chem Engrs*, **44**, T253 (1966), **46** T213, T222 (1968), **51**, T75 (1973)
 Chihara, K and M Suzuki, *Chem Eng Sci*, **31**, 505 (1976).
 Kunii, D and J M Smith, *AIChE Journal*, **6**, 97 (1960)
 Kunii, D and M Suzuki, *3rd Int Dev on Heat Transfer*, IV, 344 (1966)
 Kunii, D, M Suzuki and N Ono, *J Chem Eng Japan*, **1**, 21 (1968)
 Meyer, O W and T W Weber, *AIChE Journal*, **13**, 457 (1967)
 Pan, C Y and D Basmadjian, *Chem Eng Sci*, **25**, 1653 (1970)
 Raghavan, N S and D M Ruthven, *Chem Eng Sci*, **39**, 1201 (1984)
 Ruthven, D M, L-K Lee and H Yucel, *AIChE Journal*, **26**, 16 (1980)
 Sagara, M, P Schneider and J M Smith, *Chem Eng J.*, **1**, 47 (1970)
 Sakoda, A and M Suzuki, *J Chem Eng Japan*, **17**, 316 (1984)
 Suzuki, M, *J Chem Eng Japan*, **6**, 540 (1973)
 Yagi, S and D Kunii, *AIChE Journal* **3**, 373 (1957)
 Yagi, S, D Kunii, and N Wakao, *AIChE Journal*, **6**, 543 (1960)
 Yoshida, H and D M Ruthven, *Chem Eng Sci*, **38**, 877 (1983)

Regeneration of Spent Adsorbent

Adsorption is an unsteady process and regeneration or reactivation of the adsorbent is needed for recyclic use. The primary objective of regeneration is to restore the adsorption capacity of exhausted adsorbent while the secondary objective is to recover valuable components present in the adsorbed phase, if any.

Since adsorption operations are a cyclic process composed of adsorption step and regeneration step, efficiency and cost of regeneration play important roles in the overall feasibility of an adsorption process.

There are several alternative processes available for the regeneration of spent adsorbents: 1) desorption by inert stream or low pressure stream, 2) desorption at high temperature where adsorption isotherm is considerably advantageous for desorption, 3) desorption by changing affinity between adsorbate and adsorbent by chemical reagent, 4) desorption by extracting adsorbates by strong solvents, and 5) removal of adsorbates by thermal decomposition or biochemical decomposition.

Methods 1 and 2 are commonly used for regeneration of adsorbents used for gaseous phase adsorption. Naturally, method 2 can be applied for liquid phase adsorption if the equilibrium relation allows in specific cases. Fig. 9.1 shows these schemes of desorption. Desorption using an inert stream free of adsorbent is essentially the same operation as adsorption, which can be analyzed by the same basic equation with different initial, and boundary conditions. The same is true of desorption at high temperature (thermal desorption) except that the equilibrium relation is very different. Also, in the actual operation of thermal desorption, nonisothermal treatment becomes important in most cases. The combination of desorption at low pressure and adsorption at high pressure is the principle of pressure swing operation (PSA), which is discussed in Chapter 11.

Methods 3 and 4 are specific to liquid phase adsorption and especially effective when recovery of adsorbate is desirable. Desorption by alkaline solution is often used for recovery of organic acids adsorbed on

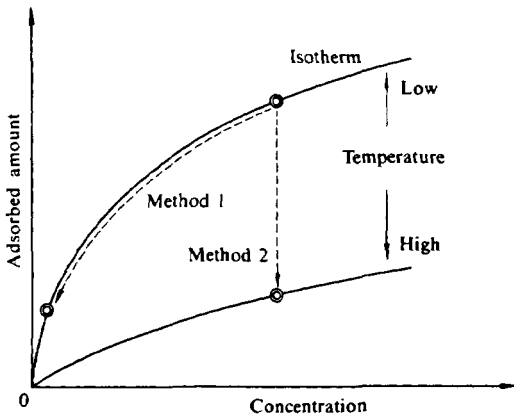


Fig. 9.1. Conceptual schemes of desorption methods.

activated carbons. In this case low adsorbability of dissociated organic acids in comparison with organic acids of molecular form is utilized. Also, extractive desorption of adsorbed organics by using organic solvents is an example of solvent regeneration, where extraction of an adsorbate by solvent as well as displacement of adsorption sites by adsorbed solvent molecules results in the effective desorption of adsorbate molecules.

When unknown multicomponent organics are adsorbed in such cases as activated carbons used in water treatment, simple desorption is not applicable to fully restore adsorption capacity. In this case, regeneration at high temperature by oxidizing gases, such as steam (thermal regeneration), which resembles activation process of activated carbon, is commonly used. When adsorbed organics are biochemically decomposable or chemically oxidizable, biochemical or chemical oxidation may be applied for regeneration of spent activated carbons from water treatment.

9.1. Thermal Desorption in Gas Phase

For the exhausted adsorbents from gas phase adsorption, regeneration by thermal desorption is most commonly used. For example, activated carbon used to prevent contamination of air by organic solvents of low concentrations, and silica gel, activated alumina or zeolite used for dehumidification of gases are regenerated by high temperature steam, air or inert gases. In the case of organic adsorbates

such as ketones and esters, polymerization reactions or oxidizing reactions which occur in micropores of adsorbent particles sometimes cause severe problems such as explosion, fire or at least insufficient recovery of adsorption sites. This type of problem should be considered first when selecting a regenerant gas.

For estimation of desorption curves from an exhausted adsorbent bed, the basic equations for mass and heat balances in an adiabatic column are as follows.

$$u_0 \partial C / \partial z + K_f a_v (C - C^*) = 0 \quad (9-1)$$

$$K_f a_v (C - C^*) = \rho_b \partial q / \partial t \quad (9-2)$$

$$\begin{aligned} k_{cz} \partial^2 T / \partial z^2 - C_{pf} \rho_f u_0 \partial T / \partial z + Q_{st} \rho_b \partial q / \partial t \\ = C_{ps} \rho_b \partial T / \partial t \end{aligned} \quad (9-3)$$

$$C^* = C^*(q, T) \quad (9-4)$$

When high temperature inert gas is introduced to the bed, the above set of equations must be solved simultaneously under a proper set of initial and boundary conditions and concentration and temperature profiles in the effluent stream can be readily obtained.

Analogous to adsorption in a column with nonisothermal conditions, the thermal front formed by a high temperature inlet stream moves through the column and changes the equilibrium relation at and after the front. Velocity of the thermal front is described by neglecting consumption of heat due to desorption heat as

$$V_T = C_{pf} \rho_f u_0 / C_{ps} \rho_b \quad (9-5)$$

Velocity of desorption wave, V_D , is also determined by the ratio of the amount adsorbed, q , to the concentration, C^* , in equilibrium with q at temperature, T .

$$V_D = C^*(q, T) u_0 / \rho_b \quad (9-6)$$

The relation between C^* , T and q are in most cases understood as follows: C^* increases exponentially with the temperature rise for a constant q and for a constant T , q is convexly dependent on C^* .

Thus by choosing a high enough temperature, imaginary speed of desorption front can be made faster than the speed of the thermal wave. In this case, desorbed species at the thermal front is accumulated at the

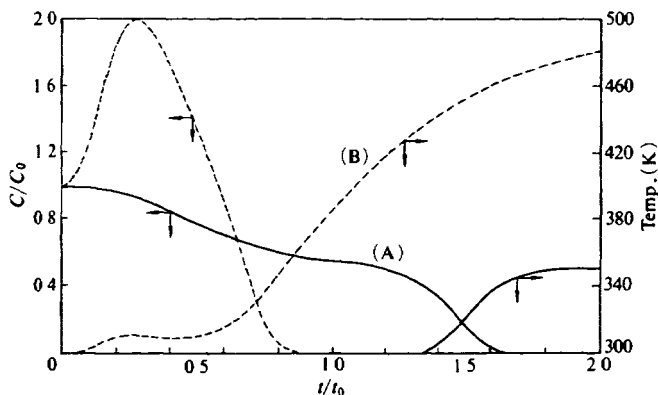


Fig. 9.2 Typical examples of calculated elution curves. Solid lines case (A), broken lines case (B)

$$C_0 = 1.0 \text{ mol/m}^3, q_0 = 4 \text{ mol/kg},$$

$$t_0 = \rho_b q_0 L / C_0 u, k_{cz} = 0.29 \text{ J/m s K},$$

$$C_{ps} = 1050 \text{ J/kg K}, C_{pf} = 1138 \text{ J/kg K},$$

$$\rho_b = 481 \text{ kg/m}^3, Q_{st} = 32930 \text{ J/mol},$$

$$L = 0.6 \text{ m}$$

$$\text{case (A)} \quad u_0 = 0.04 \text{ m/s, regeneration temp} = 350 \text{ K}$$

$$\text{case (B)} \quad u_0 = 0.004 \text{ m/s, regeneration temp} = 500 \text{ K}$$

front and a high concentration peak with less tail can be expected.

On the other hand, when the desorption temperature is not high enough, desorption gradually occurs and long tailing will be expected as in the case of desorption by an inert stream at the adsorption temperature.

Numerical examples of the solution to the above set of equations for desorption by a high temperature inert gas are shown in Fig. 9.2 for those two extreme cases.

9.2. Chemical Desorption from a Column

When the adsorption isotherm in liquid phase can be modified by changing pH or by introducing an organic solvent, desorption can be expected to occur in a manner similar to thermal desorption in the case of gas phase adsorption operation. Desorption behavior is determined by the change of adsorption isotherm and intraparticle diffusion in the desorbent phase

Fundamental equations are similar to Eqs. (9-1) to (9-4) and given as follows

$$u_o \partial C / \partial z + K_{Fa_v}(C - C^*) = 0 \quad (9-7)$$

$$K_{Fa_v}(C - C^*) = \rho_b \partial q / \partial t \quad (9-8)$$

$$u_o \partial C_d / \partial z + (K_{Fa_v})_d(C_d - C_d^*) = 0 \quad (9-9)$$

$$(K_{Fa_v})_d(C_d - C_d^*) = \varepsilon \partial C_d^* / \partial t \quad (9-10)$$

$$C^* = C^*(q, C_d^*) \quad (9-11)$$

where C_d and C_d^* respectively denote concentration of desorbent in the stream and particle phases. Adsorption or chemical consumption of desorbent by adsorbent particles or adsorbate may become significant in some cases but can usually be neglected since a large amount of desorbent is introduced in comparison with the amount consumed in the column.

Several examples for desorption of this type are given below: 1) desorption of organics from activated carbon by methanol (Sudo and Suzuki, 1985), 2) concentrating desorption of uranium from the resin adsorbent used for recovery of uranium from sea water by using an acid solution (Suzuki *et al.*, 1986), and 3) desorption of ammonium ion from the clinoptilolite used for water treatment by sodium chloride solution (Ha and Suzuki, 1984). Also, alkaline desorption for phenols adsorbed on the activated carbons or acid desorption of phosphate trapped on zirconium oxide adsorbent and many other examples may be analyzed by similar methods

9.2.1. Elution of organics adsorbed on activated carbon by methanol

Organic solvents such as alcohols and benzenes can be used for desorbing adsorbed organics. For instance, adsorption isotherms of *o*-chlorobenzoic acid on activated carbons from alcohol-water mixtures of different ratios are shown in Fig. 9.3. Obviously, the higher the alcohol content in the mixture, the less the adsorbed amount of *o*-chlorobenzoic acid on the activated carbon. This is readily understood as the change of solvophobic effect

Using this equilibrium relation and the previous set of equations, elution curves by means of methanol eluant from the activated carbon column which has adsorbed *o*-chlorobenzoic acid can be calculated. The rate of desorption is also dependent on alcohol content and the amount adsorbed, but as a rough estimation simple treatment of constant

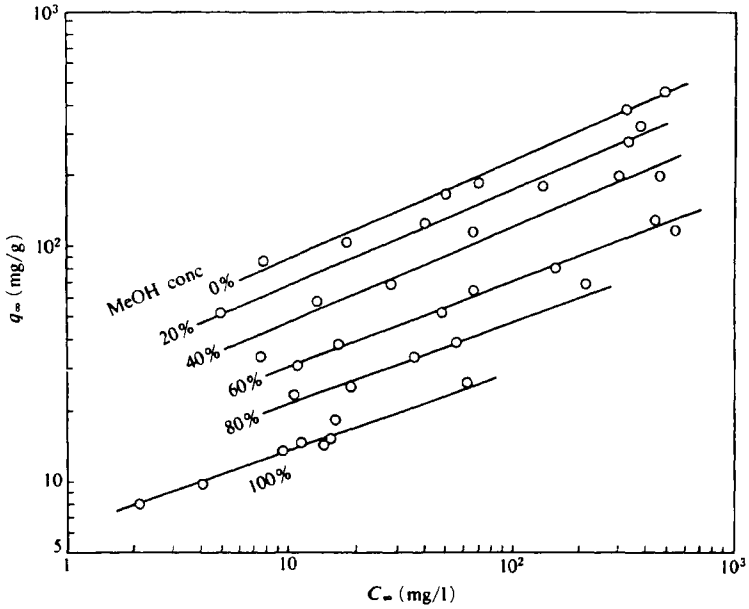


Fig 9 3 Adsorption isotherm of phenol on activated carbon from alcohol-water mixtures of different ratios

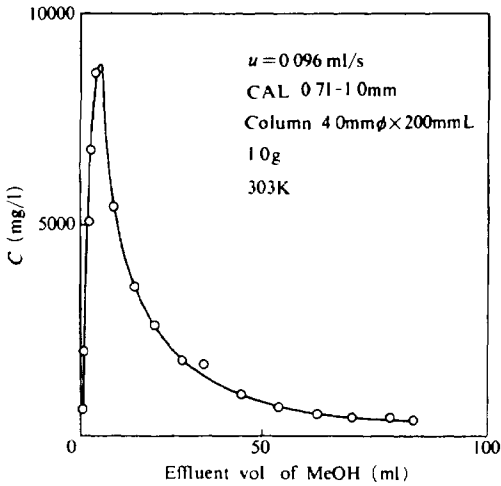


Fig 9 4 Desorption curve of phenol from activated carbon column by methanol

diffusivity; thus constant K_{Fa} 's can be adopted for breakthrough of alcohol and desorption of *o*-chlorobenzoic acid. Comparison of the measured elution curve with the calculated one is given in Fig. 9.4. Thus desorbed organics can be recovered as a high concentration solution and used as a resource.

9.2.2. Concentrating desorption of uranium from resin adsorbent by acid

Since uranium is present in sea water in such low concentrations as $3.2 \mu\text{g/l}$, adsorption recovery could become a feasible method of extraction and concentration for further utilization. Amidoxime resin is one of the promising adsorbents for this purpose and in fact after contact with sea water for more than one hundred days the resin can accumulate several hundred mg/l of uranium in the bed. The resin also adsorbs alkaline earth metals such as calcium and magnesium, which must first be removed by a weak acid solution. Desorption of uranium by hydrochloric acid solutions of different concentrations and the resultant equilibrium relations are shown in Fig. 9.5. From this result, hydrochloric acid of one mole/l was selected as an eluant. Acid elution and uranium desorption are solved simultaneously by a similar set of

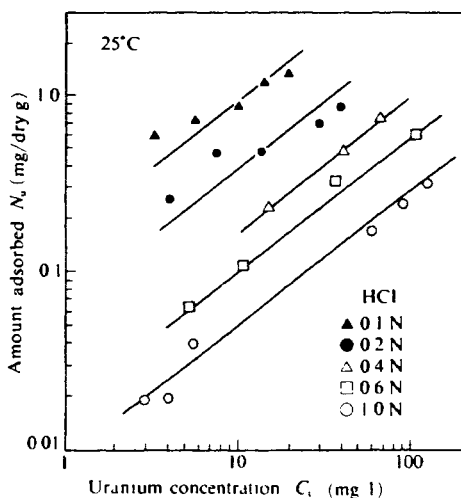


Fig 9.5 Desorption isotherms of uranium at acid concentration levels of 0.1, 0.2, 0.4, 0.6 and 1.0 mol/l

(Reproduced with permission by Suzuki, M *et al*, *2nd Int Conf on Fundamentals of Adsorption*, 545, 546 (1986), Eng Foundation)

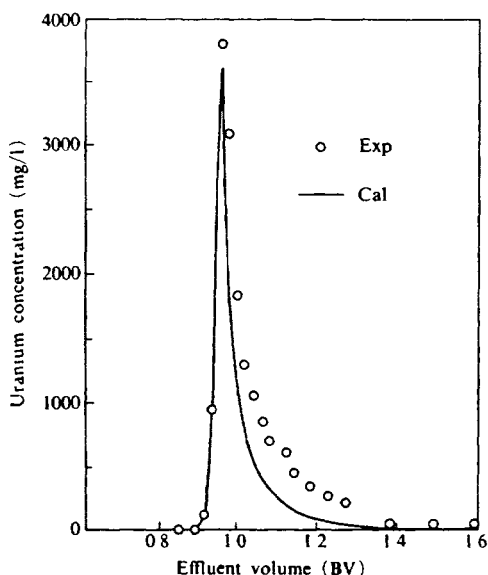


Fig. 9.6 Comparison of calculated and measured elution curves from a saturated column with hydrochloric acid solution, $SV = 3$ (Reproduced with permission by Suzuki, M *et al*, *2nd Int Conf on Fundamentals of Adsorption*, 545, 546 (1986), Eng Foundation)

equations and it was found that desorbed uranium is accumulated near the acid elution front and a concentrated peak of more than 4000 mg/l can be obtained. Comparison of the calculation and the measurement is given in Fig. 9.6.

9.2.3. Regeneration of clinoptilolite used for ammonium removal

Ammonium ion in water is effectively captured by clinoptilolite of sodium type, where sodium ion is exchanged by ammonium ion. Therefore, exchange equilibrium relation follows the mass action law and the relation is shown in Fig. 9.7. The empirical formula for equilibrium is given as

$$\left. \begin{aligned} X &= K_c Y / (1 - Y + K_c Y) \\ K_c &= 11.75 \cdot 10^{-0.52Y'} \end{aligned} \right\} \quad (9-12)$$

where Y and X respectively are fractional ionic strength of ammonium in solid phase and in aqueous phase. By using sodium chloride solution of high concentration, ammonium type clinoptilolite can be regenerated

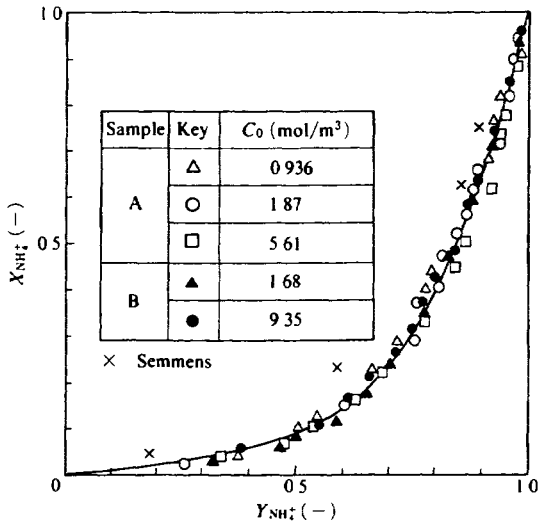


Fig 9.7 Comparison of calculated and measured ammonium ion exchange isotherms for clinoptilolite samples A and B (Reproduced with permission by Suzuki, M and K-H Ha, *J Chem Eng Japan*, 17, 142 (1984))

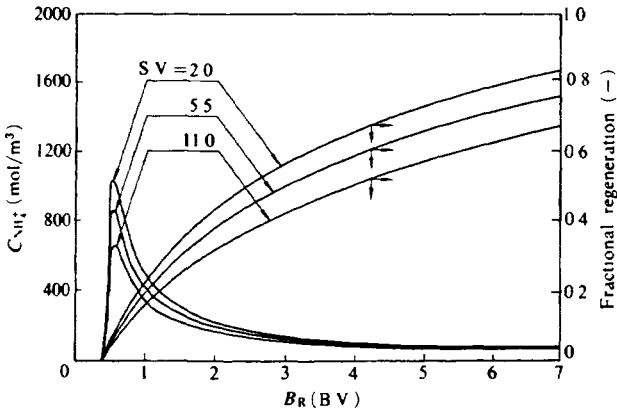


Fig 9.8 Effect of flow rate on effluent curve during regeneration of spent clinoptilolite by sodium chloride solution (Reproduced with permission by K-H Ha and Suzuki, M, *J Chem Eng Japan*, 17, 300 (1984))

the sodium type

In this case total cation mass balance and sodium ion mass balance in column are solved simultaneously and concentration of ammonium

ion is determined as the difference between total ion concentration and that of sodium ion. More detailed analysis was made using the mass balance equation based on diffusion inside particle phase,

$$\partial q_{Na}/\partial t = D_s[\partial^2 q_{Na}/\partial r^2 + (2/r)\partial q_{Na}/\partial r] \quad (9-13)$$

$$\partial q_{Na}/\partial t = k_1 a_v (C_{Na} - C_{Na,s}) = \rho_p D_s a_v (\partial q_{Na}/\partial r)_{r=R} \quad (9-14)$$

instead of Eq. (9-8).

Examples of ammonium elution curves are given in Fig. 9.8 for various space velocities of eluant.

9.3. Thermal Regeneration of Spent Activated Carbon from Water Treatment

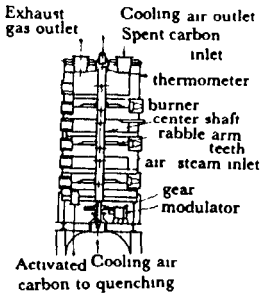
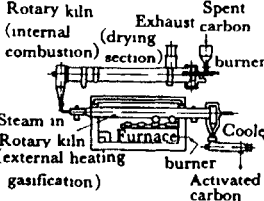
Granular activated carbon used in water treatment usually contain many different kinds of organics and chemical or extractive desorption may be effective only on some fractions of the total organics adsorbed. The most widely used regeneration method is thermal regeneration, which is similar to the production process of activated carbons.

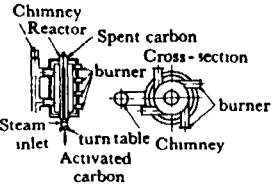
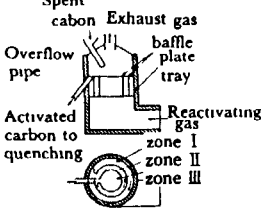
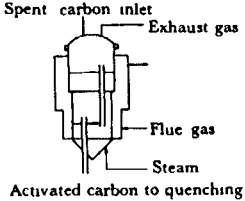
9.3.1. Reactors for thermal regeneration of activated carbon

Reactors widely used for the thermal regeneration of spent carbon are multiple hearth reactors, rotary kilns, moving bed reactors and fluidized bed reactors. Comparisons of these reactors were made in terms of residence time, steam and fuel consumption in Fig. 9.9 (Suzuki, 1976).

9.3.2. Principles of thermal regeneration

Independent of reactor type, spent activated carbons introduced in the reactor pass through three main steps during the temperature rise, as shown in Fig. 9.10. Drying of wet spent carbon occurs around 373 to 383 K where a large amount of heat is consumed for evaporation heat. Then, during temperature rise to about 1000 K, desorption of volatile organics, thermal cracking (decomposition) of fragile organics and pyrolytic polymerization of some high molecule or phenolic organics occur in the activated carbon. This step leaves carbonized residues which must be gasified by steam introduced at around 1100 to 1200 K. A problem in the last step is the selective gasification of carbonized residue since activated carbon itself is readily gasified by oxidizing gases such as

Type	Illustration	Characteristics	Deficiency	Operation data *
<p>Multiple hearth furnace</p>	<p>Herreshof furnace, BSP-Sumitomo, Nichols-Organo, Nihongaishi processes</p> 	<p>Rotating rabble arms moves carbon on each hearth toward center or outside By adjusting rotating speed, residence time of carbon is controlled Usually 4 to 8 hearths/unit For 6 hearth unit, upper 3 hearths are used for drying, next for heating and the last 2 hearths for activation Treatment capacity is 400 to 500 kg/day/m² hearth area Many existing plants in U S and Japan</p>	<p>Insufficient gas-solid contact Difficult control of solid temperature Intermittent operation is not economical Minimum reactor capacity is 1 ton/day Needs afterburner for emission control</p>	<p>Residence time 30min to 1 0hr Steam injection ca 1 kg/kg carbon Fuel required Kerosene 0 45to0 6 l/kg carbon or propane 120 l/kg carbon About the same amount of fuel is needed for an afterburner Fuel can be reduced by heat recovery</p>
<p>Rotary kiln</p>	<p>Japan Furnace—Mitsui Const Co process</p> 	<p>Internal heating at drying section and external heating at temperature rise and gasification step Slow cooling after regeneration</p>	<p>Small contact area between solid and gas and small heat exchange area at the external heating section requires large sized equipment</p>	<p>Residence time 20 min Steam injected 1 0 kg/k carbon Fuel Heavy oil 1 0 l/kg carbon</p>

<p>Moving bed</p>	<p>JGC-Takeda process</p> 	<p>Long residence time Steam is distributed from a center shaft to radial direction</p> <p>External combustion for heating acts also as an after-burner Discharged after slow cooling Low rate of attrition of particles</p>	<p>Temperature distribution and uniform supply of steam in the radial direction needs special care</p>	<p>Residence time 3 to 6 h Steam injected 0.12 kg/kg carbon Fuel Kerosene 0.31/kg carbon</p>
<p>Fluidized bed</p>	<p>Mitsubishi-Lurgi process</p> 	<p>Advantageous for solid temperature control Use of baffle plates improves residence time distribution of particles</p>	<p>Matching of conditions needed for fluidization and regeneration sometimes becomes delicate Low utilization of fluidizing (regenerating) gas High attrition of particles</p>	<p>Residence time ca 25min Steam partial pressure 39% Fuel Kerosene 0.28 to 0.3 kg/kg carbon (0.15 kg/kg carbon for afterburning)</p>
	<p>Chiyoda process</p> 	<p>Two-stage fluidized bed First stage (upper) for drying and desorption (400°C) and lower stage for gasification</p> <p>Attrition problem is waived by using spherical carbon particles Internal heating is also possible</p>	<p>Matching of conditions needed for fluidization and regeneration sometimes becomes delicate Wide residence time distribution in each stage is expected Thermal shock to the carbon introduced</p>	<p>Residence time 1 to 2 h Steam injected 2.5 kg/kg carbon Fuel 2500 kcal/kg carbon</p>

* kgcarbon refers to 1 kg of activated carbon after regeneration

Fig. 9.9 Comparison of regeneration reactors for spent activated carbon

steam if conditions such as temperature are not carefully chosen. Naturally, the regenerant gases must be free of oxygen since it easily burns activated carbon even at lower temperatures.

9.3.3. Changes in the temperature rise step

Below 1000 K, gas stream is considered inert unless it contains oxygen. Thus change of organics adsorbed on activated carbon during the temperature rise step may be estimated by thermal gravity analysis (TGA) of activated carbon samples which have adsorbed different kinds of organics (Suzuki *et al.*, 1978).

TGA curves of adsorbed organics were classified by shape into three different types, which are shown in Fig. 9.11. They are:

- (I) Thermal desorption type: concave TGA curves.
- (II) Thermal cracking type: convex TGA curves.
- (III) Carbonization type: gradual TGA curves.

By observing TGA curves of thirty-two different organics loaded on activated carbon (TABLE 9.1), classification into three types were attempted based on the boiling points of the organics and the aromatic

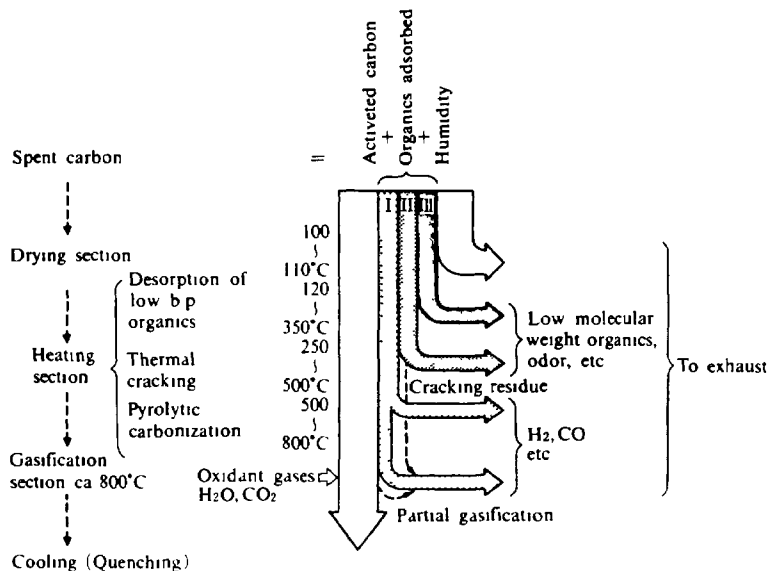


Fig 9 10 Principle of thermal regeneration of spent activated carbon—change of adsorbed organics
(Reproduced with permission by Suzuki, M., *Kagaku Kogaku*, 40, 408 (1976))

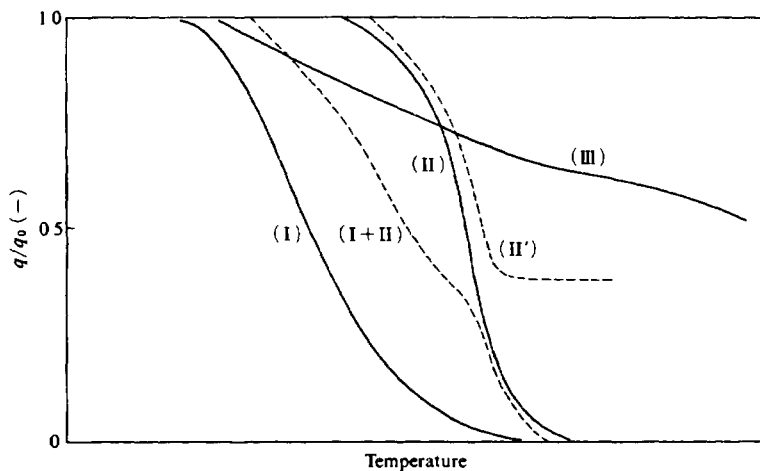


Fig 9 11 a Phenomenological classification of thermo-gravity-analysis (TGA) curves of adsorbed organics on activated carbons (Reproduced with permission by Suzuki, M *et al*, *Chem Eng Sci*. 33, 274 (1978))

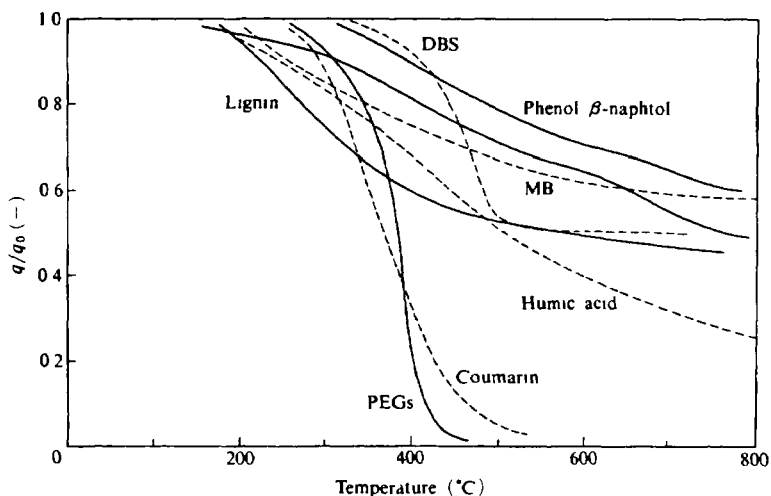


Fig 9 11 b Typical TGA curves of organics of groups 2 and 3 (Reproduced with permission by Suzuki, M *et al*, *Chem Eng Sci* 33, 275 (1978))

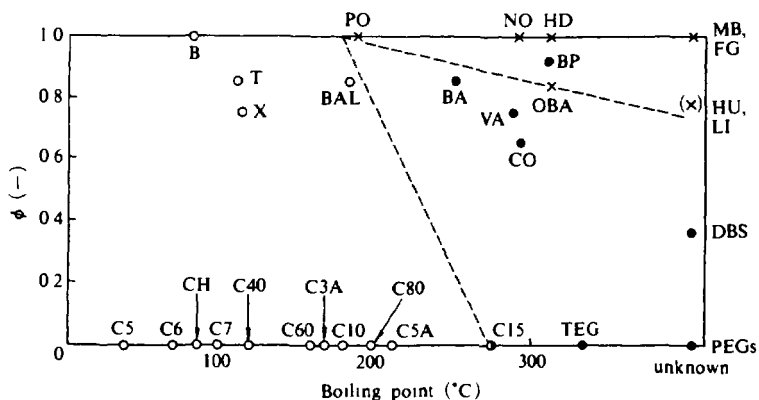


Fig 9.12. Boiling point- ϕ (aromatic carbon fraction) plots of the organics examined. Hollow circles, solid circles and crosses, respectively correspond to groups I, 2 and 3. Keys refer to TABLE 9.1. ϕ values of humic acid and lignin are unknown (Reproduced with permission by Suzuki, M *et al*, *Chem Eng Sci*, 33, 278 (1978)).

carbon content, ϕ , defined as

$$\phi = \frac{\text{number of aromatic carbon in the molecule}}{\text{total number of carbon in the molecule}}$$

Then, as shown in Fig. 9.12, the organics that have low boiling points belong to Type I. Obviously, low boiling point corresponds to low heat of vaporization of the organic, which is a measure of low heat of adsorption of the organic on activated carbon. The organics with higher boiling points cannot be desorbed before they undergo thermal cracking on the adsorbent surface. The cracking temperature is strongly dependent on the nature of the cracking reaction of the molecule. Type II assumes that fragmented reaction products are easily desorbed from the activated carbon surface. Type III probably corresponds to those organics which form polymeric products after some type of sequential cracking reaction on the carbon surface, resulting in relatively high ratio of carbonized residue.

9.3.4. Models for TGA kinetics

Two models were proposed to explain TGA behavior of types I and II

Model (a): For the thermal desorption type, equilibrium desorption

TABLE 9-1 Results of the TGA Experiments of Organics Loaded on Activated Carbon

Adsorbate	Molecular weight	Boiling point °C	q_b	q_{100}/q_0	Organic type	$T_{1/2}$	ΔT	Q_{100}	E	Key for Fig. 9-12
n pentane	72	36	0.108 ^{d)}	0 ¹⁾	I	152	200	7.2		C5
n hexane	86	69	0.259 ^{d)}	0	I	155	155	9.4	5.34 ^{d)}	C7
n heptane	100	98.4	0.259 ^{d)}	0	I	175	200	7.9		C10
n-decane	142	174	0.224 ^{d)}	0	I	270	290	8.1		C15
p pentadecane	212	270	0.215 ^{d)}	0.10	I+II					CH
cyclohexane	84	83	0.312 ^{d)}	0.12	I	182	190	8.6		B
benzene	78	80	0.254 ^{d)}	0	I	162	159	9.4		X
toluene	92	110.6	0.229 ^{d)}	0	I	185	185	11.3		PO
p xylene	106	114	0.364 ^{d)}	0.03	I	180	236	7.0		NO
phenol	94	182	several	0.61	III					FG
β naphthol	144	285	0.111	0.68	III					HD
fluoroglucinol	126	177	0.181	0.37	III					DBS
p hydroxydiphenyl	170	308	0.111	0.49	III					TEG
DBS ^{a)}	326		0.092	0.50	II	460	100		27.7	
TEG ^{b)}	194		0.102	0	II	375	85		25.7	
PFG ^{c)} 400	~400		several		II	375	85		25.7	
PEG 1000	~1000		several		II	375	85		25.7	
PTG 4000	~4000		several	0.105	II	375	85	19.1 ^{d)}	25.7	
Benzaldehyde	106	179.1	0.434	0.07	I	350	190			CBA
p oxybenzaldehyde	122	310	0.118	0.15	III					OBA
lignin			0.0398	0.45	III					LI
humic acid	320		0.035	0.26	III					HU
methylene blue	122		0.084	0.58	III					MB
benzoic acid	122	250	0.267	0.150	III					BA
caproic acid	116	205.4	0.500	0.04	II	347	157		12.0	C5A
butyric acid	88	164.1	0.425	0.01	I	243	260	8.11		C3A
hexanol	102	157.5	0.348	0.04	I	180	182	10.8		C40
octanol	130	194.5	0.460	0.03	I	234	213	8.91		C60
coumarin	146	290	0.404	0	I	360	360	9.56		C80
benzophenone	182	305.9	0.210	0.20	II	372	195	5.52		COU
viamin	120	285	0.175	0.28	II	385	115		10.2	BP
									19.1	VA

a) Sodium dodecyl benzenesulfonate

b) Tetrathylene glycol

c) Polyethylene glycol

d) loaded by immersion and drying overnight at room temperature

e) 0 denotes $q_{100} < 0.01$ g/g carbon

f) obtained by applying improper model

(Reproduced with permission by Suzuki M *et al Chem. Eng. Sci.* 33: 273 (1978))

with the Langmuir isotherm is considered as a first approximate. When an activated carbon loaded with q grams of an organic per gram of the carbon is in equilibrium with pressure p , the temperature dependence of q is given as follows:

$$q = q_{\infty} K p / (1 + K p) \quad (9-15)$$

where K is an equilibrium constant expressed in terms of isosteric heat of adsorption, Q_{st} , as

$$K = K_0 \exp(Q_{st} / RT) \quad (9-16)$$

Then, assuming that both p and q_0 are temperature independent, Eqs. (9-15) and (9-16) give

$$q/q_0 = (q_{\infty}/q_0) / [1 + (1/K_0 p) \exp(-Q_{st}/RT)] \quad (9-17)$$

By fitting this equation with experimentally obtained curves, Q_{st} can be determined. For use in practical comparison with TGA curves of type I, the temperature at $q/q_0 = 1/2$, $T_{1/2}$, and the slope of the tangential line of TGA curve at $q/q_0 = 1/2$ are recommended. Since $T_{1/2}$ and the reciprocal slope, ΔT , are given as

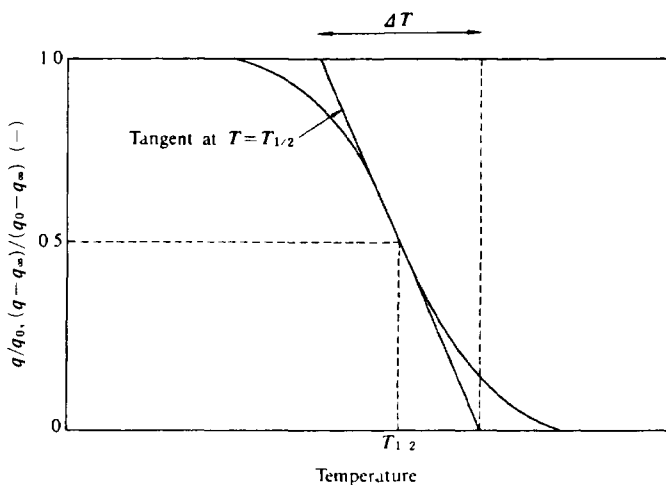


Fig. 9.13 Definition of $T_{1/2}$ and ΔT of experimental TGA curves

$$T_{1/2} = -(Q_{st}/R)/[\ln(K_o P) + \ln\{2(q_\infty/q_0) - 1\}] \quad (9-18)$$

$$\begin{aligned} [d(q/q_0)/dT]_{T_{1/2}} &= -1/\Delta T \\ &= -\frac{1}{4T_{1/2}} \cdot \frac{Q_{st}}{RT_{1/2}} \left(2 - \frac{q_0}{q_\infty}\right) \end{aligned} \quad (9-19)$$

Fig. 9.13 shows definitions of $T_{1/2}$ and ΔT . If the ratio of ΔT and $T_{1/2}$ is taken, then

$$\xi \equiv \Delta T/T_{1/2} = \frac{4}{2 - q_0/q_\infty} \cdot \frac{RT_{1/2}}{Q_{st}} \quad (9-20)$$

and in the case when $q_0 = q_\infty$ holds

$$\xi \equiv \Delta T/T_{1/2} = 4RT_{1/2}/Q_{st} \quad (9-21)$$

Medel (b): For thermal cracking type, the first order reaction kinetics is assumed as a first approximation. The basic equation is

$$dq/dt = -kq \quad (9-22)$$

where k is given by the Arrhenius equation

$$k = k_o \exp(-E/RT) \quad (9-23)$$

By setting the heating rate as $m = dT/dt$, Eqs. (9-22) and (9-23) give

$$dq/q = -k_o/m \exp(-E/RT) dT \quad (9-24)$$

Integration of the above equation becomes

$$q/q_0 = \exp[(k_o/m)(E/R)E_1(E/RT) - (RT/E)\exp(-E/RT)] \quad (9-25)$$

where

$$E_1(x) = \int_0^x [\exp(-x)/x]dx \quad (9-26)$$

Similar to the thermal desorption model, $T_{1/2}$ and ΔT of TGA curves defined by Fig. 9.13 can be related to the above solution.

$$\xi \equiv \Delta T/T_{1/2} = (2/\ln 2)\psi(E/RT_{1/2}) \quad (9-27)$$

where

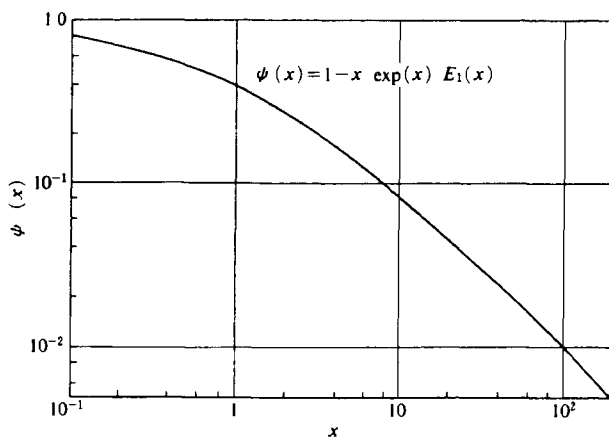
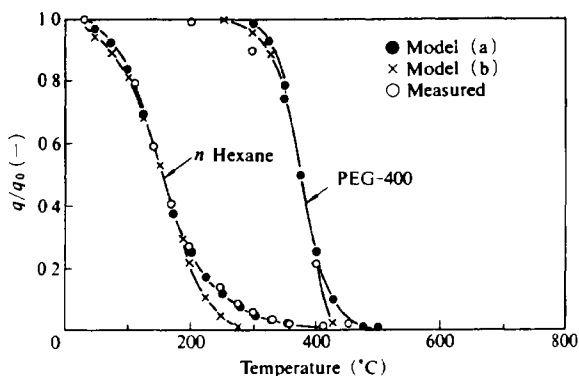

 Fig. 9.14 Diagrams for obtaining $x = E/RT_{1/2}$ from $\psi(x)$


Fig. 9.15 Comparison of models with measured TGA-curves

$$\psi(x) = 1 - x \exp(x) E_1(x) \quad (9-28)$$

The function $\psi(x)$ vs. x is shown in Fig. 9.14. From the above relation, it is clear that the activation energy E can be determined from ξ by employing Fig. 9.14. Obviously, the pre-exponential factor k_0 is obtained from E as

$$k_0 = (2m/\Delta T) \exp(E/RT_{1/2}) \quad (9-29)$$

These two models are compared with the TGA curves of *n*-hexane and polyethylene glycol (PEG) in Fig. 9.15. In the figure the thermal desorption model compares better than the thermal cracking model with the TGA curve of *n*-hexane while the reverse is true for the TGA curve of PEG 400. The model fittings were made at $q/q_0 = 1/2$ for both models with both curves.

9.3.5. TGA of spent activated carbon from multicomponent adsorption

When adsorption is done from wastewater which contains many types of organics, the problem of regeneration becomes more severe if the water contains a relatively large fraction of organics of Type III. As can be seen from the previous discussions, organics of Types I and II may be desorbed or cracked and desorbed and can be expected to leave only small amounts of carbonized residues. This suggests that if organics in wastewater are composed only of Types I and II, thermal regeneration may become very easy since most of the organics adsorbed can be removed during the temperature rise step. However, organics of Type III, if present in the adsorbate phase, are anticipated to leave a considerable fractional amount of residual carbonized material after being heated up to about 1000 K. From TABLE 9.1, apparently phenols, lignin and humic acid are the main components of organics of Type III.

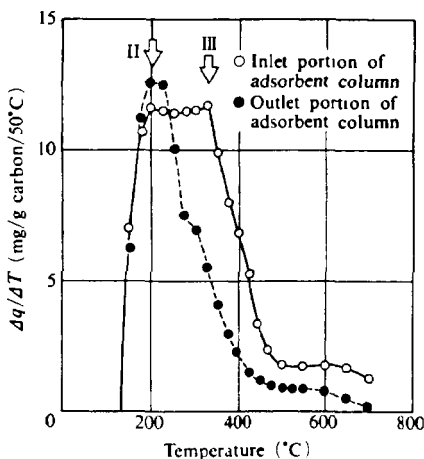


Fig 9.16 Differential TGA curves of spent activated carbon used for treatment of sugar refinery wastewater
(Reproduced with permission by Suzuki, M., *Kagaku Kogaku*, **40**, 408 (1976))

These organics may be removed by washing with alkaline solution before going into the regeneration step.

From the classification of organics those which belong to Type I may be replaced by organics of Type II, which are then replaced by Type III, i.e., organics of Type III will accumulate in the entrance part of the adsorption column while Type II and Type I are pushed forward to the exit of the column. Fig. 9.16 shows the DTG curves (differentiation of TGA curves) of the spent carbons used for treatment test for wastewater from a sugar refinery. Type II organics are concentrated more on the carbon sample taken from near the entrance than on the sample from the latter half of the column.

9.3.6. Gasification of residual carbon

At temperatures higher than 1000 K, oxidizing gases such as steam or carbon dioxide are introduced to gasify the residual carbonized material left from the temperature rise step. As a result, micropores which are

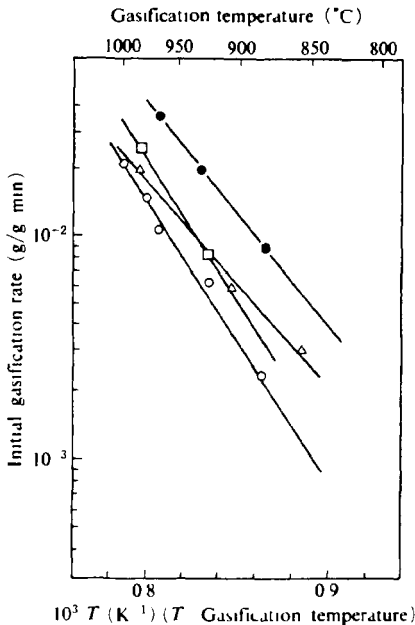


Fig 9 17 Gasification rates of various activated carbon by superheated steam (1 atm, pure steam)
(Reproduced with permission by Suzuki, M, *Kagaku Kogaku*, 40 408 (1976))

responsible for adsorption capacity are recovered. The problem here is that since activated carbon itself is made of carbon, it is easily gasified to result in a significant loss of adsorption characteristics or weight.

Obviously, the carbon residue from the adsorbed organics is expected to be more amorphous than the base carbon structure of the activated carbon and thus more easily gasified. However, how to select the conditions to accomplish selective gasification has not yet been ascertained. Appropriate gasification conditions can probably be determined by watching closely the gasification rates of base-activated carbons.

Gasification rates of several activated carbons were measured in superheated steam at 1 atm and compared in Fig. 9.17 (Suzuki, 1975). First order kinetics was assumed for the initial weight decrease of the activated carbon samples kept in a gravimetric balance and the rate constants, k , were determined.

$$k = -\ln (w/w_0)/t \quad (9-30)$$

where w and w_0 are the carbon weights after a small time lapse t and at the beginning. The difference in gasification rates may arise from different degrees of graphitization of the base carbon or catalytic effects of ash metals contained in the carbon. As shown in Fig. 9.17, activated carbons produced from lignite are the most easily gasified. Generally speaking, wood-base carbons are considered more reactive with steam than coal-base carbons, a fact which may be attributed to the degree of graphitization of the carbon structure.

Matsui *et al.* (1984) applied TGA analysis to determine activation energy of gasification rate of activated carbon in various steam concentrations. Change of activation energies in the course of gasification may suggest the catalytic effect of inorganic ashes contained in the carbon, which is expected to be more pronounced with progress of burnout.

In the case of spent carbon from wastewater treatment plants, it is likely that inorganic salts are trapped in the activated carbons. Alkali metals and alkaline earth metals are especially found to enhance gasification of carbon and also to enlarge micropore sizes. Prior removal of metals deposited in spent carbons is desirable for stable regeneration. This is clearly demonstrated in Fig. 9.18 by the change of micropore volume and surface area in the course of regeneration of the spent carbon from the treatment of wastewater from a petrochemical plant (Kawazoe, 1978). The effect of pretreatment by acid washing is distinguishable, since the pretreated sample does not show decrease of

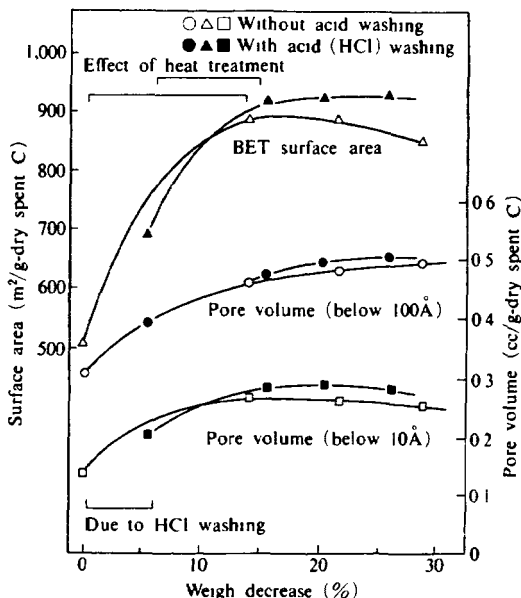


Fig 9.18 Change of surface area and pore volume of spent activated carbons from pet rochemical wastewater treatment during thermal regeneration, comparison of regeneration with and without initial acid washing. Reproduced with permission by (Kawazoe, K and T Osawa, *Seisan Kenkyu*, 28 (3), 109 (1976))

surface area during gasification.

Change of pore volume or adsorption capacity in the course of regeneration is rather difficult to realize from a single regeneration run, since virgin activated carbon is not necessarily at the optimal activated conditions. Thus, repeated regeneration and adsorption under the same conditions may help in choosing regeneration conditions. This was done for the powdered activated carbons used for adsorption of sucrose and DBS by Smith and his colleagues (Chihara *et al.*, 1982).

REFERENCES

- Chihara, K., J M Smith and M Suzuki, *AIChE Journal*, 28, 129 (1982)
 Ha, K-S and M Suzuki, *J Chem Eng Japan*, 17, 297 (1984)
 Kawazoe, K., in *Kagaku Kogaku Benran*, 4th ed., Chapter 5, Maruzen Pub Co (1978) (in Japanese)
 Kawazoe, K and T Osawa, *Seisan Kenkyu*, 28 (3), 109 (1976) (in Japanese)

- Matsui, I, D M Misić and M Suzuki, *J Chem Eng Japan*, **17**, 13 (1984)
- Kato, I, T Kawaura, Y Sudo and M Suzuki, *Gunma Meeting. Soc Chem Engrs, Japan*, **B202**, 127 (1986) (in Japanese)
- Suzuki, M, *Kagaku Kogaku*, **40**, 408 (1976) (in Japanese)
- Suzuki, M, in *Kasseitan, Kiso to Ouyou* (Activated Carbon, Fundamentals and Application), Chapter 5, Kodansha (1975) (in Japanese)
- Suzuki, M, T Fujii, S Tanaka, T Itagaki and S Kato, *2nd Int Conf on Fundamentals of Adsorption*, Santa Barbara (1986)
- Suzuki, M, D M Misić, O Koyama and K Kawazoe, *Chem Eng Sci*, **33**, 271 (1978)

Chromatographic Separation

Chromatography is used not only for analytical purposes but also for separation of fine products on an industrial scale. The basic mechanism of separation is the same as that in analytical chromatography but on the industrial scale the use of larger amounts of sample and larger columns often introduce additional problems. These include: 1) complex adsorption problems such as nonlinearity of the adsorption isotherm which becomes non-negligible while in the analytical chromatography the linear portion of an isotherm is usually utilized because of the low concentration of the peak traveling in the column. Interaction of adsorbed molecules of the components to be separated may also play an important role in determining displacement concentration profile. 2) large-scale packed columns often introduce nonuniform packing, resulting in a large dispersion effect because of flow maldistribution in the packed bed.

For efficient separation based on chromatographic principles, several ideas have been tested and commercialized for the purpose of large size or continuous separation, e.g. moving bed processes, simulated moving bed processes, centrifugal planar chromatography and counter-current droplet chromatography. Other ideas should also be explored to utilize the attractive separation potential of the chromatographic method in the future.

10.1. Basic Relations of Chromatographic Elution Curves in Linear Isotherm Systems

Chromatographic elution curve, $C(t)$, is characterized by residence time (first absolute moment) and peak broadening (second central moment). The moments are defined as

$$\mu_1 = \int_0^{\infty} C(t) dt / m_0 \quad (10-1)$$

$$\mu_2' = \int_0^{\infty} C(t)(t - \mu_1)^2 dt / m_0 \quad (10-2)$$

where $m_0 = \int_0^{\infty} C(t)dt$ represents the area under the elution curve.

When an input of negligible width (δ -function) is introduced at $t = 0$, the moments of the elution curve are related to the equilibrium and rate parameters in the adsorbent bed as shown in Chapter 6.

$$\mu_1 = (z/u) \left[1 + \frac{1-\epsilon}{\epsilon} \epsilon_p \left(1 + \frac{\rho_p K_a}{\epsilon_p} \right) \right] \quad (10-3)$$

$$\begin{aligned} \mu_2' = (2z/u) & \left[\frac{E_z}{u^2} \left\{ 1 + \frac{1-\epsilon}{\epsilon} (\epsilon_p + \rho_p K_a) \right\}^2 + \frac{1-\epsilon}{\epsilon} \frac{R}{3k_f} (\epsilon_p + \rho_p K_a)^2 \right. \\ & \left. + \frac{1-\epsilon}{\epsilon} \frac{R^2}{15D_c} (\epsilon_p + \rho_p K_a)^2 + \frac{1-\epsilon}{\epsilon} \frac{\rho_p K_a^2}{k_a} \right] \quad (10-4) \end{aligned}$$

For a phenomenological description of chromatographic separation, the concept of theoretical plate is often used. Chromatographic column is considered to consist of a large number of "theoretical plates," in each of which equilibrium relations between fluid and particle phases hold (Fig. 10.1). Height equivalent to theoretical plate (HETP) and number of theoretical plate (NTP) are then related to column length z as

$$z = \text{HETP} \times \text{NTP} \quad (10-5)$$

HETP and NTP are written in terms of moments as

$$\text{HETP} = z(\mu_2' / \mu_1^2) \quad (10-6)$$

$$\text{NTP} = \mu_1^2 / \mu_2' \quad (10-7)$$

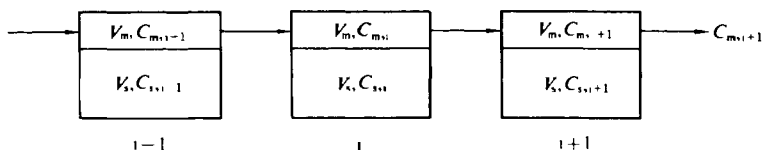


Fig. 10.1 Concept of the theoretical plate model. Well mixed in each cell and mobile phase is in equilibrium with stationary phase

μ'_2/μ_1^2 is readily obtained from Eqs (10-3) and (10-4). Usually the contribution of intrinsic adsorption rate constant, k_a , is considered negligibly small

$$\frac{\mu'_2}{\mu_1^2} = \frac{2u}{z} \left[\frac{E_z}{u^2} \left\{ 1 + \frac{1-\varepsilon}{\varepsilon} (\varepsilon_p + \rho_p K_a) \right\}^2 + \left(\frac{R}{3k_f} + \frac{R^2}{15D_e} \right) \frac{1-\varepsilon}{\varepsilon} (\varepsilon_p + \rho_p K_a)^2 \right] \quad (10-8)$$

When an adsorption equilibrium constant is large enough, $\rho_b K_a/\varepsilon \gg 1$, where ρ_b is the bed density, $(1-\varepsilon)\rho_p$, the above relation is simplified

$$\frac{\mu'_2}{\mu_1^2} = \frac{2u}{z} \left[\frac{E_z}{u^2} + \frac{\varepsilon}{1-\varepsilon} \left(\frac{R^2}{15D_e} + \frac{R}{3k_f} \right) \right] \quad (10-9)$$

In most cases the contribution of fluid-to-particle mass transfer resistance is negligible compared with that of intraparticle diffusion, and the last term in Eq (10-9) can be omitted. Furthermore, for longitudinal dispersion in packed beds, the relation defined by Eq (7-84) is modified as

$$E_z = \eta D_v + \lambda d_p u \quad (10-10)$$

Then Eq (10-9) finally gives Eq (10-11) as an expression of HETP

$$\text{HETP} = \frac{2\eta D_v}{u} + 2\lambda d_p + 2 \frac{\varepsilon}{1-\varepsilon} \frac{R^2}{15D_e} u \quad (10-11)$$

van Deemter *et al* (1956) gave the HETP relation as

$$\text{HETP} = 2\gamma D_v/u + 2\lambda d_p + C u d_p^2/D_v \quad (10-12)$$

$$C = \left[\frac{\varepsilon}{(1-\varepsilon)^2} \frac{1}{75} + \frac{\varepsilon}{\rho_b K} \right] D_v / 2\pi^2 D_e \quad (10-13)$$

This equation was derived by comparison of the elution curve approximated by the normal distribution and the equation derived from the plate theory. The similarity of Eqs (10-11) and (10-12) is not surprising. Eq (10-11) can be considered to be a more generalized form.

Eq (10-11) is further simplified in the cases of liquid phase chromatography since the contribution of the first term of R H S becomes negligible since molecular diffusion in liquid phase is small

enough.

$$\text{HETP} = 2\lambda d_p + 2\left[\frac{\varepsilon}{1-\varepsilon} \frac{R^2}{15D_c}\right]u \quad (10-14)$$

10.2. Separation of the Neighboring Peaks

When a mixture of two components is injected in the chromatographic column, separation occurs since each component moves according to its own adsorption affinity with the solid phase. While traveling in the column each peak broadens due to the nonequilibrium nature of chromatography as manifested, for example, by the existence of mass transfer resistance between fluid and solid phase. These states for each peak are qualitatively described by moment equations.

For two neighboring elution curves, *a* and *b*, the degree of separation of the two peaks is usually expressed in terms of the resolution, *R*, which is defined by means of the distance of the two peaks in terms of the duration of each peak, *t_w*, as shown in Fig. 10.2.

$$R = [\mu_{1,a} - \mu_{1,b}] / [(t_{w,b} + t_{w,a}) / 2] \quad (10-15)$$

The peak width can be defined from the tangential lines drawn at inflection points of the elution curve as the distance between the two intercepts on the abscissa.

For a good separation of the two peaks, *R* must be at least greater than unity. It is desirable to have as large an *R* as possible; when *R* is

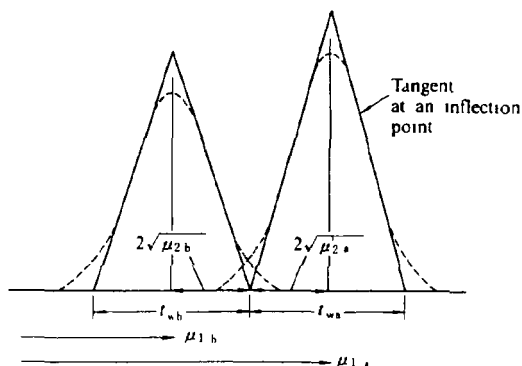


Fig 10 2 Two adjacent peaks at resolution, $R = 1$

larger than necessary productivity of the column is greatly reduced. Thus $R = 1.1-1.5$ is considered to be the optimum range when a one-path operation is used.

When the shape of the peak is close to the normal distribution curve, the peak duration time, t_w , is related to the second central moment μ_2' as

$$t_w = 4\sqrt{\mu_2'} \quad (10-16)$$

Then Eq. (10-15) can be written as

$$R = \frac{2|\mu_{1,a} - \mu_{1,b}|}{\sqrt{\mu_{2,a}'} + \sqrt{\mu_{2,b}'}} \quad (10-17)$$

Further simplification is possible when it is assumed that the two components, a and b , have similar adsorption characteristics on the adsorbent employed. For instance, the intraparticle diffusion coefficients, D_e , of both components may be approximated as the same when the two peaks are adjacent, then resolution for liquid phase can be written as

$$R = \frac{\sqrt{z/u} |1 - K_{a,a}/K_{a,b}|}{(1 + K_{a,a}/K_{a,b}) \sqrt{\lambda \cdot d_p/u + \{\varepsilon/(1 - \varepsilon)\} R^2/15D_e}} \quad (10-18)$$

This relation suggests that a longer column consistently gives better resolution with proportionality to the square root of the column length and that if longitudinal dispersion in the column is a dominant factor for peak broadening then selection of velocity has little effect on improving resolution while slow velocity usually gives higher resolution.

10.3. Large Volume Pulses

For the efficient use of a chromatographic column, cyclic introduction of pulses of the mixture becomes necessary. Furthermore, it is desirable for the size of the pulse introduced each time to be as large as allowable. But when a large volume sample of mixture is introduced in a column in the form of a square pulse, an elution peak can no longer be approximated by the normal distribution curve shown in Fig. 10.3.

In the case where each component travels independently, concentration profiles established in the bed can be described by applying the method shown for breakthrough calculations to the transport of each component.

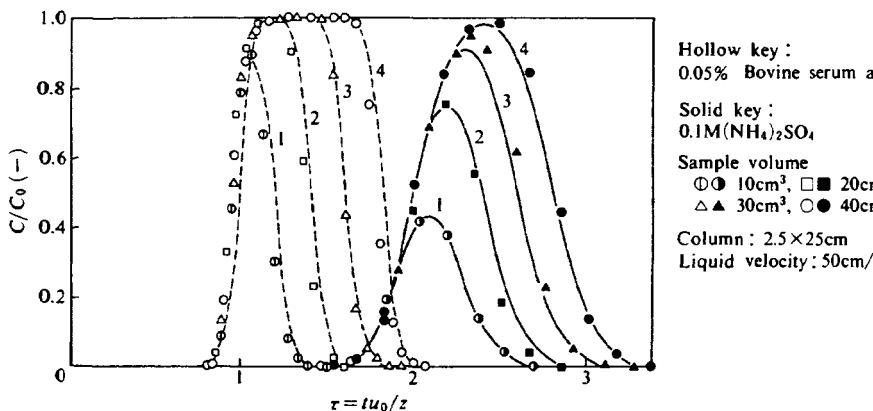


Fig. 10.3. Examples of large volume peaks for gel chromatography. (Reproduced with permission by Nakanishi, K. *et al.*, *Agric. Biol. Chem.*, 43, 2510 (1979)).

For instance, the pulse introduced at the inlet of the column is given as

$$\begin{aligned} C &= C_0 && \text{for } 0 \leq t \leq \tau \\ C &= 0 && \text{for } t < 0 \text{ and } \tau < t \end{aligned} \quad (10-19)$$

Then the concentration change at the exit of the column, $C_c(t)$, is given by

$$C_c(t) = C_b(t) - C_b(t - \tau) \quad (10-20)$$

Here $C_b(t)$ is the response curve for the step change of inlet concentration from $C = 0$ to C_0 , which is a so-called breakthrough curve.

The change of shape of the response peak with increase of pulse size, τ , as shown experimentally in Fig. 10.3, can be also calculated by employing an appropriate model and its parameters. Fig. 10.4.a shows an example from a two-phase exchange model.

Eq. (10-20) assumes a linear relation for the adsorption isotherm. This may be fulfilled in most cases of adsorptive separation of low concentration mixtures or gel permeation chromatography where no adsorption effect is expected. But when nonlinearity must be taken into account, $C_c(t)$ should be obtained by means of numerical method. As an example, a similar calculation as Fig. 10.4.a is shown for a Langmuir isotherm system with $R = 0.7$ in Fig. 10.4.b.

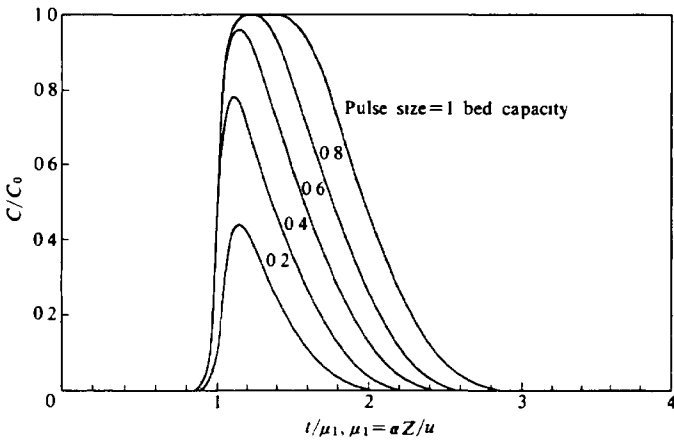
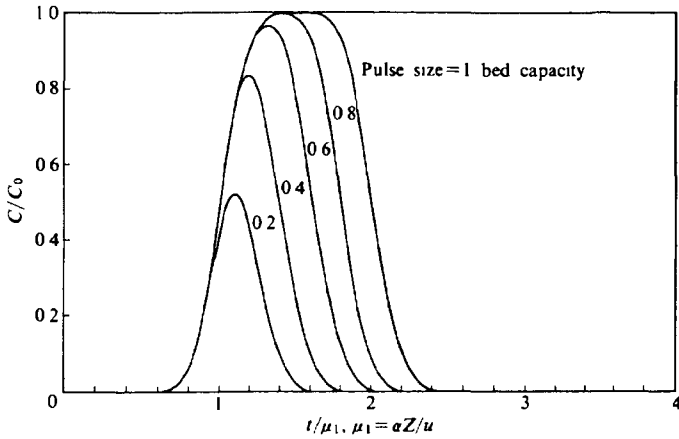


Fig 10.4 Chromatographic elution curve estimated from the two phase exchange model ($S = 100$).

Also in large pulses, overlapping of the mixture for a considerable length of a traveling distance in a column may introduce interaction effect of both components. This effect may be quantitatively checked by using numerical methods based on a bi-component adsorption isotherm.

Even when separation of the two components is not completed,

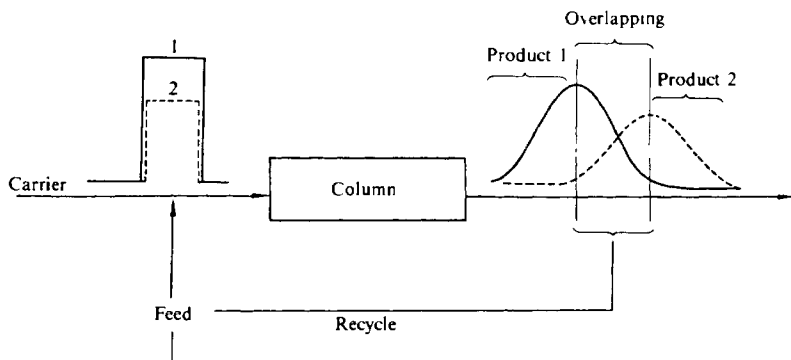


Fig. 10.5. Production chromatography with recycle of overlapping part.

production of each pure component is possible by recycling the overlapping part to the feed of the column (Fig. 10.5). This type of operation is done as a preparative separation method.

As is obvious from the discussions so far, minimization of peak broadening is one of the key factors in the design and operation of chromatographic separation. Employment of small and homogeneous size particles is advantageous in reducing peak broadening due to intraparticle diffusion, and uniform packing of particles in the column is also needed for reducing the effect of longitudinal dispersion of flowing liquid. Seko *et al.* (1982) conducted equipment trials for this purpose.

10.4. Elution with Concentration Gradient Carrier

When some of the species in the mixture introduced to a separation column are strongly adsorbed on the adsorbent, chemical elution becomes necessary. Desorption by chemical eluant follows a situation similar to that described in Chapter 9, except that the concentration of chemical eluant and hence the adsorption isotherm of adsorbates in the carrier change gradually in the course of chromatography.

Concentration gradient in the carrier is achieved by flow-programmed mixing of two different carrier streams or more simply by using a mixing tank of the finite volume of the order of the volume of the column as shown in Fig. 10.6. In the latter case, concentration change in the entering carrier is expressed in the following form.

$$C_d(t) = C_{d,1} + (C_{d,2} - C_{d,1})\exp[-t/(V/F)] \quad (10-21)$$

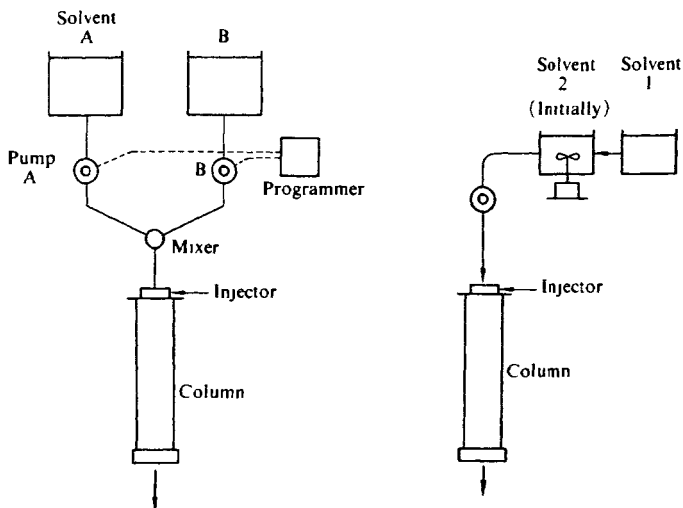


Fig 10.6. Principles of concentration gradient apparatus.

where $C_{d,1}$ and $C_{d,2}$ respectively represent the initial carrier concentration in the tank and that in the carrier entering the tank. F and V correspond to the flow rate of the carrier and the volume of the tank.

As shown in Figs. 9.3 and 9.5, adsorption isotherm can be given as a function of concentration of eluant in the carrier stream. In the case of chromatographic separation, for the sake of simplicity, an adsorption isotherm relation often is written as a Henry type equation.

$$q = KC \quad (10-22)$$

The adsorption equilibrium constant K is then considered to be a function of eluant concentration, C_d . For the case where K is changing, mass balance in the column is given as

$$u_0 dC/dz + K_f a_v (C - C^*) = 0 \quad (10-23)$$

$$K_f a_v (C - C^*) = \rho_p (1 - \varepsilon) dq/dt \quad (10-24)$$

$$u_0 dC_d/dz + (K_f a_v)_d (C_d - C_d^*) = 0 \quad (10-25)$$

$$(K_f a_v)_d (C_d - C_d^*) = (1 - \varepsilon) \rho_p dC_d^*/dt \quad (10-26)$$

$$C^* = q/K(C_d^*) \quad (10-27)$$

with

$$C_d = C_d(t), \quad C = M\delta(t) \quad \text{at } z = 0 \quad (10-28)$$

where C^* and C_d^* correspond to the equilibrium concentration of the adsorbate and the concentration of the eluant in the particle phase. The above set of equations should be solved simultaneously to obtain the concentration peak curve in the effluent stream. Parameters involved in the above model, however, are not yet completely clarified. For instance, the unclear dependence of K_{fd} on the eluant concentration, C_d , may influence the retention of the peak.

In the simplest case where equilibrium between the fluid phase and the particle phase can be assumed and C_d is assumed to be uniform throughout the column, the above set of equations reduces to the simple form as

$$u_o dC/dz = \rho_p(1 - \epsilon)K(C_d(t))dC/dt \quad (10-29)$$

Then residence time, t_R , in the column of the length, Z , can be given as

$$Z = \frac{u_o}{\rho_p(1 - \epsilon)} \int_0^{t_R} \frac{dt}{K(C_d(t))} \quad (10-30)$$

Hence, if the change of the eluant concentration in the entrance of the column and the dependence of the equilibrium constant on the eluant concentration is known, the first order approximation of the residence time of the peak can be estimated from the above relation. Mass transfer resistance between the fluid phase and the particle phase may give additional delay of elution of the peak.

Obviously change of adsorption equilibrium constant can be achieved by increase of temperature or in some cases of gas phase adsorption by increase of pressure. In any case, the same treatment is possible for estimating the residence time of the peak.

10.5. Chromatography for Large-scale Separation

10.5.1. Cyclic chromatographic operation

Chromatographic separation of mixtures has the advantage of good

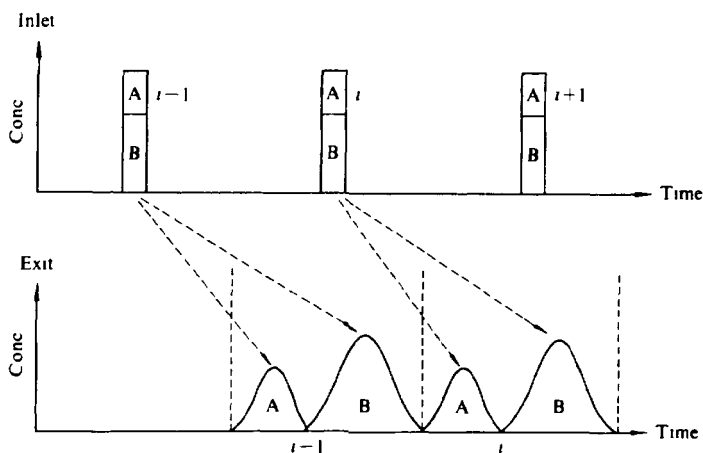


Fig 10.7 Sequential periodic chromatography

separation efficiency provided that suitable adsorbent and adsorption conditions are selected. For applying the chromatographic principle to large-scale separations, the cyclic operation shown in Fig. 10.7 is widely used as a direct extension of chromatographic operation. For designing cyclic operations, the treatment introduced in the previous sections can be utilized.

In the case when separation of two components, A and B, is required, the length of a column necessary to obtain good resolution is determined by Eq. (10-17).

Also it should be noted that only the time period of $t_{wa} + t_{wb}$ is utilized for separation of components a and b. Then repetitive introduction of mixture impulses with the time interval of $(t_{wa} + t_{wb})$ can accomplish resolution of the peaks from the peaks deriving from the preceding or following pulses (Fig. 10.5).

10.5.2. Moving bed chromatography

When a mixture is introduced into a moving bed of adsorbents with countercurrent carrier flow, components are separated according to adsorbability. The ratio of the amount of adsorbable component, i , transported by moving solids and by flowing fluid is defined as

$$R_i = u_s \rho_b k_{d,i} / u_f \quad (10-31)$$

where u_s and u_f are velocity of solid and superficial fluid velocity, ρ_b represents the bed density and $K_{a,i}$ is the adsorption equilibrium constant of component i .

In the case of $R_i > 1$ then component i moves in the direction of the solid flow and in the case of $R_i < 1$ it is transported in the direction of the fluid flow.

By choosing the proper velocity ratio of u_s/u_f , it is possible to satisfy the condition of $R_A > 1$ and $R_B < 1$ for component A (strongly adsorbable) and component B (weakly adsorbable). Then by the moving bed process shown in Fig. 10.8, it is possible to achieve separation of components A and B contained in the feed stream. In sections I, II, III and IV, R_A and R_B should satisfy the conditions shown in TABLE 10.1.

Here feed stream is introduced between sections II and III, while desorbent fluid is introduced from the bottom of the bed and components A and B are extracted from the point between III and IV

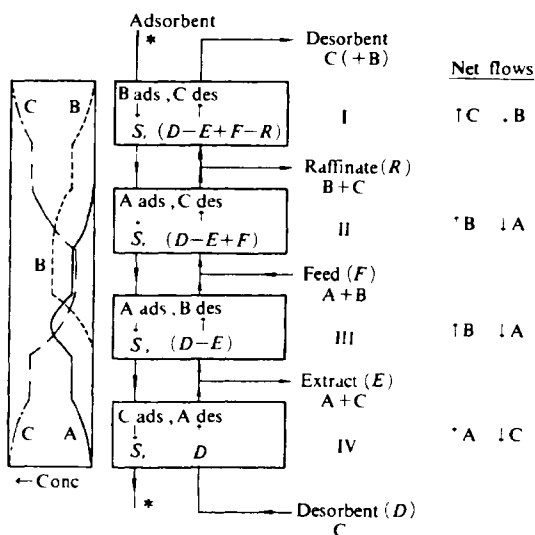


Fig. 10.8 Schematic diagram of a moving bed adsorber, S , D , E , F , R denote flow rates

TABLE 10.1 Ratio of the Amounts of Components A and B Transported by Solid and Fluid Needed to Achieve Good Separation

Section	I	II	III	IV
R_A	>1	>1	>1	<1
R_B	>1	<1	<1	<1

and the point between I and II.

10.5.3. Simulated moving bed chromatography

Since a moving bed conveys solid particles, erosion or partial crushing of the particles is inevitable. Simulated moving bed technology was developed so that a function similar to moving beds can be accomplished by using a multi-fixed bed (Fig. 10.9). By simultaneously rotating the fluid paths of the feed, the desorbent, extract product and raffinate by the manipulation of valves, moving bed separation can be simulated.

This process was developed and commercialized by UOP and called the "Sorbex process," a general name applied to the separation of *p*-xylene from C8 reformates (Parex) (Broughton *et al.*, 1970; deRosset *et al.*, 1978, Broughton, 1984), normal paraffins from isoparaffins and aromatic hydrocarbons (Molex), linear olefins from paraffins (Olex) and fructose from dextrose and polysaccharides (Sarex) and so on.

Hirota *et al.* (1981) of Mitsubishi Kasei Co. (MKC) developed a similar simulated moving bed system by employing eight sets of columns and pumps as shown in Fig. 10.10. This process does not require a sophisticated rotary valve such as the one adopted in the Sorbex process. An example of concentration profile for fructose-dextrose separation is shown in Fig. 10.11 (Shioda, 1987).

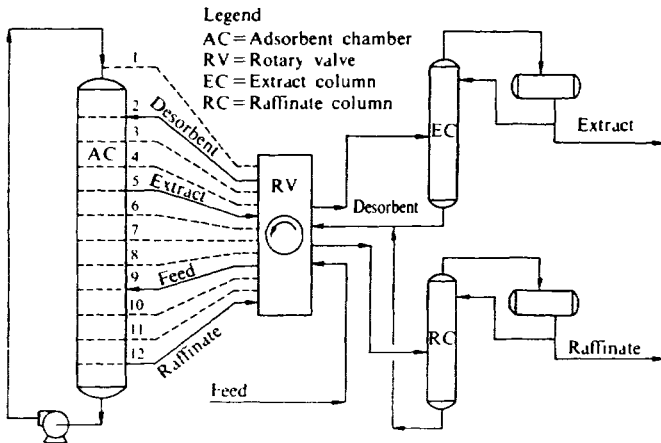


Fig. 10.9 Schematic diagram of the UOP Sorbex process
(Reproduced with permission by Broughton, B., *Separation Sci. Tech.*, 19, 733 (1984-85))

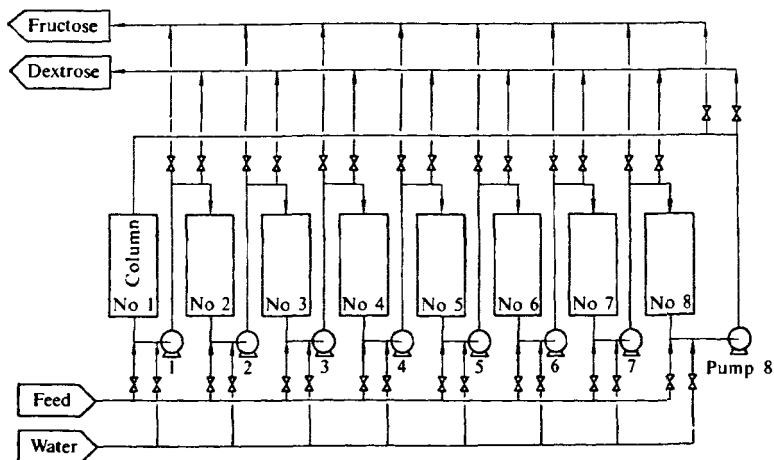


Fig 10 10 Simulated moving bed continuous system developed by MKC
(Reproduced with permission by Shioda, K , *First Japan-Korea Separation Technology Conf* , p 498 (1987))

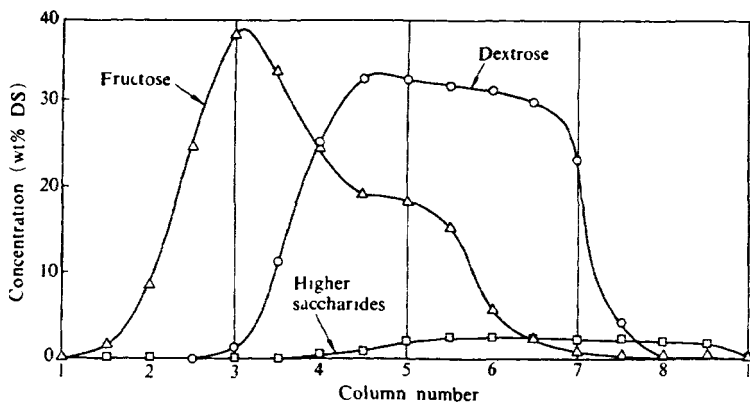


Fig 10 11 Example of a concentration profile in a simulated moving bed for fructose-dextrose separation
(Reproduced with permission by Shioda, K , *First Japan-Korea Separation Technology Conf* , p 498 (1987))

Analysis for the simulated moving bed performance was tried by Hashimoto *et al* (1983).

REFERENCES

- Broughton, D B, *Separation Sci & Tech*, **19**, 723 (1984)
- Broughton, D B, R W Neuzil, J M Pharis and C S Brearley, *Chem Eng Prog*, **66**, 70 (1970)
- deRosset, A J, R W Neuzil and D J Korous, *Ind Eng Chem Process Design & Devel*, **15**, 261 (1976)
- Hashimoto, K, S Adachi, H Noujima and H Maruyama, *J Chem Eng Japan*, **16**, 400 (1983)
- Hirota, T, H Ishikawa, M Ando and K Shioda, *Kagaku Kogaku*, **45**, 391 (1981) (in Japanese)
- Nakanishi, K *et al*, *Agric Biol Chem*, **43**, 2507 (1979)
- Seko, M, H Takeuchi and T Inada, *Ind Eng Chem Prod Res Dev*, **21**, 656 (1982)
- Shioda, K, *First Korea-Japan. Sympo on Separation Technology*, p 495 (1987)
- van Deemter, J J, F J Zuiderweg and A Klinkenberg, *Chem Eng Sci*, **5**, 271 (1956)

Pressure Swing Adsorption

In order to achieve bulk gas separation by adsorption, the adsorbent must be used repeatedly. The desorption step takes a rather long time if thermal desorption is employed because of a relatively large time constant of heat transfer due to poor thermal conduction in the adsorbent packed bed.

This problem is waived by employing low pressure desorption where the time constant of desorption is of the same order of magnitude as that of adsorption or even smaller because when pore diffusion in the adsorbent particle is a rate-determining step, effective diffusivity in the particle is inversely proportional to the operating pressure. Thus bulk separation of a mixed gas can be achieved by repeating adsorption at higher pressure and desorption at lower pressure. In principle, the less adsorbable component is the product in the adsorption step while the more adsorbable component remains in the column and is recovered through desorption. This type of operation is called pressure swing adsorption (PSA). Usually adsorbability is determined by comparing the adsorption equilibrium of each component on the adsorbent employed, but since pressure swing adsorption is a transient operation, the adsorption rate may play an important role in separation efficiency of PSA operation. As a matter of fact, adsorption rate plays a key role in the case of separation of two gases whose adsorption equilibria are about the same but whose rates are considerably different. An example of PSA of this special type is illustrated below.

In this chapter, the general background of PSA necessary for theoretical analysis is given first followed by methods for making theoretical predictions of PSA performances. Equilibrium theory, numerical simulations based on nonequilibrium models and a simplified method for obtaining a cyclic steady state profile are reviewed. The overall mass transfer parameter in cyclic operations such as PSA may be considerably different from the one usually employed in the calculation of breakthrough curves. A method for relating the overall mass transfer coefficient to intraparticle diffusivity and operating conditions is shown.

The chapter concludes with a brief discussion of PSA separation based on the difference of adsorption rates.

11.1. General Scheme of PSA Operation

The main applications of PSA are to be found in the production of oxygen from air, dehumidification of gases and purification of hydrogen. Other applications include removal of carbon dioxide, recovery of radioactive waste gas, enrichment recovery of rare gases, purification of helium, purification of natural gases, separation of isomers and separation of carbon monoxide. Separation of iso-paraffins from normal paraffins is accomplished by using a shape-selective adsorbent such as a molecular sieve. Separation of carbon monoxide involves chemical adsorption on complex adsorbents.

A typical operation mode of PSA cycle is shown in Fig. 11.1, consisting of four distinct steps. In the first step (Step 1) high pressure feed gas is introduced into Bed 2 where adsorption of adsorbable gases takes place and less adsorbable product gas is taken out as a product. During this period a small portion of product gas is drawn out to another bed, Bed 1, at low pressure to purge the accumulated adsorbate in Bed 1. Next (Step 2), Bed 1 is repressurized either by feed gas or product gas to the feed pressure (repressurization), while the pressure in Bed 2 is reduced to purge pressure (blowdown). In Steps 3 and 4, Step 1 and Step 2 are repeated with Bed 1 and Bed 2 changing roles.

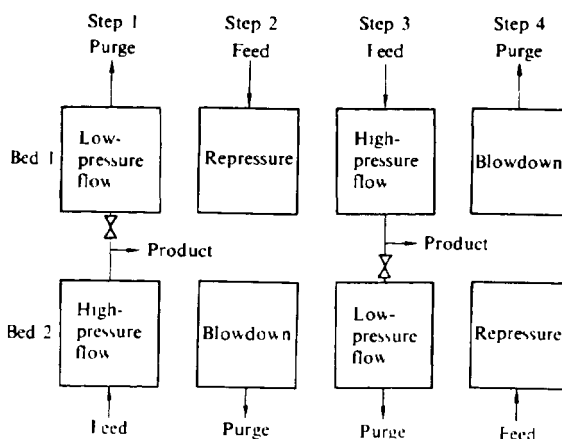


Fig. 11.1 Principal steps in a pressure swing adsorption

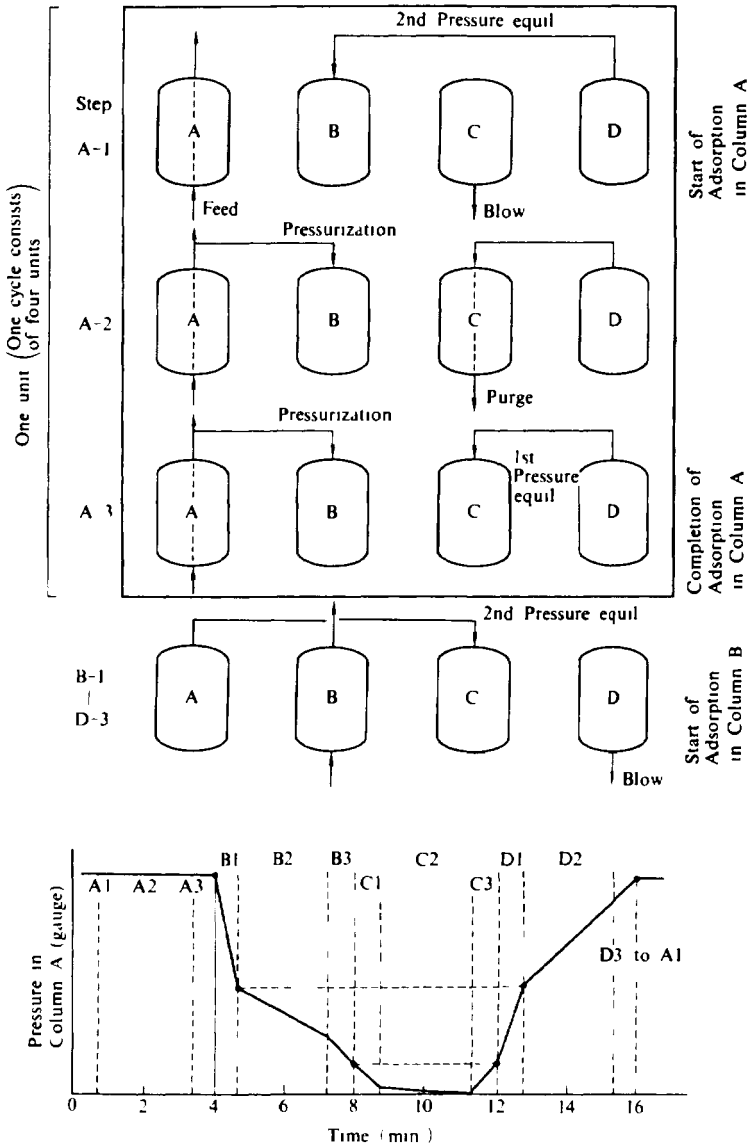


Fig 11 2 a Typical example of basic steps in four-column PSA

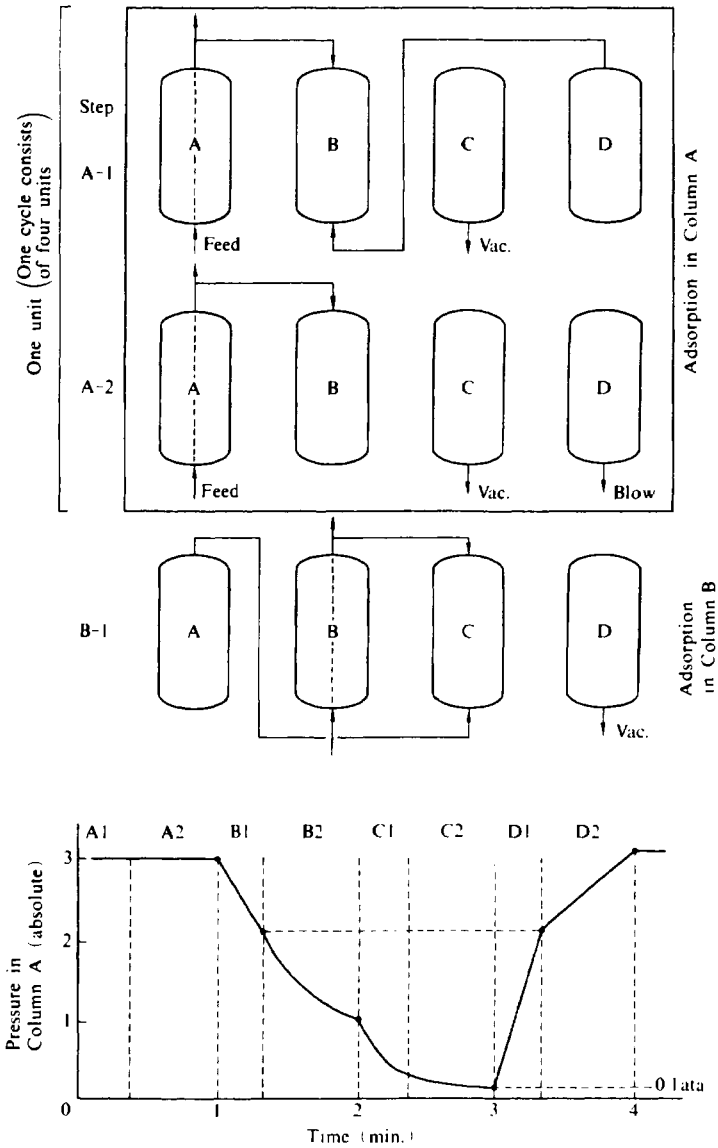


Fig. 11.2.b. Typical example of a four-bed PSA sequence (vacuum desorption for oxygen production).

Usually Steps 2 and 4 are completed in a far shorter time than Steps 1 and 3 and the adsorbed amount profiles are often assumed to remain unchanged. This is called the assumption of "Frozen Profile."

During Steps 1 and 3, a portion of the product stream is used as purge stream. Adsorption at higher pressure and desorption at lower pressure makes it possible to complete desorption with a smaller amount of purge gas compared to the amount of feed gas introduced. Skarstrom (1972) empirically showed that desorption can be accomplished employing purge gas whose volume at purge pressure is larger than the volume of the feed gas at adsorption pressure.

In actual PSA operations, more sophisticated modes are adopted mainly to increase product yield. Two examples of a four-bed PSA operation mode are shown in Fig. 11.2, where two steps of pressure equalization and repressurization with product gas (a) and vacuum desorption and pressure equalization steps are employed (b). For larger operations, multibed PSA (Fig. 11.3) with several steps of pressure equalization can give higher yield.

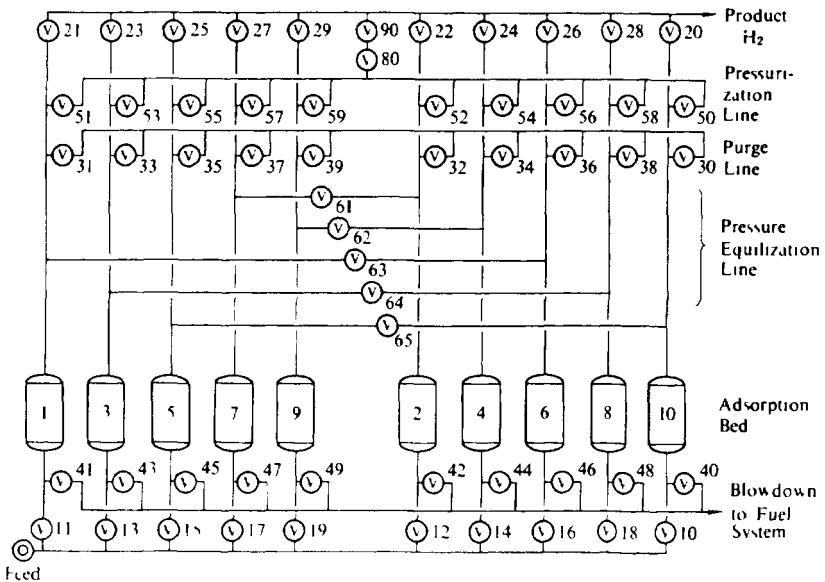


Fig. 11.3 Flow sheet of 10-bed PSA V valve (H production system by UCC)

11.2. Equilibrium Theory for PSA Criteria

As a first approach to describe the behavior of the PSA column, an equilibrium theory was developed based on negligible mass transfer resistance between gas phase and solid phase. Shendalman and Mitchell (1972) applied the theory developed for parametric pumping to prediction of movement of adsorption front in PSA operation.

When adsorption equilibrium is assumed in the column, a basic equation for mass balance of a single adsorbable component is given for an isothermal system as

$$\varepsilon\{\partial C/\partial t + \partial(\nu C)/\partial z\} + (1 - \varepsilon)\partial n/\partial t = 0 \quad (11-1)$$

Also as a total mass balance

$$dP/dt + d(\nu P) = 0 \quad (11-2)$$

By introducing equilibrium relation $n = KC$ and gas phase molar fraction $C = Py$, Eq. (11-1) is written as

$$P\{\varepsilon + (1 - \varepsilon)K\}\frac{\partial y}{\partial t} + \varepsilon P\nu\frac{\partial y}{\partial z} + (1 - \varepsilon)Ky\frac{\partial P}{\partial t} = 0 \quad (11-3)$$

A solution to the above equation is obtained using the set of ordinary differential equations given below.

$$\frac{dt}{[P\{\varepsilon + (1 - \varepsilon)K\}]} = \frac{dz}{\varepsilon P\nu} = \frac{dy}{[(1 - \varepsilon)Ky(\partial P/\partial t)]} \quad (11-4)$$

Movement of fluid element in the column during adsorption and desorption steps is obtained employing the appropriate equations with Eq. (11-4).

Adsorption step:

$$dz/dt = \beta \nu_H \quad (11-5)$$

Desorption step:

$$dz/dt = \beta \nu_l = \beta \gamma \nu_H \quad (11-6)$$

where

$$\beta = \varepsilon / [\varepsilon + (1 - \varepsilon)K] \quad (11-7)$$

and γ is the purge ratio defined as v_L/v_H .

Eqs. (11-5) and (11-6) give the velocities of adsorption front during high pressure adsorption and low pressure desorption. v_H and v_L denote linear gas velocities at high pressure and low pressure flow.

During the blowdown and repressurization steps, if the pressure drop in the column is neglected, $dP/dz = 0$ yields

$$\partial v / \partial z = -(1/P) \partial P / \partial t \quad (11-8)$$

Since $v = 0$ holds at $z = 0$,

$$v = -(1/P)(dP/dt)z \quad (11-9)$$

By combining Eq. (11-9) with Eq. (11-4) and by integrating, the location of adsorption front before and after pressure change is determined. The relation between locations of adsorption front at pressure P_H , z_H and that at pressure P_L , z_L is given as

$$z_H = z_L (P_L/P_H)^\beta \quad (11-10)$$

Penetration distance (location of adsorption front) is obtained using Eqs. (11-5, 11-6 and 11-10).

During repressurization and high pressure adsorption period, the net penetration distance, ΔL_H , is

$$\Delta L_H = L_1 (P_L/P_H)^\beta - \beta v_H t_c \quad (11-11)$$

Also, the net movement of penetration distance during blowdown and desorption at low pressure, ΔL_L , is

$$\Delta L_L = \beta \gamma v_H t_c - L_H (P_H/P_L)^\beta \quad (11-12)$$

The range of operating conditions can be determined from these parameters, i.e. in order to keep product concentration high enough, $\Delta L_H > 0$ should hold and L_H must be smaller than the column length Z . Also, if $L_1 > Z$ then breakthrough of purge stream is expected to occur and this range will not be suitable. Then the operating conditions should fall within the hatched area shown in Fig. 11.4.

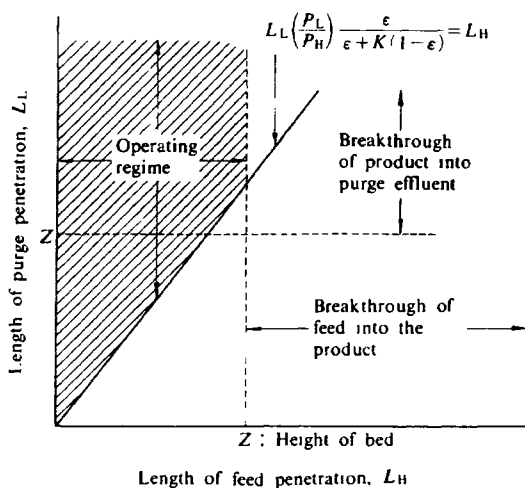
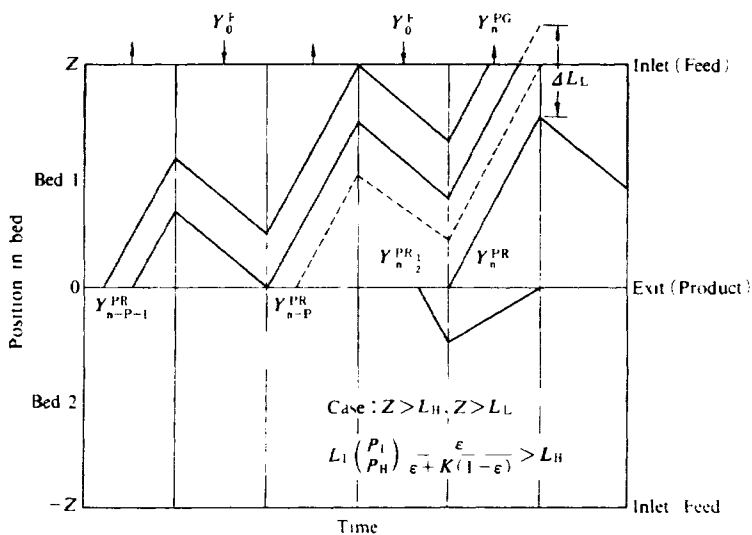
Fig. 11.4. Operating regime in L_L - L_H domain.

Fig. 11.5. Movement of characteristic points at purge-feed ratio above the critical value

Critical purge ratio, γ_{crit} , is given from the critical condition of $\Delta L = 0$ as

$$\gamma_{crit} = (v_L / v_H)_{crit} = (P_H / P_L)^\beta \quad (11-13)$$

Fig. 11.5 shows an example of movement of characteristics for a case where $\gamma > \gamma_{crit}$.

As shown briefly here, equilibrium theory can give a range of operating conditions for providing a pure product. This treatment has been further extended to apply to two adsorbable component systems (Chan, Hill and Wong, 1982 and Knaebel and Hill, 1982). Also Kawazoe and Kawai (1973) used equilibrium assumption to estimate a concentration profile during the blowdown step.

This treatment, however, cannot give product concentration since the model employs over-simplified assumptions such as infinite adsorption rate. More detailed nonequilibrium models must be employed in order to obtain relations between product concentration or yield and operating conditions.

11.3. Numerical Solution of Nonequilibrium PSA Model

Changing concentration profiles in the course of cyclic pressure swing operation can be estimated by repeated calculation of a model based on finite mass transfer rate. Several attempts have been made (Mitchell and Shendalman, 1973; Carter and Wyszynski, 1983; Chihara and Suzuki, 1983a; Raghavan, Hassan and Ruthven, 1985; Yang, and Doong, 1985).

The simplest example of numerical calculation is adopted from the treatment given by Chihara and Suzuki (1983a).

11.3.1. Isothermal cases

As a first approach, the linear driving force (LDF) model is adopted with negligible temperature effect. Mass conservation of adsorbate is given in dimensionless form as

$$\partial \bar{C} / \partial \bar{t} + \tau_a \partial \bar{C} / \partial \bar{z} + \tau_b \partial \bar{q} / \partial \bar{t} = 0 \quad (11-14)$$

$$\partial \bar{q} / \partial \bar{t} = \tau_i (\bar{q}^* - \bar{q}) \quad (11-15)$$

$$\bar{q}^* = K \bar{C} \quad (11-16)$$

with the boundary conditions for high pressure flow

$$\bar{C} = \bar{q} = 1 \quad \text{at } z = 0 \quad (11-17)$$

and for low pressure flow

$$\bar{C}(1, \bar{t}) = (P_L/P_H) \bar{C}(1, \bar{t} - \bar{t}_c) \quad \text{at } z = 1 \quad (11-18)$$

where the nondimensional parameters are

$$\tau_a = t_0/(L/v) = \frac{\text{(time for bed saturation)}}{\text{(retention time of carrier gas)}} \quad (11-19)$$

$$\begin{aligned} \tau_b &= \rho_b q_0 / \varepsilon C_0 \\ &= \frac{\text{(amount adsorbed in equilibrium with } C_0)}{\text{(adsorbate concentration in gas phase at inlet concentration } C_0)} \end{aligned} \quad (11-20)$$

$$\begin{aligned} \tau_t &= t_0/(\rho_b/K, a_s) \\ &= \frac{\text{(time for bed saturation)}}{\text{(time constant for adsorption to the adsorbent)}} \end{aligned} \quad (11-21)$$

with characteristic time, that is, saturation time, as

$$t_0 = L r_b q_0 / \varepsilon v_H C_0 \quad (11-22)$$

\bar{C} and \bar{q} denote C/C_0 and q/q_0 where C_0 is concentration in feed gas and q_0 is the amount adsorbed in equilibrium with C_0 . $\bar{Z} = Z/L$ and $\bar{t} = t/t_0$ also hold $\bar{t}_c = t_c/t_0$ where t_c is the half cycle time. For repressurization and blowdown steps (Steps 2 and 4 in Fig. 11.1), frozen profile assumption is used.

An example of calculation results for the case of dehumidification of air by silica gel is shown in Fig. 11.6. The conditions adopted for the calculation are given in TABLE 11.1. Calculation was started from an evacuated bed and it was found that the cyclic steady state was reached after about 40 cycles.

11.3.2. Nonisothermal cases

Temperature change due to heat generation or absorption which

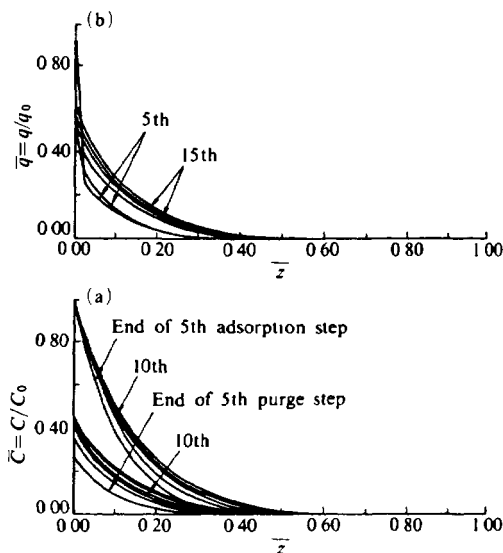


Fig. 11.6 Change of profiles of \bar{C} and \bar{q} from startup to the cyclic steady state in the case of isothermal operation (Reproduced with permission by Chihara, K. and Suzuki, M., *J. Chem. Eng. Japan*, **16**, 58 (1983))

TABLE 11.1 Physical Parameters for Computation

Adsorbent bed		Feed gas	
L	= 1 m	v_H	= 0.25 m/s
R_H	= 0.1 m	P_H	= 5.07×10^5 Pa
r	= 0.4	C_0	= 0.79 mol/m ³
ρ_b	= 0.72×10^3 kg/m ³	T_0	= 303 K
ρ_s	= 1.2×10^3 kg/m ³	t_1	= 0.01 t_0 (9 min)
C_{ps}	= 1.26×10^3 J/kg·K	Purge gas	
ρ_g	= 1.2 kg/m ³ (at atmospheric pressure)	v_L	= 0.5 m/s
C_{pr}	= 1.00×10^3 J/kg·K	P_L	= 1.01×10^5 Pa
K	= 7.57 m ³ kg (at 303 K)*	x	= $\frac{v_L}{v_H} = 2.0$
Q	= 5.19×10^4 J/mol*	t_2	= 0.01 t_0
$K_{a,1}$	= 0.2 kg m ⁻¹ s (at P_H)*, 1.0 kg/m ³ s (at P_1)*		
k_{cr}	= 0.293 J m ⁻¹ s·K**		
h_0	= 40.0 J m ⁻¹ s·K***		

* $\lambda_{s,1} = \frac{15D(1-t)}{K R_p}$ (Kawazoe *et al.* 1978)

** Yagi *et al.* (1961) for nonisothermal and adiabatic cases

*** Yagi and Kuniti (1961), for nonisothermal case

follow adsorption or desorption must be taken into account in order to describe the behavior of a PSA column especially when a large column is employed. Rapid repetition of adsorption and desorption may not provide enough time for heat exchange through the column wall.

Temperature effect can be checked by adding a heat balance equation and a relation describing temperature dependency of adsorption equilibrium coefficient to the above set of equations. Temperature dependency of adsorption equilibrium constant in Eq. (11-16) is given as

$$K = \exp[-(Q/RT_0) \bar{T}/(\bar{T} + 1)] \quad (11-23)$$

where \bar{T} denotes $(T - T_0)/T_0$ where T_0 is the temperature of feed gas. Heat balance in the bed is described by means of an overall heat transfer model for the exchange of heat between bed and the column wall and axial conduction of heat for the dispersion of heat inside the bed (Chapter 8).

$$\partial \bar{T} / \partial \bar{t} + \tau_H \partial \bar{T} / \partial \bar{z} - \tau_L \partial^2 \bar{T} / \partial \bar{z}^2 + \tau_w \bar{T} - b \partial \bar{q} / \partial \bar{t} = 0 \quad (11-24)$$

As additional boundary conditions

$$\bar{T} = 0 \quad \text{at} \quad \bar{z} = 0, \quad \text{and} \quad \bar{T}(1, t) = 1 \quad \text{at} \quad \bar{z} = 1 \quad (11-25)$$

are employed. In the above equations

$$\begin{aligned} \tau_H &= (\varepsilon_v \rho_g C_{pg} t_0) / L(\varepsilon \rho_g C_{pg} + \rho_b C_{ps}) \\ &= \frac{\text{(heat capacity of total gas introduced in } t_0\text{)}}{\text{(heat capacity of the bed)}} \end{aligned} \quad (11-26)$$

$$\begin{aligned} \tau_L &= t_0 / \{(\varepsilon \rho_g C_{pg} + \rho_b C_{ps}) L^2 / k_{er}\} \\ &= \frac{\text{(time for bed saturation)}}{\text{(time constant for effective longitudinal thermal conduction)}} \end{aligned} \quad (11-27)$$

$$\begin{aligned} \tau_w &= t_0 / \{(\varepsilon \rho_g C_{pg} + \rho_b C_{ps}) R_w / 2h_w\} \\ &= \frac{\text{(time for bed saturation)}}{\text{(time constant for heat transfer through wall)}} \end{aligned} \quad (11-28)$$

$$\begin{aligned} b &= \rho_b Q q^*_{0'} / \{(\varepsilon \rho_g C_{pg} + \rho_b C_{ps}) T_0\} \\ &= \frac{\text{(total heat generated by saturation per unit bed volume)}}{\text{(heat sustained per unit bed volume at } T_0\text{)}} \end{aligned} \quad (11-29)$$

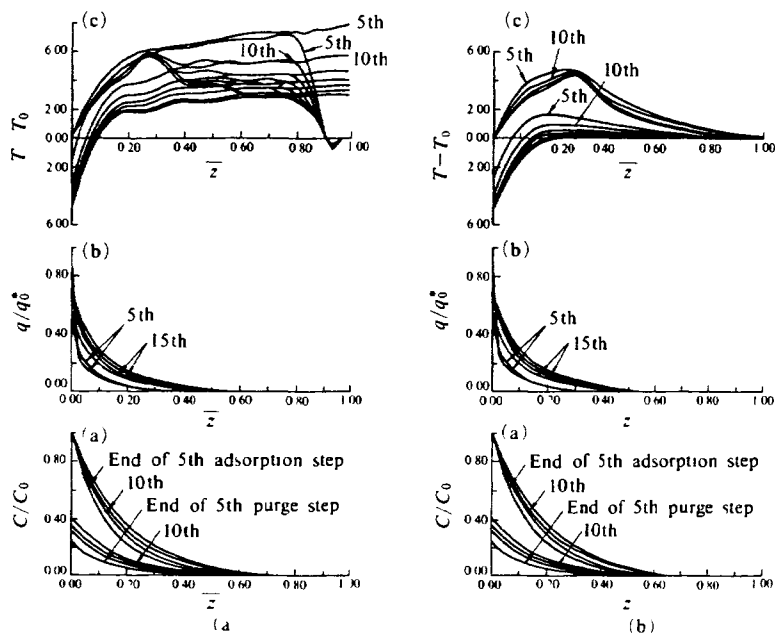


Fig. 11.7 Change of profiles of \bar{C} , q and $T-T_0$ in (a) adiabatic adsorption ($\tau_w = 0$) and (b) nonisothermal adsorption ($\tau_w = 48.5$) (Reproduced with permission by Chihara, K. and Suzuki, M. *J. Chem. Eng. Japan*, **16**, 58 (1983))

TABLE 11.2 Outlet Concentration at End of 40th Adsorption Step

	C_{out}/C_0	Dew point ($^{\circ}\text{C}$)
(Isothermal)	0.750×10^{-1}	-60
(Adiabatic)	0.338×10^{-1}	-48
(Nonisothermal)	0.134×10^{-1}	-55

(Reproduced with permission by Chihara, K. and Suzuki, M. *J. Chem. Eng. Japan* **16**, 56 (1983))

Parameter τ_w is the measure of heat transfer through column wall and $\tau_w = 0$ corresponds to the adiabatic condition while $\tau_w = \infty$ indicates an extreme case of isothermal operation. From the case shown in TABLE 11.1, a general case of nonisothermal operation and a special case of adiabatic operation were simulated using the same operating conditions given for the isothermal case (Fig. 11.6). The results are shown in Fig. 11.7 where pronounced temperature profiles are illustrated in the adiabatic case.

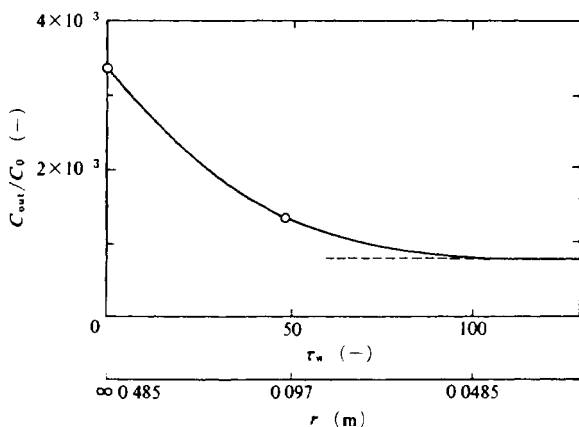


Fig 11 8 Example of dependency of final outlet concentration in adsorption step on heat transfer parameter through the wall
(Reproduced with permission by Chihara, K and Suzuki, M, *J Chem Eng Japan*, 16, 59 (1983))

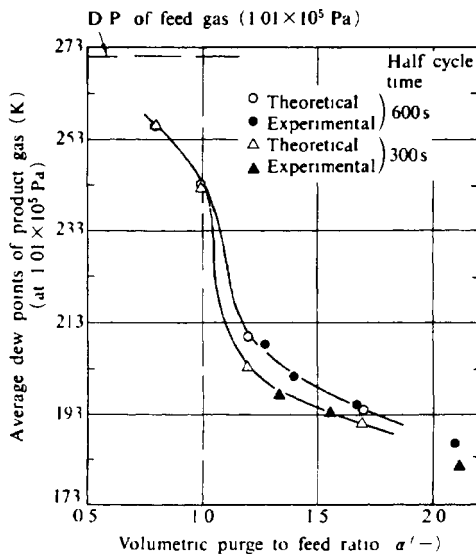


Fig 11 9 Comparison of calculated and experimental dependence of dew points of product gas on volumetric purge to feed ratio
(Reproduced with permission by Chihara, K and Suzuki, M, *J Chem Eng Japan*, 16, 297 (1983))

The resultant dew points of the product gases are compared in TABLE 11.2. Effects of heat transfer parameter τ_w is thus clearly shown by plotting product purity versus τ_w in Fig. 11.8. τ_w larger than 100 in this case may allow the assumption of isothermal operation.

Effects of purge ratio, bed length and length of cycle time (throughput ratio) were determined employing this model (Chihara and Suzuki, 1983a). Experimental observations were also made for air drying with a shorter bed of silica gel and compared with the theoretical calculation of the same model (Chihara and Suzuki, 1983b). A reasonable agreement of product dew points between experiment and theory was obtained as shown in Fig. 11.9. For shorter beds it was demonstrated that larger τ_w is necessary to justify isothermal treatment.

11.4. Simplified Solution of Dynamic Steady State Profile from Continuous Countercurrent Flow Model

The treatment given in the previous section is inevitable for

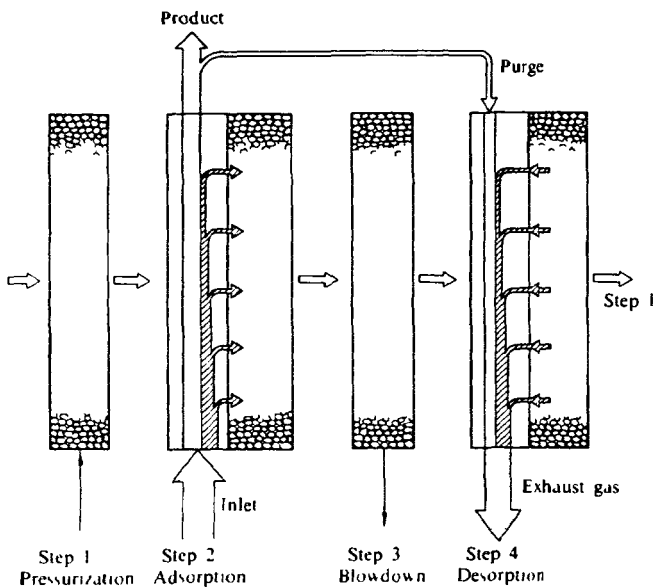


Fig 11 10 Conceptual scheme of pressure swing operation
(Reproduced with permission by Suzuki, M, *AICHE Sympo Series*, 81, 68 (1985))

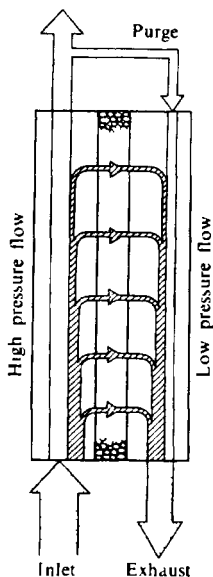


Fig 11 11 Conceptual scheme of steady concurrent flow contactor
(Reproduced with permission by Suzuki, M, *AIChE Sympo Series*, **81**, 69
(1985))

complicated estimations, such as estimation of startup PSA behavior or nonisothermal effect. But in many cases, separation efficiency of PSA or selection of design and operation parameters for desirable separation can be determined from functions in the cyclic steady state. It is advantageous if a quick estimate can be made for the cyclic steady state performance of PSA directly from the set of basic equations.

A simple method for evaluating cyclic steady state profiles of the amounts adsorbed was proposed by assuming equivalence of the pressure swing operation with the countercurrent flow contacting system (Suzuki, 1985). This idea is illustrated in Figs 11 10 and 11 11.

In the ordinary four-step PSA, each bed undergoes four steps as shown in Fig 11 1. For the sake of simplicity, it is often assumed that during both the pressurization and blow-down steps the longitudinal profiles of the amount adsorbed in the column remains unchanged (frozen) since both steps are very rapid.

Also, when the cycle time of PSA is far smaller than the time constant of saturation of the bed, i.e. throughput ratio is far smaller than unity, profiles of the amount adsorbed in the bed during adsorption and desorption steps remain almost unchanged, though concentrations in the

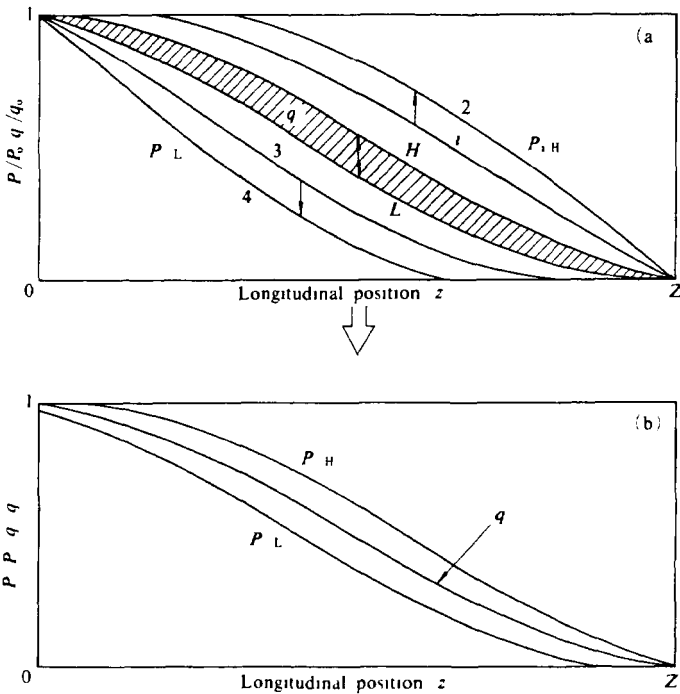


Fig 11.12 Longitudinal profiles of concentration in gas phase and amount adsorbed in the column during cyclic steady state of PSA operation in normal mode (a) and with extremely small throughput ratio (b) (Reproduced with permission by Suzuki M, *AIChE Sympo Series* 81, 68 (1985))

fluid phase in both steps are considerably different from each other. Namely, throughput ratio corresponds to the ratio of the hatched area to the total rectangular area in Fig 11.2 a. If the cycle time becomes smaller, the hatched area diminishes and the standing profile of the amount adsorbed, q_s , will be established as shown in Fig 11.2 b.

This profile of q_s is established from the balance of mass transfer during adsorption step and that during desorption step.

At any longitudinal position, the amount of mass transfer (the adsorbed amount) during the adsorption step is equal to the amount desorbed from solid phase during the desorption step. Then the assumption of a frozen profile suggests that the profile may be estimated by analogy to a continuous countercurrent flow contactor, where the mass flow from a high pressure flow to the adsorbent particle and that

from the particle to the low pressure flow take place in series.

Figure 11.11 shows the basic idea of the countercurrent flow model corresponding to the PSA shown in Fig. 11.10.

The basic equations for the adsorption step (duration time t_H) and the desorption step (t_L) are given in the simplest form below. Adsorption Step ($t = 0$ to t_H):

$$P = P_H \quad (11-30)$$

$$u_{H0} \partial C_{i,H} / \partial z + N_{i,H} = 0 \quad (11-31)$$

$$N_{i,H} = \rho_b \partial q_i / \partial t = (K_F a_v)_{i,H} (p_{i,H} - p^*) / RT \quad (11-32)$$

$$B.C.: C_{i,H} = C_{i,0} \quad \text{at} \quad z = 0 \quad (11-33)$$

Desorption Step ($t = 0$ to t_L):

$$P = P_L \quad (11-34)$$

$$u_{L0} \partial C_{i,L} / \partial z + N_{i,L} = 0 \quad (11-35)$$

$$N_{i,L} = \rho_b \partial q_i / \partial t = (K_F a_v)_{i,L} (p_{i,L} - p^*) / RT \quad (11-36)$$

$$B.C.: C_{i,L} = C_{i,0} \quad \text{at} \quad z = 0 \quad (11-37)$$

Profile of $q_i(z)$ at the end of the other step must be employed as an initial condition for each step. In Eqs. (11-32) and (11-36) an LDF model with partial pressure difference as a driving force is used. u_{H0} and u_{L0} are molar flow rates of the inert component in the adsorption and desorption steps, where total pressures are P_H and P_L . $N_{i,H}$ and $N_{i,L}$ represent the rates of mass transfer of component i between particle and fluid at the adsorption step and at the desorption step expressed in terms of linear driving force (LDF) model by taking the partial pressure difference or difference in amount adsorbed as the driving force of mass transfer.

Concentration of component i for high pressure flow, $C_{i,H}$, and that for low pressure flow, $C_{i,L}$, are defined here in terms of molar ratio to the inert component. The molar flow rate of the inert component is taken as the standard, since the flow rate of the inert component remains unchanged even though adsorption or desorption takes place in the bed. Then partial pressure of component i for the high pressure flow, $p_{i,H}$, and that for the low pressure flow, $p_{i,L}$, are given as

$$p_{i,H} = C_{i,H}P_H / (1 + \sum C_{i,H}) \quad (11-38)$$

$$p_{i,L} = C_{i,L}P_L / (1 + \sum C_{i,L}) \quad (11-39)$$

From the equations given for ordinary PSA (Eqs. (11-30) to (11-37)), corresponding basic equations for the continuous countercurrent flow model are derived as follows:

$$u_H dC_{i,H} / dz + N_i = 0 \quad (11-40)$$

$$-u_L dC_{i,L} / dz + N_i = 0 \quad (11-41)$$

Equivalent flow rates of inert component in high pressure flow, u_H , and low pressure flow, u_L , are defined as

$$u_H = \delta u_{HO}, \quad u_L = (1 - \delta)u_{LO} \quad (11-42)$$

where δ denotes the fractional duration time of the adsorption step in the PSA cycle defined as

$$\delta = t_H / (t_H + t_L) \quad (11-43)$$

Equivalent mass transfer rate of component i between high pressure flow and low pressure flow in the model, N_i , can be written in terms of $N_{i,H}$ and $N_{i,L}$ defined for the ordinary PSA model (Eqs. (11-32) and (11-36)). When an LDF model with partial pressure difference as the driving force of mass transfer is employed, the equivalent mass transfer rate, N_i , is written as

$$\begin{aligned} N_{sci} &= \delta N_{i,H} = \delta (K_F a_v)_{i,H} (p_{i,H} - p^*_i) / RT \\ &= (1 - \delta) N_{i,L} = (1 - \delta) (K_F a_v)_{i,L} (p^*_i - p_{i,L}) / RT \end{aligned} \quad (11-44)$$

Then finally N_i is given by eliminating p^*_i , which is the equilibrium partial pressure with q_i , the amount adsorbed.

$$N_i = (K_F a_v)_o (p_{i,H} - p_{i,L}) \quad (11-45)$$

where $(K_F a_v)_o$ is the effective overall mass transfer coefficient between high pressure flow and low pressure flow and is given as

$$1 / (K_F a_v)_o = 1 / [\delta (K_F a_v)_{i,H}] + 1 / [(1 - \delta) (K_F a_v)_{i,L}] \quad (11-46)$$

Equilibrium concentration p^* , is obtained after $p_{i,H}$ and $p_{i,L}$ are obtained. p^* , is given as the weighted average of $p_{i,H}$ and $p_{i,L}$ then q_i is calculated from the adsorption equilibrium relation.

$$p^*_i = \frac{[\delta(K_{Fav})_{i,H}p_{i,H} + (1 - \delta)(K_{Fav})_{i,L}p_{i,L}]}{[\delta(K_{Fav})_{i,H} + (1 - \delta)(K_{Fav})_{i,L}]} \quad (11-47)$$

$$q_i = q_i(p^*_i, s) \quad (11-48)$$

For boundary conditions, the inlet concentrations of both flows should be given.

$$z = 0: C_{i,H} = C_{i,0} \quad (11-49)$$

$$z = Z: C_{i,L} = C_{i,P} = C_{i,H}|_{z=Z} \quad (11-50)$$

The last equation shows that part of the product gas is used as the purge stream. Outlet concentration of the purge stream, $C_{i,L}|_{z=0}$, is given from the overall mass balance as

$$C_{i,L}|_{z=0} = (C_{i,0} - C_{i,H}|_{z=Z})u_H/u_L + C_{i,H}|_{z=Z} \quad (11-51)$$

In general, when the inlet concentrations of the high pressure flow and the low pressure flow are given, concentration distributions are solved as a boundary value problem. Calculation of the concentration distribution requires iteration.

TABLE 11.3 Composition and Conditions Used as a Computation Example of Hydrogen Separation

Composition of raw gas		
nitrogen	26.5 mol%	$C_{1,H} = 0.38$
carbon monoxide	3.5	$C_{2,H} = 0.05$
hydrogen	70.0	
Conditions		
Pressure of adsorption step,		$P_H = 10 \text{ kg/cm}^2$
desorption step		$P_L = 1 \text{ kg/cm}^2$
Flow rate of inert gas at		
ads. step,		$u_H = 2.0 \text{ mol m}^{-2}\text{s}$
des. step,		$u_L = 0.22 \text{ mol m}^{-2}\text{s}$
Mass transfer coefficient at		
ads. step,		$(K_1 a_1)_{1,H} = (K_1 a_1)_{2,H} = 0.1 \text{ s}^{-1}$
des. step,		$(K_1 a_1)_{1,L} = (K_1 a_1)_{1,H} (P_H/P_L)$
Column length		$Z = 3 \text{ m}$

(Reproduced with permission by Suzuki, M., *AIChE Sympo Series* 81:70 (1985))

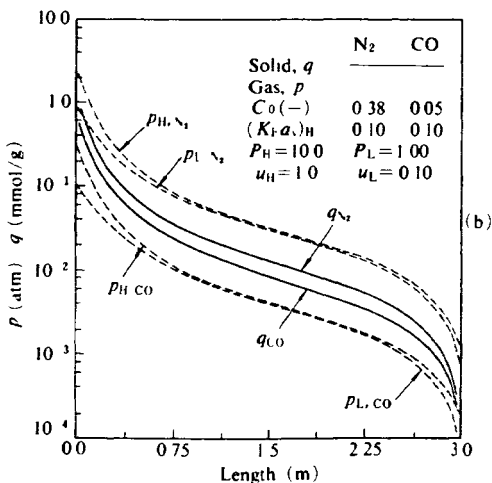
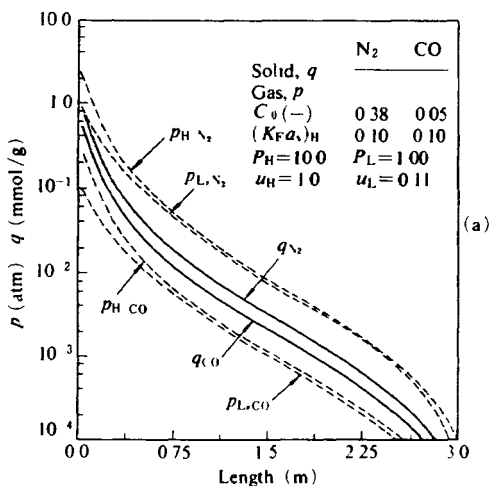


Fig. 11.13 Calculation results for the example of hydrogen separation from cracked gas. Composition is given in TABLE 11.3 (a) Purge ratio of inert gas (u_L/u_H) = 0.11 and (b) 0.1

(Reproduced with permission by Suzuki, M., *AIChE Sympo Series*, 81, 71 (1985))

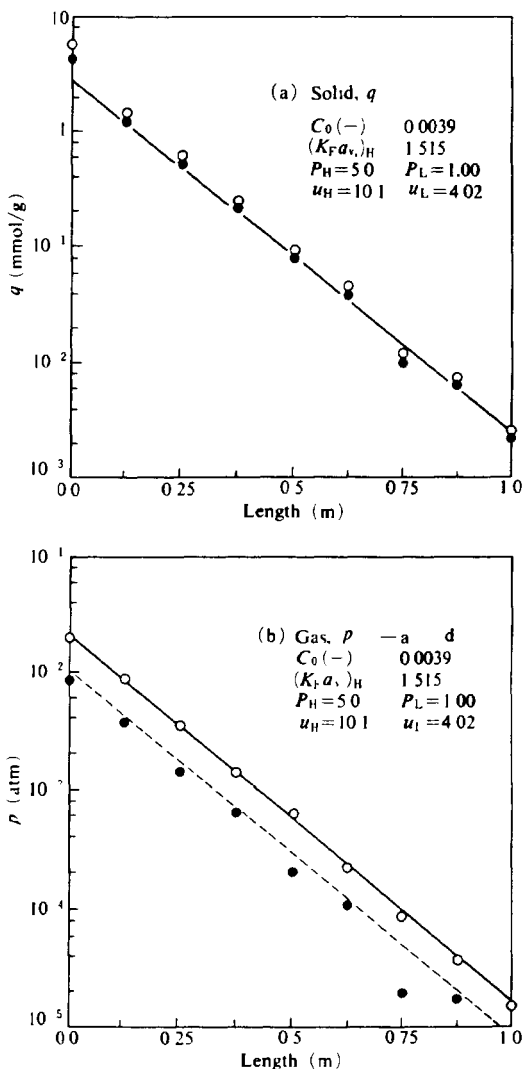


Fig. 11.14 Comparison of the calculated profiles of (a) amount adsorbed and (b) gas phase concentrations with the numerical calculation for air drying given by Chihara and Suzuki (1983a). Open circles and solid circles show their results of the amount adsorbed at the end of adsorption step and at the end of desorption step, respectively. Solid and broken lines show the results from the detailed model.

(Reproduced with permission by Suzuki, M., *AIChE Sympo Series*, **81**, 72 (1985))

Application of this model to the separation of hydrogen from hydrocarbon cracking gas has been attempted (Suzuki, 1985). TABLE 11.3 shows the conditions for calculation and Fig. 11.13.a and 11.13.b show the results for profiles of partial pressures and amounts adsorbed of carbon monoxide and nitrogen at purge ratios (u_L/u_H) of 0.11 and 0.1. Adsorption isotherm is of the Markham-Benton type.

$$q_i/q_0 = K_i p_i / (1 + \sum K_i p_i) \quad (11-52)$$

where $q_0 = 4.5$ mmol/g, $K_{N_2} = 0.1$ atm⁻¹ and $K_{CO} = 0.5$ atm⁻¹ were used. The effect of purge ratio is clearly shown by comparing these figures.

As another example, the case of air drying was calculated and compared with the complex calculation result obtained by the method introduced in the previous section (Chihara and Suzuki, 1983a). The case of isothermal operation (Fig. 11.6, solid and open circles) is compared with the results of the continuous countercurrent flow model (solid and broken lines) in Fig. 11.14. Rigorous calculation was done for a throughput ratio of 0.01 and the change in the profiles of the amount adsorbed after adsorption and desorption steps found to be reasonably small. Thus the simple model simulated quite well the cyclic steady state profile of PSA.

11.5. Mass Transfer Coefficient in Rapid Cyclic Adsorption and Desorption

For a rigorous set of differential equations for mass balance in the bed and for adsorption rate in the particle, partial differential equations are introduced for both processes, making for lengthy computation time. In order to finish numerical computation with in a reasonable amount of time it is desirable to use as simple a model as precision will allow.

The linear driving force (LDF) model may be considered to be one reliable model which can be used for this purpose. In the LDF model, overall mass transfer coefficient $k_s a_v$ is the only rate parameter, which is usually related to the intraparticle diffusion coefficient, D_s , as

$$k_s a_v = 15 D_s / R^2 \quad (11-53)$$

where R denotes the radius of the adsorbent particle.

Equation (11-53) is derived for long-term adsorption or desorption from a uniform initial distribution of amount adsorbed in the particle.

For the rapid adsorption-desorption cycles such as those encountered in PSA, application of the above relation becomes dubious since, when the cycle time is much smaller than the time constant of diffusion inside the particle, change of concentration distribution during the adsorption or desorption process is very complicated. Nakao and Suzuki (1983) compared solutions of the LDF model and the rigorous partial differential equation for the case of cyclic adsorption and desorption in a spherical adsorbent particle and found that the proportionality constant, K , defined by Eq. (11-54) becomes a function of cycle time factor defined by Eq. (11-55).

$$K_s a_v = K D_s / R^2 \quad (11-54)$$

$$\theta_c = D_s t_c / R^2 \quad (11-55)$$

where t_c is the half cycle time. Fig. 11.15 shows change of K against θ_c . By numerically solving the following basic equation with the boundary conditions shown by Eqs. (11-57) and (11-58), concentration distribution in the particle is obtained as a function of time.

$$\partial q / \partial t = D_s \{ \partial^2 q / \partial r^2 + (2/r) \partial q / \partial r \} \quad (11-56)$$

$$r = 0 : \partial q / \partial r = 0 \quad (11-57)$$

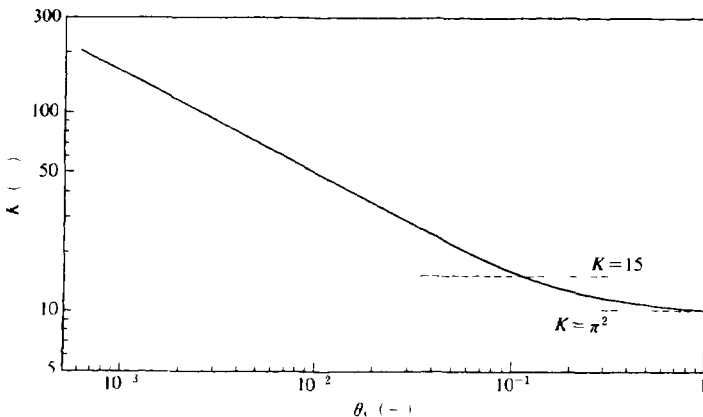


Fig. 11.15 Dependency of overall mass transfer coefficient on cycle time (Reproduced with permission by Nakao, S. and Suzuki, M., *J. Chem. Eng. Japan*, 16, 118 (1983))

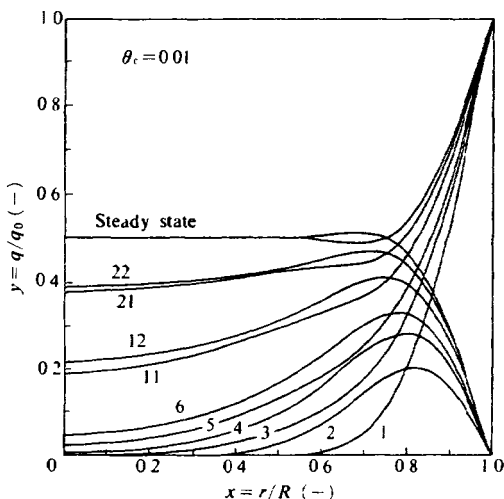


Fig 11.16 Profiles of amount adsorbed in an adsorbent particle with time at unsteady state $\theta_c = 0.01$. Numbers correspond to profiles at the end of $2n + 1$ (adsorption) and $2n + 2$ (desorption) periods (Reproduced with permission by Nakao, S and Suzuki, M, *J Chem Eng Japan*, 16, 116 (1983))

$$\begin{aligned}
 r = R: q = q_0 & \text{ at } 2nt_c < t \leq (2n + 1)t_c \\
 q = 0 & \text{ at } (2n + 1)t_c < t \leq (2n + 2)t_c
 \end{aligned}
 \quad (11-58)$$

where n is an integer. Typical concentration profiles with the initial condition of $q = 0$ at $t = 0$ is shown in Fig. 11.16 for the case of $\theta_c = D_s t_c / R^2 = 0.1$. Numbers shown in the figure correspond to the end of $2n + 1$ or $2n + 2$ half cycles. As can be understood from the figure, after several tenths of a cycle, profiles after adsorption and desorption reach dynamic steady state and the amount adsorbed in the center of the particle stays almost constant, 0.5 in this case, and only the fractional part near the surface is utilized for adsorption and desorption. Concentration profiles during one cycle in the dynamic steady state are illustrated in Fig. 11.17 for $\theta_c = 0.1, 0.01$ and 0.001 . When cycle time becomes smaller, the fractional volume of the adsorbent utilized becomes naturally restricted to the vicinity of the surface and then diffusion distance becomes smaller. From this calculation, change of the amount adsorbed in the dynamic steady state is obtained as illustrated in Fig. 11.18. The figure shows the amounts adsorbed after the adsorption and desorption steps. The difference of the two lines represents the mass transfer amount during the half cycle. LDF model is defined as

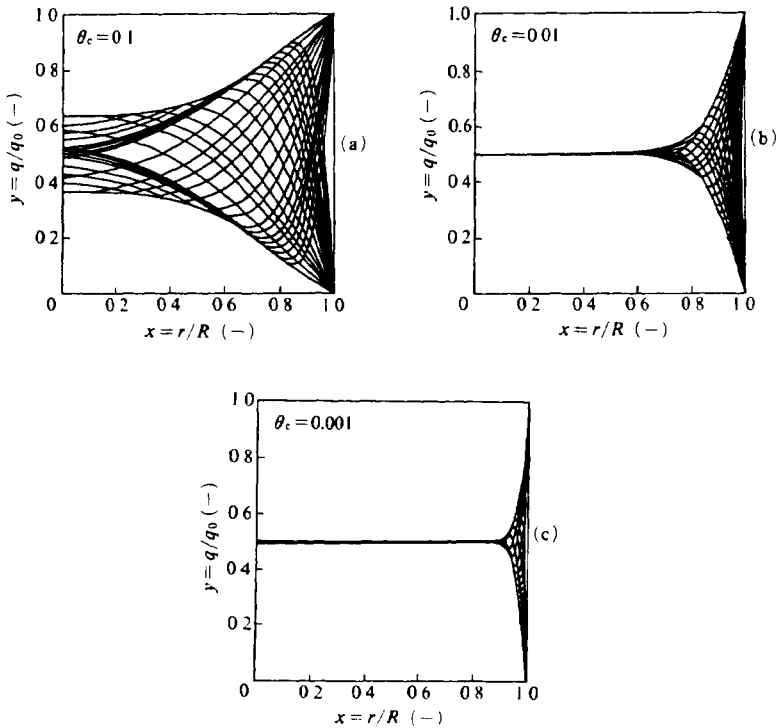


Fig. 11.17 Profiles of amount adsorbed in an adsorbent particle with time at dynamic steady state for cases (a) to (c). (a) $\theta_c = 0.1$: (b) $\theta_c = 0.01$ (c) $\theta_c = 0.001$
 (Reproduced with permission by Nakao, S. and Suzuki, M., *J. Chem. Eng. Japan*, 16, 116 (1983)).

$$dq/dt = k_s a_v (q_0 - q) \quad (11-59)$$

where q_0 is the amount adsorbed in equilibrium with the fluid phase in the adsorption step and $q_0 = 0$ for the desorption step. From this model, the amount adsorbed after the adsorption step and that after the desorption step in the dynamic steady state were obtained as

$$q/q_{0,ads} = 1/(1 + T_c) \quad (11-60)$$

$$q/q_{0,des} = T_c/(1 + T_c) \quad (11-61)$$

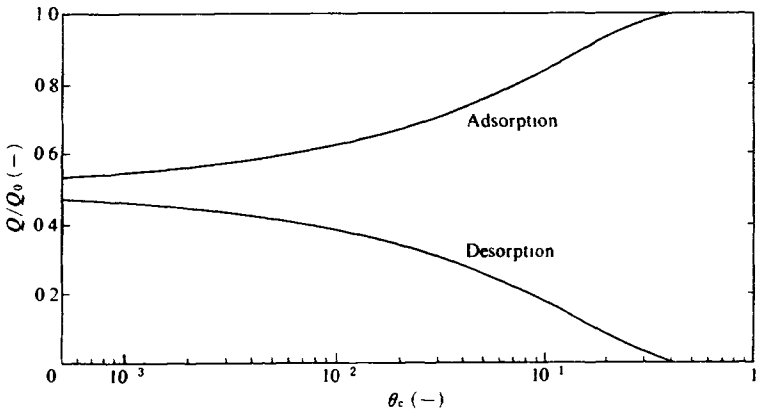


Fig 11 18 Dependency of total amount adsorbed at end of adsorption and desorption period on half-cycle time in dynamic steady state (Reproduced with permission by Nakao, S and Suzuki, M *J Chem Eng Japan*, 16, 117 (1983))

where

$$T_c = \exp(-k_s a_v t_c) = \exp(-K\theta_c) \quad (11-62)$$

Then by fitting Eqs (11-60) and (11-61) with the results from the differential equation shown in Fig 11 18, $k_s a_v$ or K is defined as a function of θ_c , which is shown by Fig 11 15 For further details, refer to Nakao and Suzuki (1983)

11.6. PSA Based on Difference of Adsorption Rates

By considering PSA as a separation process based on transient characteristics, it is also possible to construct a PSA process for the separation of two components whose equilibrium relations are similar but whose adsorption rates are quite different This example is shown for the case of separation of oxygen and nitrogen by carbon molecular sieve Carbon molecular sieves for this concept were originally shown by Juntgen, Knoblauch and their colleagues (1973) and a PSA process utilizing this principle for the production of oxygen and/or nitrogen from air was developed (Juntgen *et al* 1973, Knoblauch, Reichenberger and Juntgen, 1975 Later Takeda Chemical Co, Kuraray Chemical Co and Calgon Corp developed similar carbon molecular sieves for the purpose of producing nitrogen from air When air is introduced from

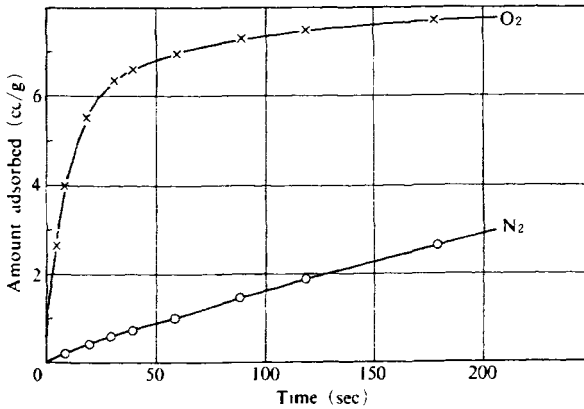


Fig 11.19 Adsorption uptake of oxygen and nitrogen by carbon molecular sieves (25°C 1 atm) Source Kuraray Catalogue

the bottom of the column packed with the carbon molecular sieves at high SV , only nitrogen appears at the exit in the beginning. Then by desorption, oxygen-rich air is recovered from the blow-down and regeneration gas.

An example of oxygen and nitrogen uptake curves of the carbon molecular sieve produced by Kuraray Chemical Co is shown in Fig 11.19.

Control of the size of micropore of carbon molecular sieve is an essential factor in obtaining large differences in diffusivities of oxygen and nitrogen. Several trials were made to control micropore diffusivities of carbon molecular sieves by the deposition of carbon produced by thermal cracking of hydrocarbons (Moore and Trimm, 1977, Chihara and Suzuki, 1979, 1982). Chihara and Suzuki (1982) showed that by starting from MSC 5A of Takeda Chemical Co., benzene cracking at 700°, 780° and 850°C in nitrogen carrier stream was effective for this purpose. The amount of deposited carbon was followed by weight change of the carbon molecular sieve sample by gravity equipment and adsorption rates of oxygen and nitrogen were measured by a constant volume method. The results are shown in Fig 11.20. By this method, ratio of diffusivities of O₂ and N₂ reached as high as 45, as shown in Fig 11.21.

Numerical simulation of this type of PSA has been done for oxygen production (Chihara and Suzuki, 1982). The principle is almost the same as that introduced in the previous section except that in this case the use of proper rate parameters is necessary.

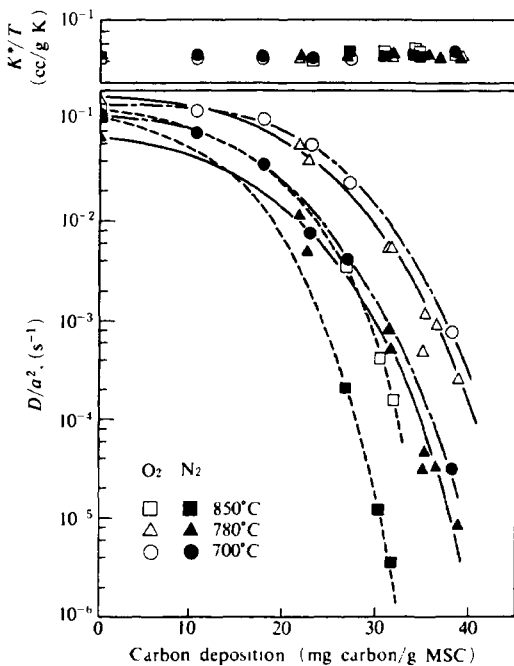


Fig 11 20 Dependence of adsorption equilibrium constants and micropore diffusivities of O₂ and N₂ on carbon deposition.

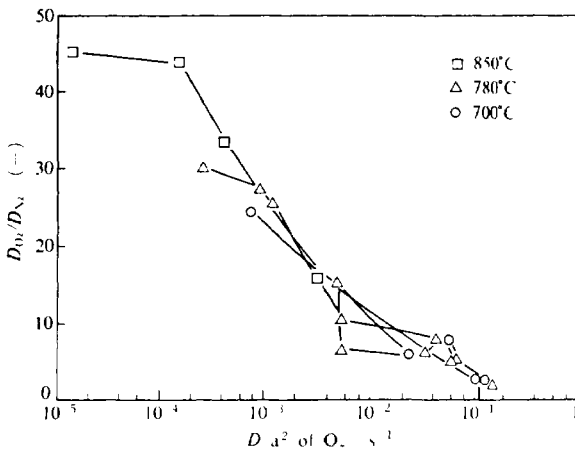


Fig 11 21 Variation of D_{O_2}/D_{N_2} with D/a^2 of O₂

REFERENCES

- Carter, J W and M L Wyszynski, *Chem Eng Sci*, **38**, 1093 (1983).
- Chan, Y N I, F B Hill and Y W Wong, *Chem Eng Sci*, **36**, 243 (1982)
- Chihara, K and M Suzuki, *J Chem Eng Japan*, **16**, 53 (1983a)
- Chihara, K and M Suzuki, *J Chem Eng Japan*, **16**, 293 (1983b)
- Chihara, K and M Suzuki, *Bunri Gijyutu*, **12**, 95 (1982) (in Japanese)
- Chihara, K and M Suzuki, *Carbon*, **17**, 339 (1979)
- Chihara, K, Y Sakon and M Suzuki, *Int Symposium on Carbon*, **4A12**, 435 (1982)
- Juntgen, H, K Knoblauch and H J Schroeter, *Berichte der Bensen-Gesellschaft fur physikalische Chemie*, **79**, 824 (1975)
- Juntgen, H, K Knoblauch, H Munzner and W Peters, *Chem Ing Tech*, **45**, 533 (1973)
- Kawai T *Atsurvoku Sungu Kyuuchaku Gijyutsu Shuusei*, Kogyo gijyutsukai (1986) (in Japanese)
- Kawazoe, K and T Kawai, *Kagaku Kogaku*, **37**, 288 (1973) (in Japanese)
- Knaebel, K S and F B Hill, *AIChE Ann Meeting*, 91d, L A., November (1982)
- Kawazoe, K, in *Kagaku Kogaku Benran*, p 847 (1978) (in Japanese)
- Knoblauch, K J Reichenberger and H Juntgen, *Gas/erdgas*, **113**, 382 (1975)
- Mitchell, J E and L H Shendalman, *AIChE Sympo Series* **69**, No 134, 25 (1973)
- Moore S V and D L Trimm, *Carbon*, **17**, 339 (1979)
- Nakao, S and M Suzuki, *J Chem Eng Japan*, **16**, 114 (1983)
- Raghavan, N S, M M Hassan and D M Ruthven, *AIChE Journal*, **31**, 385 (1985)
- Shendalman L H and J E Mitchell *Chem Eng Sci*, **27**, 1449 (1972)
- Skarstrom, C W, *Recent Development in Separation Science*, Vol 2, 95, CRC Press Cleveland (1972)
- Suzuki M, *AIChE Sympo Series*, **81**, No 242, 67 (1985)
- Yagi S and D Kunii *Int Devel in Heat Transfer* 750 ASME IME (1961)
- Yagi, S, D Kunii and N Wakao, *Int Devel in Heat Transfer*, 742 ASME, IME (1961)
- Yang, R T and S J Doong, *AIChE Journal* **31**, 1829 (1985)

Adsorption for Energy Transport

Adsorption is accompanied by evolution of heat. Also the heat of adsorption is usually 30% to 100% higher than heat of vaporization (condensation) of the adsorbate. Thus, if a fresh adsorbent and adsorbate in liquid form coexist separately in a closed vessel, transport of adsorbate from the liquid phase to the adsorbent occurs in the form of vapor, since adsorption is stronger than condensation to liquid phase.

During this step, the temperature of the liquid phase becomes lower while the adsorbent temperature rises. Air conditioning and refrigeration utilize this phenomenon.

The adsorption cooling system has drawn attention since it employs no moving parts and it may be possible to utilize low grade thermal energy such as solar energy or waste heat from industry for regeneration of the adsorbent. A demonstration unit of a refrigerator was first commercialized by Tchernev (1978) by using zeolite-water system. Guillemot (1980) suggested the feasibility of utilizing this principle in an adsorption-cooling system from the view point of thermodynamics. The principle of this process as well as a model investigation is presented here.

Another use of heat of adsorption is in heat pump systems to produce high pressure steam from low-grade waste steam. The principle of this system is also discussed in this chapter.

12.1. Principle of Adsorption Cooling

The principle of operation of the cooling system is illustrated in Fig. 12.1. The system consists of an adsorbent bed, a condenser and an evaporator. A combination of adsorbent and adsorbate is confined in a closed system. In the adsorption cycle shown in Fig. 12.1 a, adsorption takes place in the adsorbent bed, while evaporation of adsorbate occurs in the evaporator, which absorbs heat from outside of the system. Cooling can be achieved by making use of this heat absorption. In the